

Fall 2005

The Role of Histidine-Rich Proteins in the Biomineralization of Hemozoin

Lisa Pasierb

Follow this and additional works at: <https://dsc.duq.edu/etd>

Recommended Citation

Pasierb, L. (2005). The Role of Histidine-Rich Proteins in the Biomineralization of Hemozoin (Doctoral dissertation, Duquesne University). Retrieved from <https://dsc.duq.edu/etd/1021>

This Immediate Access is brought to you for free and open access by Duquesne Scholarship Collection. It has been accepted for inclusion in Electronic Theses and Dissertations by an authorized administrator of Duquesne Scholarship Collection. For more information, please contact phillips@duq.edu.

The Role of Histidine-Rich Proteins in the Biomineralization of Hemozoin

A Dissertation presented to the Bayer School of Natural and Environmental Sciences
of Duquesne University

As partial fulfillment of the requirements
for the degree of Doctor of Philosophy

By
Lisa Pasierb
August 26, 2005

Dr. David Seybert, thesis director
Dr. David W. Wright, advisor

In memory of Anna Pasierb
April 24, 1924 – May 31, 2005

Acknowledgements

First and foremost, I would like to express my sincerest gratitude to my advisor, Dr. David W. Wright. His exuberating energy and conviction attracted me to his research group, while his unwavering faith in me taught me more than he could ever know. Secondly, of course, I would like to extend my appreciation to Glenn Spreitzer and James Ziegler, the other two original members of the Wright group, whom initially tried to exert male dominance, but eventually became very faithful friends and colleagues. Finally, to all the other members of the Wright group over the years, thanks for all of your help, suggestions, and camaraderie.

Next, I would like to thank the members of my committee, Dr. Mitchell Johnson, Dr. Partha Basu, and Dean David Seybert, for their advice and counsel. Particularly, I would like to thank Dean Seybert, for his role as my graduate advisor while I completed my research abroad. Finally, I would like to add the Duquesne University Department of Chemistry and Biochemistry and Vanderbilt University Department of Chemistry to my list of acknowledgements, since both faculties and staffs made my transitions between schools an eased and enjoyable experience.

I would like to thank my parents, for their committed love and support; my sister and brother, for all of their phone calls while I was away; and my uncles, for their staunch belief in the abilities of their niece. A special thanks goes out to my boyfriend, who traveled this journey by my side with lots of love and support.

In closing I would like to dedicate this work to my grandmother Anna, who has taught me countless lessons in life, family, and love. I miss her dearly.

Abstract

Hemozoin formation, the consequential end product of the proteolysis of hemoglobin by *Plasmodium falciparum*, is essentially a biomineralization process whereby toxic free heme is aggregated into an inert crystalline solid, also known as malaria pigment or β -hematin. The histidine-rich protein II (HRP II), isolated from the digestive vacuole of the parasite, has been implicated in the mediation of this biomineral through the protein's ability to bind heme, aggregate the biomineral, and be effectively inhibited by known antimalarials, including chloroquine. The HRP II sequence, which is comprised of 76% of histidine and alanine residues, has a specific amino acid repeat motif which is reminiscent of nucleating scaffold proteins utilized by other biological systems in biomineralization processes. Using a peptide dendrimer previously developed in our laboratory as a functional HRP II mimic, we examined two domain repeats, Ala-His-His-Ala-His-His-Ala-Ala-Asp and Ala-His-His-Ala-Ala-Asp-Ala-His-His, as putative hemozoin nucleating sequences. Results indicated the Ala-His-His-Ala-His-His-Ala-Ala-Asp repeat of peptide dendrimer BNT II was the most probable nucleating domain within the HRP II sequence. Site-directed mutagenesis studies were then utilized to elucidate the role of the nucleating domain per active site amino acids.

Table of Contents

Chapter 1	An Historical Perspective of Hemozoin Formation	
1.1	Introduction	2
1.2	Historical Perspective of the Malaria Pigment (Hemozoin)	9
1.3	Structural Characterization of Hemozoin	12
1.4	Hypotheses Surrounding Hemozoin Formation	18
1.5	Chemical Synthesis of Hemozoin	31
1.6	Hemozoin Quantification	40
1.7	Hemozoin Formation – A Promising Route Towards Discovering New Antimalarials	43
	References	47
Chapter 2	Design and Synthesis of the <u>B</u>ionucleating <u>T</u>emplates (BNTs)	
2.1	Background and Significance	57
2.2	The Histidine-Rich Proteins Evidenced as Templates in the Biomineralization of Hemozoin	63
2.3	Design and Development of a Model HRP System	67
2.4	The Ala-His-His-Ala-His-His-Ala-Ala-Asp Putative Domain – Initial Studies of a Model HRP System	72
2.5	Site-Directed Mutagenesis Studies of the HRP II Mimic	87
2.6	BNT II and Mutant Modeling	102
	References	111
Chapter 3	Putative Domain Template Studies	
3.1	Introduction	121
3.2	Functional Screening of the BNTs	126
3.3	Preliminary Studies	131
3.4	Putative Domain Studies	132
	BNT II	132
	BNT IIA	141
3.5	Discussion	148
3.6	Conclusions	163
	References	166
Chapter 4	Site-directed Mutagenesis Studies of BNT II	
4.1	The Mutants of BNT II – An Introduction	174
4.2	General Information	176
	Mutant BNT IID	177
	Mutant BNT IIX	184
	Mutant BNT IYY	189
	Mutant BNT IIZ	195
4.3	Conclusions	200
	References	213

Chapter 5	Application of the BNT II Model System Inhibition of Hemozoin Aggregation by N₄O₂ Schiff Base Complexes	
5.1	Introduction	215
5.2	Synthesis and Characterization of N ₄ O ₂ Complexes	218
5.3	Experimental Methods	221
5.4	Results and Discussion	223
5.5	Conclusions	232
	References	234
Chapter 6	Concluding Remarks	
6.1	Hemoglobin Proteolysis as an Antimalarial Strategy	238
6.2	Biochemical Involvement of HRP II	239
6.3	Role of BNT II Model System	241
6.4	Summary	243
	References	245
Appendix I	Automated Peptide Synthesis Program	A-1
Appendix II	Titration Binding Curves	A-4
Appendix III	Circular Dichroism Titration Experiments	A-28

Table of Figures

1.1	Map of malaria endemic regions	2
1.2	Electron micrograph of hemozoin within an erythrocyte	4
1.3	Life cycle of <i>Plasmodium falciparum</i>	5
1.4	Schematic of hemoglobin proteolysis	6
1.5	Structure of hemozoin	7
1.6	UV-Vis spectrum of hemozoin and ferriprotoporphyrin IX	13
1.7	IR spectra of native hemozoin, synthetic β -hematin and hematin	14
1.8	EXAFS of hemin and hemozoin	14
1.9	Powder diffraction of hemozoin and synthetic β -hematin	15
1.10	EPR spectra of hemozoin and synthetic β -hematin	16
1.11	Mössbauer spectra of hemozoin and synthetic β -hematin	17
1.12	The sequence of histidine-rich protein II (HRP II) from <i>P. falciparum</i>	25
2.1	<i>Plasmodium falciparum</i> trophozoite residing in an erythrocyte	57
2.2	Abiological synthesis of hemozoin	59
2.3	Field emission inlens scanning electron microscopy of hemozoin produced by <i>Plasmodia</i> and non- <i>Plasmodium</i> species	65
2.4	Illustration of Fmoc-4-branch MAPS resin	69
2.5	Substrate binding curves for BNT I	75
2.6	Substrate binding curves for BNT II	76
2.7	Template and other protein mediated hemozoin production	77
2.8	Time evolution for the BNT mediated formation of hemozoin	78
2.9	pH dependence of the BNT mediated formation of hemozoin	79
2.10	Effect of acetate buffer concentration on the BNT mediated formation of hemozoin	79
2.11	FT-IR spectra of hemozoin from <i>P. falciparum</i> and that mediated by the BNTs	80
2.12	Synchrotron x-ray diffraction patterns of hemozoin from <i>P. falciparum</i> and that mediated by BNT II	80
2.13	Inhibition of the BNT II mediated production of hemozoin	81
2.14	Circular dichroism spectra of HRP II, linear multimers of HRP II sequence, BNT I, and BNT II	84
2.15	Scale-up equations for HPLC peptide purification	94
2.16	Semi-preparative HPLC chromatogram of BNT II	95
2.17	Semi-preparative HPLC chromatogram of BNT IIA	96
2.18	Semi-preparative HPLC chromatogram of BNT IID	97
2.19	Semi-preparative HPLC chromatogram of BNT IIX	98
2.20	Preparative HPLC chromatogram of BNT IIY	99
2.21	Preparative HPLC chromatogram of BNT IIZ	100
2.22	MALDI-TOF mass spectrometry for BNT II	103
2.23	ESI ⁺ mass spectrometry for BNT IIA	103

2.24	9-mer sequence of BNT II modeled as a right-handed 3-10 helix and a left-handed polyproline type II conformation	106
2.25	9-mer sequence of BNT IIA modeled as a right-handed 3-10 helix and a left-handed polyproline type II conformation	107
2.26	9-mer sequence of BNT IID modeled as a right-handed 3-10 helix and a left-handed polyproline type II conformation	107
2.27	9-mer sequence of BNT IIX modeled as a right-handed 3-10 helix and a left-handed polyproline type II conformation	108
2.28	9-mer sequence of BNT IYY modeled as a right-handed 3-10 helix and a left-handed polyproline type II conformation	108
2.29	9-mer sequence of BNT IIZ modeled as a right-handed 3-10 helix and a left-handed polyproline type II conformation	109
3.1	Binding equilibration study for BNT IIA	131
3.2	UV-Vis spectra of the interaction of hemin chloride with BNT II	133
3.2	<i>(inset)</i> UV-Vis spectra of BNT II	133
3.3	Hemin chloride titration binding curve for BNT II	134
3.4	Zn(II)PPIX titration binding curve for BNT II	136
3.5	Fluorescence quenching studies of Zn(II)PPIX with BNT II	137
3.5	<i>(inset)</i> Fluorescence quenching studies of Zn(II)PPIX with BNT I	137
3.6	Circular dichroism spectra of BNT II at various pH values	138
3.7	Circular dichroism spectra of BNT II and spectral changes associated with binding Fe(III)PPIX and Zn(II)PPIX	139
3.8	UV-Vis spectra of the interaction of hemin chloride with BNT IIA	142
3.9	Hemin chloride titration binding curve for BNT IIA	143
3.10	Zn(II)PPIX titration binding curve for BNT IIA	144
3.11	Fluorescence quenching studies of Zn(II)PPIX with BNT IIA	145
3.12	Circular dichroism spectra of BNT IIA and spectral changes associated with binding Fe(III)PPIX	147
3.13	Substrate binding of the hypothesized putative nucleation domains	151
3.14	Fluorescence quenching of BNT II vs. BNT IIA	153
3.15	Hemozoin production mediated by the putative nucleation domains	154
3.16	Thermal denaturation of BNT II	158
3.17	Circular dichroism spectra of collagen vs. polyproline II	159
3.18	Circular dichroism spectra of BNT II vs. BNT IIA	159
3.19	Thermal denaturation of linear multimer of BNT II	160
3.20	Representation of BNT II and BNT IIA sequences	165
4.1	UV-Vis spectra of the interaction of hemin chloride with BNT IID	178
4.2	Hemin chloride titration binding curve for BNT IID	179
4.3	Zn(II)PPIX titration binding curve for BNT IID	180
4.4	Fluorescence quenching studies of Zn(II)PPIX with BNT IID	181
4.5	Circular dichroism spectra of BNT IID and spectral changes associated with binding Fe(III)PPIX	183

4.6	UV-Vis spectra of the interaction of hemin chloride with BNT IIX	184
4.7	Hemin chloride titration binding curve for BNT IIX	185
4.8	Zn(II)PPIX titration binding curve for BNT IIX	186
4.9	Fluorescence quenching studies of Zn(II)PPIX with BNT IIX	187
4.10	Circular dichroism spectra of BNT IIX and spectral changes associated with binding Fe(III)PPIX	188
4.11	UV-Vis spectra of the interaction of hemin chloride with BNT IY	190
4.12	Hemin chloride titration binding curve for BNT IY	191
4.13	Zn(II)PPIX titration binding curve for BNT IY	191
4.14	Fluorescence quenching studies of Zn(II)PPIX with BNT IY	192
4.15	Circular dichroism spectra of BNT IY and spectral changes associated with binding Fe(III)PPIX	193
4.16	UV-Vis spectra of the interaction of hemin chloride with BNT IZ	195
4.17	Hemin chloride titration binding curve for BNT IZ	196
4.18	Zn(II)PPIX titration binding curve for BNT IZ	197
4.19	Fluorescence quenching studies of Zn(II)PPIX with BNT IZ	198
4.20	Circular dichroism spectra of BNT IZ and spectral changes associated with binding Fe(III)PPIX	199
4.21	Comparison of the UV-Vis spectra BNT II and its mutants	201
4.22	Substrate binding of BNT II and its mutants	202
4.23	Fluorescence quenching of Zn(II)PPIX by BNT II and its mutants	204
4.24	Hemozoin production mediated by BNT II and its mutants	205
4.25	Comparison of CD spectra of 2 nmoles of BNT II and its mutants in 10 mM acetate buffer, pH 4.8	207
5.1	Representation of the N ₄ O ₂ Schiff base compound	224
5.2	Effect of salt concentration on hemozoin aggregation and drug inhibition	226
5.3	Fluorescence quenching studies of ENBPI complexes by Fe(III)PPIX	228
5.4	Fluorescence aggregation studies of ENBPI complexes	229
5.5	Fluorescence emission time studies for Mg ^{II} ENBPI and Fe ^{III} ENBPI	230
5.6	NMR spectrum of Mg ^{II} ENBPI in 25 mM acetate buffer, pH 4.8	231
5.7	NMR stability study of Mg ^{II} ENBPI	232
5.8	Integration of spectra for NMR stability study of Mg ^{II} ENBPI	233
6.1	Scanning electron microscopy of β -hematin synthesized by the dehydrohalogenation of 2,6-lutidine according to methods published by Bohle	242
6.2	Scanning electron microscopy of β -hematin synthesized in aqueous solution according to methods published by Blauer	242

Table of Tables

2.1	Sequence homology of the histidine-rich proteins of <i>P. falciparum</i>	62
2.2	Substrate binding stoichiometries of BNT I and BNT II	73
2.3	Site-directed mutagenesis of the 9-mer sequence of BNT II	89
F2.16	Gradient table for semi-preparative HPLC of BNT II	95
F2.17	Gradient table for semi-preparative HPLC of BNT IIA	96
F2.18	Gradient table for semi-preparative HPLC of BNT IID	97
F2.19	Gradient table for semi-preparative HPLC of BNT IIX	98
F2.20	Gradient table for preparative HPLC of BNT ILY	99
F2.21	Gradient table for preparative HPLC of BNT IIZ	100
2.4	Amino acid analysis of BNT II and BNT mutants	101
3.1	CD spectral markers for Fe(III)PPIX titration with BNT II	141
3.2	CD spectral markers for Zn(II)PPIX titration with BNT II	141
3.3	CD spectral markers for Fe(III)PPIX titration with BNT IIA	147
3.4	Absorbance maxima values for BNT II and BNT IIA binding to Fe(III)PPIX and Zn(II)PPIX	150
4.1	Site-directed mutagenesis of the 9-mer sequence of BNT II	175
4.2	CD spectral markers for Fe(III)PPIX titration with BNT IID	183
4.3	CD spectral markers for Fe(III)PPIX titration with BNT IIX	189
4.4	CD spectral markers for Fe(III)PPIX titration with BNT ILY	194
4.5	CD spectral markers for Fe(III)PPIX titration with BNT IIZ	200
4.6	Summary of the functional analyses of BNT II and its mutants	210
5.1	Acetate buffer dependence of the IC ₅₀ of the N ₄ O ₂ Schiff base complexes	226

*F denotes a Figure that contains a corresponding table.

Table of Equations and Schemes

1.1	Acid catalyzed hemozoin formation	39
1.2	Anhydrous non-coordinating base hemozoin formation	39
2.1	Standard Fmoc-peptide synthesis protocol	91
F2.15	Scale-up equations for HPLC peptide purification	94

*F denotes a Figure that contains equations.

Table of Abbreviations

¹H NMR - proton nuclear magnetic resonance spectroscopy
AA - amino acid
ACN - acetonitrile
BHIA - β-hematin inhibitory activity
BNT I - bionucleating template I, a first generation peptide dendrimer with the sequence (Ala-His-His-Ala-His-His-Ala-Ala-Asp)
BNT II - bionucleating template II, a second generation peptide dendrimer with the sequence (Ala-His-His-Ala-His-His-Ala-Ala-Asp)₂
BNT IIA - bionucleating template II alternate, a second generation peptide dendrimer with the sequence (Ala-His-His-Ala-Ala-Asp-Ala-His-His)₂
BNT IIC - mutant of BNT II with the sequence of (Ala-Ala-Ala-Ala-Ala-Ala-Ala-Ala-Asp)₂
BNT IID - mutant of BNT II with the sequence of (Ala-His-His-Ala-His-His-Ala-Ala-Ala)₂
BNT IIX - mutant of BNT II with the sequence of (Ala-His-Ala-Ala-His-Ala-Ala-Ala-Asp)₂
BNT IYY - mutant of BNT II with the sequence of (Ala-Ala-His-Ala-Ala-His-Ala-Ala-Asp)₂
BNT IIZ - mutant of BNT II with the sequence of (Ala-His-His-Ala-His-His-Ala-Ala-Lys)₂
BSA - bovine serum albumin
CD - circular dichroism spectroscopy
CD₂Cl₂ - deuterated methylene chloride-*d*₂
CD₃CO₂Na - deuterated sodium acetate-*d*₃
CD₃COOD - deuterated glacial acetic acid-*d*₄
CD₃OH - deuterated methanol-*d*₃
CDCl₃ - deuterated chloroform-*d*
cDNA - complementary deoxyribonucleic acid
CH₃COOH - acetic acid
COUP - coupling mixture
cpm - counts per minute
CQ - chloroquine
D₂O - deuterated water
DAB - diaminobenzidine
DCM - dichloromethane
DIEA - N,N'-diisopropylethylamine
DMF - dimethylformamide
DMSO - dimethyl sulfoxide
DNA - deoxyribonucleic Acid
ENBPI - ethylenediamine-*N,N'*-bis[propyl(2-hydroxy-*R*-benzylimino)] ligand

EPR - electron paramagnetic resonance
ESI - electrospray ionization mass spectrometry
EXAFS -extended x-ray absorption fine structure
Fe(acac)₃ - iron (III) acetylacetonate
Fe(III)PPPIX - iron (III) protoporphyrin IX
FEISEM - field emission inlens scanning electron microscopy
Fmoc – 9-fluorenylmethyloxycarbonyl
Fmoc-Ala-OH - N- α -Fmoc-L-alanine
Fmoc-Asp-OtBu - N- α -Fmoc-L-aspartic acid α -t-butyl ester
Fmoc-His(Trt)-OH - N- α -Fmoc-N-im-trityl-L-histidine
Fmoc-Lys(Mtt)-OH - N- α -Fmoc-N- ϵ -4-methyltrityl-L-lysine
FT-IR - Fourier transform infrared spectroscopy
Ga(acac)₃ - gallium (III) acetylacetonate
H₃Mabi - 2-(2'-hydroxy-3'-methoxyphenyl)-1,3-bis[4-aza-5-(2''-hydroxy-3''-methoxyphenyl)but-4'-4n-1'-yl]1,3'-imidazolidine
HAP - histoaspartic protease
HBTU - 2-(1H-benzotriazole-1-yl)-1,1,3,3-tetramethyluronium hexafluorophosphate
HCl - hydrochloric acid
HOBt - N-hydroxybenzotriazole
HPIA - heme polymerization inhibitory activity
HPLC - high performance liquid chromatography
HRG - histidine-rich glycoprotein
HRP I - histidine-rich protein I
HRP II - histidine-rich protein II
HRP III - histidine-rich protein III
HRP IV- histidine-rich protein IV
HRPs- histidine-rich proteins, collectively speaking
IC₅₀ - effective concentration at 50% inhibition
ICT - immunochromatographic test method for malaria detection
IR - infrared spectroscopy
IR - infrared, referring to this specific region of the spectrum of light
KAHRP – knob-associated histidine-rich protein
KBr - potassium bromide
LPS - lipopolysaccharide
MALDI-TOF - matrix-assisted laser desorption/ionization time-of-flight (mass spectroscopy)
MAPS - multiple antigen peptide system
Mech - mechanical shaker
MeOH - methanol
MOE - molecular operating environment
NaOH - sodium hydroxide
Ni(II)PcS - nickel (II) tetrasulfanatophthalocyanine
P. berghei - *Plasmodium berghei*

P. falciparum - *Plasmodium falciparum*
PAGE - polyacrylamide gel electrophoresis
PcS - tetrasulfanatothalocyanine
PfEMP1 - *Plasmodium falciparum* erythrocyte membrane protein 1
PIP - piperidine
PM I - plasmepsin I, an aspartic protease
PM II - plasmepsin II, an aspartic protease
PM IV - plasmepsin IV, an aspartic protease
PPII - polyproline type II secondary structure
PPIX - protoporphyrin IX
PVDF – polyvinylidene difluoride membrane
RBC - red blood cell
RHRP II - recombinant histidine-rich protein II
rpm - revolutions per minute
RV-1 - reaction vessel 1
SDS- sodium dodecyl sulfate
SDS-PAGE - sodium dodecyl sulfate
SEM - scanning electron microscopy
TFA - trifluoroacetic acid
TFE - trifluoroethanol
TIS - triisopropyl silane
TLC - thin layer chromatography
UV-Vis - ultraviolet-visible, referring to this specific region of the spectrum of light
XRD- x-ray diffraction
YAC - yeast artificial chromosome
Zn(II)PPIX - zinc (II) protoporphyrin IX

Chapter 1

Historical Perspective of Hemozoin Formation

1.1. Introduction

Malaria is endemic in one hundred and seven countries¹ infecting 350-500 million people annually (**Figure 1.1**).² Reported clinical cases confirm 1.5-2.7 million deaths per year, with the majority of the claimed lives belonging to children. In Africa, the continent which tallies 90% of all malaria related deaths,³ the disease kills one child in twenty before the age of five years old, correlating to a death rate of 2,800 children per day, or approximately 1 million children per year.⁴ Recent data suggests that although childhood mortality in Africa is decreasing, the percentage of deaths attributed to malaria is actually increasing. The direct economic burden is substantial for both poverty-stricken and industrialized countries.⁵ Economic growth reductions of at least one percent per year constrain some regions in Africa.^{6,7} The United States alone concedes over 2 billion dollars annually to offset costs incurred in malaria plagued regions.⁸

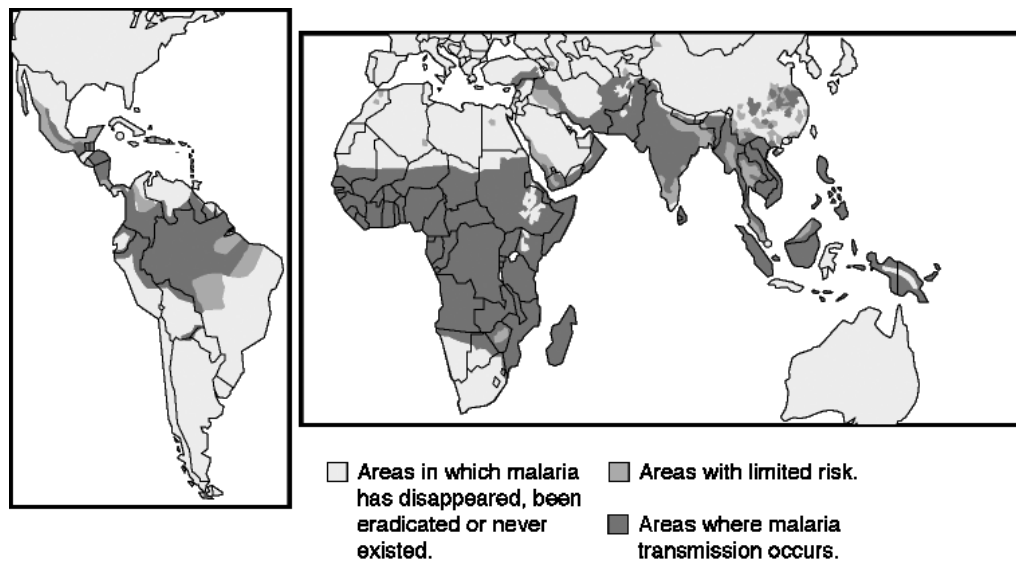


Figure 1.1. Malaria endemic regions, adapted from the World Health Organization.

From the early 1970's through the late 1990's, research in malaria was minimal, contributable to the fact the United States and most of Europe had eradicated the disease during the first half of the twentieth century.⁸ This lapse in research paralleled the development of only three antimalarials during the past twenty-five years, the same time frame in which over one thousand other drugs had been synthesized.⁹ The resurgence of malaria is due to drug and insecticide resistance,¹⁰⁻¹³ as well as social and environmental changes. *Plasmodium*, the parasitic carrier of malaria, is resistant to most antimalarial drugs including chloroquine. Vector resistance to pyrethroid insecticides now threatens the effectiveness of insecticide-treated bednet programs. Additionally civil wars, travel,¹⁴ and population increases contribute to heightened transmission of this deadly disease. Malaria-endemic countries alone have doubled in population and the disease is once again reaching across the oceans into both North America and Europe.¹⁵

Many antimalarials are developed on the premise that resulting drug efficacies are correlated to the ability of a compound or combination of compounds to interfere with aspects of parasitic metabolism, which differs significantly from the human host. *Plasmodia* catabolism involves a detoxification mechanism in which liberated free heme is sequestered into a metabolically inert crystalline material known as hemozoin (**Figure 1.2**).¹⁶ Of the four species of parasites that infect humans (*Plasmodium falciparum*, *Plasmodium vivax*, *Plasmodium ovalae*, and *Plasmodium malariae*), *P. falciparum* is the deadliest, accounting for 90% of all malaria cases in Africa and 50% in Asia and Latin America, being responsible for 95% of all malaria deaths.

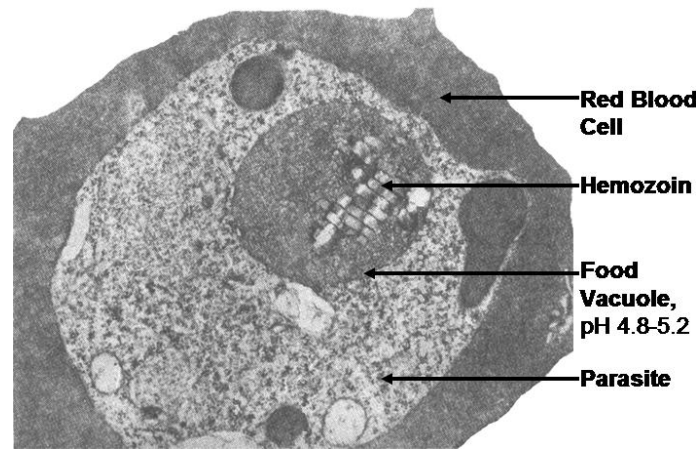


Figure 1.2. Electron micrograph of hemozoin localized inside an erythrocyte. Reproduced from reference 16.

The life cycle of *Plasmodia* is complex, (**Figure 1.3**) with developmental stages and corresponding symptoms differing according to the species involved. Typically, malaria infection is initiated when an infected female *Anopheles* mosquito injects sporozoites subcutaneously into the circulatory system of a human host. The sporozoite-stage parasites rapidly invade hepatocytes in the liver, undergoing asexual multiplication (exoerythrocytic schizogony) for 5-8 days before rupturing and releasing merozoites into the blood stream. The merozoites invade host erythrocytes and begin a maturation period of 48 hours, assuming several distinctive growth phases (blood-stage schizogony). The early trophozoite “ring” stage includes the ingestion of host cytoplasm and hemoglobin proteolysis. This trophic period ceases after several nuclear divisions result in the formation of schizonts. New merozoites

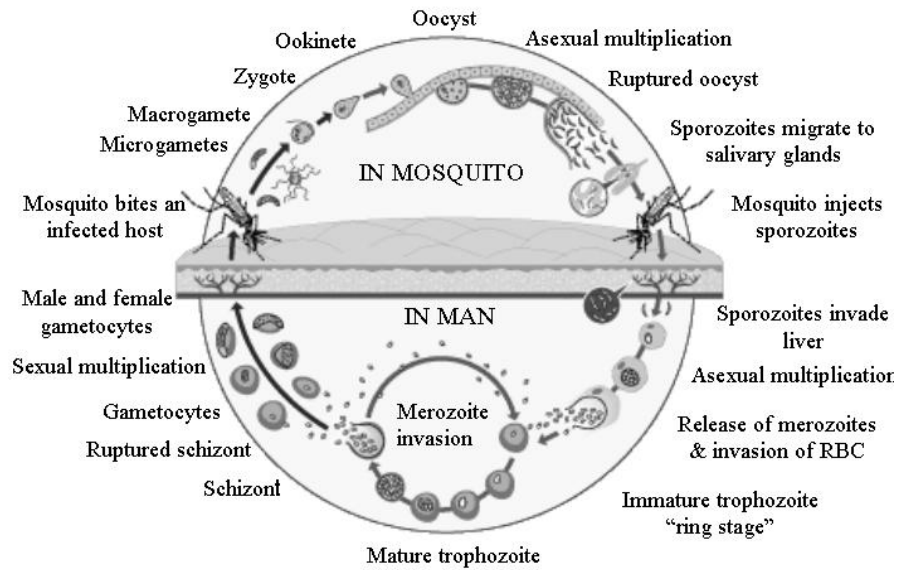


Figure 1.3. Life cycle of *Plasmodium falciparum* adapted from The Wellcome Trust.

bud from mature schizonts and are released from red blood cells, spawning a new invasion of host erythrocytes.

Some parasitic merozoites sexually differentiate into gametocytes, the developmental form which is transmittable back to the vector once a mosquito bites an infected host (gametogenesis). Inside the mosquito midgut, the gametocytes transform into male and female gametes, which then unite to form zygotes. The zygotes mature into motile ookinetes, which migrate through the midgut wall and develop into oocysts. The oocysts undergo several cycles of asexual replication, producing sporozoites. Upon maturation, the oocyst ruptures releasing the sporozoites, which then migrate through the mosquito hemocoel to the salivary glands, where these stage-specific parasites now await injection into another host, thereby completing the life cycle.

During the intraerythrocytic phase of its life cycle, the malaria parasite can degrade up to 80% of an infected erythrocyte's hemoglobin in order to obtain requisite amino acids.¹⁷ Hemoglobin catabolism occurs in the digestive vacuole of *Plasmodium falciparum* (pH 4.8-5.4) as a semi-ordered process^{18,19} involving the sequential action of several different proteases (**Figure 1.4**). Two aspartic proteases, plasmepsin-I and plasmepsin-II (PM I and PM II) initially cleave hemoglobin between phenylalanine and leucine at positions 33 and 34 along the peptide chain.²⁰⁻²² These residues, located in a conserved domain known as the hinge region, are crucial to the overall stabilization of hemoglobin. Cleavage at this site partially unfolds the polypeptide, exposing additional sites along the peptide chain for other proteases to cleave. Falcipain, a cysteine protease,²³ along with the plasmepsins (I, II, and IV²⁴) and HAP,²⁵ a histioaspartic protease,²⁶ further degrade the globin fragments into peptides. Plasmepsin I prefers to cleave phenylalanine in the P1 position, while

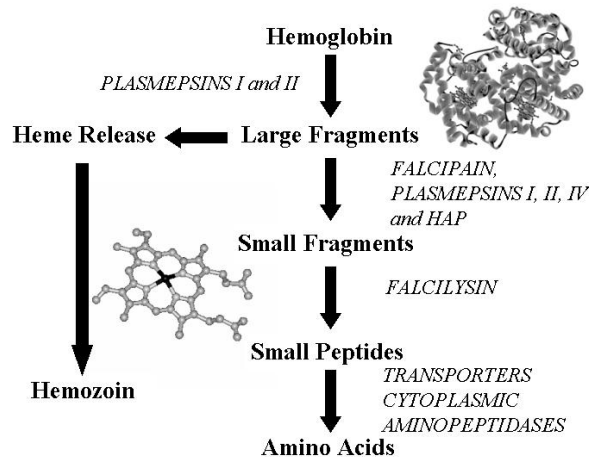


Figure 1.4. Schematic of hemoglobin proteolysis.

plasmepsin II targets hydrophobic residues, especially leucine in the P1' position.¹⁹ Falcilysin, a metalloprotease, then trims fragmented peptides to a metabolically useful size of about 6-8 amino acid residues

in length.²⁷ These small peptides are further reduced to simple amino acid residues once such fragments are transported from the digestive vacuole to the cytoplasm.²⁸

Hemoglobin proteolysis consequently releases free heme (iron(III)protoporphyrin IX, Fe(III)PPIX), which is toxic to the parasite. Accumulated free heme concentrations estimated as high as 0.4 M can disrupt metabolic function via the peroxidation of membranes, the inhibition of enzymes, and the generation of oxidative free radical species, all of which can damage the cell wall ultimately resulting in cell lysis. To balance the metabolic requirements for amino acids against the toxic release of free heme, malaria parasites, which lack a heme oxygenase for the subsequent breakdown of the iron porphyrin, have evolved a unique detoxification mechanism which involves the formation of the brown crystalline heme aggregate known as hemozoin (malaria pigment, β -hematin).

Recent spectroscopic evidence (x-ray powder diffraction and Raman spectroscopies) confirms the structure of hemozoin as a coordination aggregate of Fe(III)PPIX monomers in which the oxygen from a propionate of one group serves as the axial ligand to the ferric ion of another (Figure 1.5).²⁹ Hydrogen bonding between the propionic acid side chains

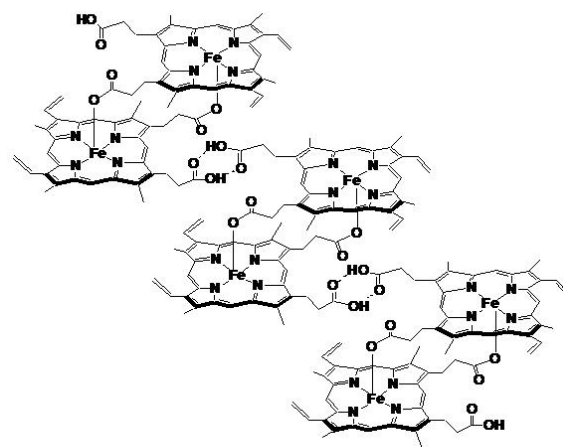


Figure 1.5. Structure of hemozoin.

of the porphyrin rings reveals an aggregate of Fe(III)PPIX dimers.³⁰

Hemozoin is released along with the merozoites during oxidative burst and is engulfed by macrophages, where it appears to impair macrophage function³¹ and suppress cytokine production.³² Such immunological impairment of the host alone prompts further investigation of the biochemical nature of hemozoin. However, before a comprehensive understanding of the pathogenesis of *Plasmodium falciparum* is understood, the biochemical basis for the formation of this biomineral must be unraveled.

Despite the recent completion of the sequencing of the genomes of *Plasmodium falciparum*, the *Anopheles* mosquito, and the human host, which will yield thousands of new target proteins,³³ the complexity of the life cycle of *Plasmodia* makes it difficult to determine which life cycle stages drug therapies should target for vaccines. Vaccine delivery systems and adjuvant technology must be improved before stage-specific immunotherapies will be effective.³⁴ While vaccine development may seem like a promising new route to combating malaria, blood stage antigens may not be completely effective in eliciting immunity.³⁵ Socio-economical and topological factors may also dictate the type of vaccine conjured based on the polymorphisms sustained by the parasite in a specific region.

An alternative drug therapy would include the inhibition of hemozoin production, since this metabolic process is unique to the parasite. If the malaria parasite's metabolic processing were halted at this stage, accumulation of free heme would ultimately result in parasite lysis. In fact, many of the most effective

antimalarials are thought to mechanistically proceed by disrupting the parasite's ability to synthesize hemozoin. Though the exact mechanisms remain elusive, some members of the quinoline family of antimalarials are hypothesized to sterically cap the formation of hemozoin through π - π interactions. While chemoprophylaxis continues to be the most effective means by which to combat malaria, multi-drug resistant parasites are emerging at an alarming rate. Intensifying efforts to develop new antimalarials may only have limited successes; therefore probing the mechanism of hemozoin formation may provide the best insight towards the development of new antimalarial strategies.

1.2. Historical Perspective of the Malaria Pigment (Hemozoin)³⁶

Hemozoin, known more commonly as the malaria pigment in its infancy, was first documented in the early 1700's by Giovanni Maria Lancisi, a physician who noted dark discolorations in the internal organs of malarial victims. He coined the name malaria, literally meaning "bad air," believing the deaths were linked to a poisonous vapor originating from swamps. In 1849, Rudolph Virchow first linked the brown-black tincture to the disease, sketching "pigmented bodies" that he discovered in the blood of a patient inflicted with chronic malaria. Thirty years later Charles Louis Alphonse Laveran linked the dark granules to a parasitic infection, observing "oscillating bodies" in the blood of an infected Algerian soldier and documenting an additional twenty-six cases where the motility of such "dark crescent spheres" indicated the presence of a living organism.

Five years later (1884) at the Bayview Hospital in Baltimore, Councilman and Abbot performed autopsies on two malaria fatalities, recording the brains as being “dull chocolate in color,” while the livers, spleens, and lungs were enlarged with distinctive black discolorations. Microscopic examination of the organs revealed that an irregularly shaped pigment was located not only on the outside of the organs, but also confined within the “red corpuscles.” This distinctive brown staining developed into such an archetypical marker of malaria and progression of the parasitic life cycle that in 1889 Johns Hopkins Hospital instituted blood smear analyses in the diagnosis of the disease. Through this effort, Camillo Golgi photographed the malaria parasite and correlated the amount of pigment to the severity of the infection. Several years later, William George MacCallum observed the sexual formation of male and female gametocytes merging into a zygote.

In 1897 Sir Ronald Ross examined a female *Anopheles stephensi* mosquito and noted comments about cells outside the mosquito midgut ... “these bodies contained a few granules of black pigment” being identical in appearance to the “large quartans and crescent-derived spheres” characteristic of the substance found in malaria victims. This finding first linked the mosquito as the vector in the transmission of malaria.

In 1911 W.H. Brown identified the chromogenic species in the malaria pigment as heme, confirming its origination from hemoglobin and establishing the theory these dark granules were a hemoprotein.³⁷ Moreover, Brown physically differentiated the malaria pigment from melanin (skin pigment), noting differences in

solubility and bleaching effects, given that potassium permanganate and hydrogen peroxide solutions failed to bleach malaria crystals, disintegrating the compound instead. In 1934, Louis Sambon replaced the outdated terminology of “plasmodin” and “haemo-melanin” for the malaria pigment with its present terminology, hemozoin.³⁸ That same year, B. N. Gosh and J. A. Sinton demonstrated the spectrum of hemozoin in alkaline solution was identical to that of hematin,³⁹ and its elemental composition by C, N, O, and Fe was also matched,⁴⁰ reinforcing the characterization of hemozoin as a hemoprotein.

In 1936 a similarly insoluble synthetic compound was reported by Antonin Hamsik, who first identified that when the porphyrin hematin was modified in the β -position in acidic medium the resulting compound could no longer convert back to the original soluble hematin species.⁴¹ This new compound, β -hematin, was insoluble in most solvents, and considered an “inactive” form of hematin.

In 1956 Deegan and Maegraith first reported the differential solubilities of crude hemozoin and hematin. Hemozoin remained insoluble in sodium bicarbonate buffer (pH 9.5), whereas hematin was solubilized. This finding provided additional support for the theory of a structural scaffold (protein) enveloping the heme unit in hemozoin, protecting the compound from solvation. Since heme was also known to bind specifically to the hydrophobic sites of other proteins, the involvement of a novel proteinacious material in hemozoin formation remained a sound hypothesis. More importantly, this notable difference in solubility became the basis for the

modern differential solubility assay, which permits the quantitation of hemozoin free of other types of hemozoin aggregates.

Until the early 1990's, chemical analyses obtained from the isolation and purification of native hemozoin supported the premise of the malaria pigment as a hemoprotein; however results were often conflicting.^{42,16} Most researchers agreed the protein component was of relatively low mass (<16 kDa), but some argued the proteinaceous material originated from the degradation of hemoglobin during parasitic feeding, while others maintained the protein was a novel parasite specific polypeptide.

The early history of malaria spawned three Nobel laureates in the twentieth century. In 1902 Sir Ronald Ross was awarded the Nobel Prize in medicine, not solely for his establishment of the mosquito as the vector in the disease, but also for his development of the mathematical models used to study the epidemiology of malaria. In 1906 the Nobel honor was jointly presented to Camillo Golgi and Santiago Ramon y Cajal in recognition for their contributions to the physiology of the nervous system of the *Anopheles* mosquito. One year later Laveran was the recipient of this same award for his contributions in establishing the role of protozoa as a causative agent in this disease.

1.3. Structural Characterization of Hemozoin

Despite its early identification, the structural and chemical nature of hemozoin has only been elucidated in the past fifteen years. In 1987, Fitch and Kanjanangulpan first reported that hemozoin could be purified from proteins,

reporting the malaria pigment was 82-99% Fe(III)PPIX by weight.⁴³ Native hemozoin was purified in sequential steps, first removing any hemozoin-associated proteins by incubation with a nonspecific protease from *Streptomyces griseus*, followed by a phospholipid extraction with a chloroform/methanol mixture according to procedures described by Bligh and Dyer.⁴⁴ Most importantly the protein/peptide free product was microscopically⁴⁵ and spectroscopically similar to synthetic β -hematin, dissolving the notion that hemozoin was a hemoprotein. Both crude hemozoin and synthetically aggregated β -hematin recorded UV-Vis spectrums with absorbances at 655 nm and a broad Soret band at 400 nm in 2.5% SDS solution (**Figure 1.6**). Both native and synthetic pigments were insoluble in ethanol, sodium bicarbonate, and chloroform, notably different from the solubility properties of hematin. The relative solubility was then quantitated from the height of the Soret band (400 nm) of the remaining solid sample dissolved in 0.02 N NaOH after a two-hour incubation in each solvent.

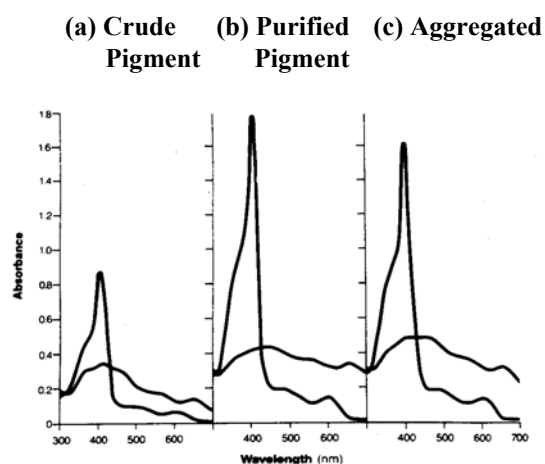


Figure 1.6. UV-Vis spectra of hemozoin isolated from *Plasmodium berghei* (a,b) and (c) aggregated ferriprotoporphyrin in NaOH. Reproduced from reference 43.

Four years later Slater and coworkers published a seminal paper in which hemozoin and synthetic β -hematin were determined by infrared and x-ray spectroscopies to be the same compound.⁴⁶ The infrared spectra exhibited sharp peaks at 1664 and 1211 cm^{-1} , indicative of a carboxylate coordinated to an iron center from

the stretching frequencies of a C=O and C-O vibration respectively (**Figure 1.7**). EXAFS of both compounds confirmed an oxygen atom in the coordination sphere of the iron atom (1.886 \AA)²⁹ and a carbon atom further away (3.4 \AA) (**Figure 1.8**). Elemental analysis and mass spectrometry (m/z 616.3, hemozoin dissolved in basic solution) revealed the pigments only consisted of Fe(III)PPIX, which led to the conclusion that hemozoin was an aggregate of dimers in which the Fe of one heme unit is coordinated to the propionate side chain of another.

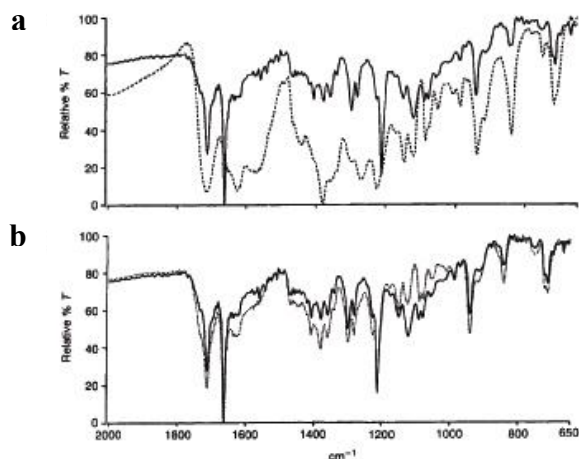


Figure 1.7. Fourier-transform IR spectra of (a) Hemozoin (—) and hematin (---) and (b) native hemozoin (—) and β -hematin (---). Reproduced from reference 46.

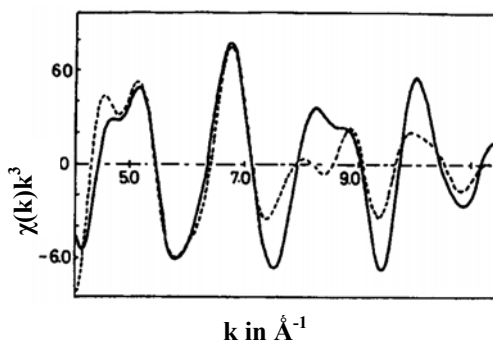


Figure 1.8. EXAFS of hemin (—) and hemozoin (---). Reproduced from reference 46.

Bohle and coworkers provided additional evidence that native hemozoin and its synthetic analog were chemically and spectroscopically similar via high resolution powder diffraction patterns (**Figure 1.9**). The group discovered the diffraction patterns in malarial trophozoites had a unique Bragg diffraction spike that was different from the powder diffraction pattern determined in uninfected erythrocytes.⁴⁷ When the two spectra were subtracted from each other, not only were the broadened

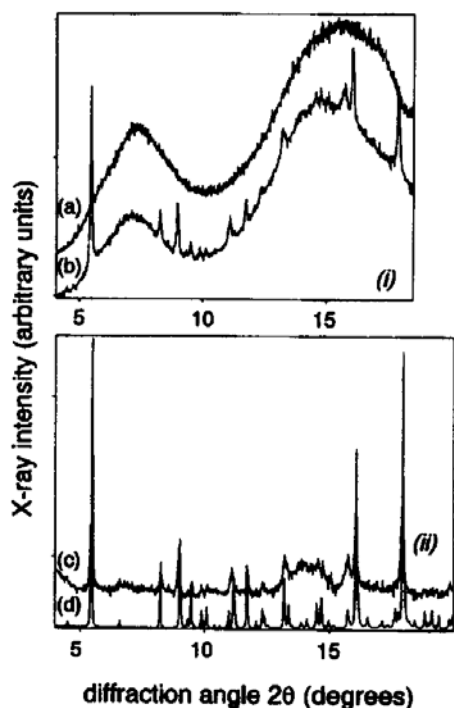


Figure 1.9. Powder diffraction patterns ($\lambda = 1.1495 \text{ \AA}$). (a) lyophilized uninfected erythrocytes (b) lyophilized trophozoites from *Plasmodium falciparum* (c) difference of (a) and (b) (d) synthetic β -hematin. Reproduced from reference 47.

bands from the lipid bilayer in the spectra removed, but also the resultant spectrum matched the diffraction pattern of synthetic β -hematin.

Other physical characterizations of hemozoin were not so unambiguous. Slater reported an EPR spectrum at 10K to have peaks at $g = 3.80$ and 1.95 , indicative of a low spin iron center.⁴⁶ Four years later Cammack and coworkers assigned both high spin and low spin EPR signals for hemozoin isolated from *Plasmodium berghei*.⁴⁸ These conflicting results were not

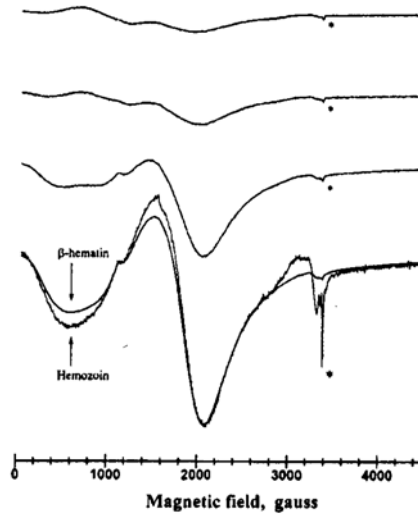


Figure 1.10. EPR spectra for β -hematin at (a) 21 K (b) 15.5 K (c) 9.0 K and (d) 5.6 K. The spectra of hemozoin is overlaid for comparison. Reproduced from reference 49.

resolved until 1998 when Bohle *et al.* performed carefully controlled temperature dependent EPR studies which found hemozoin to have signals at $g = 5.79, 3.80,$ and 2.04 at 21 K and below (**Figure 1.10**).⁴⁹ Spectra recorded above this temperature exhibited a loss in absorption intensity and accounted for the discrepancies in the spectra amongst the previous groups. Monomeric Fe(III)PPIX had similar signals at $g = 5.80$ and 2.04 , ascribing both species as high spin

iron compounds. These findings supported the structural information that hemozoin was a dimer of reciprocating heme units.

Mössbauer studies provided similarly litigious results. Initially isomer shifts reported by Yayon were at 0.46 and 0.47 mm s^{-1} with quadrupole splittings of 0.80 and 0.92 mm s^{-1} and line widths of 0.50 and 0.44 mm s^{-1} , respectively for both native (*P. berghei*) and synthetic hemozoin.⁵⁰ Egan and coworkers then reported isomer shifts of 0.24 mm s^{-1} for hemozoin (*P. falciparum*) and 0.20 mm s^{-1} for synthetic hemozoin at 78 K.^{51,52} Bohle characterized synthetic hemozoin at 4.2 K to have an isomer shift at 0.275 mm s^{-1} with a quadrupole splitting of 0.588 mm s^{-1} and a line width of 0.35 mm s^{-1} .⁴⁹ Such discrepancies were not resolved until the Egan lab (2002) reported identical spectra for both synthetic β -hematin and trophozoite isolated

hemozoin which had been lyophilized to avoid the strong attenuation of the signal by water (**Figure 1.11**).⁵³ Such results highlight the importance of temperature on electronic relaxation effects of iron containing species and the meticulous workup of biological samples in order to avoid background scatter.

Such discrepancies highlight the difficulties in the isolation and purification of native hemozoin, as well as the synthetic analog. *Plasmodium berghei* derived hemozoin used by the Yayon group is not known to produce significant quantities of hemozoin, so questions lie in the actual composition of the product analyzed. Nonetheless, tedious extractions and copious washes are necessitated to obtain

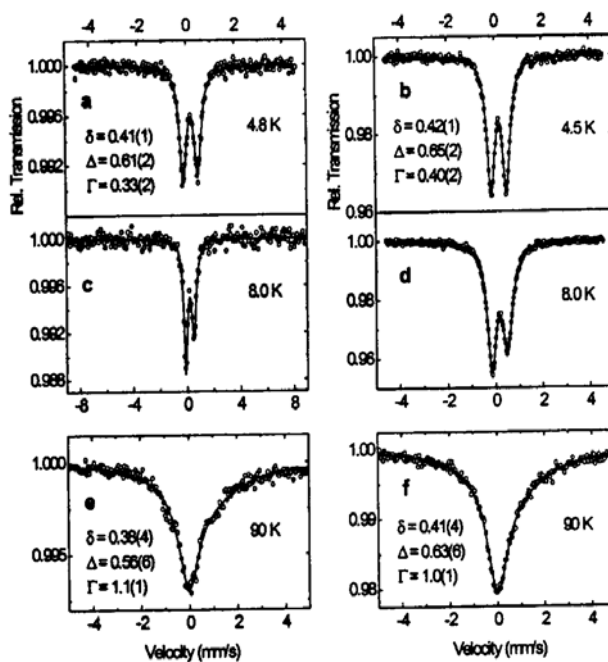


Figure 1.11. Mössbauer spectra of lyophilized trophozoites (a, c and e) and β -hematin (b, d and f). (δ), isomer shift, (Δ), quadrupole splitting, (Γ), linewidth, all in mm s^{-1} . Reproduced from reference 53.

reproducible results. The complete removal of protein components and free heme from hemozoin are invaluable in both qualitative and quantitative analyses. Characterizations should be carried out routinely to ensure that hemozoin is void of all contaminants.

Though hemozoin has long been both a marker for the diagnosis of malaria and an indicator of the parasitic life cycle, little is known about its chemical mechanism of formation. *In vivo* attempts to investigate hemozoin formation have not been successful and thus, most studies have been confined to synthetic β -hematin formation in either aqueous or non-aqueous reaction conditions.

1.4. Hypotheses Surrounding Hemozoin Formation

The formation of hemozoin *in vivo* has numerous proposed mechanisms reporting the process is either enzyme catalyzed,^{54,55} lipid catalyzed,⁵⁶⁻⁶⁰ histidine-rich protein initiated,⁶¹⁻⁶³ spontaneous,⁶⁴ or autocatalytic⁶⁵ (For the most recent reviews see Egan⁶⁶ and Sullivan.⁶⁷).

In 1992 Slater and Cerami first reported the formation of hemozoin as an enzyme catalyzed process,⁵⁴ which occurred upon overnight trophozoite incubation at 37°C with hematin in 500 mM sodium acetate buffer, pH 4.8. ¹⁴C labeled heme was used to detect *de novo* synthesized hemozoin from the quantity of hemozoin already present in the trophozoites extracted from the acetonitrile layer of cells. Uninfected red blood cells and macrophages failed to incorporate the radiolabeled heme in hemozoin formation, as did synthetic and native β -hematin.⁴⁶ Denatured hemoglobin and albumin, serving as controls, also tested negative for hemozoin formation.

Chloroquine and amodiaquin, two known antimalarials, inhibited the formation of hemozoin, with reported IC_{50} values (the effective concentration at 50% inhibition) of 120 μ M and 250 μ M respectively. Moreover, the authors uncovered the pH optimum for the formation of hemozoin was between the pH of 5.0 and 6.0, the approximate pH of the parasite's digestive vacuole. Pigment formation was greatly diminished above pH > 6.0, leading the authors to speculate that hemozoin would not assemble outside of the digestive vacuole because the carboxylate side chains of the heme moiety would then be protonated, not allowing the formation of the axial Fe-O propionate bond. Hemozoin formation also increased linearly over time and with increasing protein concentration, leading the authors to conclude a novel "heme polymerase" was responsible for the formation of the malaria pigment.

A short time thereafter Egan, mimicking the acidic conditions inside the digestive vacuole (pH = 5), demonstrated a spontaneous formation of hemozoin⁶⁴ from basic hematin acidified with glacial acetic acid (4.5 M acetate concentration) at nonphysiological temperatures. The synthetic product exhibited temperature and acetate concentration dependence, reporting complete hemozoin formation within 30 minutes at 60°C, within 2 hours at 37°C, and within 8 days at 6°C. UV-Vis spectroscopy studies showed that increasing the concentration of acetate buffer (0-6.0 M), solubilized increasing concentrations of hemin chloride, which supported their finding of increased reaction rates when the volume of acetate buffer was increased and the amount of hemin remained constant. Besides refuting an enzymatic mechanism of formation, the authors hypothesized that ionic strength (flux into and

out of a cell) could possibly play a role in the organization of malarial hemozoin, rationalizing that carboxylate groups from free amino acids and/or peptides resulting from hemoglobin proteolysis¹⁶ or an unidentified protein were able to provide an environment analogous to that supplied by the acetate buffer, aiding the nucleation of heme in the formation of hemozoin.

Controversies revolving around the exact mechanism of hemozoin formation were heightened during the next few years. Three years after the hypothesis of a “heme polymerase” was introduced, Dorn *et al.* assessed that hemozoin formation was an autocatalytic process,⁶⁵ uncovering that both denatured parasite lysates and synthetic β -hematin promoted the aggregation of hemozoin. Knowing Slater’s results were quantitated against quantities of hemozoin already existing in the trophozoites and that the insoluble extract promoted *de novo* pigment, Dorn proposed that the existing hemozoin could theoretically provide an interface capable of nucleating additional hemozoin. Additionally, Dorn reported active hemozoin formation under the same experimental conditions (140 μ M ¹⁴C labeled heme, overnight incubation at 37°C, 500 mM sodium acetate buffer, pH 4.8) when parasite lysates were boiled for 10 minutes at 100°C, denaturing any enzymes. When the parasite lysates were subjected to Percoll density-gradient fractionation, the vacuole fraction and hemozoin fraction supported the formation of ¹⁴C labeled hemozoin, while the fractionated trophozoite lysate and membrane layers failed to do so. Isolated hemozoin from the gradient fractionation was then treated with proteinase K, a chloroform-methanol mixture, and purified by SDS-PAGE analysis. This hemozoin, devoid of all proteins,

still produced radiolabeled pigment, leading the author to conclude that hemozoin formation could proceed by an autocatalytic process. Additionally, both chloroquine and mefloquine inhibited the formation of hemozoin from the cultured extract, as well as the synthetic analog. Although refuting the theory of enzymatic formation of hemozoin in favor of an autocatalytic mechanism, the authors did not refute the possibility of a protein providing the structural framework for the active site of hemozoin nucleation.

A few months later in a *Nature* correspondence, Cerami released new data involving the HPLC elution profiles of trophozoite extracted hemozoin.⁶⁸ The acetonitrile extract, which had no absorbance at 400 nm, the characteristic wavelength of the porphyrin ring structure, still supported hemozoin formation. Mass spectrometry of this fraction revealed methyl esters of oleic, palmitic, and stearic acids. The insoluble pigment formed in this extract displayed an HPLC elution profile similar to that of synthetic β -hematin. This fraction also contained significant amounts of organically bound phosphorous and was cleavable with phospholipase B, suggestive of a phospholipid-catalyzed mechanism of hemozoin formation. The author maintained that a novel “heme polymerase” could still exist, although one had not yet been isolated. Notably, Cerami acknowledged the crucial importance of determining the parasite’s biological mode of heme sequestration *in vivo* in order to resolve the underlying scientific discrepancies arising amongst the *in vitro* investigations.

Included in this same issue of *Nature* was a reply from the Dorn lab, which independently reported the possibility of a phospholipid mechanism of hemozoin formation.⁵⁶ Dorn now reported acetonitrile extracts from the trophozoite lysate could also provide the framework for hemozoin nucleation in the absence of any existing preformed pigment. More surprising was the fact that the acetonitrile extract from uninfected erythrocytes could also initiate hemozoin nucleation. Furthermore, besides extraction techniques, the lab noted the relative importance that pH could possibly play in the formation of hemozoin since that under aqueous conditions of sodium acetate buffer, pH 4.8, 50% of the propionic acid side chains of the heme moiety are deprotonated, the necessary chemical constraint needed for the structural formation of hemozoin via the Fe-O propionate linkage.

One year later Amit V. Pandey and Babu L. Tekwani discredited the Egan hypothesis that the formation of hemozoin was a spontaneous process,⁶⁴ citing the authors failed to purify the collected hematin product.⁶⁹ Egan clearly cited problems with centrifugations and the adsorption of heme onto the cellulose acetate filters, nonetheless, he only washed the samples with H₂O, which failed to remove any free heme based upon the differential solubilities of the species. A necessitated wash with sodium bicarbonate (pH=9.1) was required but omitted. While the IR analyses of the samples exhibited the characteristic stretching frequencies associated with hemozoin, the product in all likelihood was a mixture of both hemozoin and hematin. Replication of the experiment by Pandey's group demonstrated the product described by Egan *et al.* was readily soluble in bicarbonate buffer, as well as sodium dodecyl

sulfate (SDS). Further analyses by TLC showed a product migration similar to that of soluble hemozoin. Longer incubations at higher temperatures formed a product that was insoluble in sodium bicarbonate, but the authors argued the experimental conditions were no longer physiological (high acetate concentration, 80°C, 12 hours). They also uncovered that under the employed experimental conditions (37°C, 6 hours), hemozoin only formed at acetate buffer concentrations of 1.0 M or higher. In order to further probe the heme-acetate interactions first suggested by Egan, the group used ¹⁴C-labeled acetate to examine the possibility of a carboxylate-iron linkage between hemozoin and acetate. Their studies illustrated distinct binding between heme and the radiolabeled acetate, suggesting a heme-acetate adduct (complex) as a plausible intermediate in the production of hemozoin under these conditions.

Shortly thereafter, the heme-acetate theory of complexation in the formation of hemozoin was scrutinized. Foremost, Pandey and Tekwani themselves demonstrated that hemozoin (based on the characteristic IR frequencies) could form in 1 M phosphoric acid.⁶⁹ Additionally, Riscoe's group demonstrated hemozoin formation in 0.2 M phosphate buffer, pH 5.2, when examining xanthenes as possible antimalarials.⁷⁰ Comparisons were made again amongst the various methods employed to synthesize the malaria pigment. Elemental analyses showed that hemozoin, malaria hemozoin, and synthetic β-hemozoin formed in various buffers, pH 5.2 (0.02 M phosphate buffer, 0.02 M acetate buffer, and 4 M acetate buffer) agreed reasonably well in composition, however the differential solubilities of the products in methanol, ethanol, 2.5 % SDS, DMSO, and an acetic acid:water:methanol mixture

(1.5:0.5:8) varied. Reactions in 4 M acetate yielded a precipitate that was soluble in all solvents, displaying solvation properties similar to hematin. Hemozoin derived from the 0.02 M phosphate buffer was insoluble in all of the examined solvents, exhibiting solubility properties like the native malaria pigment. Reactions incubated in the lower ionic strength acetate buffer synthesized a solid product that was partially soluble in the alcoholic and acetic acid solvents, but insoluble in 2.5% SDS and DMSO. A pH profile for hemozoin formation in phosphate buffer demonstrated the rate of hemozoin formation above pH 6 was drastically reduced, comparing well to the pH profile compiled for reactions run in acetate buffer.

A more substantial argument was made by Egan when he further criticized the hypothesis of a heme-acetate complex in the formation of hemozoin suggested by Pandey and Tekwani with a few simple solubility tests.⁷¹ Hematin, which has heightened solubility in increased acetate concentrations, did not form hemozoin in 11.4 M acetate under the prescribed reaction conditions, but did precipitate a material when the buffer was diluted to 4.5 M. The IR of this material failed to show any similarities with that of β -hematin. If the heme-acetate postulate were valid, then increasing the ionic strength of the buffer should have facilitated the reaction to proceed more quickly. Additionally, since the solubility of hematin increased as the concentration of acetate buffer increased, the reaction yield should have also been amplified.

By this time native and synthetic hemozoin were considered to be structurally identical, being synthesized *in vitro* either under non-physiological conditions or in

seeded reactions, but no enzyme to date had been isolated nor delineated the structural focus for the formation of hemozoin. In 1996, Goldberg and coworkers added yet another theory to the mechanics of the formation of hemozoin. Using monoclonal antibodies to investigate the proteins of the digestive vacuole of *P. falciparum*, they identified a class of histidine-rich proteins (HRP's) that mediated the formation of hemozoin.⁶¹

The sequence of HRP II is comprised of 76% alanine and histidine (M_r 27 kD), possessing 51 repeats of an Ala-His-His repeat motif (**Figure 1.12**),⁷² a sequence closely resembling the Gly-His-His-Pro-His-Gly heme binding domain in the human histidine-rich glycoprotein (HRG).⁷³ Specifically, each molecule of HRP bound approximately 17 equivalents of heme in 100 mM acetate buffer, pH 4.8. Moreover, the recombinant protein mediated the formation of hemozoin while concurrently other proteins and homo- and polypeptides such as bovine serum albumin (BSA), lysozyme, polylysine, and polyasparagine failed to generate the

```
MVSFSKNKVL SAAVFASVLLLDNNNSAFNNNLCSKN
AKGLNLNKRL LHETQAHVDDAHHAHHVADAHHAH
HAHHAADAHHAHHAADAHHAHHAADAHHAHHA
DAHHAHHAADAHHAHHAADAHHAHHAADAHHAH
HAADAHHAHHAADAHHAHHAAYAHHAHHASDAH
HAADAHHAAYAHHAHHAADAHHAADAHHAAYAH
HAHHAADAHHAADAHHATDAHHAHHAADAHHAT
DAHHAADAHHAADAHHATDAHHAADAHHATDAH
HAADAHHAADAHHATDSHHAHHAADAHHAAAH
ATDAHHAAAHHAADAHHAAAHHEAATHCLRH
```

Figure 1.12. The sequence of histidine-rich protein II (HRP II) isolated from *Plasmodium falciparum*.

insoluble malarial pigment. Human HRG also failed to promote the *in vivo* aggregation of hemozoin, suggesting the binding domains of the two sequentially related proteins have diverse functions.

HRP II mediated hemozoin also increased in amount with increasing reaction time, protein concentration and hemin concentration, forming at optimal rates within the pH range of 4.0-6.0. The nature of the buffer failed to affect the rate of reaction, though again the authors noted a increased production of the biomineral with increasing ionic strength. HRP III, of which 56% of the protein is comprised of alanine and histidine residues, (28 Ala-His-His repeats, M_r 27 kD) also mediated the formation of hemozoin. HRP IV,⁷⁴ a 10 kD genetic clone lacking HRP II and HRP III (31% histidine), reacted positively with the HRP II monoclonal antibody, but heme polymerization assays were not completed. These findings, along with the fact that preformed hemozoin promoted additional malaria pigment in *in vitro* assays, weakened the theory of an enzyme catalyzed mechanism of formation.

When ³H labeled chloroquine and quinidine antimalarials were incubated with HRP II in the presence of heme (100 mM sodium acetate buffer, pH 4.8), the hemozoin formed exhibited considerable radioactivity.⁶² Incubation of HRP alone with labeled drugs failed to record any counts per minute (cpm). Conversely, purified hemozoin without heme substrate did not accumulate the radiolabel, implicating a drug-heme complex in the mode of hemozoin inhibition rather than the direct binding of the antimalarial to hemozoin. Moreover, this suggested the degradation of hemoglobin and sequestration of heme into hemozoin as independent processes, both

as viable targets for antimalarial strategies. As a caveat, the binding of the drug to proteolyzed heme may not be indicative of the associative inhibition of the hemozoin formation,⁶³ since drugs with strong heme binding affinities do not have a direct correlation with the potency of the antimalarial. Blockade of either process would ultimately result in parasite death. In retrospect, if the HRP's served as a three dimensional template for the nucleation of hemozoin, the disruption of protein interactions could produce novel antimalarials. Others began acknowledging the possibility of a recognizable nucleation site for the formation of hemozoin, dismissing the classical hypothesis of enzymatic processing.⁷⁵⁻⁷⁷

From the structural information elucidated from the sequence of HRP II, Pandey and Chauhan postulated a pH mechanism of hemozoin formation.⁷⁸ Though numerous experimental conditions effected the formation of hemozoin *in vitro*, the pH of the digestive vacuole was critical for *in vivo* formation; for at this critical pH one-half of the propionate groups of the heme moiety are deprotonated, facilitating the binding of the propionate group of one side chain to the central iron core of another. Heme binding to the HRPs spatially orients two heme molecules into a preferred conformation for this iron-carboxylate bond formation. The repetitive binding sequence of Ala-His-His-Ala-Ala-Asp, prepared as a linear hexapeptide, did not promote the nucleation of hemozoin.

The hypothesis involving a lipid mediated formation of hemozoin resurrected in 1999 in two separate articles from Fitch and Tekwani. Fitch, previously knowing the acetonitrile extract from infected red blood cells promoted the formation of

hemozoin^{68,65} and this extract also yielded the methyl esters of unsaturated fatty acids,⁶⁸ found that lipids from both infected and uninfected erythrocytes promoted the formation of hemozoin. After the lipids in the extract were hydrolyzed, his group also detected the presence of fatty acids via gas chromatography/mass spectrometry. Based on this observation, he then found arachidonic, linoleic, oleic, and palmitic acids, and the mono and di-oleoylglycerol, as standards, also promoted the formation of hemozoin. This production of β -hematin exhibited the same dependency on pH, temperature and acetate concentration that previous studies on the formation of hemozoin recorded, but in addition, the concentration of the lipids and the nature of detergents also displayed a profound effect on hemozoin nucleation.

In 2001, though Pandey *et al.* did not study the mechanism of hemozoin formation, support for the histidine-rich protein mediated formation of hemozoin was supplanted in an attempt to elucidate the mechanism of chloroquine inhibition.⁷⁹ Besides confirming that native HRP II bound approximately 18 equivalents of heme, PAGE analysis stained with Coomassie Brilliant Blue revealed a heme:peptide complex discernable from the native protein. Incubation with chloroquine coincided with the disappearance of the diaminobenzidine (DAB, a heme peroxidase) staining, demonstrating at least, the disruption of the heme:protein complex.

In 2002 Tekwani *et al.* appended the lipid postulated formation of hemozoin to proceed by a free radical mechanism of formation.⁶⁰ Since malaria patients were known to have reduced levels of antioxidants in the blood, he predicted that since antioxidant levels were at a diminished capacity no longer available to prevent the

oxidation of lipids, once oxidized, the unsaturated lipids promoted hemozoin formation via a free radical chain reaction. This hypothesis was initially supported by the fact Orjih had concluded that both uninfected and infected cells upon treatment with NaOH, HCl, or CH₃COOH formed hemozoin.⁸⁰ Antioxidants and reducing agents tested positive for β-hematin inhibition, including glutathione, sodium dithionite, β-mercaptoethanol, ascorbic acid, superoxide dismutase, and dithiothreitol, as well as p-aminophenol, a compound known to terminate free radical reactions. This however, suggests the parasite must first ascertain control over host metabolism in order to manage its metabolic catabolism of hemoglobin and the subsequent formation of hemozoin.

Though both the lipid mediated formation of hemozoin and HRP nucleation remain valid hypotheses for the assembly of this biomineral, a direct comparison of the two proposals has yet to be studied. Which mechanism most efficiently processes hemozoin? Here the rate of formation remains a critical, yet still unanswered question. Which process would involve the least expenditure of energy on part of the parasite in order for it to obtain its requisite amino acids in the relatively short amount of time it spends in the trophic stage? Moreover, why doesn't the parasite choose a physiochemical mechanism that is unique to the organism? If lipids from uninfected cells and chemically processed standards still promote the formation of hemozoin, why is β-hematin compartmentalized in only a few organisms?

All in all, these scientific discrepancies in the underlying chemical mechanisms of hemozoin formation are exacerbated by the arguments as to the

structural characterization of the compound itself. Despite the dismissal of hemozoin as a hemoprotein, until quite recently, garnering advances in spectroscopic characterizations, hemozoin was referred to as a “heme polymer” and the formation process was coined a polymerization mechanism. Subsequently, at one point in time the malaria pigment and its synthetic analog were coined the different names of hemozoin and β -hematin, respectively.

In 1998, Dorn *et al.* compiled a review of the methods of hemozoin formation at physiological temperature (37°C), not so as to assess the methods of isolation and purification, but to clarify differing inhibition values.⁵⁷ Chloroquine was a consistent inhibitor in the ability to disrupt the formation of hemozoin, but the IC₅₀ values varied significantly as based upon the research group’s methodologies of native hemozoin isolation. Assessing the inhibitory effects of various antimalarials in 500 mM sodium acetate buffer, pH 4.8, the results demonstrated the hemozoin isolated from trophozoite lysates tended to have much higher IC₅₀ values than those obtained from an acetonitrile trophozoite lysate or digestive vacuole extract. More relevant however, was the finding that chemically synthesized hemozoin had inhibitory effects similar to the hemozoin obtained from the digestive vacuole. This first supported the idea that chemically synthesized hemozoin may be the optimum method for synthesizing large amounts of the pigment for evaluation in *in vitro* assays.

Later Bohle *et al.* unequivocally characterized native hemozoin and synthetic β -hematin as being of the same chemical composition through synchrotron x-ray diffraction studies.²⁹ This same group then provided evidence of reciprocating heme

dimers for the structure of hemozoin,³⁰ coining the more appropriate terminology of “heme aggregate” or biomineral. Later these authors suggested that although β -hematin is chemically and structurally similar to the malaria pigment, consideration must also be given to its morphological form when assessing the mechanism of formation of hemozoin and its reactivity *in vivo*.⁸¹ Different synthetic preparations of the malaria pigment produced an assortment of crystal sizes, each with dissimilar reactive faces. Others supported the novel term of “biocrystallite,”⁸² only adding to the complexity of the history of this unique heme compound.

Classically nucleation and crystal growth involves a supersaturated solution. No direct evidence exists that once hemoglobin is catabolized by the parasite, that free heme accumulates in any appreciable concentration. Furthermore, the oxidative damage that can result from one molecule of heme could have a cascade of detrimental effects on the very sustenance of the parasite. The parasite needs to prevent any toxic and deleterious effects of heme as efficiently as possible. With the above arguments and the fact that biocrystallization rarely involves a detoxification pathway or excretory mechanism, we chose to classify hemozoin as a biomineral.

1.5. Chemical Synthesis of Hemozoin

Due to the tedious extraction and isolation of hemozoin from trophozoites, many research groups sought chemical means by which to synthesize larger quantities of the pigment. Beyond the first synthesis by Hamsik, hemozoin can be formulated either in aqueous solution with hematin and acetic acid,^{46,64,83,65,84-86} or via an organic synthesis involving the dehydrohalogenation of hemin with 2,6-lutidine.

Since Slater *et al.* first characterized that both native and chemically prepared hemozoin were spectroscopically the same compound,⁴⁶ their preparation of β -hematin is one of the most frequently referenced preparations. Their formulation involves dissolving 60 μ moles of hematin in 8 mL of 0.1 M NaOH followed by the subsequent precipitation of the porphyrin with 49 mmol of acetic acid (or benzoic, propionic, or succinic acid substitution). The suspension is heated overnight at 70°C. The initial precipitate is then washed four times with water, followed by two 3 hour washes with 0.1 M sodium bicarbonate buffer, pH 9.1, to remove any free heme. The remaining insoluble material is washed an additional four times with water, lyophilized, and dried over P₂O₅, reporting yields of 40-50%.

Egan later modified this method,⁶⁴ demonstrating that hemozoin could be formed under less corrosive reaction conditions. He dissolved 23 μ moles of hemin in 3.0 mL of 0.1 M NaOH in a 60°C temperature controlled cell and then added dilute HCl (0.30 mL, 1.0 M) and acetate (1.74 mL, 12.0 M), incubating the solution for thirty minutes (or at various other times), before quenching the reaction mixture on ice for five minutes. The solution was then filtered over an 8 μ m cellulose acetate/nitrate filter and washed with copious amount of water. This method not only produced hemozoin, but also suggested its formation to be a time dependent process, as evidenced by the increase in the C=O and C-O stretching frequencies in the recorded IR spectra. Consequently, the authors failed to dissolve any residual hematin with a sodium bicarbonate wash, so the results obtained as to the reactivity and inhibition of hemozoin were skewed. Nonetheless, this synthesis formed

hemozoin under milder conditions than those employed by Slater (60°C vs. 70°C, 30 min vs. 16 hours, 4.5 M sodium acetate buffer vs. concentrated acid).

In 1995 while examining the formation of hemozoin, Blauer and Akkawi termed B-hematin,^{83,85} an insoluble form of ferriprotoporphyrin IX isolated as an intermediate in the production of hemozoin. Herein, the product was formed by incubating hemin in 0.4 N NaOH with acetic acid under magnetic stirring. The mixture was quenched on ice, centrifuged, and the precipitate transferred onto a filter. The solid was washed profusely with water and then with DMSO until the filtrate ran clear. The material was rewashed with water and then ethanol and dried under vacuum until all residual water was removed. The authors noted that at reaction temperatures of 70°C, the IR spectra were similar to β -hematin prepared via the method of Slater *et al.*,⁴⁶ with strong absorption bands at 1663 and 1209 cm^{-1} . Samples however prepared at lower temperatures and with lower concentrations of acetic acid had additional broad absorption bands at 1647 and 1020 cm^{-1} , which deviated from the IR frequencies of hemin chloride as well, which are centered near 1715 and 1620 cm^{-1} . These novel absorption bands and the products' slight difference in solubility in acidic medium led the authors to speculate that "B-hematin" was an isolated intermediate in the chemical transformation of hemin chloride into β -hematin. Though additional spectroscopic evidence was lacking, the authors suggested the differences in the IR spectra were a result of the differing coordination environments between the intermediate and final hemozoin product.

When investigating the rates of formation of B-hematin,⁸⁵ the overall yields of the reactions were dependent upon the pH of the solution (maximum yields were obtained between pH 4-5) and the reaction times. Yields also varied according to the type of acid used, but all acids promoted the formation of B-hematin, so long as the solution remained acidic during the course of the reaction. The relative yields also increased with decreasing concentrations of ferriprotoporphyrin IX. Coincidentally, the antimalarial chloroquine inhibited the formation of the B-hematin intermediate as effectively as it suppressed the formation of hemozoin. These kinetic investigations pioneered the relationship between the rate of hemozoin formation and reaction conditions (e.g. pH, time, concentration, ionic strength etc.).

Egan's preparation of hemozoin⁶⁴ was later adopted by Basilico with modifications for β -hematin synthesis in a 96-well plate.⁸⁶ This protocol was used in the rapid screening for antimalarial drug inhibition based on previous work showing that both hematoporphyrin and protoporphyrin IX inhibited malaria pigment formation through cofacial π - π stacking interactions between the drug and hematin.⁸⁴ This microtiter plate assay was also used by Dorn to analyze the various methods of hemozoin production (trophozoite lysate, acetonitrile extract from the trophozoite lysate, digestive vacuole lysate, hemozoin isolated from the malaria parasite, and synthetic β -hematin).⁵⁷

Basilico again used this assay when examining the consequential effects of the initial porphyrin on inhibition assays. Hemozoin inhibition assays performed with hematin in sodium hydroxide (heme polymerization inhibitory activity, HPIA) and

alternatively with hemin chloride in DMSO (β -hemin inhibitory activity, BHIA) both demonstrated a pH dependence of drug effectiveness on hemozoin inhibition.⁸⁷ The antimalarials probed demonstrated optimal effectiveness in acetate buffer around pH 5.1, the approximate pH of the digestive vacuole. Interestingly, the effect was less pronounced when hemin chloride was the chosen initial porphyrin rather than hematin. Along with this, the inhibitory effects of the salts were nearly reversed for hematin and hemin chloride. This highlighted the importance in experimental design in assay protocols, since differences in the homogeneity of the two compounds in solution may account for such discrepancies. Hematin, when in sodium hydroxide exists mainly as μ -oxo dimers and displays a decreased solubility with decreasing pH levels so inhibitory effects may be weakened merely because less monomeric porphyrin is in solution. When the iron porphyrin is dissolved in DMSO, the solvent disrupts the formation of the μ -oxo dimers, thus no interference in drug:heme interactions occurs because of reduced solubility. The BHIA mainly adjusts the microenvironment of the porphyrin facilitating π - π stacking interactions between the antimalarial and hemozoin. If a drug interacts via a different mechanism, the results may be biased based upon the interactions between the drug and heme, the drug and hemozoin, or the possibility of a drug:heme complex interacting with hemozoin.

In 1999 Egan revalidated his acetate buffered preparation of hemozoin,⁶⁴ providing additional supporting spectroscopic evidence.⁷¹ In addition to elemental analysis and IR spectroscopy, x-ray powder diffraction and scanning electron microscopy identified the hemozoin samples. The XRD patterns for both the author's

preparation of hemozoin and Slater's preparation from trophozoites matched well with Bohle's chemical dehydrohalogenation of hemin (see below) analyzed using high resolution synchrotron radiation. Microscopy samples revealed the synthetic hemozoin to be slightly smaller than the scans obtained from two different *P. falciparum* strains, but the overall morphological features were comparable. The authors suggested that hemozoin solubility could be affected by particle size and the water content of the sample.

In 2000 Blauer and Akkawi published another article suggesting the formation of synthetic β -hematin only formed upon prolonged drying of the reaction products.⁸⁸ Following the hemozoin preparation by Egan,⁷¹ the authors recorded the IR spectrum of the insoluble pigment washed only with water, but it failed to display the iron carboxylate peaks characteristic of hemozoin. When however, this product was washed with DMSO, the insoluble product, now in a significantly lower yield, resembled the IR spectra of the earlier B-hematin, again isolating the "intermediate" involved in the formation of hemozoin. A spectrum matching that of the malaria pigment was only obtained after the precipitate collected from Egan's protocol was kept wet for an additional 2 hours at 70°C and then washed with DMSO until the filtrate was faintly colored. A control where the sample was not heated for the additional amount of time produced "B-hematin." The authors suggested that under these reaction conditions that pure crystalline β -hematin only formed upon a structural reorganization of the substance, which occurred during the drying process. A revised the protocol for synthesizing hemozoin to ensure product formation

included dissolving hemin in aqueous sodium hydroxide, followed by the addition of diluted acetic acid (final concentration 5.9 M) at 37°C with constant stirring for 2 hours. The reaction is then cooled in water, centrifuged, and the precipitate collected onto a filter. The insoluble substance is then washed with copious amounts of water and DMSO, followed by additional washes of water and ethanol, before drying the product *in vacuo* at room temperature.

The debates on the mechanics of hemozoin formation continued beyond the year 2000. Little research was completed on the kinetics of formation or the conditions affecting its formation. Egan first compiled such information for hemozoin prepared from acetate in a 2001 *Biochemistry* article,⁸⁹ examining the effects of reaction conditions including temperature, pH, acetate concentration, stirring and seeding on the rate of hemozoin formation. By monitoring the increase in IR frequency at 1210 cm⁻¹ at various reaction times, while maintaining a constant acetate concentration (4.5 M), pH (pH = 4.5), and temperature (60°C), the rate of hemozoin formation under the prescribed conditions followed a sigmoidal kinetic profile with an approximate induction period of 15 minutes. Magnetic stirring increased the reaction rate significantly. The authors found that decreasing the reaction temperature decreased the rate of formation and resulted in a longer induction phase, as did lowering the concentration of the acetate buffer (pH 4.5, 60°C). The pH dependency exhibited maximal formation at pH 3.5, with the rate diminishing significantly above the pH of 5.0. Seeding the reactions with either 10%

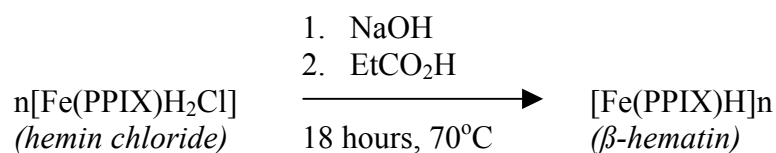
or 50% of preformed hemozoin at both 4.5 and 8.5 M acetate buffer had no effect on the rate of formation.

Similar effects were observed when monitoring the reaction via XRD. The peak for hematin disappeared over time giving rise to the hemozoin peak, which has 20 peaks that are different from the starting material. In parallel, the recorded XRD of a wet sample of hemozoin displayed the same diffraction pattern as the dried product; dispelling the hypothesis that hemozoin chemically synthesized from acetate was reorganized into its crystalline form during the drying process (IR data sampled in Nujol mulls compared comparably as well.). SEM data collected at differing reaction times failed to be quantitative, but provided supportive insight into the mechanism of hemozoin formation. Spectroscopic evidence previously supplied by Bohle *et al.* demonstrated that hemozoin is a dimer of reciprocal iron-propionate linkages with strong evidence of hydrogen bonding between the other unionized heme propionates.^{29,30} The SEM data collected by Egan illustrated a surface growth phenomenon whereby a nearly amorphous starting material transformed into small crystallites, indicative of possibly a nucleation and growth phase. This invalidates the old notion that hemozoin is comprised of polymeric units and is formed under the mechanics of a polymerization mechanism.

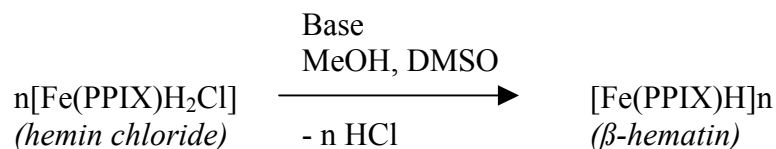
Egan's review of hemozoin formation in acetate solution and the effects of the reaction conditions thereto, collectively summarize the enormous amount of scientific discrepancies seen throughout the literature. Subtle changes in the reaction conditions have a profound effect on the rate of synthesis and on the formation of the hemozoin

itself. A alcohol-water medium presented by Blauer and Akkawi was also shown to increase the rate of formation of hemozoin, with a maximal yield of β -hematin achieved in 40% ethanol,⁹⁰ but the authors weaken a solvation theory by not focusing on the solubility issues surrounding hemin, but instead insist that β -hematin can be isolated as an intermediate in the formation of hemozoin.

In contrast to the acetate preparation of hemozoin, Bohle *et al.* pioneered the preparation of hemozoin via the dehydrohalogenation of hemin.⁹¹ This reaction requires relatively mild conditions (room temperature) and produces high yields (>90%) compared to the approximately 50-80% yields recorded from the acetate preparations (**Equations 1.1 and 1.2**). The chemical synthesis, which is carried out in an inert atmosphere, involves suspending hemin (0.489 g., 0.75 mMol) in 70 mL of dry methanol and then treating the suspension with excess dry 2,6-lutidine (0.5 mL, 4.3 mMol). The solution is then stirred in the dark for 18 hours before centrifuging the product at 300 rpm for 10 minutes. After decanting the supernatant, the black solid is resuspended, centrifuged, and washed 5 times with 50 mL of methanol and



Equation 1.1 Aqueous acid-catalyzed method of hemozoin formation.



Equation 1.2 Anhydrous non-coordinating base method.

then 4 times with 50 mL of deionized water or until the filtrate is colorless. The solid is then subjected to a three hour wash in 0.1 M sodium bicarbonate, before centrifuging and decanting again, repeating the cycle until the filtrate is colorless. A final water wash is incorporated before drying the product over phosphorous pentoxide *in vacuo*.

The anhydrous and anaerobic conditions of the reaction play a crucial role in the overall yield of hemozoin, for experiments completed without dry solvents or on the benchtop decreased the overall yield of hemozoin and noticeably increased the amount of material soluble in the sodium bicarbonate wash. Additionally, the use of 2,6-lutidine as the base in the reaction is thought to increase product formation, since this compound has a lower affinity for transition metals due sterics encountered from the *ortho*-substituted methyl groups. In contrast, the hydroxide ion used in the aqueous preparation of hemozoin could lead to the formation of an iron oxo-bridged dimer, accounting for lower yields of the insoluble β -hematin.

1.6. Hemozoin Quantification

Numerous attempts have been made to quantitatively assess the conversion of free hematin into the insoluble crystalline biomineral hemozoin either by microscopy or spectrophotometry. Such attempts have provided merely qualitative assessments and such results are discussed hereto. More sensitive methods are being developed, but major obstacles involve the insoluble nature of the hemozoin crystal and the fact that once hemozoin is in solution it is spectroscopically indistinguishable from ferriprotoporphyrin IX.⁷⁷

1.6.1. Direct spectroscopic measurement of heme

1.6.1a. UV-Vis Spectroscopy

The heme moiety from hemozoin absorbs from 388-400 nm depending on the substance used to dissolve the pigment. Quantitation based solely on this methodology requires the sample to be relatively pure and free of all unreacted heme before analysis since extraneous hematin also absorbs at this wavelength. Purification based on differential solubilities is not only tedious and time-consuming, but also does not guarantee that any appreciable hemozoin mass is not lost. This method however, remains the primary means by which to analyze hemozoin formation.

1.6.1b. IR Spectroscopy

Attempts to quantitate the formation of hemozoin through infrared analysis have been achieved with limited successes. Monitoring the growth in intensity of the carboxylate stretching frequencies is only as quantitative as the reaction itself. The rate of reaction *in vitro* is already known to be affected by pH, temperature, acetate concentration etc., thus why should one assume that aliquots removed from the same sampled reaction over time will not have an effect the formation of hemozoin afterwards? Even samples prepared simultaneously for individual analysis have discrepancies in the absolute peak intensities.

1.6.1c. HPLC Analysis

Many have attempted to quantitate hemozoin production based on the differential solubility of hematin and this biomineral using high-performance liquid

chromatographic (HPLC) methods. One such group⁹² used 4.6 x 75 mm TSK phenyl-5PW normal and reversed phase columns (Supleco, Bellefonte, PA), injecting a quenched assay for hemozoin formation in water directly onto the HPLC system. An initial buffer of 10 mM tetramethylammonium chloride/10 mM heptane sulfonate/40% acetonitrile/60% water/H₃PO₄ at pH 2.5 ran at 1.0 mL/min for 20 minutes eluted the free heme (400 nm), while retaining the hemozoin. The hemozoin was then eluted by adjusting the gradient to 10 mM tetramethylammonium chloride/10 mM heptane sulfonate/40% acetonitrile/60% water/NaOH, pH 12.0. Assays with ¹⁴C hemin demonstrated relatively little mass was lost based on scintillation counts of the recovered fractions. When injecting free heme, the retention times were comparable to the heme elution profile of the reaction mixture. Fault within this methodology relies on the fact that all of the free heme may not be disassociated from the hemozoin when in the first buffer system. Copious washes with sodium bicarbonate, pH 9, or 2% SDS is necessitated in order to remove any free heme associated with the hemozoin. Moreover, does the environment of the HPLC system supply an amenable replacement for the profuse washes? If the separation by the pH gradient fails to remove all associated free heme, then quantitation of the solubilized hemozoin at higher pH is not verifiable.

1.6.1d. Mössbauer Spectroscopy

Egan and coworkers employed Mössbauer spectroscopy in a somewhat novel application to probe the kinetics of hemozoin formation.⁵² Following a standard acetate preparation of hemozoin (4.5 M acetate buffer, pH 4.3, 60°C) the group

monitored the formation of hemozoin, determining the reaction to be zero-order with both seeded and unseeded reactions. Zero-order kinetics were also observed in 3 M and 6 M acetate. The unique concept in their analysis via Mössbauer (78 K) is that hemozoin purification is not necessitated since hematin and β -hematin have differing isomer shifts. Six years later under carefully temperature controlled experiments, the group rescinded the notion that hematin and β -hematin were discernable by Mössbauer spectroscopy, reporting temperature dependent electronic relaxation effects for both β -hematin and hemozoin isolated from trophozoites.⁵³

1.6.2. Highlighted Difficulties

In retrospect, the identification of hemozoin as a marker for the progression of malaria is not that difficult, with the simplest diagnostics being the visible marker of hemozoin itself. Quantification is however, seemingly more problematic, with relatively few simplistic methods of analysis available, especially when assessing the pathogenesis of malaria in the field. Additionally, *in vitro* correlations may not adequately mimic the environment of the digestive vacuole, while the physical limitations of microscopy have not been withstanding in the *in vivo* attempts at hemozoin quantification.

1.7. Hemozoin Formation – A Promising Route towards Discovering New Antimalarials

Hemozoin formation is an aggregation process unique to the parasite, making its chemical route a potential target for drug therapies.^{75,78} Though the parasite proteolysis of hemoglobin and subsequent formation of hemozoin seem unlikely to be

controlled by enzymatic processes,⁷⁵ understanding the chemical mechanism of β -hematin formation is a prerequisite for understanding the process *in vivo*. Most researchers agree the formation of hemozoin within the parasite must have some nucleation site or template, which serves to initiate the growth of the non-toxic sequestered porphyrin. Until recently this concept was supported by the fact a concentration dependent precipitation of the heme seemed unlikely due to the fact not all of the heme is detoxified via this mechanism.⁹³⁻⁹⁵ Ginsburg *et al.* alternatively proposed glutathione degraded heme once it was transported into the parasite cytosol,^{93,95} while Loria argued a degradation mediated by hydrogen peroxide occurred inside the digestive vacuole.⁹⁴ Both glutathione and hydrogen peroxide are known to chemically decompose hemin, and the effects of these species on hemozoin are under intense investigation in our lab, as well as in others.⁹⁶ Egan *et al.* contradicted both authors reporting the fate of heme to be unequivocally incorporated into hemozoin.⁵³ Parasitized cells contained the same amount of hemoglobin as unparasitized cells, with the parasitized cells digesting up to 80% of the hemoglobin contained in the infected red blood cell, incorporating 95% of the degraded heme into hemozoin.

Given that hemozoin crystals are uniform in shape and size, *Plasmodium falciparum* must exert a great deal of control over its synthesis; hence it is termed a biomineralization process. Biology thus plays an active role in this chemical process. *In vitro*, the conversion of hematin into β -hematin can be promoted in several ways. The methods differ in reaction conditions, yet all methods unequivocally produce

β -hematin. Which pathway is biochemically more significant remains to be seen. This however, does not diminish the valuable information gained from probing such model systems. Drug screens however can be most effective once a more knowledgeable understanding of the process of hemozoin formation is achieved.

Despite lingering discrepancies amongst the route to hemozoin formation (i.e. whether hemozoin formation is promoted by phospholipids or proteins), several sites of potential interactions along this route are targets for new antimalarials. Iron chelators, such as deferoxamine, attempt to sequester iron before the parasite can utilize it in hemozoin formation. Several cysteine and aspartic acid protease inhibitors serve as antimalarials, inhibiting the initial steps in the breakdown of hemoglobin.

Though the formation of hemozoin *in vitro* can occur in the absence of any preformed hemozoin or added “initiators,” the detoxification of heme by the parasite must occur in a timely manner. *Plasmodium falciparum* evolves from the early ring stage through the trophozoite stage in a mere 24 hours therefore our conclusion is that within the parasitic digestive vacuole, hemozoin formation must be a mediated process. Given that to date, no lipid was isolated from the digestive vacuole, while in fact the histidine-rich protein, HRP II, had been localized within this organelle and been shown to promote the formation of hemozoin, we attempted to investigate the mechanistic role of the histidine-rich proteins in the nucleation of hemozoin. Though no discredit is given to a lipid driven mechanism of hemozoin formation, this route is likely improbable in the parasite. Lipids may very well provide a structural

framework in which hemozoin formation can be initiated, and commercial unsaturated fatty acids have nucleated hemozoin. While 80% of the lipids identified in the malaria parasite are unsaturated,⁹⁷ their precise role inside the digestive vacuole has yet to be determined. Could the lipids exact the same effect encountered in the acetate preparation of hemozoin and function merely as an agent increasing the solubility of hematin?⁶⁶ Hemozoin has been formed under aphysiological conditions with only hemin chloride and acetate buffer. Moreover, other compounds that merely bound heme (i.e. serum albumin and polyhistidine) did not nucleate the formation of hemozoin. So why wouldn't the malaria parasite chose a novel means by which to detoxify free heme? Why would an organism evolve a biomineralization scheme that wasn't unique to itself? How could the parasite genetically sustain its very existence over time if the chosen route to hemozoin synthesis shares commonalities with its host and vector? Why would the parasite synthesize such an extremely insoluble biomineral, and not protect its mode of formation? Genetic preservation and the localization of four histidine-rich proteins within digestive vacuole support the role of these species-specific proteins in the formation of hemozoin.

References

- [1] *World Malaria Report 2005*, Roll Back Malaria, World Health Organization, UNICEF: Geneva, **2005**.
- [2] Bremen, J. "The ears of the hippopotamus: manifestations, determinants, and estimates of the malaria burden." *Am. J. Trop. Med. Hyg.* **2001**, *64*, 1-11.
- [3] *What is malaria*, RBM Infosheet No. 1; World Health Organization: **2002**.
- [4] Anderson, J.; MacLean, M.; Davies, C. *Malaria Research: An Audit of International Activity*, Prism Report 7; The Wellcome Centre for Medical Sciences: London, **1997**.
- [5] Sachs, J.; Malaney, P. "The economic and social burden of malaria." *Nature* **2002**, *415*, 680-685.
- [6] *Report of the Commission on Macroeconomics and Health of the World Health Organization*, WHO: Geneva, **2002**.
- [7] *Economic costs of malaria*, RBM Infosheet No. 10; World Health Organization: **2002**.
- [8] Greenwood, B.; Mutabingwa, T. "Malaria in 2002." *Nature* **2002**, *415*, 670-672.
- [9] Trouiller, P.; Olliaro, P. L. "Drug development output from 1975 to 1996: what proportion for tropical diseases?" *Int. J. Infect. Dis.* **1998**, *3*, 61-63.
- [10] Childs, G. E.; Boudreau, E. F.; Wimonwattatee, T.; Pang, L.; Milhous, W. K. "In vivo and clinical correlates of mefloquine resistance of *Plasmodium falciparum* in eastern Thailand." *Am. J. Trop. Med. Hyg.* **1991**, *44*, 484-487.
- [11] Wellems, T. E. "Molecular genetics of drug resistance in *Plasmodium falciparum* malaria." *Parasitol. Today* **1991**, *7*, 110-112.
- [12] Brassuer, P.; Kouamouo, J.; Moyuo, R. S.; Druilhe, P. "Multidrug resistant malaria in Camaroom in 1987-1988." *Am. J. Trop. Med. Hyg.* **1992**, *46*, 8-14.
- [13] Foley, M.; Tilley, L. "Quinoline antimalarials: Mechanism of action and resistance." *Int. J. Parasitol.* **1997**, *27*, 231-240.
- [14] Meuentener, P.; Schlagenhauf, P.; Steffen, R. "Imported malaria (1985-95): trends and perspectives." *Bull. WHO* **1999**, *77*, 560-566.

- [15] Schlagenhauf, P.; Steffen, R.; Loutan, L. "Migrants as a major risk group for imported malaria in European countries." *J. Travel Med.* **2003**, *10*, 106-107.
- [16] Goldie, P.; Roth, E. F. J.; Oppenheim, J.; Vanderberg, J. P. "Biochemical characterization of *Plasmodium falciparum* hemozoin." *Am. J. Trop. Med. Hyg.* **1990**, *43*, 584-596.
- [17] Orjih, A. U.; Fitch, C. D. "Hemozoin production by *Plasmodium falciparum*: Variation with strain and exposure to chloroquine." *Biochim. Biophys. Acta* **1993**, *1157*, 270-274.
- [18] Goldberg, D. E.; Slater, A. F.; Cerami, A.; Henderson, G. B. "Hemoglobin degradation in the malaria parasite *Plasmodium falciparum*: An ordered process in a unique organelle." *Proc. Natl. Acad. Sci. U. S. A.* **1990**, *87*, 2931-2935.
- [19] Francis, S. E.; Sullivan, D. J., Jr.; Goldberg, D. E. "Hemoglobin metabolism in the malaria parasite *Plasmodium falciparum*." *Annu. Rev. Microbiol.* **1997**, *51*, 97-123.
- [20] Goldberg, D. E.; Slater, A. F.; Beavis, R.; Chait, B.; Cerami, A.; Henderson, G. B. "Hemoglobin degradation in the human malaria pathogen *Plasmodium falciparum*: A catabolic pathway initiated by a specific aspartic protease." *J. Exp. Med.* **1991**, *173*, 961-969.
- [21] Gluzman, I. Y.; Francis, S. E.; Oksman, A.; Smith, C. E.; Duffin, K. L.; Goldberg, D. E. "Order and specificity of the *Plasmodium falciparum* hemoglobin degradation pathway." *J. Clin. Invest.* **1994**, *93*, 1602-1608.
- [22] Tyas, L.; Moon, R. P.; Loetscher, H.; Dunn, B. M.; Kay, J.; Ridley, R. G.; Berry, C. "Plasmepsins I and II from the malarial parasite *Plasmodium falciparum*." *Adv. Exp. Med. Biol.* **1998**, *436*, 407-411.
- [23] Rosenthal, P. J.; McKerrow, J. H.; Aikawa, M.; Nagasawa, H.; Leech, J. H. "A malarial cysteine proteinase is necessary for hemoglobin degradation by *Plasmodium falciparum*." *J. Clin. Invest.* **1988**, *82*, 1560-1566.
- [24] Wyatt, D. M.; Berry, C. "Activity and inhibition of plasmepsin IV, a new aspartic proteinase from the malaria parasite, *Plasmodium falciparum*." *FEBS Lett.* **2002**, *513*, 159-162.

- [25] Berry, C.; Humphreys, M. J.; Matharu, P.; Granger, R.; Horrocks, P.; Moon, R. P.; Certa, U.; Ridley, R. G.; Bur, D.; Kay, J. "A distinct member of the aspartic proteinase gene family from the human malaria parasite *Plasmodium falciparum*." *FEBS Lett.* **1999**, *447*, 149-154.
- [26] Banerjee, R.; Liu, J.; Beatty, W.; Pelosof, L.; Klemba, M.; Goldberg Daniel, E. "Four plasmepsins are active in the *Plasmodium falciparum* food vacuole, including a protease with an active-site histidine." *Proc. Natl. Acad. Sci. U. S. A.* **2002**, *99*, 990-995.
- [27] Eggelson, K. K.; Goldberg, D. E. "Identification and characterization of falcilysin, a metallopeptidase involved in hemoglobin catabolism with the malaria parasite *Plasmodium falciparum*." *J. Biol. Chem.* **1999**, *274*, 32411-32417.
- [28] Kolakovich, K. A.; Gluzman, I. Y.; Duffin, K. L.; Goldberg, D. E. "Generation of hemoglobin peptides in the acidic digestive vacuole of *Plasmodium falciparum* implicates peptide transport in amino acid production." *Mol. Biochem. Parasitol.* **1997**, *87*, 123-135.
- [29] Pagola, S.; Stephens, P. W.; Bohle, D. S.; Kosar, A. D.; Madsen, S. K. "The structure of malaria pigment β -hematin." *Nature* **2000**, *404*, 307-310.
- [30] Bohle, D. S.; Kosar, A. D.; Madsen, S. K. "Propionic acid side chain hydrogen bonding in the malarial pigment β -hematin." *Biochem. Biophys. Res. Commun.* **2002**, *294*, 132-135.
- [31] Schwarzer, E.; Turrini, F.; Ulliers, D.; Giribaldi, G.; Ginsburg, H.; Arese, P. "Impairment of macrophage function after ingestion of *Plasmodium falciparum* infected erythrocytes or isolated malaria pigment." *J. Exp. Med.* **1992**, *176*, 1033-1041.
- [32] Prada, J.; Malinowski, J.; Muller, S.; Bienzle, U.; Kremsner, P. G. "Hemozoin differentially modulates the production of interleukin 6 and tumor necrosis factor in murine malaria." *Eur. Cytokine Netw.* **1995**, *6*, 109-112.
- [33] Hoffman, S., L.; Subramanian, G. M.; Collins, F. H.; Venter, J. C. "*Plasmodium*, human and *Anopheles* genomics and malaria." *Nature* **2002**, *415*, 702-709.
- [34] Richie, T. L.; Saul, A. "Progress and challenges for malaria vaccines." *Nature* **2002**, *415*, 694-701.

- [35] Long, C. A.; Hoffman, S. L. "Malaria - from infants to genomics to vaccines." *Science* **2002**, *297*, 345-347.
- [36] Wernsdorfer, W. H.; McGregor, I. *Malaria: Principles and Practice of Malariology*; Churchill-Livingstone: Edinburgh, 1988
- [37] Brown, W. H. "Malarial pigment (so called melanin): Its nature and mode of production." *J. Exp. Med.* **1911**, *13*, 290-299.
- [38] Sinton, J. A.; Ghosh, B. N. "Studies of malarial pigment (hemozoin). Part I. Investigation of the action of solvents on hemozoin and the spectroscopical appearances observed in the solutions." *Rec. Malar. Surv. India* **1934**, *IV*, 15-42.
- [39] Ghosh, B. N.; Sinton, J. A. "Studies of malaria pigment (haemozoin). Part II. The reactions of haemozoin to test for iron." *Rec. Malar. Surv. India* **1934**, *IV*, 44-59.
- [40] Ghosh, B. N.; Nath, M. C. "The chemical composition of malaria pigment (haemozoin)." *Rec. Malar. Surv. India* **1934**, *IV*, 321-325.
- [41] Hamsik, A. "Über additionsvermögen des hämatins." *Z. Physiol. Chem.* **1930**, *190*, 199-221.
- [42] Ashong, J. O.; Blench, I. P.; Warhurst, D. C. "The composition of hemozoin from *Plasmodium falciparum*." *Trans. R. Soc. Trop. Med. Hyg.* **1989**, *83*, 167-172.
- [43] Fitch, C. D.; Kanjanangulpan, P. "The state of ferriprotoporphyrin IX in malaria pigment." *J. Biol. Chem.* **1987**, *262*, 15552-15555.
- [44] Bligh, E. G.; Dyer, W. J. "A rapid method of total lipid extraction and purification." *Can. J. Biochem. Physiol.* **1959**, *37*, 911-917.
- [45] Schwarzer, E.; Turrini, F.; Arese, P. "A luminescence method for the quantitative determination of phagocytosis of erythrocytes, of malaria-parasitized erythrocytes and of malaria pigment." *Br. J. Haematol.* **1994**, *88*, 740-745.
- [46] Slater, A. F.; Swiggard, W. J.; Orton, B. R.; Flitter, W. D.; Goldberg Daniel, E.; Cerami, A.; B., H. G. "An iron-carboxylate bond links the heme units of malaria pigment." *Proc. Natl. Acad. Sci. U. S. A.* **1991**, *88*, 325-329.

- [47] Bohle, D. S.; Dinnebier, R. E.; Madsen, S. K.; Stephens, P. W. "Characterization of the products of the heme detoxification pathway in malarial late trophozoites by X-ray diffraction." *J. Biol. Chem.* **1997**, *272*, 713-716.
- [48] Cammack, R.; Patil, D. S.; Linstead, D. "EPR spectroscopic studies of haemoglobin breakdown in malarial parasite-infected erythrocytes." *J. Chem. Soc., Faraday Trans.* **1994**, *90*, 3409-3410.
- [49] Bohle, D. S.; Debrunner, P.; Jordan, P. A.; Madsen, S. K.; Schulz, C. E. "Aggregated heme detoxification byproducts in malarial trophozoites: β -hematin and malaria pigment have a single $S=5/2$ iron environment in the bulk phase as determined by EPR and magnetic Mössbauer spectroscopy." *J. Am. Chem. Soc.* **1998**, *120*, 8255-8256.
- [50] Yayon, A.; Bauminger, E. R.; Ofer, S.; Ginsburg, H. "The malarial pigment of rat infected erythrocytes and its interaction with chloroquine: A Mossbauer effect study." *J. Biol. Chem.* **1984**, *259*, 8163-8167.
- [51] Adams, P. A.; Berman, P. A. M.; Egan, T. J.; Marsh, P. J.; Silver, J. "The iron environment in heme and heme-antimalarial complexes of pharmacological interest." *J. Inorg. Biochem.* **1996**, *63*, 69-77.
- [52] Adams, P. A.; Egans, T. J.; Ross, D. C.; Silver, J.; Marsh, P. J. "The chemical mechanism of β -hematin formation studied by Mössbauer spectroscopy." *Biochem. J.* **1996**, *318*, 25-27.
- [53] Egan, T. J.; Combrinck, J. M.; Egan, J.; Hearne, G. R.; Marquess, H. M.; Ntenteni, S.; Sewell, B. T.; Smith, P. J.; Taylor, D.; van Schalkwyk, D. A.; Walden, J. C. "Fate of haem iron in the malaria parasite *Plasmodium falciparum*." *Biochem. J.* **2002**, *365*, 343-347.
- [54] Slater, A. F.; Cerami, A. "Inhibition by chloroquine of a novel haem polymerase enzyme activity in malaria trophozoites." *Nature* **1992**, *355*, 167-169.
- [55] Slater, A. F. "Chloroquine: Mechanism of drug action and resistance in *Plasmodium falciparum*." *Pharmacol. Ther.* **1993**, *57*, 203-235.
- [56] Ridley, R. G.; Dorn, A.; Matile, H.; Kansy, M. "Haem polymerization in malaria (*reply*)." *Nature* **1995**, *378*, 138-139.

- [57] Dorn, A.; Vippagunta, S. R.; Matile, H.; Bubendorf, A.; Vennerstrom, J. L.; Ridley, R. G. "A comparison and analysis of several ways to promote hemozoin (heme) polymerization and an assessment of its initiation *in vitro*." *Biochem. Pharmacol.* **1998**, *55*, 737-747.
- [58] Fitch, C. D.; Cai, G.-z.; Chen, Y.-F.; Shoemaker, J. D. "Involvement of lipids in ferriprotoporphyrin IX polymerization in malaria." *Biochim. Biophys. Acta* **1999**, *1454*, 31-37.
- [59] Tripathi, A. K.; Tekwani, B. L. "Mechanism of formation of β -hemozoin in malaria parasite: Lipids edge over proteins as possible mediators." *J. Parasit. Dis.* **1999**, *23*, 61-70.
- [60] Tripathi, A. K.; Garg, S. K.; Tekwani, B. L. "A physicochemical mechanism of hemozoin (β -hemozoin) synthesis by malaria parasite." *Biochem. Biophys. Res. Commun.* **2002**, *290*, 595-601.
- [61] Sullivan, D. J., Jr.; Gluzman, I. Y.; Goldberg, D. E. "Plasmodium hemozoin formation mediated by histidine-rich proteins." *Science* **1996**, *271*, 219-222.
- [62] Sullivan, D. J., Jr.; Gluzman, I. Y.; Russell, D. G.; Goldberg Daniel, E. "On the molecular mechanism of chloroquine's antimalarial activity." *Proc. Natl. Acad. Sci. U. S. A.* **1996**, *93*, 11865-11870.
- [63] Sullivan, D. J., Jr.; Matile, H.; Ridley, R. G.; Goldberg Daniel, E. "A common mechanism for blockade of heme polymerization by antimalarial quinolines." *J. Biol. Chem.* **1998**, *273*, 31103-31107.
- [64] Egan, T. J.; Ross, D. C.; Adams, P. A. "Quinoline antimalarial drugs inhibit spontaneous formation of β -haematin (malaria pigment)." *FEBS Lett.* **1994**, *352*, 54-57.
- [65] Dorn, A.; Stoffel, R.; Matile, H.; Bubendorf, A.; Ridley, R. G. "Malarial hemozoin/ β -hemozoin supports heme polymerization in the absence of protein." *Nature* **1995**, *374*, 269-271.
- [66] Egan, T. J. "Physico-chemical aspects of hemozoin (malaria pigment) structure and formation." *J. Inorg. Biochem.* **2002**, *91*, 19-26.
- [67] Sullivan, D. J. "Theories on malaria pigment formation and quinoline action." *Int. J. Parasitol.* **2002**, *32*, 1645-1653.
- [68] Bendrat, K.; Berger, B. J.; Cerami, A. "Haem polymerization in malaria." *Nature* **1995**, *378*, 138.

- [69] Pandey, A. V.; Tekwani, B. L. "Formation of hemozoin/ β -hematin under physiological conditions is not spontaneous." *FEBS Lett.* **1996**, *393*, 189-192.
- [70] Ignatushchenko, M. V.; Winter, R. W.; Baechinger, H. P.; Hinrichs, D. J.; Riscoe, M. K. "Xanthenes as antimalarial agents; studies of a possible mode of action." *FEBS Lett.* **1997**, *409*, 67-73.
- [71] Egan, T. J.; Hempelmann, E.; Mavuso, W. W. "Characterization of synthetic β -hematin and effects of the antimalarial drugs quinidine, halofantrine, desbutylhalofantrine and mefloquine on its formation." *J. Inorg. Biochem.* **1999**, *73*, 101-107.
- [72] Wellems, T. E.; Howard, R. J. "Homologous genes encode two distinct histidine-rich proteins in a cloned isolate in *Plasmodium falciparum*." *Proc. Natl. Acad. Sci. U. S. A.* **1986**, *83*, 6065-6069.
- [73] Koide, T.; Foster, D.; Yoshitake, S.; Davie, E. W. "Amino acid sequence of human histidine-rich glycoprotein from the nucleotide sequence of its cDNA." *Biochemistry* **1986**, *25*, 2220-2225.
- [74] Lenstra, R.; d'Auriol, L.; Andrieu, B.; Le Bras, J.; Galibert, F. "Cloning and sequencing of *Plasmodium falciparum* DNA fragments containing repetitive regions potentially coding for histidine-rich proteins: identification of two overlapping reading frames." *Biochem. Biophys. Res. Commun.* **1987**, *146*, 368-377.
- [75] Meshnick, S. R. "Is haemozoin a target for antimalarial drugs?" *Ann. Trop. Med. Parasitol.* **1996**, *90*, 367-372.
- [76] Ridley, R. G. "Haemozoin formation in malarial parasites: Is there a haem polymerase?" *Trends Microbiol.* **1996**, *4*, 253-254.
- [77] Sullivan, A. D.; Meshnick, S. R. "Haemozoin: Identification and quantification." *Parasitol. Today* **1996**, *12*, 161-163.
- [78] Pandey, A. V.; Chauhan, V. S. "Heme polymerization by malarial parasite: a potential target for antimalarial development." *Curr. Sci.* **1998**, *75*, 911-918.
- [79] Pandey, A. V.; Bisht, H.; Babbarwal, V. K.; Srivastava, J.; Pandey, K. C.; Chauhan, V. S. "Mechanism of malarial haem detoxification inhibition by chloroquine." *Biochem. J.* **2001**, *355*, 333-338.

- [80] Orjih, A. U. "On the mechanism of hemozoin production in malaria parasites: activated erythrocyte membranes promote β -hematin synthesis." *Exp. Biol. Med.* **2001**, *226*, 746-752.
- [81] Bohle, D. S.; Kosar, A. D.; Stephens, P. W. "Phase homogeneity and crystal morphology of the malaria pigment β -hematin." *Acta Crystallogr., Sect. D: Biol. Crystallogr.* **2002**, *D58 10*, 1752-1756.
- [82] Hempelmann, E.; Egan, T. J. "Pigment biocrystallization in *Plasmodium falciparum*." *Trends Parasitol.* **2002**, *18*, 11.
- [83] Blauer, G.; Akkawi, M. "B-hematin." *Biochem. Mol. Biol. Int.* **1995**, *35*, 231-235.
- [84] Basilico, N.; Monti, D.; Olliario, P. L.; Taramelli, D. "Non-iron porphyrins inhibit β -haematin (malaria pigment) polymerisation." *FEBS Lett.* **1997**, *409*, 297-299.
- [85] Blauer, G.; Akkawi, M. "Investigations of B- and β -Hematin." *J. Inorg. Biochem.* **1997**, *66*, 145-152.
- [86] Basilico, N.; Pagani, E.; Monti, D.; Olliario, P. L.; Taramelli, D. "A microtitre-based method for measuring the haem polymerization inhibitory activity (HPIA) of antimalarial drugs." *J. Antimicrob. Chemother.* **1998**, *42*, 55-60.
- [87] Parapini, S.; Basilico, N.; Pasini, E.; Egan, T. J.; Olliario, P.; Taramelli, D.; Monti, D. "Standardization of the physicochemical parameters to assess *in vitro* the β -hematin inhibitory activity of antimalarial drugs." *Exp. Parasitol.* **2000**, *96*, 249-256.
- [88] Blauer, G.; Akkawi, M. "On the preparation of β -hematin." *Biochem. J.* **2000**, *346*, 249-250.
- [89] Egan, T. J.; Mavuso, W. W.; Ncokazi, K. K. "The mechanism of β -hematin formation in acetate solution. Parallels between hemozoin formation and biomineralization processes." *Biochemistry* **2001**, *40*, 204-213.
- [90] Blauer, G.; Akkawi, M. "Alcohol-water as a novel medium for β -hematin preparation." *Arch. Biochem. Biophys.* **2002**, *398*, 7-11.
- [91] Bohle, D. S.; Helms, J., B. "Synthesis of β -hematin by dehydrohalogenation of hemin." *Biochem. Biophys. Res. Commun.* **1993**, *193*, 504-508.

- [92] Berger, B. J.; Bendrat, K.; Cerami, A. "High-performance liquid chromatographic analysis of biological and chemical heme polymerization." *Anal. Biochem.* **1995**, *231*, 151-156.
- [93] Ginsburg, H.; Famin, O.; Zhang, J.; Krugliak, M. "Inhibition of glutathione-dependent degradation of heme by chloroquine and amodiaquine as a possible basis for their antimalarial mode of action." *Biochem. Pharmacol.* **1998**, *56*, 1305-1313.
- [94] Loria, P.; Miller, S.; Foley, M.; Tilley, L. "Inhibition of the peroxidative degradation of haem as the basis of action of chloroquine and other quinoline antimalarials." *Biochem. J.* **1999**, *339*, 363-370.
- [95] Zhang, J.; Krugliak, M.; Ginsburg, H. "The fate of ferriprotoporphyrin IX in malaria infected erythrocytes in conjunction with the mode of action of antimalarial drugs." *Mol. Biochem. Parasitol.* **1999**, *99*, 129-141.
- [96] Schwarzer, E.; Kuhn, H.; Valente, E.; Arese, P. "Malaria-parasitized erythrocytes and hemozoin nonenzymatically generate large amounts of hydroxy fatty acids that inhibit monocyte functions." *Blood* **2003**, *101*, 722-728.
- [97] Mishra, N. C.; Sharma, A. "Biochemistry of the malaria parasite: an overview." *J. Basic Appl. Biomed.* **1995**, *3*, 11-23.

Chapter 2

Design and Synthesis of the Bionucleating Templates (BNTs)

2.1. Background and Significance

While the complexity of the life cycle of *Plasmodium falciparum* harnesses the development of thousands of novel stage-specific antimalarials, the recent genome sequencing¹⁻⁴ will not only aid in our understanding of this deadly parasite, but also proliferate the number of potential chemotherapeutic agents. Even with high-throughput screening tools, the time frame for the development of new and effective drug therapies (**Figure 2.1**)⁵ shortfalls the transmission rate of *P. falciparum* and its emerging drug resistance.⁶ Analysis of the genome sequence has failed to reveal any novel parasitic enzymes which are capable of synthesizing amino acids,

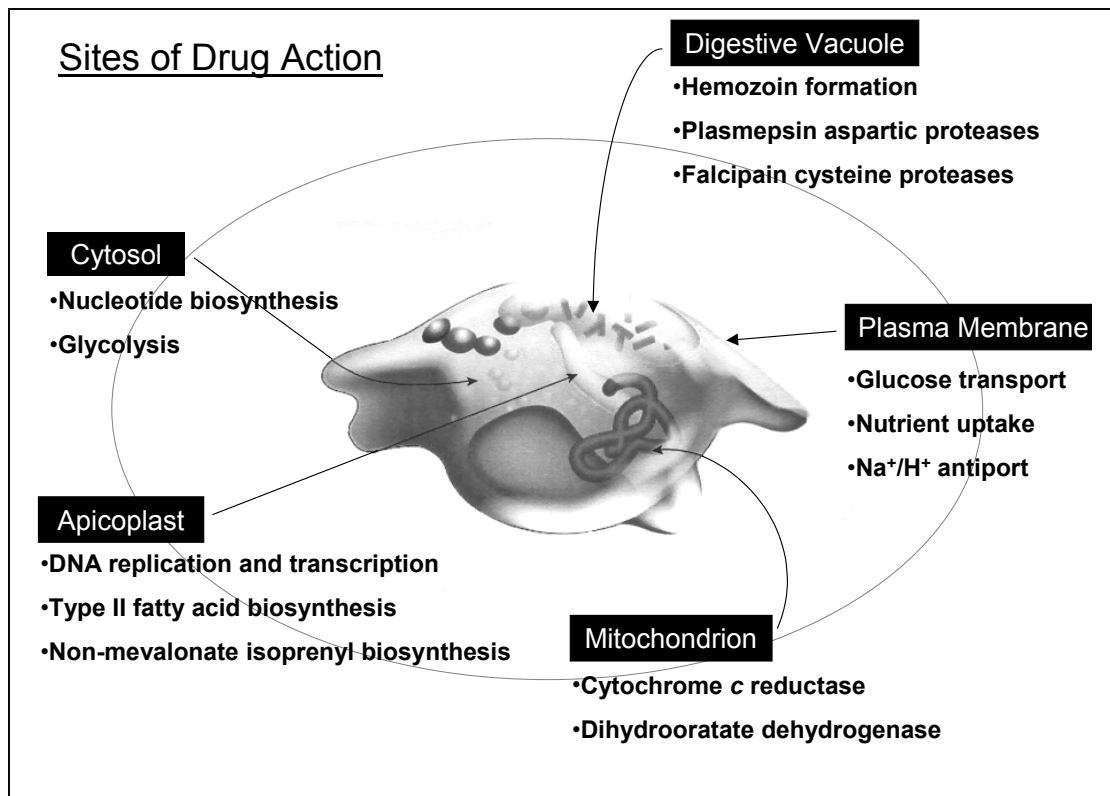


Figure 2.1. A schematic of a *Plasmodium falciparum* trophozoite residing in a host erythrocyte. The major organelles are highlighted with potential chemotherapeutic agents. Reproduced from reference 5.

thus the disruption of hemoglobin degradation and subsequent formation of hemozoin remain viable antimalarial targets,^{7,8} since the parasite must rely on host hemoglobin as its main source of requisite amino acids. Though few direct methods for examining antimalarial effectiveness in terms of hemozoin inhibition exist to date,⁹⁻¹¹ this route remains one of the most promising means by which to combat malaria. Antimalarials, which function to antagonize the nucleation and/or formation of hemozoin, will indubitably result in parasite death due to unavoidable toxic accumulation of free heme. Additionally, disrupting heme detoxification via this mechanistic approach should have little consequential effect on the host, since humans can biologically process free heme through the heme oxygenase/biliverdin reductase pathway.

The size and shape uniformity of hemozoin crystals indicates that *Plasmodium* must precisely control its biosynthetic route of β -hematin formation. *In vitro*, the conversion of hematin into hemozoin may be promoted via several pathways. Lipids,¹²⁻¹⁶ histidine-rich proteins (HRPs),¹⁷⁻¹⁹ and preformed hemozoin²⁰ mineralize the crystalline malaria pigment *de novo* (For the most recent reviews see Egan²¹ and Sullivan²²). The mechanics of β -hematin formation *in vivo* however, are largely controversial due to the fact the biochemical processing of hemozoin involves the intimate contact of the parasite with a host erythrocyte. Such interactions are further complicated by the numerous asexual growth and developmental stages that the parasite undergoes while residing in the human host.

The proposal that hemozoin formation was controlled through catalytic events was rejected when Dorn²⁰ demonstrated that hemozoin, isolated from the parasite, as well as chemically synthesized β -hematin, could seed the reaction of the malarial pigment. The biochemical processing of hemozoin was then theorized as a template mediated nucleation event rather than an enzymatic route to formation. Since both lipids and HRPs bind heme and nucleate the formation of hemozoin *in vitro*, the question is then redirected to which model template is more physiologically relevant in the metabolic processing of the malarial parasite? In other words, which controls the task of sequestering free heme inside the digestive vacuole and ultimately safeguarding the proliferation of the parasitic life form?

Hemozoin either formed by *Plasmodium falciparum* or chemically synthesized is identical in both its chemical composition and spectroscopic properties. Knowing that *P. falciparum* evolves from the early ring stage through the trophozoite stage in a mere 24 hours and that the abiological synthesis of the malaria pigment requires 6 days and nonphysiological conditions²³ (Figure 2.2), our hypothesis is that within the parasitic digestive vacuole, hemozoin formation must be a mediated process.

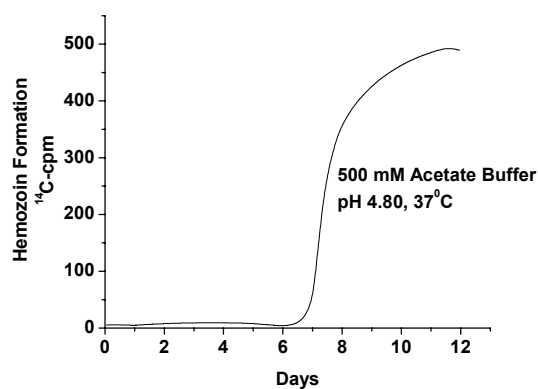


Figure 2.2. The abiological synthesis of hemozoin. Reproduced from reference 23.

Plasmodium must carefully regulate its susceptibility to oxidative stress, avoiding the toxic effects of free heme accumulation and the ensuing potential oxidative damage that can occur in the digestive vacuole. Though the parasite's obvious portal is the sequestration of hemozoin, other metabolic processes can be hypothesized to prevent or reduce oxidative damage. A secondary line of defense can be envisioned upon consideration of the acidic nature of the digestive vacuole. Chemically, the reactivity of iron (III) protoporphyrin IX, the monomeric unit of hemozoin, is reduced in acidic environments. At low pH, free heme aggregates as less chemically reactive μ -oxo dimers. Though this dimer formation would link two molecules of heme via an oxygen atom in the axial position and not by the required propionate linkage necessary for the formation of hemozoin, the acidic nature of the digestive vacuole could suppress oxidation reactions and represent an additional targeted mode of antimalarial drug action. As a consequence, the consideration of the complex homeostatic equilibrium within the digestive vacuole, and **particularly the acidic pH (4.8-5.2), is fundamental to studying the underlying mechanics of hemozoin formation.**

Though there is little doubt that lipids can mediate the formation of hemozoin *in vitro*, many questions surround a lipid-mediated formation of hemozoin *in vivo*. Since as early as the late 1960's when S. B. Brown reported the hydrogen peroxide oxidation of iron protoporphyrin IX,²⁴⁻²⁶ free heme has been known to have deleterious oxidative effects on several substrates including polyunsaturated fatty acids. However, once hemozoin is engulfed by macrophages, it promotes the

oxidation of fatty acid substrates, specifically arachidonic and linoleic acid to a mixture of hydroxy eicosatetraenoic and hydroxy octadecadienoic acids respectively.²⁷⁻²⁹ Why then, would *Plasmodium falciparum* choose to nucleate hemozoin on a template that it could later potentially destroy?

In addition to this, the debate continues as to whether or not *Plasmodium falciparum* can synthesize its own fatty acids. Originally *Plasmodium falciparum* was thought to scavenge fatty acids from host erythrocytes; being truly parasitic, relying on its host not only for requisite amino acids, but also supplying the template for its heme detoxification process. New evidence of a type II fatty acid biosynthesis now exists both *in vivo* and *in vitro* for the parasite,³⁰ originating from the identification of several fatty acid synthase (FAS) genes. Waller and colleagues recently determined that fatty acid inhibitors, such as thiolactomycin and triclosan, exhibited pronounced sensitivities in the early ring stage of parasite growth. If lipids were structural scaffolds for the nucleation of hemozoin then why would inhibitors display markedly increased activities in the growth stage that has relatively little or no hemozoin formation occurring? Obviously more detailed studies, including fatty acid quantification, are needed.

The HRPs appear to be the parasite's most probable template for the nucleation of hemozoin. A histidine-rich protein, HRP II, isolated from the digestive vacuole of *P. falciparum* (refer to **Figure 1.12** for the sequence of HRP II), not only promoted the formation of hemozoin, but also bound 17 equivalents of heme.¹⁷ Given that the parasites can multiply an estimated eight times every two days,³¹ the

efficiency of sequestering heme is of utmost importance for the viability of *Plasmodia*, especially since each proteolyzed molecule of hemoglobin releases four molecules of heme. Simply in terms of binding affinities, the HRPs appear to expend less metabolic energy based on effective arrest of free heme. A HRP templated formation of hemozoin can also be argued from the perspective of genetic preservation. Why would the parasite not evolve a detoxification scheme that was unique to itself?

Given that to date, no lipid was isolated from the digestive vacuole, while in fact the histidine-rich protein, HRP II, had been localized within this organelle and been shown to promote the formation of hemozoin, we investigated the role of the histidine-rich proteins in the nucleation of hemozoin.

To date, four histidine rich proteins (HRP I, HRP II, HRP III, and HRP IV) have been isolated from *P. falciparum* and share sequence homology. HRP I is knob associated and thought to be involved in cytoadherence and red blood cell rosetting, being only synthesized in the early stages of gametocyte development.³² HRP II, HRP III, and HRP IV are localized in the digestive vacuole of *Plasmodium falciparum* and possess an usually high percentage of alanine and histidine (**Table 2.1**). HRP II, a 35 kD protein, is synthesized by the parasite during all stages

Table 2.1. Sequence Homology of the HRPs.

Protein	% Composition (His & Ala)	# of Ala-His-His Repeats
HRP II	76%	51
HRP III	56%	28
HRP IV	31%	

of intraerythrocytic growth^{17,33} and metabolically exported to the cytoplasm, as evidenced by its detection as a water soluble protein in culture supernatant.³⁴ HRP II not only aggregated hemozoin, but also was effectively inhibited by chloroquine, a known antimalarial. Additionally when HRP II was used antigenically in *Aotus* monkey trials, the protein elicited protective immunity against *Plasmodium falciparum*.^{35,36} HRP III, a 27 kD protein, was isolated in the digestive vacuole of mutants devoid of HRP II expression. A genetic cross strain which did not contain HRP II or HRP III still cross reacted with monoclonal antibodies from both proteins and was characterized as HRP IV (M_r 10 kD).³⁷

2.2. The Histidine-Rich Proteins Evidenced as Templates in the Biomineralization of Hemozoin

Despite the fact the HRPs have definitive sequence characterizations, the biological roles of these proteins remain obscure. Recent site-directed mutagenesis studies of non-overlapping synthetic peptides of HRP I, HRP II, and HRP III have demonstrated that only HRP I possessed multiple high activity red blood cell (RBC) binding sites found in the central lysine rich region II (residues 301-480) of the native protein.³⁸ More specifically, the screening of the HRP II mutants presented only one RBC binding sequence, which was a non-repetitive N-terminal sequence rich in asparagine residues, while HRP III failed to exhibit any specific erythrocyte binding. Though it has long been proposed the highly repetitive nature of *Plasmodium falciparum* proteins is advantageous to the parasite,³⁹ its exact molecular role as a scaffolding protein in heme detoxification has yet to be determined. Specific

interactions between the HRPs and heme remain elusive, though HRP II has been widely used in immunochromatographic methods for the detection of malaria (ParaSight F® and ICT®) and was recently highlighted as an unexplored antimalarial strategy.⁴⁰

Research collected thus far on the plausible role of the HRPs in the formation of hemozoin is indicative of a nucleation process rather than a catalytic event. The presence of a specific amino acid repeat motif [Ala-His-His-Ala-His-His-Ala-Ala-Asp in HRP II, and Ala-His-His-Ala-Ala-Asn-Ala-His-His-Ala-Ala-Asn (N-terminus) and Asp-Asp-Ala-His-His-Asp-Gly-Ala-His-His (C-terminus) in HRP III] is reminiscent of nucleating scaffold proteins utilized by other biological systems in biomineralization processes.^{41,42} Such systems exploit the three-dimensional structure succumbed by protein folding as a surface on which to organize well-defined inorganic solid state materials, which function as structural supports or defense mechanisms⁴³ for the organisms. Much like diatoms precipitate species specific hydrated silica from silaffin proteins,⁴⁴ and the carnivorous marine worm *Glycera* biomineralizes atacamite, a copper chloride mineral with an associated but uncharacterized protein rich in glycine and histidine,⁴⁵ *P. falciparum* controls hemozoin nucleation and formation on the surface of the histidine-rich protein.

Like other known biominerals (e.g. calcite, hydroxyapatite, magnetite, etc.), hemozoin has a rather straightforward mineral composition, but a more complex structural characterization in which the lattice organization somehow reduces solubility.⁴¹ Besides *P. falciparum*, all other members of the *Plasmodium* species, as

well as a few non-*Plasmodium* species such as *Schistosoma mansoni*, *Rhodnius prolixus*, and *Haemoproteus columbae*, synthesize the malarial pigment. The pigment deposited by these organisms varies slightly amongst species in crystalline surface morphologies (**Figure 2.3**).⁴⁶ Intrinsic parasite differences, physiological variations (i.e. hemoglobin concentration, ion and salt concentration, and pH), or host dissimilarities are postulated to contribute to the final morphological shape of the crystal.⁴⁷ Such variances in three-dimensional structure are also predicted to alter not only hemozoin formation, but also pigment degradation and reactivity. The shape heterogeneity of the crystals is reminiscent of yet another property of biominerals, most demonstratively visualized in the variation amongst the intricate details of the silicon dioxide shells of diatoms of different species.

In all instances, understanding how biology deposits inorganic materials into or onto an organic matrix with precisely controlled spatial and temporal details has intrigued scientists such that biomimetic chemistry has evolved as an attempt to synthesize advanced materials with specifically tailored properties. Belcher *et al.* have recently determined that calcium carbonate biomineralization *in vivo* in red abalone (a marine snail) is controlled morphologically by the sequential release of

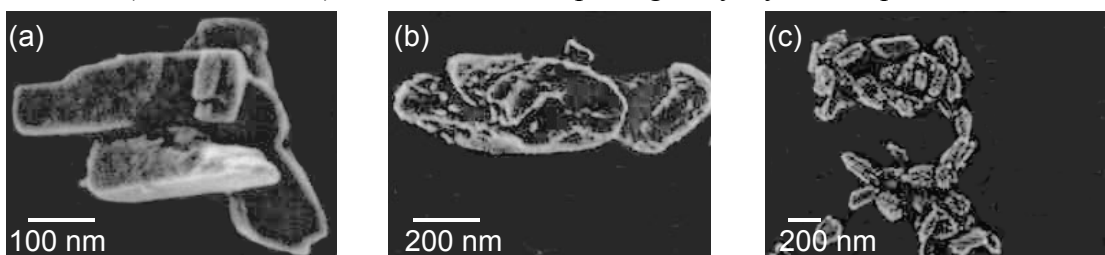


Figure 2.3. Field emission inlens scanning electron microscopy (FEISEM) of hemozoin purified from (a) *Plasmodium falciparum* (b) *Schistosoma mansoni* and (c) *Haemoproteus columbae*. Reproduced from reference 46.

differing proteins.⁴⁸ Moreover, a peptide, rich in proline, tyrosine, and glycine, is secreted prior to inorganic calcium nucleation, highlighting the importance of a protein scaffold in directing biomineral formation.

From the perspective of biomineralization, we believe the HRPs play a critical role in the biological initiation/nucleation of hemozoin. We hypothesize the organization of the alanine-histidine-histidine repeats within the histidine-rich proteins of *P. falciparum* create unique nucleation sites for the crystallization of hemozoin.

Using *Plasmodium falciparum* derived proteins for biomineralization studies pose several problems. First and foremost, rationally designing a synthetic gene that would encompass simultaneous changes in a putative nucleating domain is both problematic and laborious. Secondly, these proteins come from a highly infectious organism and culturing infectious agents musters great safety concerns. Additionally, the highly repetitive DNA sequences in the HRPs make sequencing and expression difficult since the high adenine (A) and thymine (T) content (80%) causes replication problems in typical *E. coli* cultures since these simplistic organisms can not effectively replicate cDNA greater than 5 kb. Some success has been met with yeast artificial chromosome (YAC) systems and fusion proteins, but effective sequencing remains challenging. Additionally, cell cultures must be kept synchronized in order to keep the parasites in the same developmental stage.

In retrospect, the culmination of these synthetic difficulties highlights the necessity of a model system. Understanding the biochemical processing of hemozoin

formation will not only aid in the development of novel antimalarials, but it may also provide insight into the very sustenance of *Plasmodium*, the causative agent of a deadly disease that has subsisted for over 1000 centuries.

2.3. Design and Development of a Model HRP System

While previous experiments using polyhistidine and linear multimer peptides comprised of Ala-His-His-Ala-Ala-Asp⁴⁹ bound heme, all failed to nucleate the formation of hemozoin. With this in mind, synthetic peptides attempting to bionucleate the formation of hemozoin must adhere to several design criteria. First, the template must contain a minimal set of recognition motifs necessary to not only bind heme, but also nucleate β -hematin. Secondly, to effectively mimic the native protein, the template should bind approximately the same number of heme as HRP II. Finally, the template should possess some secondary structure since *in vivo* observations have determined that secondary, tertiary, and quaternary structure is imperative in attempts to mimic biological biomineralization processes. Inherent intermolecular aggregations and intra-template interactions should be minimized in the overall topology to avoid blocking or capping the plausible nucleating domain, preventing the aggregation of hemozoin at the inorganic-organic interface.

With a limited understanding of protein folding mechanisms, difficulties arise when attempting to predict amino acid sequences that will yield desired three-dimensional scaffolds. Dendrimers, synthetic compounds that have highly symmetrical polymeric branches radiating from a central core, have allowed scientists to ascertain some structural control in materials science. The interspatial voids

stemming from the regularly repetitive nature of the branches have permitted the inclusion and/or confinement of ions and molecules. The exploitation of such “host-guest” chemistry has attracted the attention of scientists as a means of constraining size and shape in three-dimensional space. While short linear peptides lack conformation, peptide dendrimers provide an appealing framework on which to incorporate non-conventional vectoral growth and porosity. Furthermore, dendrimeric branches can be fine-tuned to control not only the architecture, but also functional interactions between the template and substrate. Molecular recognition sites can be directly engineered into the structural design, insomuch that inorganic binding sites can be spatially arranged to control both physical properties and spectroscopic characterizations.

Peptide dendrimers are broadly defined as dendrimers with peptide bonds^{50,51} having found applications in the development of vaccines,⁵²⁻⁵⁶ diagnostic reagents,^{57,58} drug delivery systems,⁵⁹ catalysts,^{60,61} inhibitors,⁶² and antimicrobials,⁶³ while also functioning as protein models.⁶⁴⁻⁶⁶ The assembly of synthetic peptides onto a template or scaffolding permits the construct not only to obtain the three-dimensional bulk characteristic of classical dendrimers, but moreover to ascribe to the globular nature of proteins. The most common peptide dendrimers are constructed on a multiple antigen peptide system (MAPS), which unlike classical dendrimers, which have a central core, branching segments and terminal functionality, lack a centered focal point, branching from only one end. These systems were first developed by Tam in attempt to present multiple copies of antigens from a single core in order to

increase immunogenic activities.^{67,52}

MAPS are often preferred over tandem peptide multimers⁶⁸ since the polymeric peptide may possess an altered secondary structure due to its peptide chain elongation. Along this same line of reasoning, MAPS often exhibit enhanced sensitivities over multimeric peptide copies due to an increased number of interactions per given unit surface area (i.e. increased density of potential binding sites). Lysine is the most commonly used amino acid in the core, providing sites for branching segments through the α and ϵ amino ends.⁶⁹ Multiple copies of peptide segments are conjugated either directly or through standard solid phase peptide synthesis protocols. Commercially available MAPS include 4-branch or 8-branch lysine cores typically conjugated to a solid polymer resin of polystyrene with 1% divinylbenzene through an alanine or glycine linkage (**Figure 2.4**).

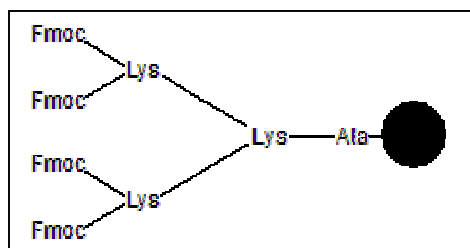


Figure 2.4. Fmoc-4-branch MAPS resin.

MAPS offer several advantages over other peptide conjugates,^{69,70} both kinetically and thermodynamically. MAPS are stable in solution over a pH range from pH 2-9 and can also be lyophilized as a powder, which is advantageous over the storage conditions of

recombinant proteins. Additionally, the relatively small size of the lysine core allows the peptide to comprise the majority of the conjugate mass, which contrasts other peptide carriers in which the peptide mass is small compared to the relative mass of the carrier. This same design construct permits the N-terminus (distal end) of the

peptide to be more flexible, while the C-terminus is constrained against the lysine scaffolding. This, plus the close packing of the peptide segments allows the branches to conform to some secondary structure and enhance the overall stabilization of the peptide. Conversely, the restricted space against the lysine core could also become problematic by increasing the steric hinderance between the peptide chains. These interactions generate smaller, less accessible interstitial spaces near the core compared to other sites further along the peptide branch.

Standard solid phase peptide synthesis on MAPS resins is far from trivial. Though many have successfully constructed peptide segments on the lysine core, inter-chain interactions are often problematic.⁷¹ Using lower loading resins (< 0.4 mmole/g and < 0.8 mmole/g for 4-branch and 8-branch MAPS respectively) improve synthetic yields and homogeneity by minimizing chain aggregations and enhancing solvent permeability. Fewer substitutions on the resin (less coverage) increase the interstitial distance between peptide segments and decrease the steric constraints near the surface. Controlling the population of lysine residues on the surface of the resin allows a greater surface area for resin swelling, which also leads to more efficient coupling since hydrogen bonding between the peptide chains and N-termini is diminished. Efficient coupling is essential in MAPS syntheses since deletions in the amino acid sequences are more prevalent, since all branches must be coupled simultaneously. Interestingly, the tetrameric MAPS have no real advantages over the 8-branch MAPS when greater than 15 amino acid residues are used in the synthesis of the peptide.^{69,68}

Recalling that native HRP II bound 17 equivalents of heme per molecule^{17,72} (pH 4.8), MAPS offer an excellent template on which to incorporate multiple heme binding sites so as to mimic a heme binding efficiency similar to that of the native protein. Moreover, the constructive design of the MAPS with a certain degree of rigidity near the lysine core, not only allows for the incorporation of secondary structure along the peptide chain, but also maintains sufficient interbranching distance which permits the allocation of three-dimensional space necessary for the crystalline aggregation of hemozoin, a critical feature missing in the linear peptide and multimer constructs.

Upon examining the sequence of HRP II, in which histidine and alanine comprise 76% of the native protein, Ala-His-His is repeated 51 times. Knowing that histidine can bind a variety of metals, this tripeptide was further scrutinized as a possible repeat unit within a putative nucleating domain for the formation of hemozoin. Knowing that native HRP II bound 17 equivalents of heme, while also nucleating the formation of hemozoin, this trimeric repeat was examined for a plausible higher-ordered organizational scheme. From this, two possible nucleating domains can be identified: the 9-mer sequence **Ala-His-His-Ala-His-His-Ala-Ala-Asp** (repeated 16 times within the native protein), and **Ala-His-His-Ala-Ala-Asp-Ala-His-His** (repeated 23 times). **These two amino acid sequences were hypothesized to be putative nucleating domains within HRP II** and were evaluated for possible roles in the formation of hemozoin through synthetic site-directed mutagenesis studies.

2.4. The Ala-His-His-Ala-His-His-Ala-Ala-Asp Putative Domain – Initial studies of a Model HRP System

2.4.1. Chemical Characterization

In order to uncover the components of the heme moiety in Fe(III)PPIX that were critical for the nucleation of hemozoin on HRP II, Ziegler *et al.* constructed a first and second generation 4-branch MAPS peptide dendrimer based on the putative 9-mer sequence Ala-His-His-Ala-His-His-Ala-Ala-Asp, where each Ala-His-His tripeptide repeat was postulated to serve as the binding domain for the natural substrate, Fe(III)PPIX.⁷³ The first **bio**nucleating **t**emplate, BNT I (a 1st generation dendrimer with 1 tandem 9-mer repeat per lysine branch), contained 8 Ala-His-His repeats, while a second model, BNT II, (a 2nd generation dendrimer with 2 tandem 9-mer repeats per lysine branch) possessed 16 such repeats, capitalizing on the branched nature of the dendrimer core to incorporate multiple binding domains. Initial studies indicated the N-acylated synthetic peptides synthesized according to standard Fmoc solid phase synthesis protocols tested positive for monoclonal antibodies for HRP II using the commercially available *ParaSight F*® test from Becton-Dickson Pharmaceutical (Sparks, MD).

In addition to Fe(III)PPIX, several other substrates [protoporphyrin IX (PPIX), Zn (II) protoporphyrin IX (Zn(II)PPIX), tetrasulfanophthalocyanine (PcS), and nickel (II) tetrasulfanophthalocyanine (Ni(II)PcS)] were recognized by the BNTs (**Table 2.2, Figure 2.5 and 2.6**). BNT I, with eight Ala-His-His trimeric repeats, bound 7.1 ± 0.7 equivalents of Fe(III)PPIX. More significantly, BNT II, with

Table 2.2. Substrate Binding Stoichiometries of BNT I and BNT II.

Substrate	BNT I (8 Ala-His-His repeats)	BNT II (16 Ala-His-His repeats)
Fe(III)PPIX	7.1±0.7	12.2±1.0
PPIX	7.7±0.2	10.4±1.0
Zn(II)PPIX	6.8±0.5	14.0±0.6
PcS	5.7±0.2	13.2±1.0
Ni(II)PcS	6.5±0.1	11.0±1.0

double the number of postulated heme binding sites, bound 12.2 ± 1.0 equivalents of Fe(III)PPIX, approximately twice as much substrate as BNT I. BNT II bound approximately twice the amount of the other substrates as well. Assuming the trimeric repeat Ala-His-His is the binding domain of the template, Fe(III)PPIX (and the other substrates) failed to be incorporated into all of the putative binding sites of BNT II (16 sites), but this was not surprising given the dendrimeric nature of the peptide restricts accessibility near the core due to inherent steric constraints. BNT I is less sterically hindered and therefore, its stoichiometric binding is more closely correlated to the number of incorporated synthetic binding sites.

Since protoporphyrin IX and tetrasulfanatophthalocyanine were also capable of binding to the templates, the association of the substrate with the BNT templates was not dependent on a metal recognition site, suggesting that substrate recognition was not mediated by axial ligation of a histidine residue to a metal ion. Under the conditions employed in the binding assay (100 mM acetate buffer, pH 4.8, mimicking the environment of the digestive vacuole of *P. falciparum*), the imidazole ring of the histidine is likely protonated since the pK_a of the side chain is 5.8. Since this moiety is likely unavailable for axial ligation, interactions must be through π -stacking and/or

electrostatic forces. A recent study of recombinant HRP II of *P. falciparum* demonstrated a similar pH dependence on heme binding.⁷⁴

After each stoichiometric binding maxima, the difference titration curves for the substrates show a slight negative divergence from the plateau expected with saturable binding of the template (**Figures 2.5 and 2.6**). At high substrate stoichiometries a number of aggregative interactions are possible that could eventually result in precipitation. Such interactions are likely responsible for this negative trend noted after maximal binding and are particularly prominent with Fe(III)PPIX, the natural substrate for the HRP proteins. This behavior may be a result of the self-aggregative properties of the porphyrin substrate, but biologically this could be indicative of the very precise management that *P. falciparum* must ascertain in its detoxification of heme.

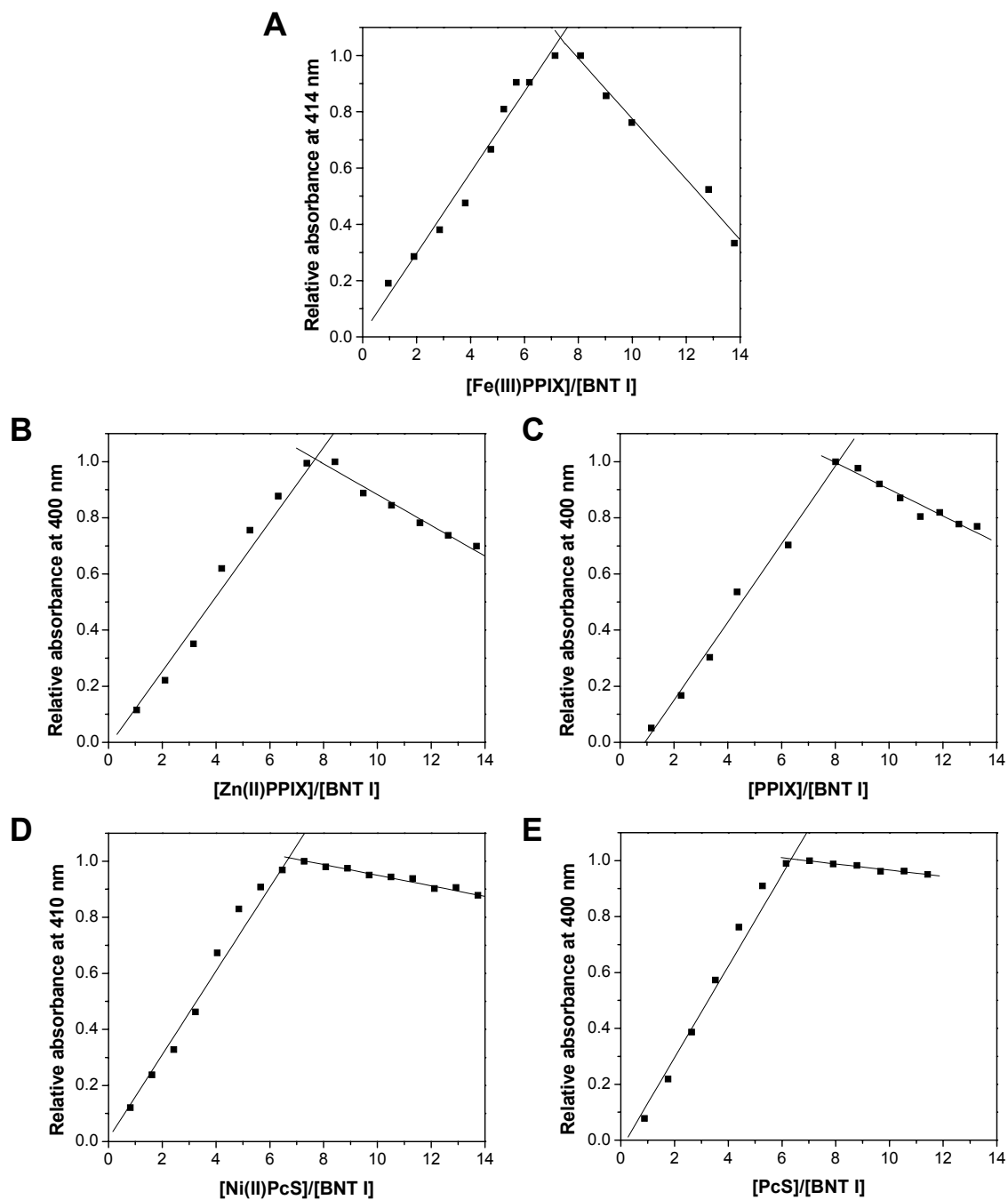


Figure 2.5. Substrate binding stoichiometries for BNT I. (A) Fe(III)PPIX (B) Zn(II)PPIX (C) PPIX (D) Ni(II)PcS (E) PcS. Briefly, aliquots of a stock solution of substrate (~ 1 mM) dissolved in 0.1 M NaOH were added to a 100 mM acetate buffer solution, pH 4.8, containing the appropriate amount of nucleating template, BNT I (2-2.5 μ M), and a 100 mM acetate buffer blank solution. Samples were equilibrated for 15 minutes prior to measurements.

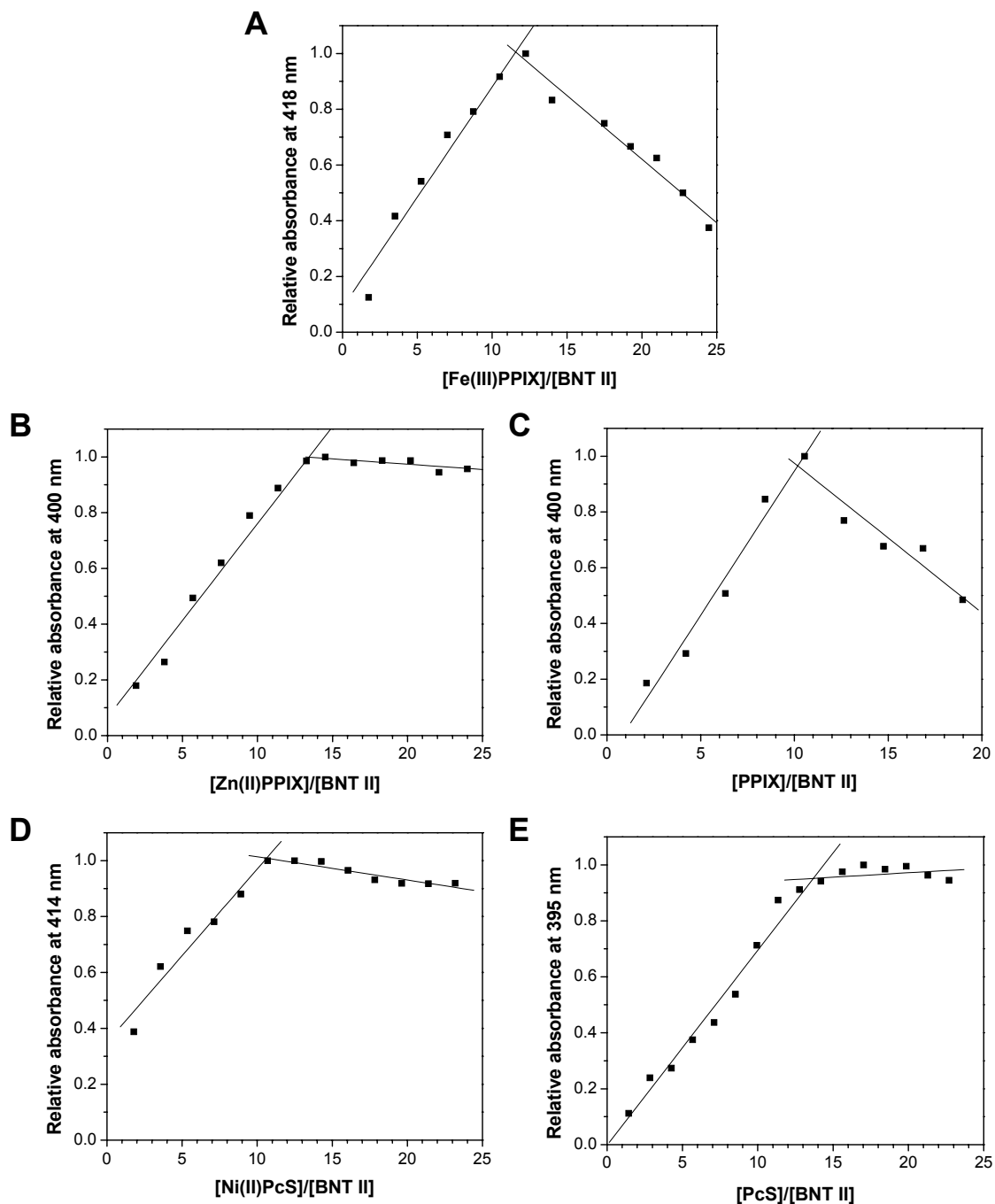


Figure 2.6. Substrate binding stoichiometries for BNT II. (A) Fe(III)PPIX (B) Zn(II)PPIX (C) PPIX (D) Ni(II)PcS (E) PcS. Briefly, aliquots of a stock solution of substrate (~ 1 mM) dissolved in 0.1 M NaOH were added to a 100 mM acetate buffer, pH 4.8, containing the appropriate amount of nucleating template, BNT II, (1-1.5 μ M) and a 100 mM acetate buffer blank. Samples were equilibrated for fifteen minutes prior to measurements.

More significant than binding substrates, the templates also mediated the formation of hemozoin (**Figure 2.7**) according to the *in vitro* heme polymerization assay of Sullivan.¹⁷ In the presence of free heme under acidic conditions, the templates promoted the formation of insoluble heme aggregates. Polyhistidine, lysozyme, bovine serum albumin (BSA) and an acetate buffer control failed to aggregate the malarial pigment. (Both Dorn¹³ and Orjih⁷⁵ reported background hemozoin formation at 1-2 nmoles under similar experimental conditions.) The results demonstrated that BNT II nucleated twice the amount of hemozoin as BNT I, which had half as many putative nucleating domains attached to the lysine core. Chloroquine (CQ) also inhibited the template-mediated production of hemozoin in

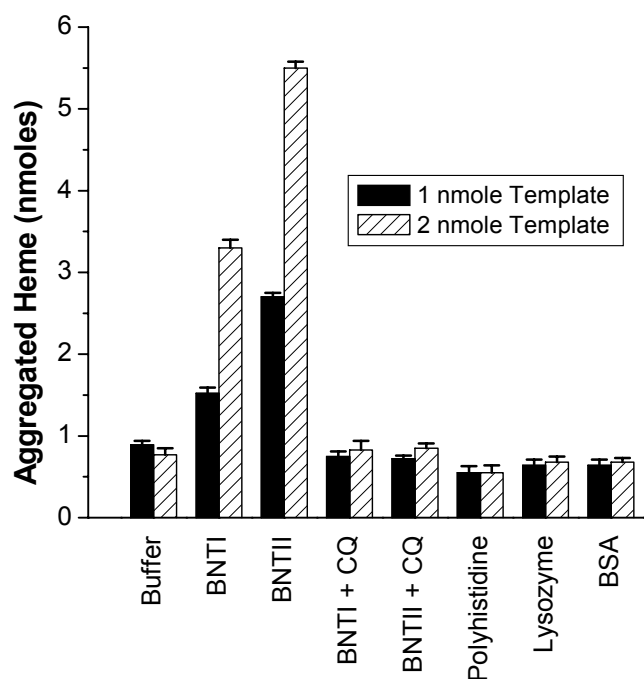


Figure 2.7. Hemozoin production mediated by the bionucleating templates and other protein substrates. The baseline amounts are consistent with previously published reports.^{13,77}

both template assays. Additionally hemozoin was formed in a concentration (Figure 2.7), time (incubation period) (Figure 2.8), and pH dependent manner (Figure 2.9), analogous to the activity of HRP II. Activity diminished above a pH of 4.8, the approximate pH of the digestive vacuole of the parasite, and as it approached the pK_a of the imidazole side chain. The ionic strength of the acetate buffer had little effect on the aggregation of hemozoin (Figure 2.10).

The BNT mediated insoluble heme aggregates were characterized by Fourier transform infrared (FT-IR) spectroscopy and exhibited the characteristic vibrational frequencies of hemozoin^{76,46,22} at 1660 cm^{-1} and 1210 cm^{-1} (Figure 2.11). The BNT mediated hemozoin also shared similar synchrotron x-ray powder diffraction (XRD) patterns with those of hemozoin isolated from *P. falciparum*⁷⁷ (Figure 2.12).

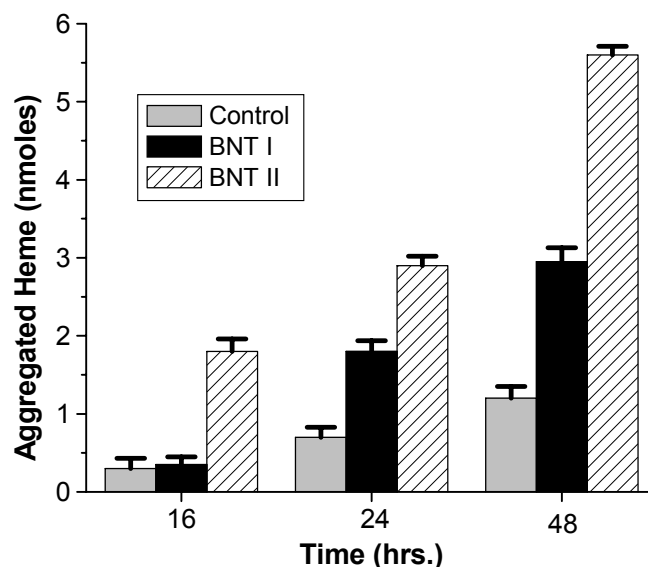


Figure 2.8. Time evolution for the BNT mediated formation of insoluble heme aggregates. Hemin ($50\text{ }\mu\text{M}$) dissolved in 0.1 M NaOH was incubated at $37\text{ }^{\circ}\text{C}$ with 2 nmoles of template in 2 mL of acetate buffer (500 mM , $\text{pH } 4.8$) for the time intervals indicated.

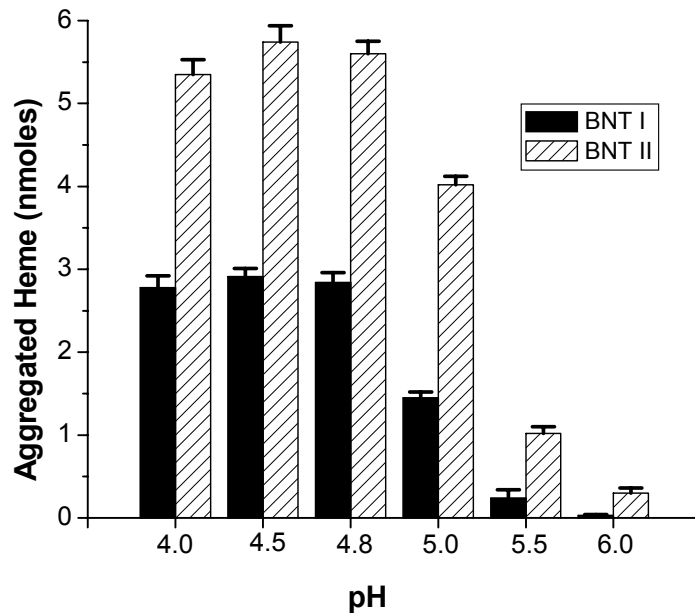


Figure 2.9. pH dependence of the BNT mediated formation of insoluble heme aggregates. Hemin (50 μ M) dissolved in 0.1 M NaOH was incubated at 37 $^{\circ}$ C with 2 nmoles of template in 2 mL of acetate buffer (500 mM) at the indicated pH for 48 hrs.

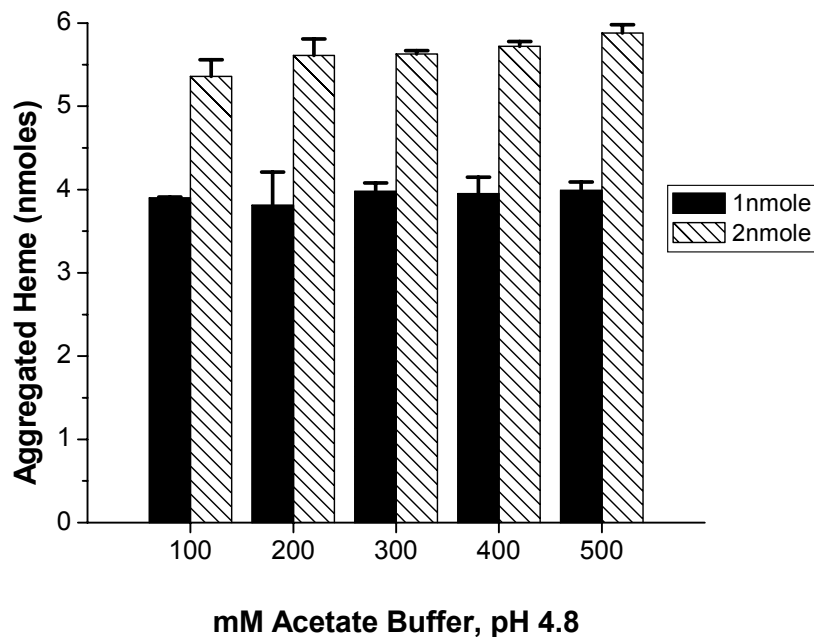


Figure 2.10. Effect of acetate buffer concentration on the BNT mediated formation of insoluble heme aggregates. Hemin (50 μ M) dissolved in 0.1 M NaOH was incubated at 37 $^{\circ}$ C with 2 nmoles of BNT II in 2 mL of acetate buffer (pH 4.8) at the various indicated ionic concentrations.

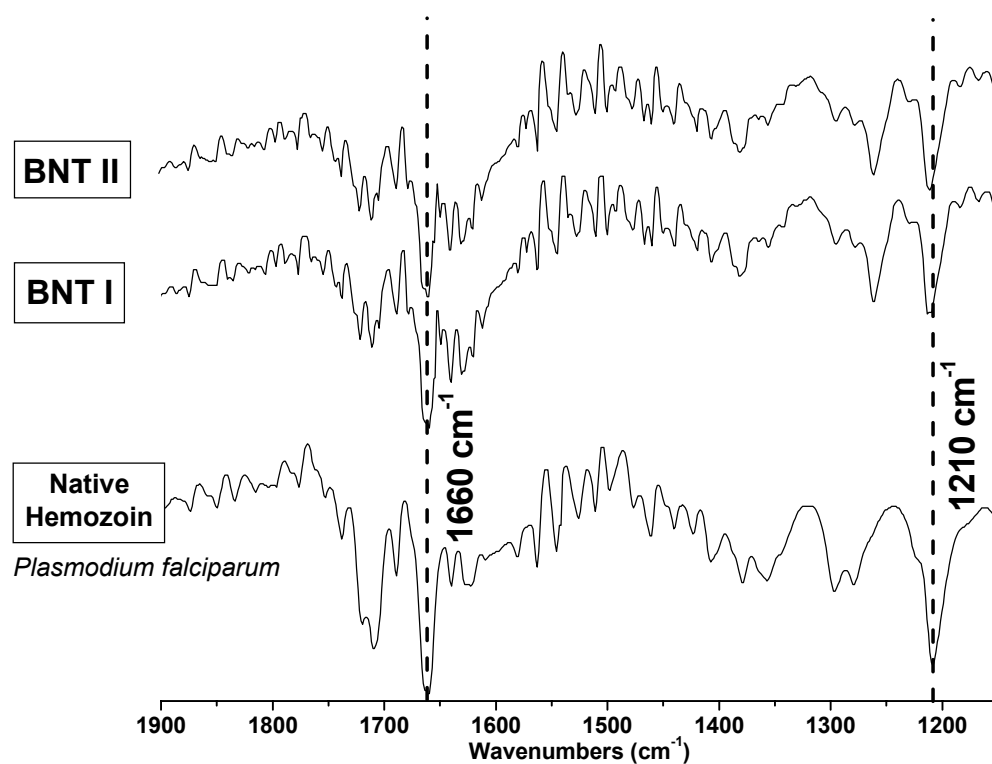


Figure 2.11. Comparison of FT-IR spectra of native hemozoin from *Plasmodium falciparum* and that mediated by the bionucleating templates, BNT I and BNT II.

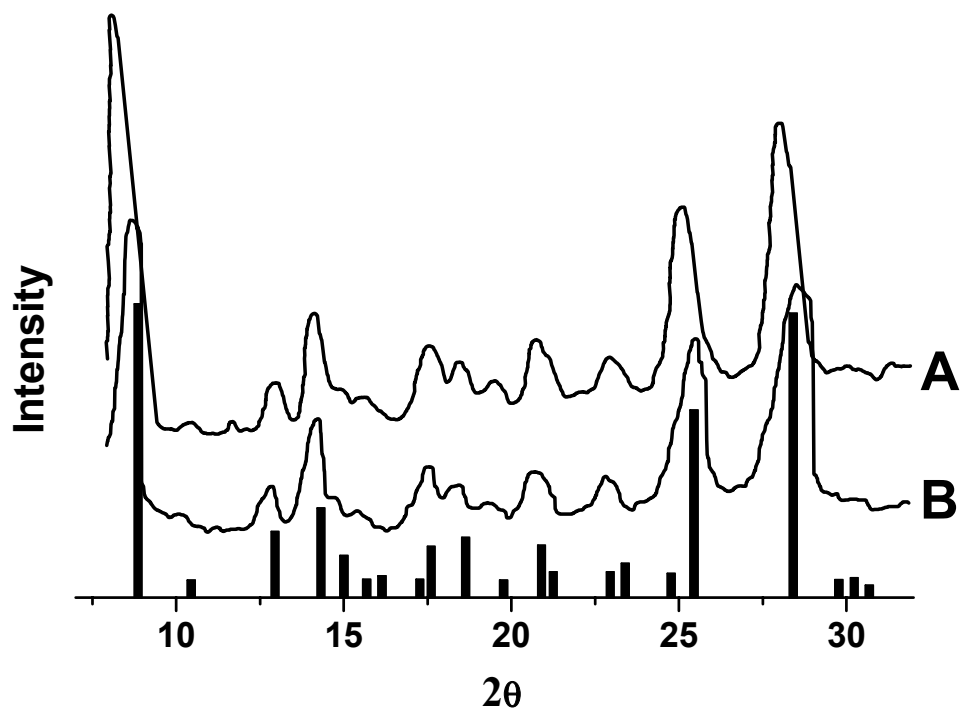


Figure 2.12. Comparison of the synchrotron x-ray diffraction patterns of (A) hemozoin mediated by BNT II and (B) hemozoin from *Plasmodium falciparum*.

Common antimalarials, chloroquine and Zn(II)PPIX, inhibited the BNT mediated formation of hemozoin in a dose dependent manner (**Figure 2.13**), with IC_{50} 's on the same order of magnitude as those previously determined for HRP II.¹⁷ Martiney *et al.* had previously shown that Zn(II)PPIX and similar analogues inhibited the formation of hemozoin in *Plasmodium falciparum* trophozoite extracts,⁷⁸ by binding to nucleation sites preventing the templating of Fe(III)PPIX. With the BNTs responding similarly in a concentration dependent manner, substrate recognition was not based solely on ferric protoporphyrin IX metal specificity, but through π - π stacking or electrostatic interactions. Though this suggested β -hematin inhibition occurred by the substrate blocking the nucleation sites on the template, other

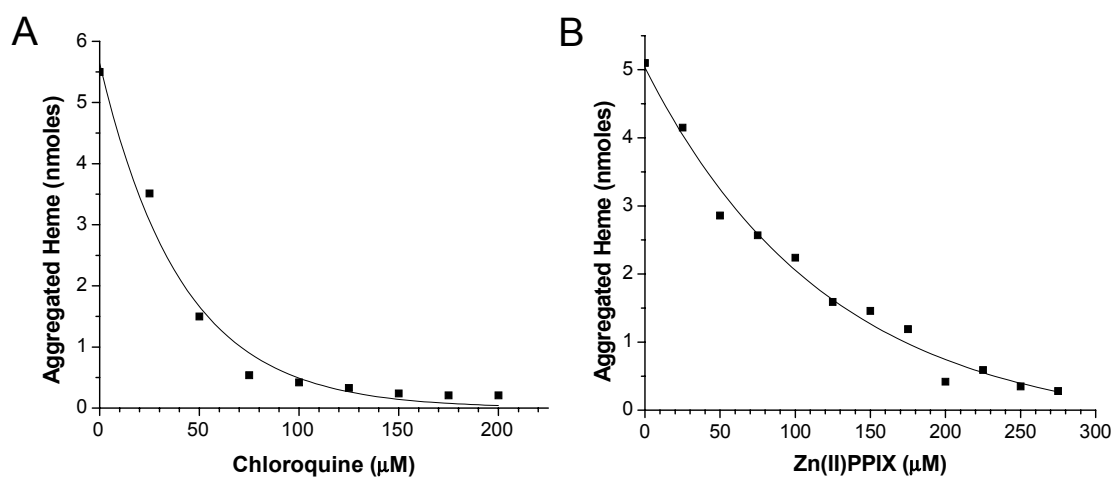


Figure 2.13. Inhibition of BNT II mediated production of hemozoin. (A) Effect of increasing concentrations of known antimalarial chloroquine. Results of the assay consisting of 50 μ M hemin and 1 μ M BNT II in 2 mL acetate buffer (500 mM, pH 4.8, 37 $^{\circ}$ C) and increasing concentrations of chloroquine revealed an $IC_{50} \approx 30 \mu$ M. (B) Effect of increasing concentrations of Zn(II)PPIX. Results of the assay consisting of 50 μ M hemin and 1 μ M BNT II in 2 mL acetate buffer (500 mM, pH 4.8, 37 $^{\circ}$ C) and increasing amounts of Zn(II)PPIX revealed an $IC_{50} \approx 125 \mu$ M. Each point represents the average of three individual assays with a standard deviation of < 5%. The line through the data represents a multi-order exponential fit.

mechanisms of β -hematin inhibition could possibly exist. Besides association with the template, the antimalarial could interact with heme, physically preventing the iron porphyrin moiety from associating with the nucleating scaffold. Additionally, the drug could interact with a possible heme:template complex blockading the faces of the biomineral impeding further hemozoin aggregation.

2.4.2. Conformational Analysis

Despite its repetitive sequence similarity to the histidine-rich glycoprotein (HRG) (Gly-His-His-Pro-His-Gly repeat units), the nucleating domain of HRP II must be in association with heme via a mechanism that is vastly different from the bis-axial coordination that occurs with HRG.^{79,80} If heme binding to the putative binding site of HRP II were to occur via bis-axial coordination, the formation of hemozoin could not proceed because the protein would cap the heme substrate, sterically blocking the propionic side chain of the heme moiety from dimerizing with another heme molecule. Moreover, under the acidic conditions that exist in the digestive vacuole as well as those mimicked *in vitro* (pH 4.8-5.2), a histidine-heme axial ligation is improbable since the imidazole of histidine is likely protonated, given the pKa of the histidine side chain has a value of 5.8. Such results are consistent with the pH dependent formation of hemozoin, as well as with the abiological growth pattern of this biomineral.

Given that the current structural model of hemozoin is a hydrogen bonded network of heme dimers, the propagation of β -hematin must permit translational growth only after heme molecules occupy two proximal sites on HRP II. A linear

peptide of the same 9-mer sequence, Ala-His-His-Ala-His-His-Ala-Ala-Asp, bound heme, but failed to mediate the formation of hemozoin. This result, along with a previous study in which a hexapeptide, Ala-His-His-Ala-Ala-Asp, and its multimers failed to promote the formation of hemozoin,⁴⁹ demonstrates the necessity of geometric and steric constraints in the formation of the malaria pigment. The BNTs, because of the designed scaffold, possess not only the correct spatial orientation for heme binding, but also a surface for which to align the heme units in a temporal fashion so as to accommodate the formation of an iron-carboxylate bond in which the iron of one heme moiety is linked to a propionate group of another, propagating hemozoin formation by providing the necessary translational symmetry.

In fact, circular dichroism (CD) studies supported this assessment (**Figure 2.14**). The CD spectra of the linear peptide models (AHHAHHAAD and (AHHAHHAAD)₂), which failed to support the formation of hemozoin, were identified as unordered or random-coiled structures (**inset of Figure 2.14**). The AHHAHHAAD peptide possessed a negative band at 201 nm, maintaining a negative CD signal throughout the remainder of the spectrum. The 18-mer model peptide, (AHHAHHAAD)₂, had a negative band red-shifted to 198 nm, but the CD signal crossed over into the positive region of the spectrum at 217 nm. The BNT models, which supported the aggregation of β -hematin, exhibited more definitive secondary structure above the 210 nm portion of the CD spectra. BNT I shared spectral markers with the linear 18-mer peptide, (AHHAHHAAD)₂, by also possessing a negative band at 198 nm and a positive crossover at 217 nm, but this dendrimer also had a

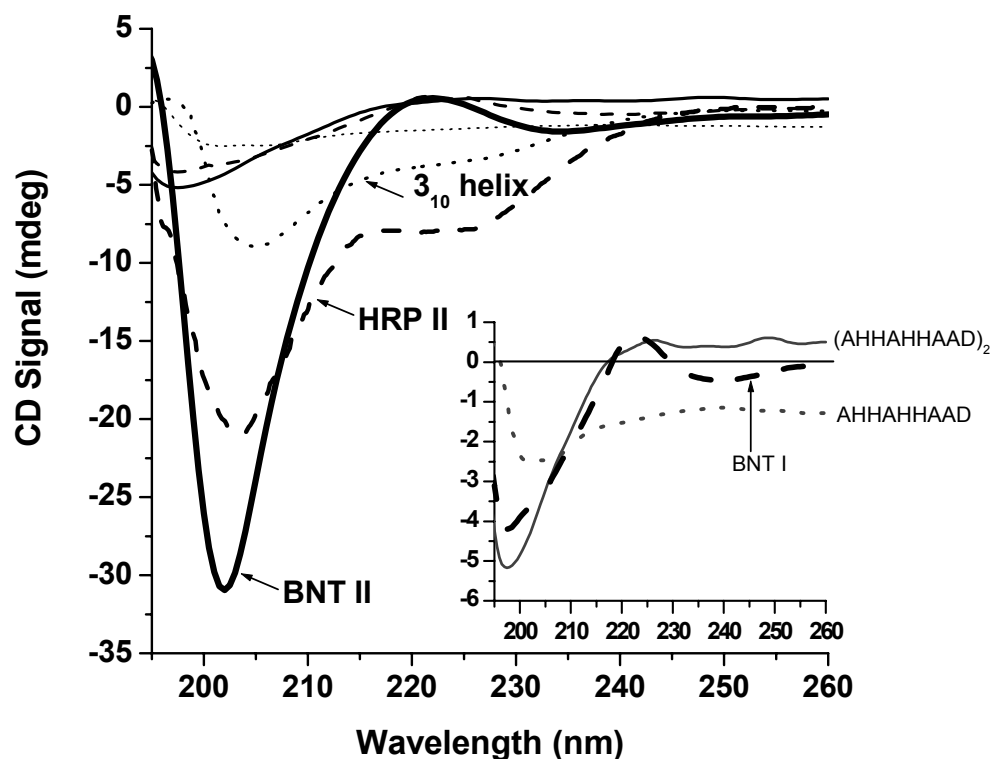


Figure 2.14. Circular dichroism spectra of the nucleating domain peptides, native HRP II from *Plasmodium falciparum* and a 3₁₀ helix. (.....) peptide AHHAHHAAD, (—) peptide (AHHAHHAAD)₂, (---) BNT I, (—) BNT II, (.....)3₁₀ helix, and (....) HRP II. Peptides lacking a definitive secondary structure are highlighted in the inset. The spectra of a 3₁₀ helix and HRP II are reproduced from references 80 and 73 respectively.

positive shoulder at 222 nm with an additional crossover at 230 nm into a deeper negative minimum at 240 nm, suggestive of a higher ordered structure. Such minor secondary structure of the BNT I template could further explain that while the model did support the template mediated formation of hemozoin, β -hematin aggregation according to the assay conditions was not above the baseline levels of 1-2 nmoles unless the concentration of the template was increased. The CD spectrum of BNT II differed, with a predominant negative blue-shifted band at 202 nm, a crossover band at 219 nm, a slightly positive shoulder at 222 nm, and a negative minimum at 234 nm.

Early conformational studies of HRP II from both *Plasmodium falciparum*⁸¹ and *Plasmodium lophurae*⁸² described similar CD spectral markers. Both of these histidine-rich proteins had relatively little absorbance above 250 nm due to its low occurrence of aromatic amino acids, and the majority of the spectrum maintained a near negative CD signal except for the predominant sharp negative band at ~200 nm, which is attributable to the high occurrence of histidine residues. Specifically, the spectrum of the HRP protein from *Plasmodium lophurae* had a deep negative band at 207 nm, a crossover band at 215 nm and a positive band at 222 nm; while the CD spectrum of the species *Plasmodium falciparum* was less well-resolved, possessing a deep negative band at 200 nm, with a possible shoulder at 225 nm that was less discernable.

The CD spectrum of *Plasmodium falciparum* HRP II was further detailed by Lynn *et al.* who examined the effects of pH on the conformation of the recombinant form of the protein (rHRP II).⁷⁴ Despite lacking a good representative CD spectrum of a 3-10 helix, the authors concluded the signature deep negative band at 200 nm, normally ascribed to random-coil/unordered structures, was anything but unordered, due to the unique stability of this protein over a broad range of pHs, ionic strengths, and temperatures, as well as its anomalous movement on SDS gel. Instead the authors compared the CD spectrum of the protein to that of polyproline in trifluoroethanol (TFE), which forms a left-handed helix with three residues per turn forming a polyproline type II secondary structure (PPII), possessing a strong negative band at 206 nm and a weak positive band at 226 nm.

Without the crystal structure of HRP II, the unambiguous characterization of the conformation of the protein cannot be determined by CD data alone. Despite this, and the fact the high histidine content of HRP proteins masks the behavior of the peptide backbone in the low ultraviolet region of the spectra, the exact conformation of the protein and our model peptides (which have also not been successfully crystallized) is not imperative for the interpretation of our experimental data. **Our explanation will instead focus on the fact that in either conformation (a 3-10 helix is right-handed, while a polyproline II type secondary structure forms a left-handed helical turn), the helix has three residues per turn, which establishes a hydrophobic face of alanine residues based on the sequence of the amino acids examined.**

By comparison, the CD spectrum of our BNT II model suggests the peptide is conformationally similar to the rHRP II reported by Lynn *et al*, having a similar deep negative band at 202 nm and a shoulder at ~ 220 nm. Despite the inherent differences in secondary structure that can occur in a globular protein like HRP II which has a molecular weight of 35 kD, the local conformation of our ~8,000 g/mole dendrimeric peptide is strikingly similar. Since our linear peptide models lack any appreciable CD signal, the MAPS core must contribute to the overall secondary structure of the peptide. The construct rigidity has not been examined in detail in the literature and the few examples of circular dichroism spectroscopy of MAPS dendrimers fail to address this very issue, insinuating that local conformation is a result of the precise arrangement of amino acid residues. Upon consideration, the contribution of the

MAPS core to the overall CD spectrum may not be its structural orientation, when considering all of the plausible interactions that could occur along the peptide branches of the dendrimer itself. Discussion focused on the dendrimeric core contributions to inherent stabilization will be introduced later.

In all, Ziegler *et al.* established the bionucleating peptide dendrimers, BNT I and BNT II, as the first synthetic model histidine-rich protein analogs based on similar chemical activities. His work is highlighted in **Table 2.2** and **Figures 2.5-2.13**, added solely for the purposes of establishing the background information pertinent to our biomineralization studies. In particular, BNT II bound heme with similar efficiency to HRP II (12 eq. vs 17 eq.) and was capable of mediating the formation of hemozoin. Known antimalarials were also capable of inhibiting the template mediated formation hemozoin with IC_{50} 's within the same order of magnitude as those tested against the native protein. Now, with the establishment of a conformational similarity between the BNTs and HRP II, the nucleating domain AHHAHHAAD may be scrutinized as a template for the biomineralization of hemozoin, where inherent changes in the amino acid sequence of the nucleating domain may elicit changes in activity based on imposed changes in conformation.

2.5. Site-Directed Mutagenesis Studies of the HRP II Mimic

2.5.1. Mutants of BNT II

With the establishment of BNT II as a functional peptide mimic for HRP II, we elucidated the role of the nucleating domain per active site amino acid through






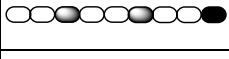
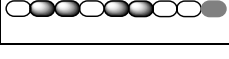
synthetic site-directed mutagenesis studies. Our first effort included synthesizing the alternate hypothetical nucleating domain Ala-His-His-Ala-Ala-Asp-Ala-His-His, to permit a direct comparison of the two postulated hemozoin templating sequences. In comparison to BNT II, swapping the trimer Ala-His-His to the end of the nucleating domain will reveal information as to both the binding and nucleating capabilities of the template when the trimeric Ala-His-His repeat is interrupted.

To decrease the exhaustive number of mutants that could possibly be synthesized, our efforts focused on targeting amino acids that were physiologically relevant to native HRP II. Preliminary results by Ziegler *et al.* in our laboratory already confirmed that metal recognition sites were not essential for substrate binding. Additionally, since polyhistidine failed to nucleate the formation of hemozoin, alanine may be a critical spacer in the 9-mer templating domain, serving to precisely orient substrate recognition motifs. The binding data also suggested that template/substrate recognition is most likely through π - π stacking and/or electrostatic interactions, thus histidine and aspartic acid could be critical residues.

Initial syntheses were confined to the six mutants below (**Table 2.3**). The mutants were named arbitrarily, with **BNT IIA** being the first alternate peptide mimic of HRP II. Once initial studies, which included substrate binding activities and the *in vitro* heme aggregation assay, indicated that the amino acid sequence of BNT II was the most probable nucleating domain within the sequence of HRP II (**see Chapter 3 for experimental results**), all other peptide mutations were envisioned with regards to the Ala-His-His-Ala-His-His-Ala-Ala-Asp sequence. Mutant **BNT IIC** assessed if

heme binding was dominated solely by histidine residues, by mutating the His-His repeat with alanine residues. **BNT IID** evaluated the necessity of a conserved aspartic acid residue, by replacing it with a nonpolar alanine. Mutants **BNT IIX** and **BNT IIY** probed the histidine binding sites in terms of the relative positioning of the amino acid on the putative nucleating face. **BNT IIX** examined conservation of the lead histidine in the Ala-His-His repeat unit, mutating the histidine at positions three and six with alanine, while **BNT IIY** explored the reverse order, mutating the histidine at positions two and five with alanine, now conserving the third and sixth residues in the Ala-His-His-Ala-His-His-Ala-Ala-Asp nucleating domain. Mutant **BNT IIZ** again surveyed the role of the highly conserved aspartic acid by mutating the ninth position with lysine, this time not exploring the effect of polarity, but the effect of charge, since lysine will be deprotonated under the experimental conditions.

Table 2.3. Site-directed mutagenesis of the 9-mer sequence of BNT II. *denotes a mutated amino acid residue. The shaded template was insoluble under the experimental conditions employed (100 mM acetate buffer, pH 4.8).

BNT II		Ala	His	His	Ala	His	His	Ala	Ala	Asp
BNT IIA						Ala*	Asp*		His*	His*
BNT IIC			Ala*	Ala*		Ala*	Ala*			
BNT IID										Ala*
BNT IIX				Ala*			Ala*			
BNT IIY			Ala*			Ala*				
BNT IIZ										Lys*

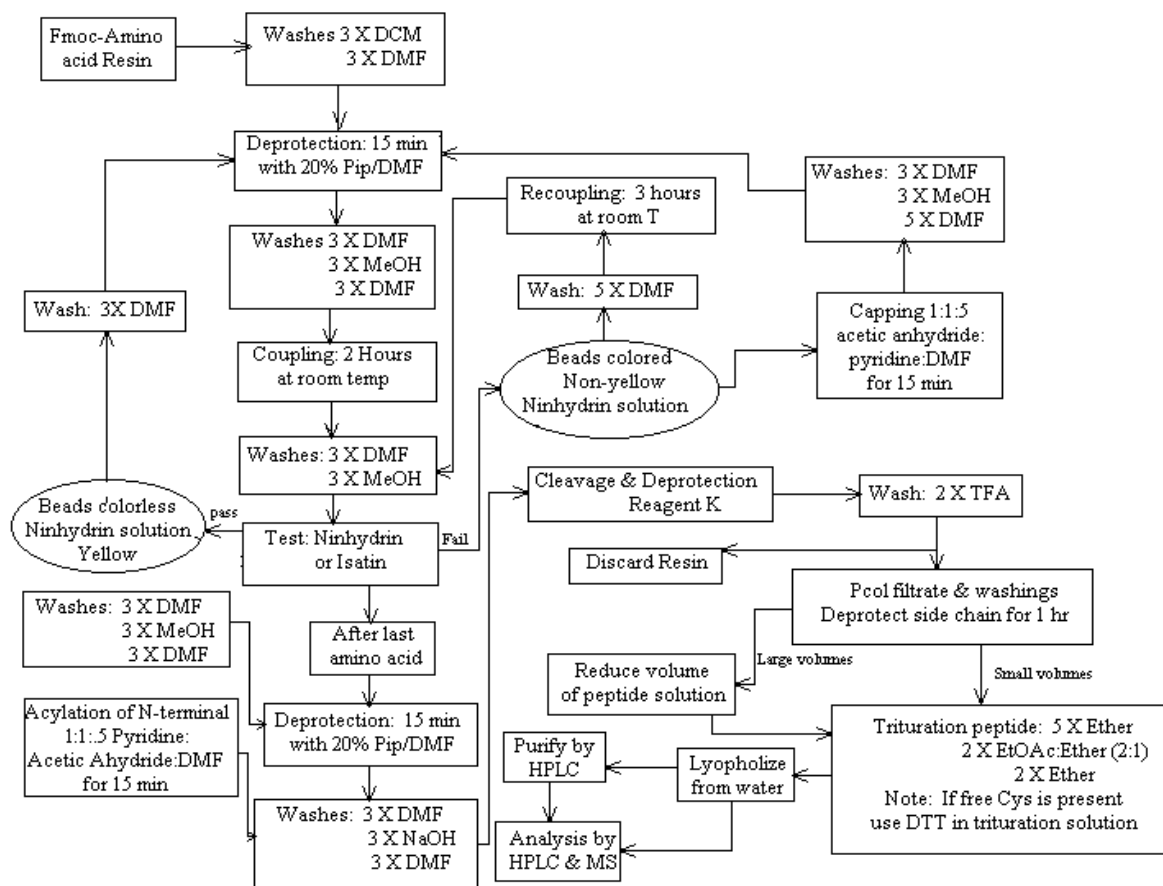
2.5.2. Synthesis of Bionucleating Templates (BNTs)

2.5.2a. Reagents

All Fmoc-4-branch MAPS resins and Fmoc-amino acids [N- α -Fmoc-L-alanine (Fmoc-Ala-OH), N- α -Fmoc-L-aspartic acid α -t-butyl ester (Fmoc-Asp-OtBu), N- α -Fmoc-N-im-trityl-L-histidine (Fmoc-His(Trt)-OH), N- α -Fmoc-N- ϵ -4-methyltrityl-L-lysine (Fmoc-Lys(Mtt)-OH)] were purchased from AnaSpec, Inc. (San Jose, CA) and kept at the recommended storage conditions until used. N,N'-diisopropylethylamine (DIEA) and 2-(1H-benzotriazole-1-yl)-1,1,3,3-tetramethyluronium hexafluorophosphate (HBTU) were obtained from Advanced ChemTech (Louisville, KY). BioReagent grade methanol (MeOH), dimethylformamide (DMF), dichloromethane (DCM), piperidine, and N-hydroxybenzotriazole (HOBt), sequencing grade pyridine, HPLC grade acetonitrile (ACN), and acetic anhydride were purchased from Fisher Scientific (Pittsburgh, PA). Trifluoroacetic acid (99.9%) (TFA) and triisopropyl silane (TIS) were acquired from Sigma-Aldrich Chemicals (Milwaukee, WI).

2.5.2b. Automated Synthesis of Templates

The dendrimeric templates were synthesized on an Advanced ChemTech Model 90 Peptide Synthesizer according to standard continuous flow Fmoc-solid phase synthesis protocols with minor modifications (**Scheme 2.1**). Detailed automated programming was generously supplied by AnaSpec, Inc. (**Appendix I, pages A-1 thru A-4**). Approximately 250 mg. of Fmoc-4-branch MAPS resin was swelled in DCM for fifteen minutes followed by an initial Fmoc-deprotection by



Scheme 2.1. Standard Fmoc-peptide synthesis protocol.

treatment with 20% piperidine in DMF. Coupling cycles were accomplished with 4-fold excess (vs. overall loading capacity of the resin) of activated amino acid for 1 hour, using Fmoc-amino acid/HBTU/HOBt/DIEA in a 1:1:1:2 mole ratio. The peptidyl resin was then washed 3X with 12.5 mL of DMF, 3X with 12.5 mL MeOH, and again 3X with 12.5 mL of DMF. Subsequent deprotections were carried out by two successive treatments of 20% piperidine in DMF (10 min. and 40 min. cycles), followed by the same washing protocol listed above: DMF, MeOH, DMF. Acylation of the N-terminal amines was accomplished by exposing the peptidyl resin to 20 mL

of 1:1:5 acetic anhydride/pyridine/DMF for 30 min. Upon acylation the peptidyl resin was washed 3X with 12.5 mL DMF and then 5X with 12.5 mL of MeOH. The resin was collected on a finely sintered glass frit, washed with additional MeOH, dried by vacuum filtration and then stored at -4 °C until cleavage occurred.

2.5.2c. Cleavage and Purification of BNTs

All branched peptides were cleaved at room temperature by mixing 1.5 mL of cleavage cocktail consisting of 95% TFA / 5% TIS per 100 mg. of peptidyl resin. The capped reaction mixture was swirled by hand every ½ hour until 4 hours had elapsed, after which the resin was filtered onto a finely sintered glass frit. The cleaved resin was washed with 5X the volume of TFA, based on the initial volume of cleavage cocktail used. The peptide was then precipitated from the filtrate by the dropwise addition of 8X the volume of cold diethyl ether, based on the volume of TFA wash. The precipitated peptide was then centrifuged on a Sorval GLC-1 or Beckman Coulter Allegra 21R swinging bucket rotor for fifteen minutes. The ether layer was decanted and the peptide pellet washed an additional three times with 30 mL of ether. The peptide pellet was then resuspended in water (v/v with 0.1% TFA) and minimal acetonitrile (v/v with 0.1% TFA, <20% total volume) and lyophilized on a LabConco FreeZone 4.5L Benchtop Freeze Dry System (Model 77500, Kansas City, MO).

Each branched peptide was purified by reversed phase high-performance liquid chromatography (HPLC) on a Waters 600 HPLC equipped with a Waters 996 Photodiode Array Detector using a Waters Nova-Pak C₁₈ 300 Å 15 µm

(3.9 X 150 mm) column before scaling for semi-preparative or preparative HPLC purifications. Briefly approximately 1 mg. of peptide was dissolved in 1 mL of water (v/v with 0.1% TFA) and filtered through a Millex-GV 0.22 μm low protein binding Durapore PVDF membrane. A 20 μL sample was injected onto the column equilibrated with water (v/v with 0.1% TFA) at 0.5 mL/min. A linear gradient of 100% water (v/v with 0.1% TFA) to 50% CH_3CN (v/v with 0.1% TFA) was performed over thirty minutes for initial purification. The gradient was then optimized for each BNT.

Analytical HPLC gradients conditions were then scaled for semi-preparative or preparative purification according to the equations listed in **Figure 2.15**. Semi-preparative peptide purification was completed on a Waters 600 HPLC equipped with a Waters 996 Photodiode Array Detector using a PrepLC™ 25 mm Radial Compression Module compressed with isopropanol. The module in series with a PrepLC™ 25 mm extension tube held two Delta-Pak™ C_{18} 300 \AA 15 μm (25 x 100 mm) columns. The initial column was fitted with Delta-Pak™ C_{18} 300 \AA 15 μm Guard-Pak™ (25 x 10 mm). All other semi-preparative and preparative HPLC was performed on a Waters Prep LC 4000 equipped with a Waters 2487 Dual Wavelength UV/Vis Detector using a Delta-Pak™ C_{18} 300 \AA 15 μm (30 x 300 mm) column. All MAPS peptides were detected at a wavelength of 210 nm.

Flow rate at constant linear velocity and equal column length

$$F_{\text{prep}} = F_{\text{anal}} \times \frac{(D_{\text{prep}})^2}{(D_{\text{anal}})^2}$$

Flow rate at different column length

$$F_{\text{prep}} = F_{\text{anal}} \times \frac{L_{\text{prep}}}{L_{\text{anal}}} \times \frac{(D_{\text{prep}})^2}{(D_{\text{anal}})^2}$$

Sample Load

$$M_{\text{prep}} = M_{\text{anal}} \times \frac{L_{\text{prep}}}{L_{\text{anal}}} \times \frac{(D_{\text{prep}})^2}{(D_{\text{anal}})^2}$$

Flow Rate

$$t_{\text{prep}} = t_{\text{anal}} \times \frac{L_{\text{prep}}}{L_{\text{anal}}} \times \frac{(D_{\text{prep}})^2}{(D_{\text{anal}})^2} \times \frac{F_{\text{anal}}}{F_{\text{prep}}}$$

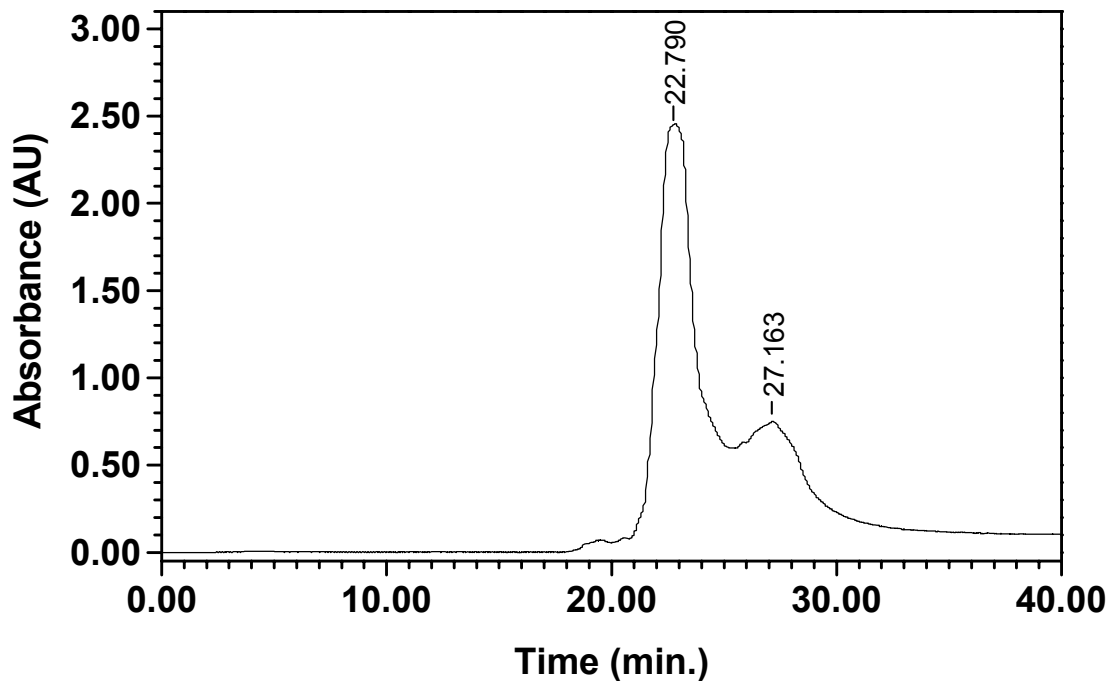
Gradient Delay Volume

$$T_d = \frac{V_d}{F_{\text{prep}}} \times \left(\frac{V_{\text{prep}}}{V_{\text{anal}}} - 1 \right)$$

F_{anal} = analytical flow rate
 F_{prep} = preparative flow rate
 D_{anal} = diameter of analytical column
 D_{prep} = diameter of preparative column
 L_{anal} = length of analytical column
 L_{prep} = length of preparative column
 M_{anal} = analytical sample load
 M_{prep} = preparative sample load
 t_{anal} = gradient run time for analytical column
 t_{prep} = gradient run time for preparative column
 V_d = delay volume of instrument
 V_{anal} = volume of analytical column
 V_{prep} = volume of preparative column

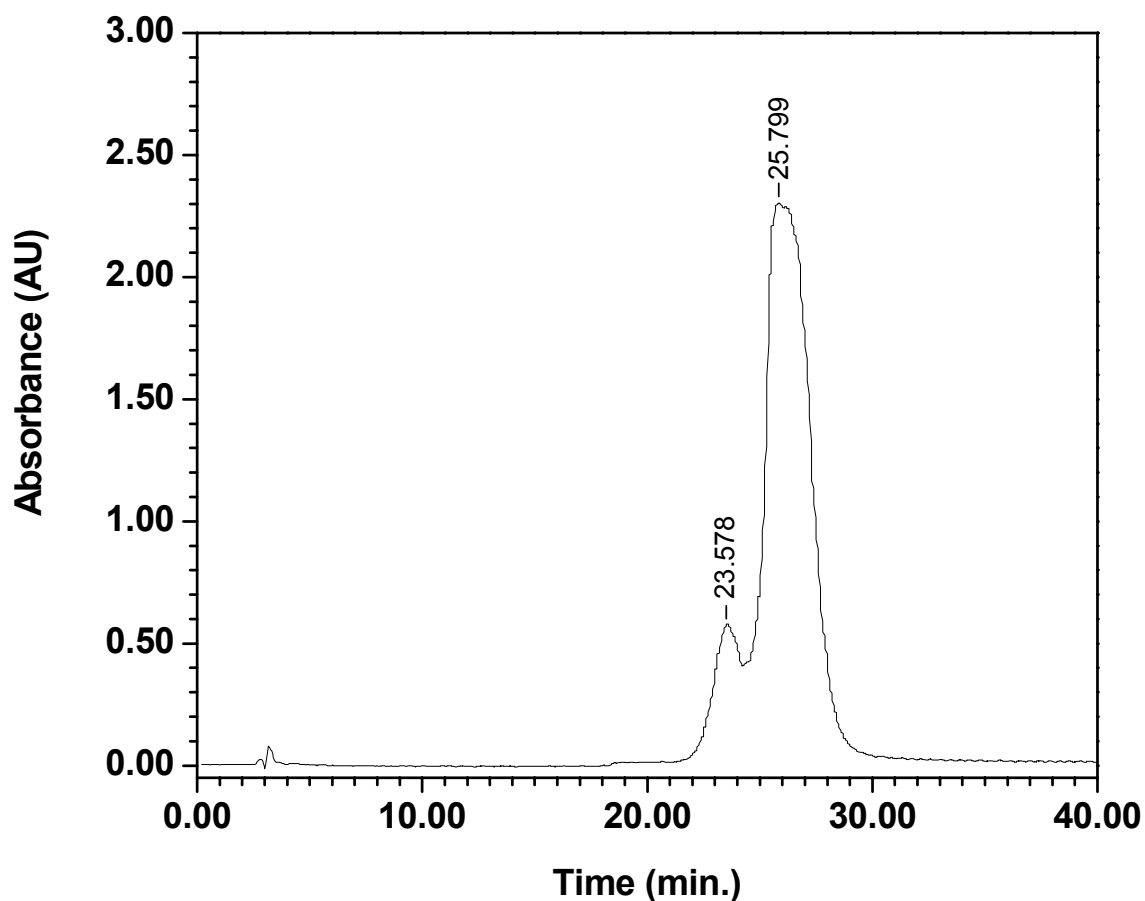
Figure 2.15. Scale-up equations for HPLC peptide purification.

Specific flow rates and gradient conditions for each BNT are listed below with a representative sample chromatogram (Figures 2.16 - 2.21). BNT IIC was insoluble in aqueous media, eluting with 100% CH₃CN (v/v with 0.1% TFA) and therefore not a viable mutant for analysis according to our experimental conditions (pH 4.8).



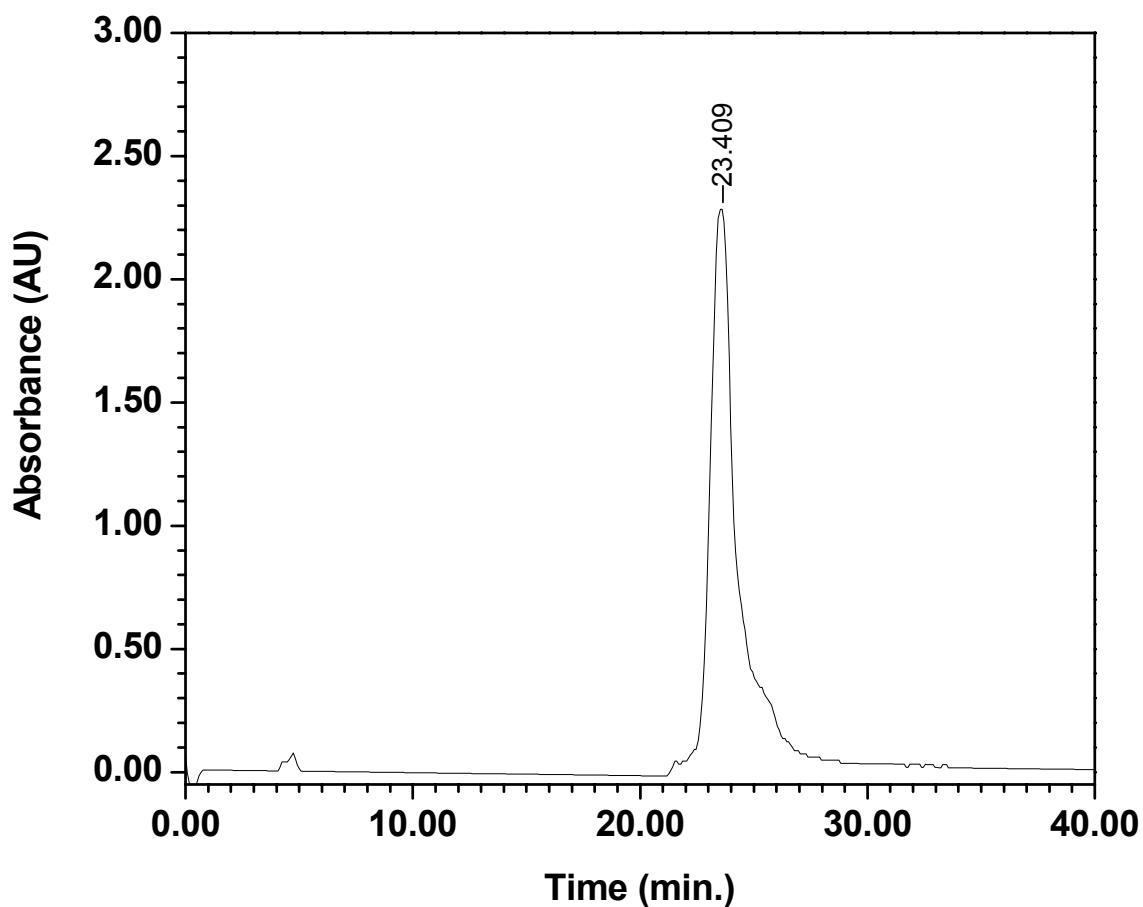
Time (min.)	Flow Rate (mL/min.)	%A	%B
0.00	13.70	100	0
11.50	13.70	100	0
21.50	13.70	70	30
46.50	13.70	50	50

Figure 2.16. Semi-preparative HPLC chromatogram of BNT II and corresponding gradient table. %A = H₂O with 0.1% TFA. %B = ACN with 0.1% TFA. BNT II was purified using a Waters 600 HPLC equipped with a PrepLC™ 25 mm Radial Compression Module with two Delta-Pak™ C₁₈ 300 Å 15 µm (25 x 100 mm) columns run in series. BNT II was the major peak eluting from ~21.5 – 24.0 min. as determined by amino acid analysis.



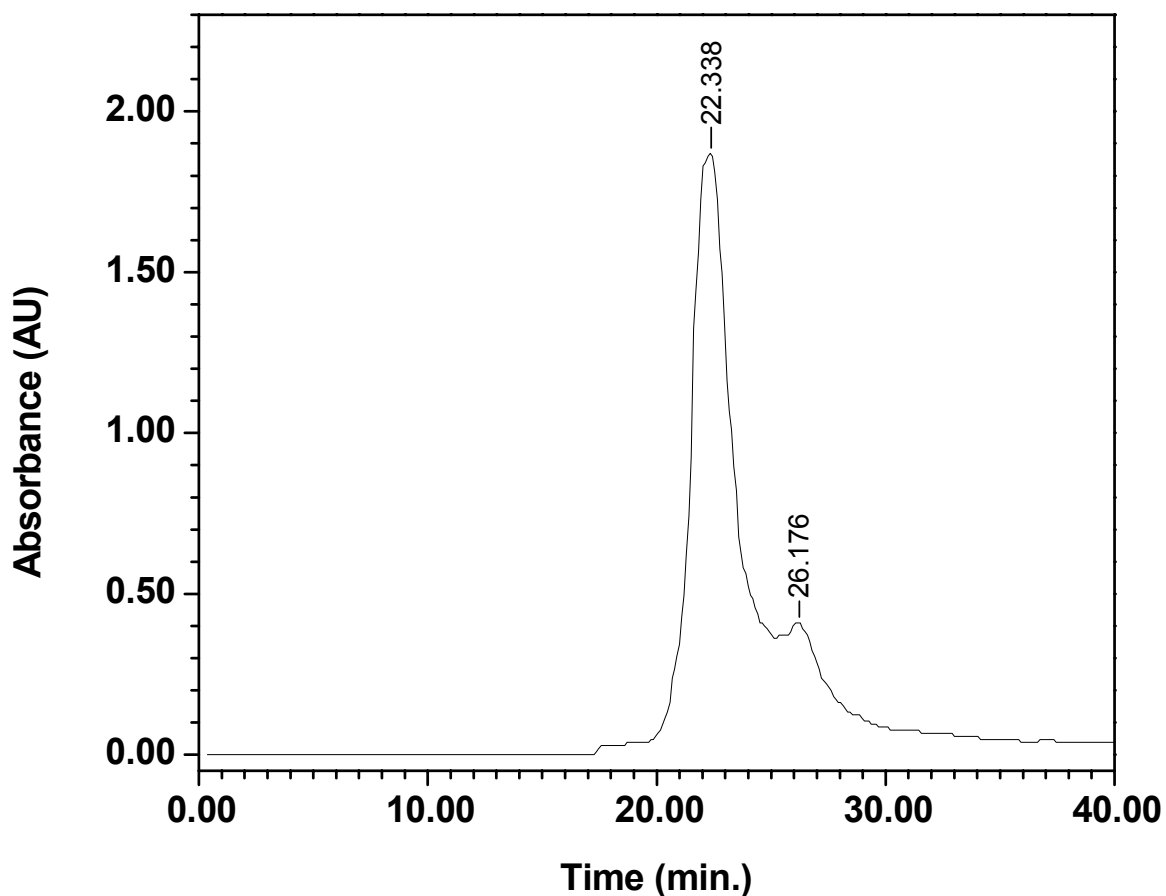
Time (min.)	Flow Rate (mL/min.)	%A	%B
0.00	13.70	90	10
11.50	13.70	90	10
51.50	13.70	80	20

Figure 2.17. Semi-preparative HPLC chromatogram of **BNT IIA** and corresponding gradient table. %A = H₂O with 0.1% TFA. %B = ACN with 0.1% TFA. BNT IIA was purified using a Waters 600 HPLC equipped with a PrepLC™ 25 mm Radial Compression Module with two Delta-Pak™ C₁₈ 300 Å 15 μm (25 x 100 mm) columns run in series. BNT IIA was the major peak eluting from ~24.8 – 29.5 min. as determined by amino acid analysis.



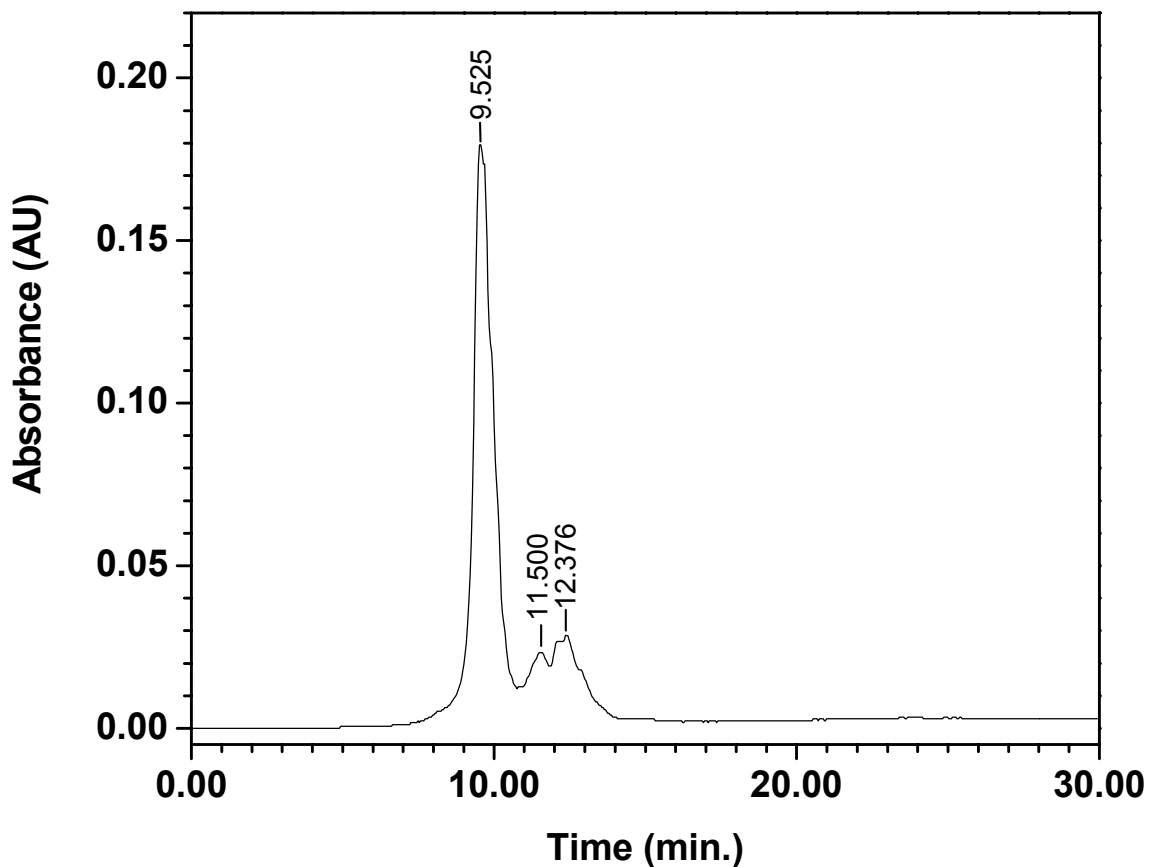
Time (min.)	Flow Rate (mL/min.)	%A	%B
0.00	17.50	100	0
15.75	17.50	100	0
20.75	17.50	70	30
30.75	17.50	65	35
50.00	17.50	60	40

Figure 2.18. Semi-preparative HPLC chromatogram of **BNT IID** and corresponding gradient table. %A = H₂O with 0.1% TFA. %B = ACN with 0.1% TFA. BNT IID was purified using a Waters 600 HPLC equipped with a PrepLC™ 25 mm Radial Compression Module with two Delta-Pak™ C₁₈ 300 Å 15 µm (25 x 100 mm) columns run in series. BNT IID was the major peak eluting from ~22.6 – 24.5 min. as determined by amino acid analysis.



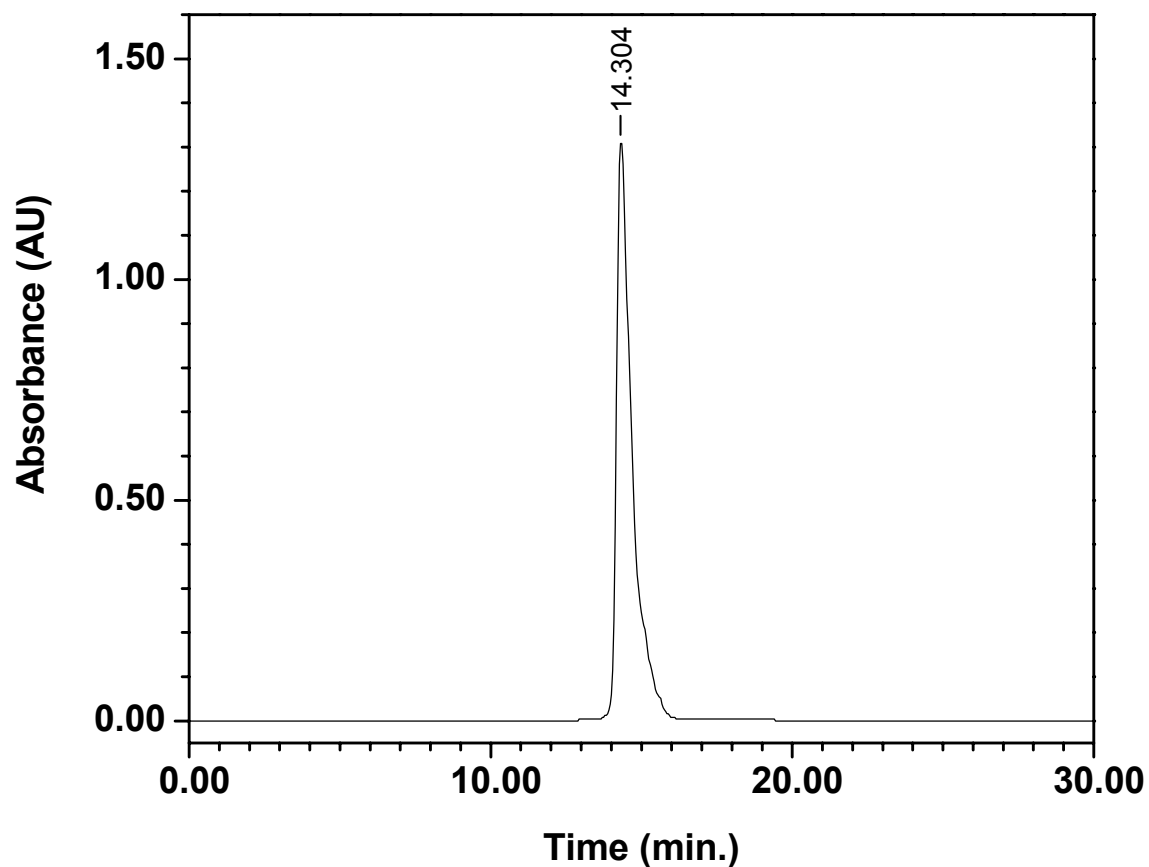
Time (min.)	Flow Rate (mL/min.)	%A	%B
0.00	19.50	100	0
11.50	19.50	100	0
21.50	19.50	70	30
36.50	19.50	50	50

Figure 2.19. Semi-preparative HPLC chromatogram of **BNT IIX** and corresponding gradient table. %A = H₂O with 0.1% TFA. %B = ACN with 0.1% TFA. BNT IIX was purified using a Waters 600 HPLC equipped with a PrepLC™ 25 mm Radial Compression Module with two Delta-Pak™ C₁₈ 300 Å 15 µm (25 x 100 mm) columns run in series. BNT IIX was the major peak eluting from ~20.8 – 24.1 min. as determined by amino acid analysis.



Time (min.)	Flow Rate (mL/min.)	%A	%B
0.00	50.00	100	0
5.00	50.00	90	10
10.00	50.00	60	40
20.00	50.00	50	50
30.00	50.00	50	50

Figure 2.20. Preparative HPLC chromatogram of **BNT IIY** and corresponding gradient table. %A = H₂O with 0.1% TFA. %B = ACN with 0.1% TFA. BNT IIY was purified using a Waters Prep LC 4000 with a Delta-Pak™ C₁₈ 300 Å 15 μm (30 x 300 mm) column. BNT IIY was the major peak eluting from ~8.9 – 10.4 min. as determined by amino acid analysis.



Time (min.)	Flow Rate (mL/min.)	%A	%B
0.00	50.00	100	0
10.00	50.00	90	10
30.00	50.00	50	50

Figure 2.21. Preparative HPLC chromatogram of **BNT IIZ** and corresponding gradient table. %A = H₂O with 0.1% TFA. %B = ACN with 0.1% TFA. BNT IIZ was purified using a Waters Prep LC 4000 with a Delta-Pak™ C₁₈ 300 Å 15 μm (30 x 300 mm) column. BNT IIZ was the major peak eluting from ~14.0 – 15.6 min. as determined by amino acid analysis.

After HPLC purification, all peptides were analyzed for purity based on amino acid analysis either performed by AnaSpec, Inc. (San Jose, CA) or the Vanderbilt Peptide Sequencing and Amino Acid Analysis Shared Resource (Nashville, TN) except for template BNT IIA, which was previously analyzed at Boston College by collaborator Richard T. Chang. From the amino acid analysis results below (**Table 2.4**), all templates synthesized in house were greater than 98% pure after HPLC purification and lyophilization (BNT IIA synthesized and purified at Boston College was 94.5% pure). For amino acid analysis, the MAPS core adds 0.75 lysine residues per chain ($0.75 \times 4 = 3$ lysine residues) and 0.25 alanine residues per chain ($0.25 \times 4 = 1$ alanine residue) for the 4-branch peptide.⁸³ For the bionucleating templates BNT II, BNT IIC, BNT IID, and BNT IIZ, the experimental values for lysine are typically higher than the theoretical values due to the high signal from the

Table 2.4. Amino acid analysis of BNT II and BNT mutants. Experimental values are in bold text while the predicted values are indicated in parentheses. ^a – *lysine values are high due to high signal from histidine.* ^b – *aspartic acid value is high and low due to high signal from alanine.* ^c - *alanine is low.*

Template	BNT II	BNT IIA	BNT IIC	BNT IID	BNT IIX	BNT ILY	BNT IIZ
<i>Amino Acid</i>							
Ala	32.90 (33)		64.87 (65)	40.88 (41)	48.81 (49)	47.81^c (49)	32.92 (33)
His	31.90 (32)		----	31.86 (32)	16.05 (16)	15.91 (16)	31.60 (32)
Asp	8.00 (8)		7.80^b (8)	----	8.14^b (8)	8.08 (8)	---
Lys	3.14^a (3)		3.33^a (3)	3.26^a (3)	3.00 (3)	3.03 (3)	11.14^a (11)
% purity	99.55	94.55	99.14	99.31	99.52	98.17	99.19

histidine residues. BNT IIX and BNT IY with only 16 histidine residues yielded lysine values (3.00 and 3.03 respectively) more closely correlated to the actual value than those mutants that had double the number of histidine residues. In addition to the interference resulting from the high number of histidine residues, the high number of alanine residues also masks the aspartic acid signals as seen in BNT IIC and BNY IIX.

Mass spectral analyses were performed on both MALDI-TOF and electrospray ionization (ESI) mass spectrometers at both the University of Pittsburgh Biotechnology Center (Pittsburgh, PA) and at Vanderbilt University (Nashville, TN), but the results were inconclusive. ESI chromatograms were typically very broad in both positive and negative ionization modes, while the MADLI-TOF chromatograms exhibited only those peaks associated with the matrix, despite the array of matrix components used. Such results are not uncharacteristic of MAPS peptides, since mass spectral analyses typically yield poor, unresolved results. MALDI-TOF and electrospray ionization data was obtained for BNT II (**Figure 2.22**) and BNT IIA (**Figure 2.23**), respectively, which suggests that stabilization may be sequence dependent, since both BNT II and BNT IIA have the same number and type of amino acids.

2.6. BNT II and Mutant Modeling

At the outset of any biomineralization process, an organic matrix with a functionalized surface must be arranged within a reaction environment.⁸⁴ Next, interfacial recognition between the inorganic mineral and organic substrate occurs via

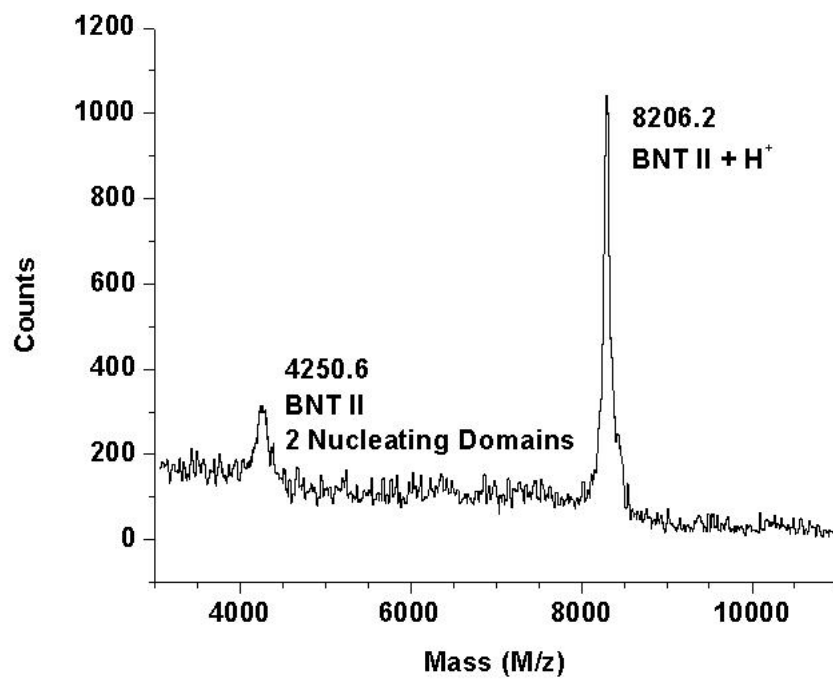


Figure 2.22. MALDI-TOF mass spectrometry for BNT II.

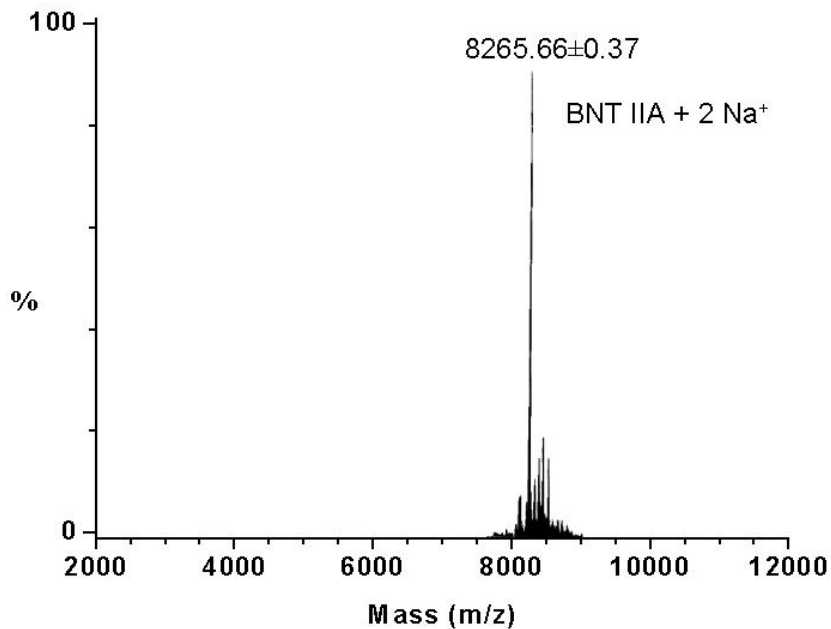


Figure 2.23. Electrospray ionization mass spectrometry for BNT IIA in the positive ionization mode.

complementarity of lattice geometry, topography, spatial symmetry, stereochemistry, polarity, electrostatic interactions, or a combination of the above.⁴² Afterward, the templated two-dimensional biomineral undergoes vectoral expansion in three dimensions, having its orientation and growth specifically directed by the template in such that crystalline size, shape, and morphology are often constrained to the physical and compositional domain of the architecture. Finally, during the last stage of biomineralization, additional cellular components participate in the storage, transport and/or removal of the biomineral.

Though the biosynthetic route of hemozoin formation involves the intimate and complex interactions of *Plasmodium falciparum* with a host erythrocyte, β -hematin formation can be paralleled to the four generically classified stages of biomineralization processes. Specifically, before hemozoin formation can begin, the HRP II protein must be localized within the digestive vacuole of *Plasmodium falciparum*. Next, free inorganic heme, a requisite byproduct of the parasitic proteolysis of hemoglobin, interacts with HRP II in such that free heme is sequestered from the digestive organelle. Once in association with the lattice of the HRP II protein, the inorganic iron porphyrin forms a hydrogen-bonded network of dimers with neighboring heme units, constructing the architectural hierarchy of the malaria pigment. Finally during the last stage of β -hematin biomineralization, the malaria parasite transfers the pigment to other sites throughout the host through oxidative burst.

As an aside from hemozoin derived specifically from *Plasmodium falciparum*, it is interesting to note that other species that produce hemozoin, form a material that is compositionally the same as the malaria pigment. The morphological attributes however, often differ since the organic matrix has alterations in the number of repeat units in the protein sequence compared to that of HRP II.

In order to better understand the critical interactions between HRP II and heme in the binding and nucleation of hemozoin, the biomimetic peptide BNT II and its mutants were modeled as potential right-handed 3-10 helices and left-handed polyproline type II helices using the Chemical Computing Group's MOE 2002.03 program (Molecular Operating Environment, Montreal, Canada). This modeling program, nor any other currently available at the time, was capable of evaluating the entire biomimetic template, since the contribution of the dendrimer core could not be accounted for thermodynamically. However, since BNT II shared the spectral features of HRP II described by Pantou⁸¹ as well as Lynn,⁷⁴ the 18-mer peptide branches were modeled in both conformations. Recall however, that neither the 9-mer nor the 18-mer linear peptide models adhered to either conformation (**Figure 2.14**), both having only weak CD signaling throughout the wavelength of interest. This modeling was thus predicated under the assumption that each of the four peptide branches was conformationally independent of the others, having its secondary structure imparted from the MAPS core as well as possible intramolecular interactions.

For the purposes of our investigations, this conformational discrepancy is of little relevance to our research and cannot be resolved until the crystal structure of HRP II is solved. Either way, whether the helix is right or left handed, the imperative information occurs in the fact there are three amino acids per turn of the helix. This imparts similar hydrophobic and putative nucleating faces for which to analyze the nucleation and formation events surrounding hemozoin formation. Each template peptide chain in both the 3-10 and PPII conformations (**Figures 2.24-2.29**) is presented below and will be discussed in depth in the proceeding chapter.

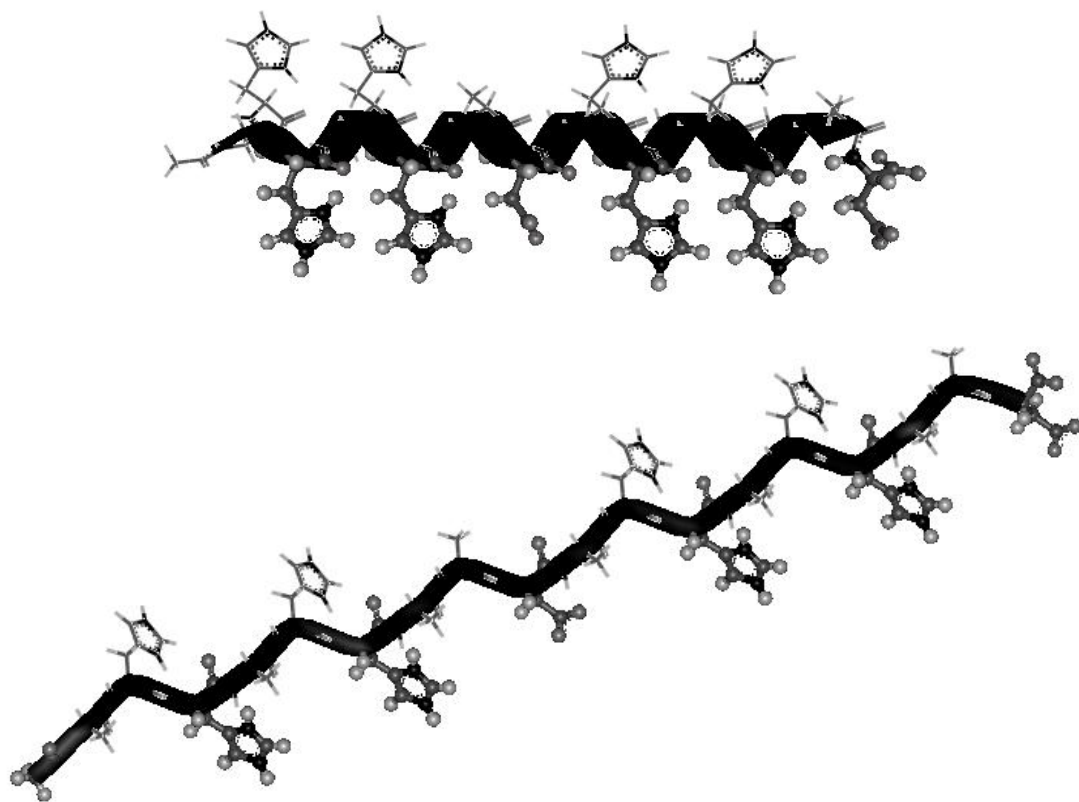


Figure 2.24. The 18-mer peptide branch of **BNT II** modeled as a right-handed 3-10 helix (top) and a left-handed polyproline type II conformation (bottom). The amino acid sequence follows **(Ala-His-His-Ala-His-His-Ala-Ala-Asp)₂**.

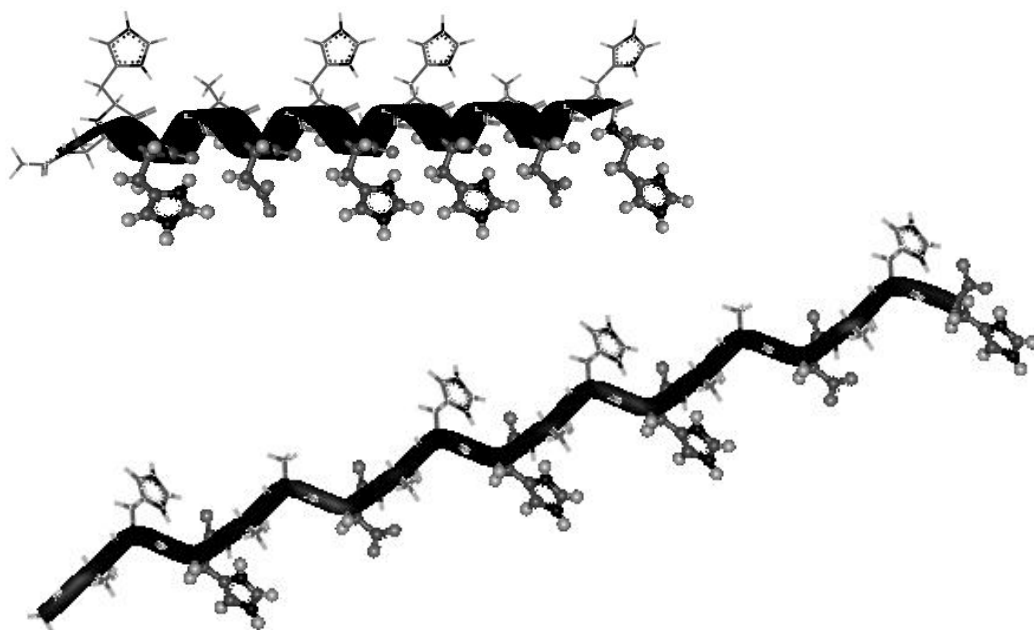


Figure 2.25. The 18-mer peptide branch of **BNT IIA** modeled as a right-handed 3-10 helix (top) and a left-handed polyproline type II conformation (bottom). The amino acid sequence follows **(Ala-His-His-Ala-Ala-Asp-Ala-His-His)₂**.

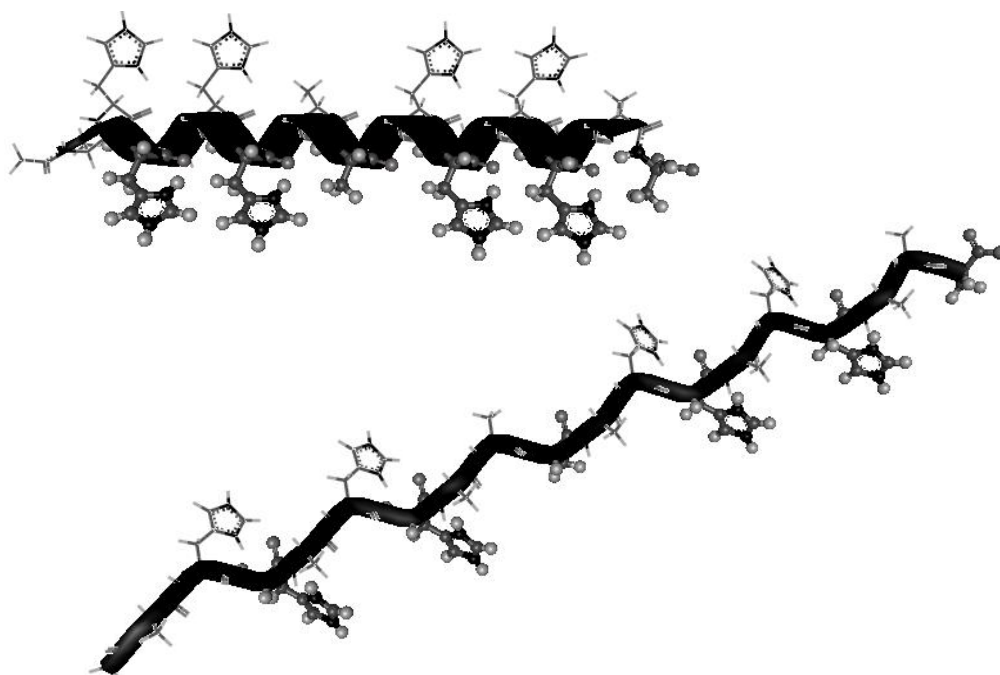


Figure 2.26. The 18-mer peptide branch of **BNT IID** modeled as a right-handed 3-10 helix (top) and a left-handed polyproline type II conformation (bottom). The amino acid sequence follows **(Ala-His-His-Ala-His-His-Ala-Ala-Ala)₂**.

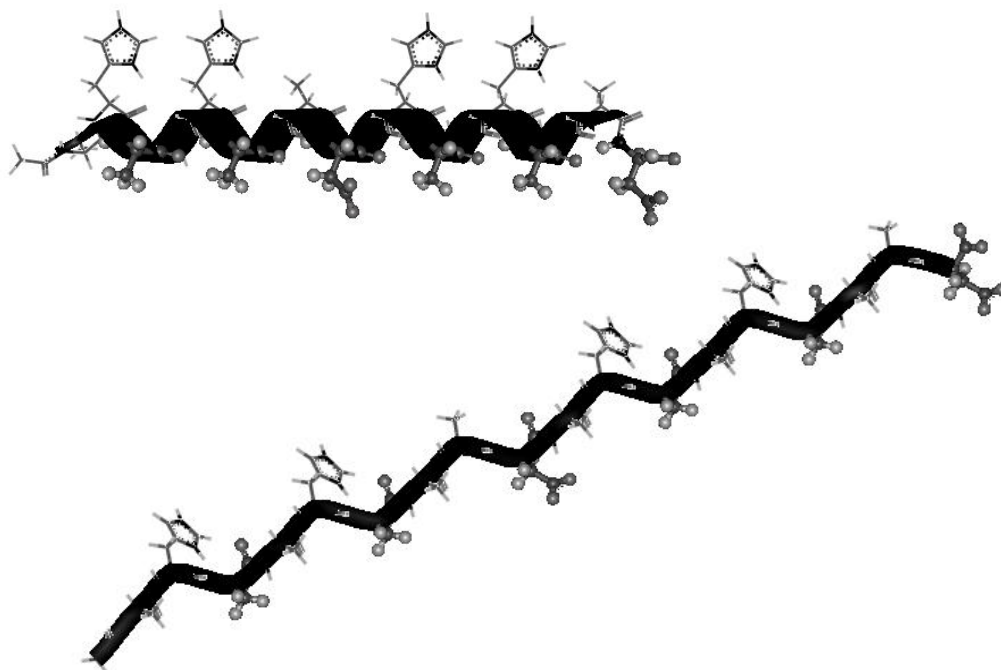


Figure 2.27. The 18-mer peptide branch of **BNT IIX** modeled as a right-handed 3-10 helix (top) and a left-handed polyproline type II conformation (bottom). The amino acid sequence follows **(Ala-His-Ala-Ala-His-Ala-Ala-Ala-Asp)₂**.

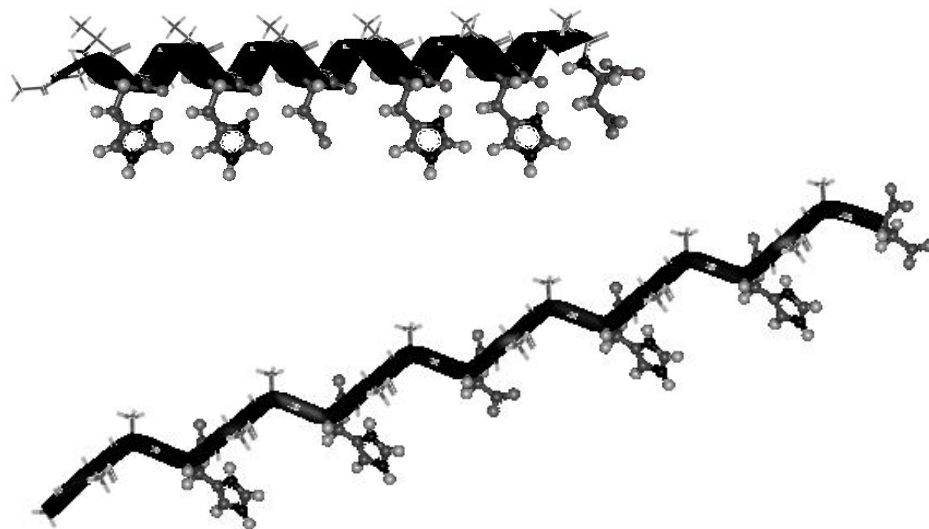


Figure 2.28. The 18-mer peptide branch of **BNT ILY** modeled as a right-handed 3-10 helix (top) and a left-handed polyproline type II conformation (bottom). The amino acid sequence follows **(Ala-Ala-His-Ala-Ala-His-Ala-Ala-Asp)₂**.

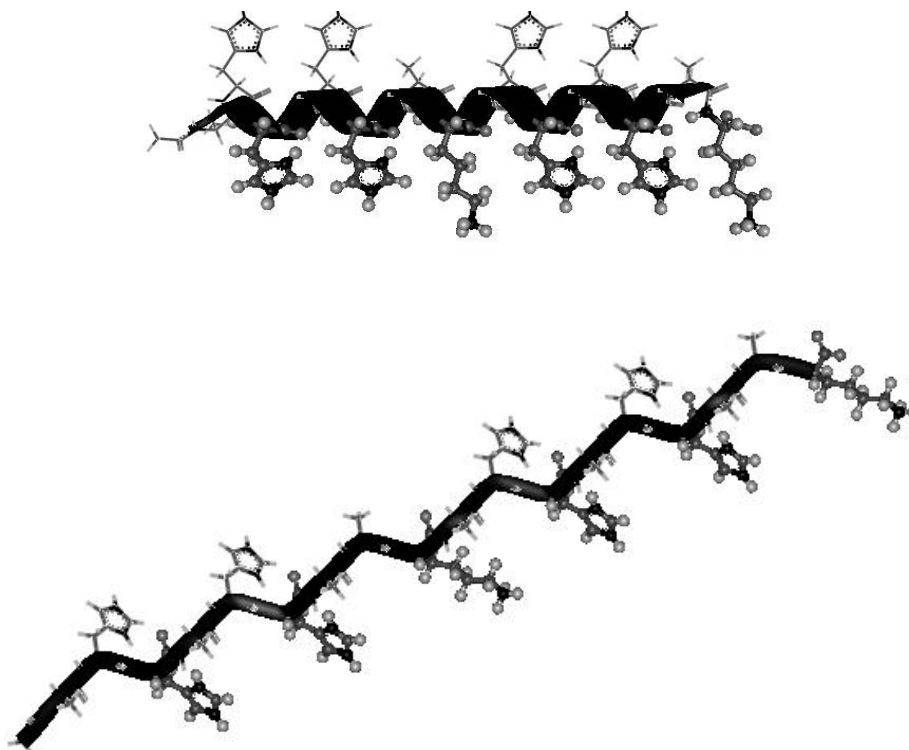


Figure 2.29. The 18-mer peptide branch of **BNT IIZ** modeled as a right-handed 3-10 helix (top) and a left-handed polyproline type II conformation (bottom). The amino acid sequence follows **(Ala-His-His-Ala-His-His-Ala-Ala-Lys)₂**.

Both conformations enable the visualization of the putative nucleating faces of the templates and the determination of the amino acid residues that are critical for substrate recognition. In such that the template orients the nucleation of the mineral, both the spatial distribution and functionality of the involved amino acids, which ultimately dictate the secondary structure and conformation of the surface groups, are imperative for successful biomineralization. Detailed knowledge of the events that underlie the structural modifications of the repetitive sequence of HRP II are imperative to understanding key mechanisms, not only in the formation of hemozoin,

but also in post invasion events such as the pathogenesis of *Plasmodium falciparum* and the corresponding host immune response. Specific interference with β -hematin formation could substantially reduce parasitism and remains a relatively unexplored antimalarial strategy.^{40,11} Though various studies have substantiated the interaction of heme with HRP II as a valid target of antimalarial drug action, this very interaction complicates the mode of action for antimalarial drugs since the drug can possibly interact with the heme component, the protein, or the complexed heme:protein unit. The result is a plethora of contradictory science surrounding hemozoin formation and antimalarial drug action often with legitimate results but unanswered mechanisms.

References

- [1] Gardner, M. J.; Hall, N.; Fung, E.; White, O.; Berriman, M.; Hyman, R. W.; Carlton, J. M.; Pain, A.; Nelson, K. E.; Bowman, S.; Paulsen, I. T.; James, K.; Eisen, J. A.; Rutherford, K.; Salzberg, S. L.; Craig, A.; Kyes, S.; Chan, M.-S.; Nene, V.; Shallom, S. J.; Suh, B.; Peterson, J.; Angiuoli, S.; Pertea, M.; Allen, J.; Selengut, J.; Haft, D.; Mather, M. W.; Vaidya, A. B.; Martin, D. M. A.; Fairlamb, A. H.; Fraunholz, M. J.; Roos, D. S.; Ralph, S. A.; McFadden, G. I.; Cummings, L. M.; Subramanian, G. M.; Mungall, C.; Venter, J. C.; Carucci, D. J.; Hoffman, S. L.; Newbold, C.; Davis, R. W.; Frase, C. M.; Barrell, B. "Genome sequence of the human malaria parasite *Plasmodium falciparum*." *Nature* **2002**, *419*, 498-511.
- [2] Gardner, M. J.; Shallom, S. J.; Carlton, J. M.; Salzberg, S. L.; Nene, V.; Shoaibi, A.; Ciecko, A.; Lynn, J.; Rizzo, M.; Weaver, B.; Jarrahi, B.; Brenner, M.; Parvizi, B.; Tallon, L.; Moazzez, A.; Granger, D.; Fujii, C.; Hansen, C.; Pederson, J.; Feldblyum, T.; Peterson, J.; Suh, B.; Angiuoli, S.; Pertea, M.; Allen, J.; Selengut, J.; White, O.; Cummings, L. M.; Smith, H. O.; Adams, M. D.; Venter, J. C.; Carucci, D. J.; Hoffman, S. L.; Fraser, C. M. "Sequence of *Plasmodium falciparum* chromosomes 2, 10, 11, and 14." *Nature* **2002**, *419*, 531-534.
- [3] Hall, N.; Pain, A.; Berriman, M.; Churcher, C.; Harris, B.; Harris, D.; Mungall, K.; Bowman, S.; Atkin, R.; Baker, S.; Barron, A.; Brooks, K.; Buckee, C. O.; Burrows, C.; Cherevach, I.; Chillingworth, C.; Chillingworth, T.; Christodoulou, Z.; Clark, L.; Clark, R.; Corton, C.; Cronin, A.; Davies, R.; Davis, P.; Dear, P.; Dearden, F.; Doggett, J.; Feltwell, T.; Goble, A.; Goodhead, I.; Gwilliam, R.; Hamlin, N.; Hance, Z.; Harper, D.; Hauser, H.; Hornsby, T.; Holroyd, S.; Horrocks, P.; Humphray, S.; Jagels, K.; James, K. D.; Johnson, D.; Kerhornou, A.; Knights, A.; Konfortov, B.; Kyes, S.; Larke, N.; Lawson, D.; Lennard, N.; Line, A.; Maddison, M.; McLean, J.; Mooney, P.; Moule, S.; Murphy, L.; Oliver, K.; Ormond, D.; Price, C.; Quail, M. A.; Rabbinowitsch, E.; Rajandream, M. A.; Rutter, S.; Rutherford, K. M.; Sanders, M.; Simmonds, M.; Seeger, K.; Sharp, S.; Smith, R.; Squares, R.; Squares, S.; Stevens, K.; Taylor, K.; Tivey, A.; Unwin, L.; Whitehead, S.; Woodward, J.; Sulston, J. E.; Craig, A.; Newbold, C.; Barrell, B. G. "Sequence of *Plasmodium falciparum* chromosomes 1, 3-9, and 13." *Nature* **2002**, *419*, 527-531.
- [4] Hyman, R. W.; Fung, E.; Conway, A.; Kurdi, O.; Mao, J.; Miranda, M.; Nakao, B.; Rowley, D.; Tamaki, T.; Wang, F.; Davis, R. W. "Sequence of *Plasmodium falciparum* chromosome 12." *Nature* **2002**, *419*, 534-537.

- [5] Ridley, R. G. "Medical need, scientific opportunity and the drive for antimalarial drugs." *Nature* **2002**, *415*, 686-693.
- [6] Olliaro, P. "Future perspectives in drug research"; UNDP/World Bank/WHO Special Programme for Research and Training in Tropical Diseases, **1995**.
- [7] Rosenthal, P. J.; Meshnick, S. R. "Hemoglobin catabolism and iron utilization by malarial parasites." *Mol. Biochem. Parasitol.* **1996**, *83*, 131-139.
- [8] Cowman, A. F.; Crabb, B. S. "A parasite genome sheds light on an old enemy." *Nat. Biotechnol.* **2002**, *20*, 1098-1099.
- [9] Kurosawa, Y.; Dorn, A.; Kitsuji-Shirane, M.; Shimada, H.; Satoh, T.; Matile, H.; Hofheinz, W.; Masciadri, R.; Kansy, M.; Ridley, R. G. "Hematin polymerization assay as a high-throughput screen for identification of new antimalarial pharmacophores." *Antimicrob. Agents Chemother.* **2000**, *44*, 2638-2644.
- [10] Parapini, S.; Basilico, N.; Pasini, E.; Egan, T. J.; Olliaro, P.; Taramelli, D.; Monti, D. "Standardization of the physicochemical parameters to assess *in vitro* the β -hematin inhibitory activity of antimalarial drugs." *Exp. Parasitol.* **2000**, *96*, 249-256.
- [11] Sahal, D.; Kannan, R.; Chauhan, V. S. "Applying malaria parasite's heme detoxification system for screening potential antimalarial drugs." *Anal. Biochem.* **2003**, *312*, 258-260.
- [12] Ridley, R. G.; Dorn, A.; Matile, H.; Kansy, M. "Haem polymerization in malaria (*reply*)." *Nature* **1995**, *378*, 138-139.
- [13] Dorn, A.; Vippagunta, S. R.; Matile, H.; Bubendorf, A.; Vennerstrom, J. L.; Ridley, R. G. "A comparison and analysis of several ways to promote hematin (heme) polymerization and an assessment of its initiation *in vitro*." *Biochem. Pharmacol.* **1998**, *55*, 737-747.
- [14] Fitch, C. D.; Cai, G.-z.; Chen, Y.-F.; Shoemaker, J. D. "Involvement of lipids in ferriprotoporphyrin IX polymerization in malaria." *Biochim. Biophys. Acta* **1999**, *1454*, 31-37.
- [15] Tripathi, A. K.; Tekwani, B. L. "Mechanism of formation of β -hematin in malaria parasite: Lipids edge over proteins as possible mediators." *J. Parasit. Dis.* **1999**, *23*, 61-70.

- [16] Tripathi, A. K.; Garg, S. K.; Tekwani, B. L. "A physiochemical mechanism of hemozoin (β -hematin) synthesis by malaria parasite." *Biochem. Biophys. Res. Commun.* **2002**, *290*, 595-601.
- [17] Sullivan, D. J., Jr.; Gluzman, I. Y.; Goldberg, D. E. "Plasmodium hemozoin formation mediated by histidine-rich proteins." *Science* **1996**, *271*, 219-222.
- [18] Sullivan, D. J., Jr.; Gluzman, I. Y.; Russell, D. G.; Goldberg Daniel, E. "On the molecular mechanism of chloroquine's antimalarial activity." *Proc. Natl. Acad. Sci., USA* **1996**, *93*, 11865-11870.
- [19] Sullivan, D. J., Jr.; Matile, H.; Ridley, R. G.; Goldberg Daniel, E. "A common mechanism for blockade of heme polymerization by antimalarial quinolines." *J. Biol. Chem.* **1998**, *273*, 31103-31107.
- [20] Dorn, A.; Stoffel, R.; Matile, H.; Bubendorf, A.; Ridley, R. G. "Malarial hemozoin/ β -hematin supports heme polymerization in the absence of protein." *Nature* **1995**, *374*, 269-271.
- [21] Egan, T. J. "Physico-chemical aspects of hemozoin (malaria pigment) structure and formation." *J. Inorg. Biochem.* **2002**, *91*, 19-26.
- [22] Sullivan, D. J. "Theories on malaria pigment formation and quinoline action." *Int. J. Parasitol.* **2002**, *32*, 1645-1653.
- [23] Gluzman, I. Y.; Francis, S. E.; Oksman, A.; Smith, C. E.; Duffin, K. L.; Goldberg, D. E. "Order and specificity of the *Plasmodium falciparum* hemoglobin degradation pathway." *J. Clin. Invest.* **1994**, *93*, 1602-1608.
- [24] Brown, S. B.; Jones, P. "Reactions between haemin and hydrogen peroxide. Part 2. - Destructive oxidation of haemin." *Trans. Faraday Soc.* **1968**, *64*, 994-998.
- [25] Brown, S. B.; Jones, P. "Reactions between haemin and hydrogen peroxide. Part 3. - Catalytic decomposition of hydrogen peroxide." *Trans. Faraday Soc.* **1968**, *64*, 999-1005.
- [26] Brown, S. B.; Jones, P.; Suggett, A. "Reactions between haemin and hydrogen peroxide. Part 1. - Ageing and non-destructive oxidation of haemin." *Trans. Faraday Soc.* **1968**, *64*, 986-993.
- [27] Green, M. D.; Xiao, L.; Lal, A. A. "Formation of hydroxyeicosatetraenoic acids from hemozoin-catalyzed oxidation of arachidonic acid." *Mol. Biochem. Parasitol.* **1996**, *83*, 183-188.

- [28] Schwarzer, E.; Ludwig, P.; Valente, E.; Arese, P. "15(S)-hydroxyeicosatetraenoic acid (15-HETE), a product of arachidonic acid peroxidation, is an active component of hemozoin toxicity to monocytes." *Parassitologia* **1999**, *41*, 199-202.
- [29] Schwarzer, E.; Kühn, H.; Valente, E.; Arese, P. "Malaria-parasitized erythrocytes and hemozoin nonenzymatically generate large amount of hydroxy fatty acids that inhibit monocyte functions." *Blood* **2003**, *101*, 722-728.
- [30] Waller, R. F.; Ralph, S. A.; Reed, M. B.; Su, V.; Douglas, J. D.; Minnikin, D. E.; Cowman, A. F.; Besra, G. S.; McFadden, G. I. "A type II pathway for fatty acid biosynthesis presents drug targets in *Plasmodium falciparum*." *Antimicrob. Agents Chemother.* **2003**, *47*, 297-301.
- [31] Simpson, J. A.; Aarons, L.; Collins, W. E.; Jeffery, G. M. "Population dynamics of untreated *Plasmodium falciparum* malaria within the adult human host during the expansion phase of infection." *Parasitology* **2002**, *124*, 247-263.
- [32] Day, K. P.; Hayward, R. E.; Smith, D.; Culvenor, J. "CD36-dependent adhesion and knob expression of the transmission stages of *Plasmodium falciparum* is stage-specific." *Mol. Biochem. Parasitol.* **1998**, *93*, 167-177.
- [33] Hayward, R. E.; Sullivan, D. J.; Day, K. P. "*Plasmodium falciparum*: histidine-rich protein II is expressed during gametocyte development." *Exp. Parasitol.* **2000**, *96*, 139-146.
- [34] Howard, R. J.; Uni, S.; Aikawa, M.; Aley, S. B.; Leech, J. H.; Lew, A. M.; Wellems, T. E.; Renner, J.; Taylor, D. W. "Secretion of a malarial histidine-rich protein (Pf HRP II) from *Plasmodium falciparum*-infected erythrocytes." *J. Cell Biol.* **1986**, *103*, 1269-1277.
- [35] Knapp, B.; Shaw, E.; Hundt, E.; Enders, B.; Küpper, H. A. "A histidine-alanine rich recombinant antigen protects Aotus monkeys from *Plasmodium falciparum*." *Behring. Inst. Res. Commun.* **1988**, *82*, 349-359.
- [36] Knapp, B.; Hundt, E.; Enders, B.; Küpper, H. A. "Protection of Aotus monkeys from malaria infection by immunization with recombinant hybrid proteins." *Infect. Immun.* **1992**, *60*, 2397-2401.

- [37] Lenstra, R.; d'Auriol, L.; Andrieu, B.; Le Bras, J.; Galibert, F. "Cloning and sequencing of *Plasmodium falciparum* DNA fragments containing repetitive regions potentially encoding for histidine-rich proteins: identification of two overlapping reading frames." *Biochem. Biophys. Res. Commun.* **1987**, *146*, 368-377.
- [38] Lopez, R.; Urquiza, M.; Curtidor, H.; Caminos, J. E.; Mora, H.; Puentes, A.; Patarroyo, M. E. "*Plasmodium falciparum*: red blood cell binding studies of peptides derived from histidine-rich KAHRP-1, HRP-II, and HRP-III proteins." *Acta Trop.* **2000**, *75*, 349-359.
- [39] Anders, R. F. "Multiple cross-reactivities amongst antigens of *Plasmodium falciparum* impair the development of protective immunity against malaria." *Parasite Immunol.* **1986**, *8*, 529-539.
- [40] Egan, T. J. "Discovering antimalarials: a new strategy." *Chem. Biol.* **2002**, *9*, 852-853.
- [41] Mann, S. "Biomineralization: the hard part of bioinorganic chemistry!" *J. Chem. Soc., Dalton Trans.* **1993**, *1*, 1-9.
- [42] Mann, S. "Molecular tectonics in biomineralization and biomimetic materials chemistry." *Nature* **1993**, *365*, 499-505.
- [43] Kaim, W.; Schwederski, B. ***Bioinorganic Chemistry: Inorganic Elements in the Chemistry of Life***; John Wiley & Sons, Inc.: West Sussex, England, 1994, 303-317.
- [44] Pohnert, G. "Biomineralization in diatoms mediated through peptide- and polyamine-assisted condensation of silica." *Angew. Chem., Int. Ed.* **2002**, *41*, 3167-3169.
- [45] Weiner, S.; Addadi, L. "At the cutting edge." *Science* **2002**, *298*, 375-376.
- [46] Chen, M. M.; Shi, L.; Sullivan, D. J. J. "*Haemoproteus* and *Schistosoma* synthesize heme polymers similar to *Plasmodium* hemozoin and β -hematin." *Mol. Biochem. Parasitol.* **2001**, *113*, 1-8.
- [47] Norland, G. S.; Briones, N.; Sullivan, D. J. J. "The size and shape of hemozoin crystals distinguishes diverse *Plasmodium* species." *Mol. Biochem. Parasitol.* **2003**, *130*, 91-99.

- [48] Belcher, A. M.; Hansma, P. K.; Stucky, G. D.; Morse, D. E. "First steps in harnessing the potential of biomineralization as a route to new high-performance composite materials." *Acta Mater.* **1998**, *46*, 733-736.
- [49] Pandey, A. V.; Joshi, R.; Tekwani, B. L.; Singh, R. L.; Chauhan, V. S. "Synthetic peptides corresponding to a repetitive sequence of malarial histidine rich protein bind haem and inhibit haemozoin formation in vitro." *Mol. Biochem. Parasitol.* **1997**, *90*, 281-287.
- [50] Cloninger, M. J. "Biological applications of dendrimers." *Curr. Opin. Chem. Biol.* **2002**, *6*, 742-748.
- [51] Sadler, K.; Tam, J. P. "Peptide dendrimers: applications and synthesis." *Rev. Mol. Biotechnol.* **2002**, *90*, 195-229.
- [52] Tam, J. P. "Synthetic peptide vaccine design-synthesis and properties of a high-density multiple antigenic peptide system." *Proc. Natl. Acad. Sci., USA* **1988**, *85*, 5409-5413.
- [53] Tam, J. P. "Incorporation of T and B epitopes of the circumsporozoite protein in a chemically defined synthetic vaccine against malaria." *J. Exp. Med.* **1990**, *171*, 299-306.
- [54] Defoort, J. P.; Nardelli, B.; Huang, W.; Ho, D. D.; Tam, J. P. "Macromolecular assemblage in the design of a synthetic AIDS vaccine." *Proc. Natl. Acad. Sci., USA* **1992**, *89*, 3879-3883.
- [55] Chaves, F.; Calvo, J. C.; Carvajal, C.; Rivera, Z.; Ramirez, L.; Pinto, M.; Trujillo, M.; Guzmán, F.; Patarroyo, M. E. "Synthesis, isolation, and characterization of *Plasmodium falciparum* antigenic tetrabranched peptide dendrimers obtained by thiazolidine linkages." *J. Pept. Res.* **2001**, *58*, 307-316.
- [56] Rivera, Z.; Granados, G.; Pinto, M.; Varón, D.; Carvajal, C.; Chaves, F.; Calvo, J.; Rodríguez, R.; Guzmán, F.; Patarroyo, M. E. "Double dimer peptide constructs are immunogenic and protective against *Plasmodium falciparum* in the experimental *Aotus* monkey model." *J. Pept. Res.* **2002**, *59*, 62-70.
- [57] Tam, J. P.; Zavala, F. "Multiple antigen peptide. A novel approach to increase detection sensitivity of synthetic peptides in solid-phase immunoassays." *J. Immunol. Methods* **1989**, *124*, 53-61.

- [58] Kim, Y.; Zimmerman, S. C. "Applications of dendrimers in bio-organic chemistry." *Curr. Opin. Chem. Biol.* **1998**, *2*, 733-742.
- [59] Sheldon, K.; Liu, D.; Ferguson, J.; Garipey, J. "Loligomers: design of de novo peptide-based intracellular vehicles." *Proc. Natl. Acad. Sci., USA* **1995**, *92*, 2056-2060.
- [60] Esposito, A.; Delort, E.; Lagnoux, D.; Djojo, F.; Reymond, J.-L. "Catalytic peptide dendrimers." *Angew. Chem., Int. Ed.* **2003**, *42*, 1381-1383.
- [61] Lagnoux, D.; Delort, E.; Douat-Casassus, C.; Esposito, A.; Reymond, J.-L. "Synthesis and esterolytic activity of catalytic peptide dendrimers." *Chem. Eur. J.* **2004**, *10*, 1215-1226.
- [62] Sinnis, P.; Clavijo, P.; Fenyó, D.; Chait, B. T.; Cerami, C.; Nussenzweig, V. "Structural and functional properties of region II-plus of the malaria circumsporozoite protein." *J. Exp. Med.* **1994**, *180*, 297-306.
- [63] Tam, J. P.; Lu, Y.-A.; Yang, J.-L. "Antimicrobial dendrimeric peptides." *Eur. J. Biochem.* **2002**, *269*, 923-932.
- [64] Hahn, K. W.; Klis, W. A.; Stewart, J. M. "Design and synthesis of a peptide having chymotrypsin-like esterase activity." *Science* **1990**, *248*, 1544-1547.
- [65] Montal, M.; Montal, M. S.; Tomich, J. M. "Synporins - synthetic proteins that emulate the pore structure of biological ionic channels." *Proc. Natl. Acad. Sci., USA* **1990**, *87*, 6929-6933.
- [66] Fields, C. G.; Mickelson, D. J.; Drake, S. L.; McCarthy, J. B.; Fields, G. B. "Melanoma cell adhesion and spreading activities of a synthetic 124-residue triple-helical 'mini-collagen'." *J. Biol. Chem.* **1993**, *268*, 14153-14160.
- [67] Posnett, D. N.; McGrath, H.; Tam, J. P. "A novel method for producing anti-peptide antibodies." *J. Biol. Chem.* **1988**, *263*, 1719-1725.
- [68] Kim, P.; Pau, C.-P. "Comparing tandem repeats and multiple antigenic peptides as the antigen to detect antibodies by enzyme immunoassay." *J. Immunol. Methods* **2001**, *257*, 51-54.
- [69] Tam, J. P. "Recent advances in multiple antigen peptides." *J. Immunol. Methods* **1996**, *196*, 17-32.
- [70] Veprek, P.; Ježek, J. "Peptide and glycopeptide dendrimers. Part I." *J. Pept. Sci.* **1999**, *5*, 5-23.

- [71] Veprek, P.; Ježek, J. "Peptide and glycopeptide dendrimers. Part II." *J. Pept. Sci.* **1999**, *5*, 203-220.
- [72] Pandey, A. V.; Bisht, H.; Babbarwal, V. K.; Srivastava, J.; Pandey, K. C.; Chauhan, V. S. "Mechanism of malarial haem detoxification inhibition by chloroquine." *Biochem. J.* **2001**, *355*, 333-338.
- [73] Ziegler, J.; Chang, R. T.; Wright, D. W. "Multiple-antigenic peptides of histidine-rich protein II of *Plasmodium falciparum*: dendrimeric biomineralization templates." *J. Am. Chem. Soc.* **1999**, *121*, 2395-2400.
- [74] Lynn, A.; Chandra, S.; Malhotra, P.; Chauhan, V. S. "Heme binding and polymerization by *Plasmodium falciparum* histidine rich protein II: influence of pH on activity and conformation." *FEBS Lett.* **1999**, *459*, 267-271.
- [75] Orjih, A. U. "On the mechanism of hemozoin production in malaria parasites: activated erythrocyte membranes promote β -hematin synthesis." *Exp. Biol. Med.* **2001**, *226*, 746-752.
- [76] Slater, A. F.; Swiggard, W. J.; Orton, B. R.; Flitter, W. D.; Goldberg, D. E.; Cerami, A.; Henderson, G. B. "An iron-carboxylate bond links the heme units of malaria pigment." *Proc. Natl. Acad. Sci., USA* **1991**, *88*, 325-329.
- [77] Bohle, S. D.; Dinnebier, R. E.; Madsen, S. K.; Stephens, P. W. "Characterization of the products of the heme detoxification pathway in malarial late trophozoites by x-ray diffraction." *J. Biol. Chem.* **1997**, *272*, 713-716.
- [78] Martiney, J. A.; Cerami, A.; Slater, A. F. G. "Inhibition of hemozoin formation in *Plasmodium falciparum* trophozoites extracts by heme analogs: Possible implication in the resistance to malaria conferred by the β -thalassemia trait." *Mol. Med.* **1996**, *2*, 236-246.
- [79] Burch, M. K.; Morgan, W. T. "Preferred heme binding sites of histidine-rich glycoproteins." *Biochemistry* **1985**, *24*, 5919-5924.
- [80] Morgan, W. T. "The histidine-rich glycoprotein of serum has a domain rich in histidine, proline, and glycine that binds heme and metals." *Biochemistry* **1985**, *24*, 1496-1501.

- [81] Panton, L. J.; McPhie, P.; Maloy, W. L.; Wellems, T. E.; Taylor, D. W.; Howard, R. J. "Purification and partial characterization of an unusual protein from *Plasmodium falciparum*: histidine-rich protein II." *Mol. Biochem. Parasitol.* **1989**, *35*, 149-160.
- [82] Margossian, S. S.; McPhie, P.; Howard, R. J.; Coligan, J. E.; Slayter, H. S. "Physical characterization of histidine-rich protein from *Plasmodium lophurae*." *Biochim. Biophys. Acta* **1990**, *1038*, 330-337.
- [83] Analysis of MAPS Peptides,
<http://www.abrf.org/ABRFNews/1997/March1997/mar97maps.html>
- [84] Mao, C.; Li, H.; Cui, F.; Feng, Q.; Ma, C. "The functionalization of titanium with EDTA to induce biomimetic mineralization of hydroxyapatite." *J. Mater. Chem.* **1999**, *9*, 2573-2582.

Chapter 3

Putative Domain Template Studies

3.1. Introduction

Despite the fact that more than one hundred years have elapsed since the discovery of the malaria parasite, the complex biochemistry of *Plasmodia* still hampers the current scientific understanding of antimalarial drug action. While the recent completion of the *P. falciparum* genome¹ will undoubtedly provide new drug targets, understanding the modes of action of any malarial antagonist is unlikely to be resolved until a better understanding of the life cycle of the parasite is evolved.

The malarial parasite invades host red blood cells, transforming through four life cycle stages, the merozoite, ring, trophozoite, and schizont stages, all within 48 hours after invasion. During this intraerythrocytic phase, *P. falciparum* can catabolize up to 80% of an infected erythrocyte's hemoglobin² in its acidified digestive vacuole (pH 4.8-5.5) in order to obtain requisite amino acids. Hemoglobin degradation consequently results in the release of free heme, which would be toxic to the parasite if not sequestered by the organism into an inert crystalline substance known as hemozoin.

The malaria parasite's heme detoxification pathway is vastly different from human heme detoxification, which utilizes a heme oxygenase/biliverdin reductase pathway. As a result, hemoglobin degradation, as well as the subsequent formation of hemozoin, has received significant attention due to its implications in drug development.³ Moreover, this essential biochemical processing of hemozoin is retained in drug resistant strains of the parasite, suggesting that a better fundamental basis of the mechanism of hemozoin formation will elicit an improved understanding

of antimalarial drug action, since many antimalarials, including chloroquine, are most active during the blood stage of infection where hemoglobin degradation occurs (trophozoite stage).

While the molecular compositions of hemozoin and its synthetic analogue, commonly known as β -hematin, have been resolved by Bohle *et al.*⁴ as being identical, the chemical mechanism of formation remains largely controversial due to fundamental differences that exist between the *in vivo* and *in vitro* methods of formation (For a more thorough review refer to Chapter 1.). Within the biological milieu of the parasite, hemozoin is synthesized in aqueous solutions, with numerous hypotheses surrounding its formation, including: mechanisms involving enzyme catalysis,^{5,6} spontaneous formation,⁷ autocatalysis with preformed hemozoin,⁸ lipid catalysis,⁹⁻¹³ and nucleation on the histidine-rich protein II (HRP II).¹⁴⁻¹⁶ Synthetically, hemozoin can be formed in aqueous solution with hematin and acetic acid, though other acids have been used,^{7,8,17-21} and also in non-aqueous solution by the dehydrohalogenation of hemin with 2,6-lutidine in an inert atmosphere.²² Whether *in vitro* or *in vivo*, the precise mechanism of hemozoin formation is mired by the fact that the progression of hemozoin formation has not yet been able to be continuously monitored by spectroscopic techniques.

Many antimalarials, including chloroquine and quinoline based drugs are thought to function by inhibiting hemozoin formation,⁵ suggesting these drugs function by disrupting the assembly and/or production of the malaria pigment. Such proposed mechanisms of antimalarial drug action include the direct interaction with

hematin via π - π stacking of its aromatic structure with that of heme,²³⁻²⁶ by drug intercalation with the growing face of the hemozoin crystal preventing further crystal development,^{4,27} or by the displacement hematin from substrates such as lipids or HRP II²⁸⁻³⁰ in such that free heme concentrations become toxic to *P. falciparum*.

Likewise, if the formation of the malaria pigment is premised as a biomineralization process three possible scenarios for disrupting the biosynthesis of hemozoin templated on HRP II can be envisioned. First, the potential drug can interact directly with hematin preventing its nucleation onto the surface of the template. Alternatively, the drug can blockade the surface of the template in such that its face is not physically accessible for hematin binding. Finally, the drug could possibly interfere by preventing the requisite bond formation between monomers of Fe(III)PPIX during the nucleation of hemozoin.

With this in mind, **it becomes imperative to understand which amino acid residues of HRP II are critical in the templating, nucleation, and formation of hemozoin.** Halting hemozoin formation at this growth stage heralds the histidine-rich protein II as an unexplored antimalarial strategy.³¹ Herein lays the inspiration and motivation for site-directed mutagenesis studies of the two putative binding domains of HRP II, functionally mimicked in our **bionucleating templates**, BNT II and the alternative putative binding domain, BNT IIA.

The earliest studies of HRP II as an antimalarial strategy began shortly after the protein was isolated and identified, though its direct implication to hemozoin formation had not yet been established. Given that the protein's usually high content

of histidine is unique to *Plasmodium falciparum* and not the host, scientists examined the effects of the incorporation of histidine analogues into culture medium and the impact of such on the asexual growth and protein synthesis of the parasites *in vitro*.³² Though few of the chemically modified histidines were inhibitory, the results were semi-quantitative at best, since asexual parasite growth was determined by microscopy and the effects of the analogues on protein synthesis had not been studied in detail. Thereafter, studies involving the histidine-rich proteins of *Plasmodium falciparum* (HRPs I-IV) received little attention until HRP II was determined to play a critical role in the detoxification of heme, binding 17 equivalents of heme and participating in the aggregation of hemozoin.¹⁵

The binding of heme alone does not elicit hemozoin formation. Numerous examples of linear multimers adapted from the sequence of HRP II have been shown to bind heme, however until now, such sequences other than the native protein have failed to promote the formation of hemozoin. Pandey *et al.* had demonstrated that heme binding to synthetic peptides based on hexapeptide repeats of Ala-His-His-Ala-Ala-Asp from HRP II was proportional to the number of repeat units in the peptides,³³ although hemozoin formation failed to occur. Obviously, template substrate interactions must be more involved, possibly invoking some conformational change in the template that could orient heme molecules into a proper spatial orientation necessary for hemozoin formation.

The bionucleating templates, the BNTs, which are essentially MAPS peptide dendrimers, possess a hierarchy of structure that enables stable and ordered

conformations. Such polymeric scaffolds do not occlude peptide assembly and are often favored over tandem repeat peptides because the majority of the peptide chain is available for substrate interactions, thereby increasing both activities and assay sensitivities.³⁴ Through defined molecular weights, monodispersity, stereoregularity and sequence and compositional control at the single amino acid residue level, inherent chemical reactivity and conformational rigidity can be assessed. Such point mutations allow for a direct comparison of the biological relevance of single amino acid residues in the highly unusual conservation of histidine and alanine containing sequences in HRP II. In the end, such novel engineering allows for the judicious manipulation of both the peptide and dendrimer fragments.

Using the dendrimeric architectures with specified peptide sequences would circumvent the problems often associated with protein folding of larger sequenced peptides. Additionally, the peptide dendrimer could allow the molecular recognition phenomena to appear as a result of the constructive interactions between amino acids and substrate. A drawback of the dendrimer however, is that the constructional constraints of the tetrameric core could possibly occlude binding near the surface due to inherent steric hinderance.

The impact of a functional model of HRP II would be invaluable for not only *in vitro* antimalarial drug susceptibility data, but also for epidemiological purposes since antimalarial drug resistance is a widespread issue in the control of *P. falciparum* malaria. Assays utilizing HRP II for malaria detection, such as the commercially available monoclonal antibody kits specific for HRP II, already have advantages over

the mainstream parasite quantification techniques.³⁵ Non-protein assays such as the isotopic assay, which measures parasitic metabolic activity via the incorporation of [³H]hypoxanthine, and a schizont maturation assay, which tallies the number of parasites that develop from the ring to schizont stage, assess parasitic activity at a partial timeframe within the parasite's 48 hour intraerythrocytic life cycle. With HRP II-based assays, since the protein is produced throughout the entire 48 hour intraerythrocytic life cycle, infection/treatment can be monitored throughout the complete blood stage of *Plasmodium falciparum*.

3.2. Functional Screening of the BNTs

Initially BNT II (which possesses the Ala-His-His-Ala-His-His-Ala-Ala-Asp sequence repeated twice per dendrimeric branch) and BNT IIA (which possesses the alternative putative binding domain, Ala-His-His-Ala-Ala-Asp-Ala-His-His sequence also repeated twice per branch), were analyzed for binding capabilities with the natural substrate of HRP II, iron (III) protoporphyrin IX [Fe(III)PPIX], and an alternate porphyrin, zinc (II) protoporphyrin IX [Zn(II)PPIX]. Such studies were adopted from Zielger³⁶ based on the UV-Vis difference titration methods of Morgan.^{37,38} Additional substrate binding was evaluated through fluorescence quenching studies of the zinc porphyrin, also adopted from Morgan.³⁹

Both putative nucleating domain templates were also monitored for the ability to aggregate hemozoin according to the *in vitro* heme polymerization assay developed by Sullivan,¹⁵ hereafter more appropriately referred to as the *in vitro* heme aggregation assay.

Circular dichroism studies of BNT II and BNT IIA evaluated any conformational changes that may have occurred upon substrate (hemin) binding. Results will be assimilated in regards to both protein/peptide conformational analysis and dendrimeric secondary structure.

3.2.1. Preparation of Stock Solutions

Stock solutions of the templates were prepared in 100 mM sodium acetate buffer, pH 4.8, from lyophilized peptide samples and refrigerated until used. Concentrations were determined based on amino acid analysis. Prior to use, the peptide solutions were equilibrated to room temperature and thoroughly mixed to ensure full peptide dissolution. Stock solutions of hemin chloride [Fe(III)PPIX, Sigma-Aldrich Chemicals, St. Louis, MO] and zinc protoporphyrin IX [Zn(II)PPIX, Mid-Century Chemicals, Chicago, IL] were prepared in 0.1 M NaOH. The porphyrin solutions were kept refrigerated until used for a maximum of two weeks before being discarded.

3.2.2. Porphyrin Binding Assay

Following the UV-Vis difference titration methods of Morgan,^{37,38} 2-10 nmoles of the bionucleating template dissolved in 100 mM sodium acetate buffer, pH 4.8, were added to a 1.0 mL semi-micro quartz cell (10 mm, Starna Cells, Atascadero, CA). Blanks contained 1.0 mL of the aforementioned buffer. Aliquots of hemin chloride or Zn(II)PPIX (~1 mM) dissolved in 0.1 M NaOH were then titrated into both the blank and reference cuvettes. Samples were equilibrated for

fifteen minutes prior to measurements on an Aligent 8453 UV-Vis spectrometer (Wilmington, DE).

The amount of the porphyrin bound to the BNT was measured by monitoring the change in absorbance at the appropriate Lambda maxima, usually near 420 nm for the hemin chloride titrations and 380 nm for the zinc porphyrin titrations, with the absorption maxima varying slightly according to the template being investigated. The change in absorbance was normalized to 1 absorbance unit and the x-axis recorded as a ratio of porphyrin to template. Additionally, templates that did not bind a significant amount of porphyrin were re-examined at higher peptide concentrations, so that a sufficient amount of data points could be recorded before binding ceased and porphyrin aggregation was apparent.

3.2.3. Fluorescence Quenching Studies with Zn(II)PPIX

In addition to the UV-Vis titration methods, template binding was also monitored by fluorescence quenching of Zn(II)PPIX. According to the assay, an appropriate amount of 100 mM sodium acetate buffer, pH 4.8, was added to a quartz spectrofluorometer cell (10 mm, Starna Cells, Atascadero, CA), along with varying amounts of the quenching template. A stock solution of Zn(II)PPIX dissolved in 0.1 M NaOH was then added, diluting the porphyrin to a final concentration of 1×10^{-5} M in a 4.0 mL sample volume. The total volume of the porphyrin did not exceed 10% of the sample volume in order to maintain buffering capacity. The sample was scanned rapidly from 450-700 nm upon addition of the fluorophore on a Cary Eclipse Fluorescence Spectrophotometer (Varian Inc., Walnut Creek, CA) using

an excitation wavelength at 410 nm, 10 mm slit width, scan rate of 120 nm/min. and photomultiplier tube set at 800 v. The data was analyzed as a direct plot of the normalized fluorescence intensity at 586 nm against the ratio of the BNT and Zn(II)PPIX.

3.2.4. *In Vitro* Heme Aggregation Assay

The templates were assayed for hemozoin formation by incubating 2 nmol of template and 100 μ M hemin chloride (dissolved in 0.1 M NaOH) in a total volume of 2.0 mL of 100 mM sodium acetate buffer, pH 4.8, for 48 hours at 37 $^{\circ}$ C. Controls contained 100 μ M hemin chloride in 2.0 mL of 100 mM sodium acetate buffer. The volume of hemin added was less than 10% of the total volume of the solution in order to maintain buffering capacity. After 48 hours the samples were vortexed, transferred to 50 mL polycarbonate Oak Ridge centrifuge tubes, and centrifuged at 19,000 g for 1 hour at 4 $^{\circ}$ C on a Sorvall RC-5B refrigerated super-speed centrifuge equipped with a SS-34 fixed angle rotor. The supernatant was discarded and the pellet resuspended in 5 mL of 0.1 M sodium bicarbonate solution, pH 9.1, to solubilize any free heme. The centrifuge tubes were then vortexed every $\frac{1}{2}$ hour for two hours before centrifuging again and decanting the supernatant. The pellet was treated with an additional sodium bicarbonate wash and centrifuged. The remaining pellet was washed with water, vortexed, and centrifuged until the pH of the decanted supernatant was neutral. The final pellet of aggregated heme was quantitated on the basis of its absorbance at 400 nm ($\epsilon = 100,000$). Briefly, the pellet was dissolved in 1.0 mL of 0.1 M NaOH and vortexed every 15 minutes for 1 hour before recording the

absorbance measurement on an Aligent 8453 UV-Vis spectrophotometer (Wilmington, DE). Hemozoin production was expressed in nmoles. Controls, with a background hemozoin production of approximately 1-2 nmoles, were routinely subtracted from the BNT mediated production of hemozoin. Background hemozoin production corresponded well with previously published results under similar experimental conditions.^{10,40}

3.2.5. Circular dichroism spectroscopy

Template stock solutions dissolved in 100 mM acetate buffer, pH 4.8, were diluted to 10 mM buffer concentrations (2-15 nmoles of template) in a 3.0 mL quartz cuvette and scanned. Aliquots of hemin chloride dissolved in 0.1 M NaOH were titrated into the cuvette and allowed to equilibrate for fifteen minutes prior to measurements. The signal from a 10 mM acetate buffer blank was also recorded and subtracted as a background signal. Titrations continued until the buffering capacity was lost and hemin aggregation apparent. All CD experiments were averaged over five scans from 190-269 nm at a scan rate of 0.5 nm/0.5 sec on an AVIV Model 215 Circular Dichroism Spectrometer (Lakewood, NJ) equipped with a pH probe. Control experiments with hemin chloride (dissolved in 0.1 M NaOH) alone in 10 mM acetate buffer, pH 4.8, under identical instrumentation settings and conditions did not give any appreciable CD signal indicating the changes in the CD spectra arise from template:heme interactions. The ellipticity was expressed as the mean residue molar ellipticity, $[\theta]$ ($\text{deg cm}^{-2} \text{dmol}^{-1}$). The spectra were smoothed by the Savitzky-Golay algorithm.

3.3. Preliminary Studies

To ensure the binding assay protocol provided an adequate equilibration time for the templates, an equilibration time study was performed with BNT IIA and compared with the equilibration times previously established by Ziegler.³⁶ Initial estimates concluded this alternate domain template bound 7-9 equivalents of hemin chloride, thus the time study involved monitoring the change in absorbance upon binding slightly fewer equivalents of hemin (6 eq.) to ensure that problems associated with saturable binding were not present. From the results below in **Figure 3.1**, the majority of the binding occurred within five to ten minutes after the addition of hemin chloride. Relatively small changes in the absorbance were observed thereafter, thus a fifteen minute equilibration time was used throughout the binding studies, similar to the binding time constraints employed by Ziegler for BNT II.³⁶

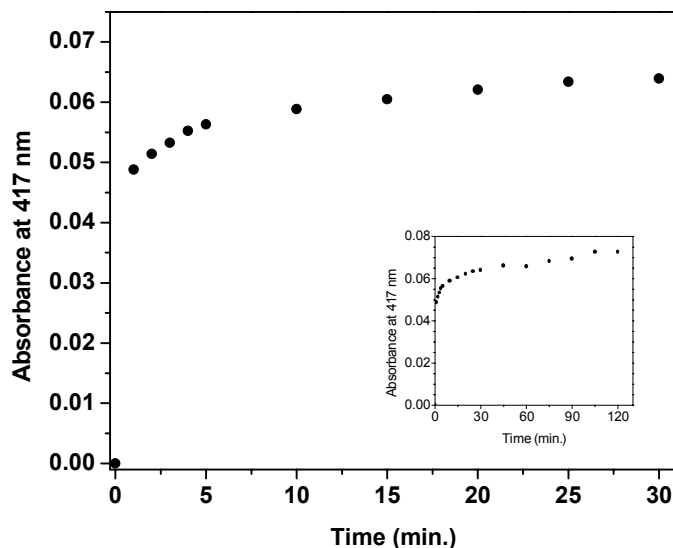


Figure 3.1. Binding equilibration study of BNT IIA with 6 equivalents of hemin chloride in 100 mM acetate buffer, pH 4.80, at 22°C. The inset depicts the complete time range of the experiment.

BNT II and BNT IIA were more soluble than recombinant forms of HRP II, dissolving to concentrations of approximately 10 mg mL⁻¹ in 100 mM acetate buffer, pH 4.8, as compared to 1 mg mL⁻¹ for the protein.⁴¹

3.4. Putative Domain Studies

(The Ala-His-His-Ala-His-His-Ala-Ala-Asp and Ala-His-His-Ala-Ala-Asp-Ala-His-His Domains)

3.4.1. BNT II (The Ala-His-His-Ala-His-His-Ala-Ala-Asp Domain)

3.4.1a. Interaction with Heme

The electronic absorption spectrum for the interaction of hemin chloride with BNT II has a single Soret peak centered around 419 nm (**Figure 3.2**). BNT II alone has no appreciable absorbance in the 300-600 nm region (**Figure 3.2 inset**). Hemin chloride in 100 mM sodium acetate buffer, pH 4.80, mimicking the pH of the digestive vacuole of *P. falciparum* (pH 4.5-5.5), has a characteristic Soret band at 385 nm. Thus upon binding, the Soret region of the spectrum red-shifted approximately 34 nm from its original value with Fe(III)PPIX. Visible changes to the absorption spectra were observed after the addition of only 1 equivalent of heme. Though the data presented is normalized to enhance the red-shift in the Soret region upon substrate binding, the spectra sharpened and continued to increase in intensity until a plateau was reached or a slight decrease in absorbance was recorded. At this point binding was noted to have ceased and hemin aggregation was visibly apparent.

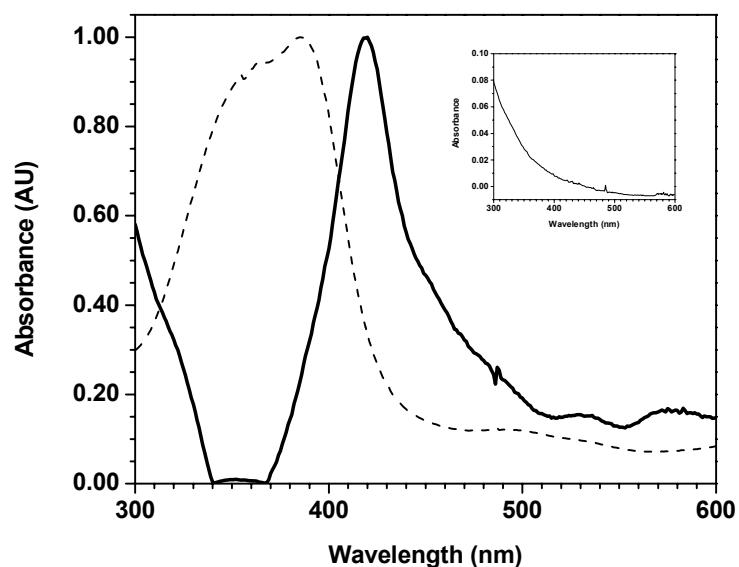


Figure 3.2. UV-Vis spectrum of the interaction of hemin chloride with BNT II, represented by the (—) solid line. Samples of approximately 1 equivalent of hemin chloride were added to 1-5 nmoles of template in 100 mM acetate buffer, pH 4.8. Hemin chloride in buffer alone is represented by the (---) dashed line. Spectra were normalized to enhance the red-shift of the Soret band upon substrate binding. The UV-Vis spectrum of BNT II had no appreciable absorbance in the 300-600 nm region (inset).

As seen in **Figure 3.3**, the first postulated putative binding domain, BNT II bound 9.83 ± 0.21 equivalents of heme. Purified HRP II bound 17 equivalents of hemin chloride under similar buffer conditions.¹⁵ Given the geometry of the MAPS core, it is not surprising that BNT II bound slightly fewer equivalents of hemin than the native protein, seeing how interior sites may be occluded near the dendrimeric core. The hemin binding stoichiometries for BNT II are also slightly lower than that reported by Ziegler *et al.*,³⁶ though with notably less error. Incidentally, the MAPS core (commercially purchased from AnaSpec Inc., San Jose, CA) was slightly

modified from the previous work, having an alanine linkage at the base of the dendrimeric scaffolding rather than a glycine residue. If the sole consideration for hemin binding concerned intermolecular interactions, the differences in the MAPS core may be insignificant, but given the dendrimeric nature of the template, intramolecular forces may also interplay.

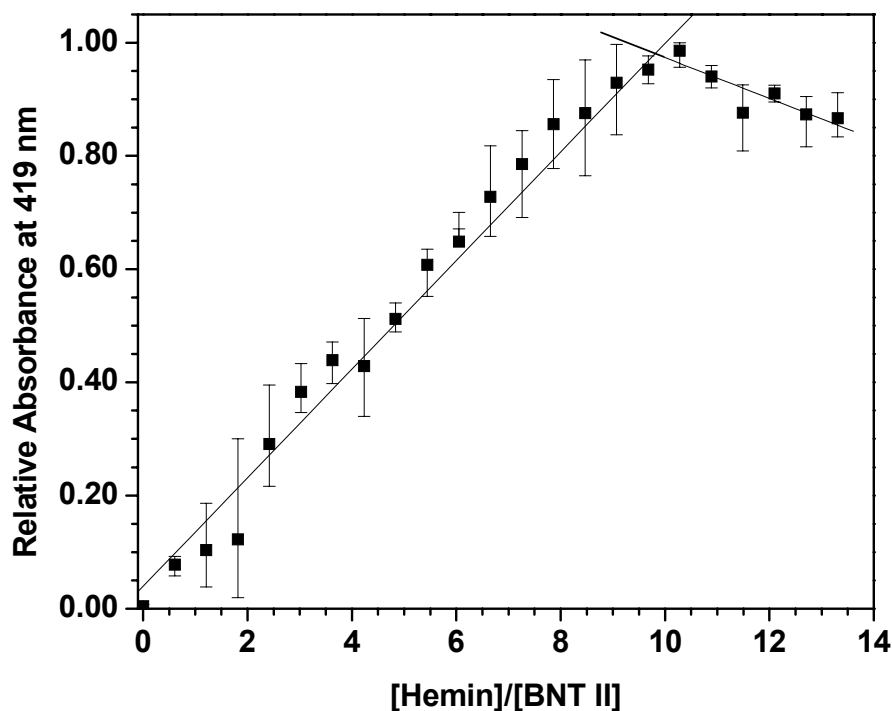


Figure 3.3. Hemin chloride titration binding curve for BNT II. The plot was generated from the UV-Vis difference absorption spectra based on methods established by Morgan.^{37,38} The data presented is the averaged result of three independent binding titration experiments. Individual binding experiments are shown in **Appendix II, page A-4**.

After the stoichiometric binding maxima, the difference titration curve seems to reflect a significant change in the electronic structure of the species in solution. Most titration binding curves exhibit only a slight divergence from the plateau upon

saturable binding, but the hemin binding curve associated with BNT II decreases drastically. Typically at such high stoichiometries of hemin substrate, this decrease in absorbance intensity was also followed by visibly apparent hemin aggregation and/or precipitation. Though a number of aggregative interactions are possible, it is intriguing to note such behavior is reminiscent of nucleation steps in biomineralization processes.

3.4.1b. Interaction with Zinc (II) Protoporphyrin IX

Zinc protoporphyrin IX was also recognized by BNT II, binding 13.40 ± 0.31 equivalents of the substrate (**Figure 3.4**). This does not necessarily imply that Zn(II)PPIX has a different binding domain from the iron porphyrin since BNT II bound more equivalents of the zinc porphyrin, but suggests such interactions between the substrate and template may slightly vary with secondary interactions occurring somewhere along the peptide dendrimer. The fact that protoporphyrin IX was also capable of binding to BNT II as determined by Ziegler,³⁶ suggests that substrate association with BNT II is not driven by the axial ligation of a histidine residue to a metal.³⁶ Furthermore, since the pK_a of histidine is 5.8, the moiety is most likely protonated under the experimental reaction conditions, and therefore axial ligation to a metal is doubtful.

The fluorescence quenching studies of Zn(II)PPIX provided additional evidence for the interaction of the zinc porphyrin with BNT II. With the final concentration of Zn(II)PPIX being 1×10^{-5} M in 4.0 mL of solution, various concentrations of BNT II in 100 mM acetate buffer, pH 4.8, quenched the

fluorescence of the fluorophore (**Figure 3.5**). The fluorescence intensity at the [BNT II]/[Zn(II)PPIX] of 0.1 was already decreased by 45% of the original value. The change in fluorescence intensity at the same 0.1:1 ratio of template to porphyrin only decreased by 23% when BNT I was examined (**Figure 3.5 inset**). These results are expected and consistent with other studies involving BNT I, since the first generation dendrimer has half as many of the designed binding domains. The fluorescence of BNT II was completely quenched at a 0.3:1 ratio of template to porphyrin.

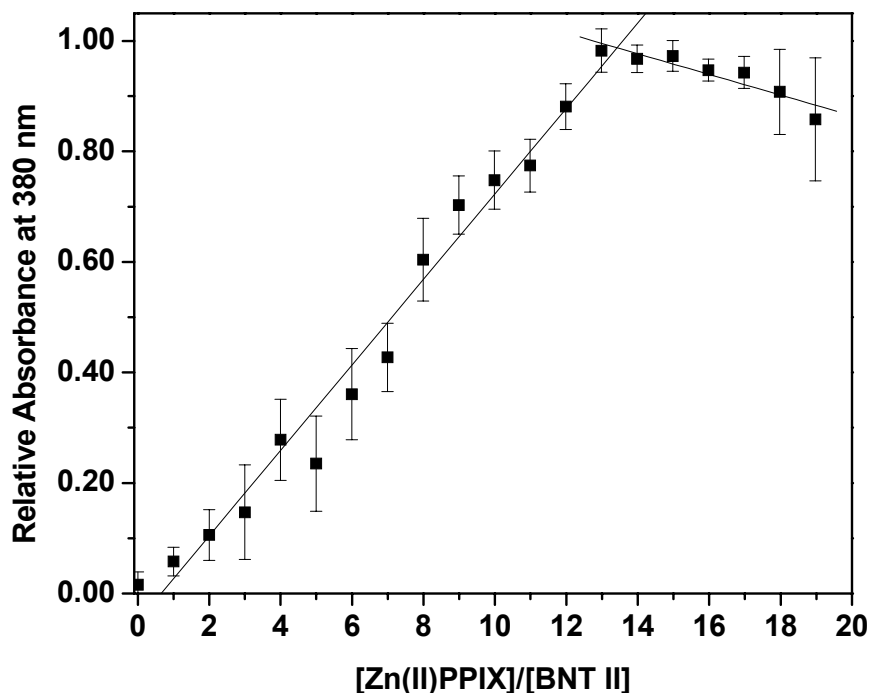


Figure 3.4. Zn(II)PPIX titration binding curve for BNT II. The plot was generated from the UV-Vis difference absorption spectra based on methods established by Morgan.^{37,38} The data presented is the averaged result of five independent binding titration experiments. Individual binding experiments are shown in **Appendix II, page A-5**.

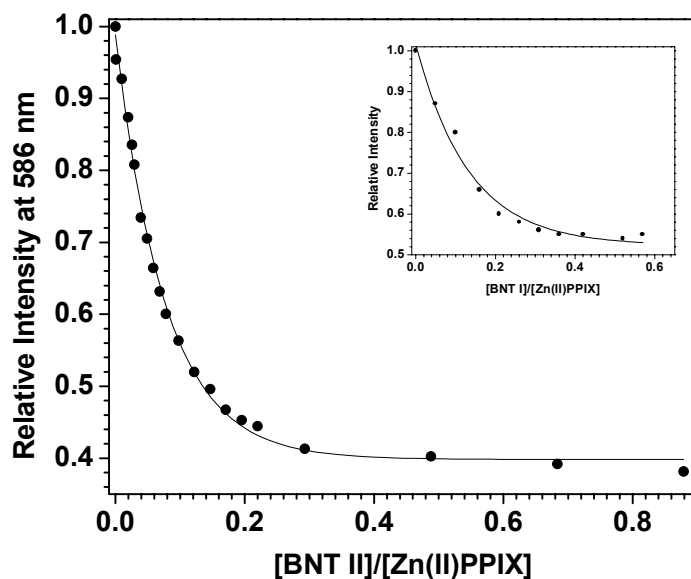


Figure 3.5. Fluorescence quenching studies of Zn(II)PPIX with BNT II. Samples were excited at 410 nm and monitored at the emission maxima of the fluorophore. The inset displays the experiment with the single nucleating domain, BNT I, for comparison.

3.4.1c. Heme Aggregation Activity

In the presence of free heme under acidic conditions, the BNT II dendrimer promoted 5.63 ± 0.04 nmoles of insoluble aggregated heme product. This value was the average of five separate reactions and compared well to the 5.5 ± 0.5 nmoles of hemozoin produced by the same template when Zielger *et al.*³⁶ performed the assay.

The assay protocol called for exhaustive washing cycles of sodium bicarbonate and water, which could ultimately lead to inconsistent results if not completed meticulously. Not only was the differential solubility of the heme products important in the processing of the samples in order to obtain values free of hematin derivatives, but also proper centrifugation was crucial in order to pellet the

small sample of hemozoin that remained. Further discussion on the heme aggregation activity of BNT II is presented in the discussion of the putative domain studies, **Section 3.5**.

3.4.1.d. Circular Dichroism Studies

Though the circular dichroism spectra of BNT II did not substantially change over a broad pH range (**Figure 3.6**), the spectra of hemin titration interacting with BNT II did (**Figure 3.7 A**). Although the 10 mM concentration of the sodium acetate buffer greatly reduced the buffering capacity of the heme titration assays, the notable changes in the circular dichroism spectra suggest a physical interaction between BNT II and hemin at pH 4.8. Such changes in the CD spectra were also noted upon the addition of Zn(II)PPIX (**Figure 3.7 B**). Despite the fact that BNT II bound a

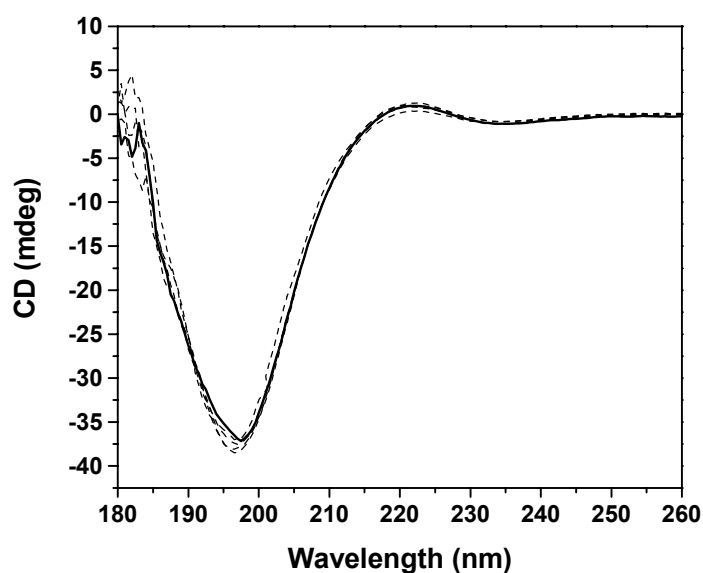


Figure 3.6. Circular dichroism spectra of BNT II at pH 4.86 (—) and (----) pH 6.03, 7.03, 8.13, and 9.05. **Note:** The change in pH was monitored by the dropwise addition of 0.1 M NaOH and therefore spectra were recorded as a change in CD signal rather than in units of molar ellipticity.

significant amount of both Fe(III)PPIX and Zn(II)PPIX, the CD titration experiments with both porphyrins exhibited some dissimilarities. Hemin binding notably altered the spectrum of BNT II after the addition of only one equivalent of the iron porphyrin, while Zn(II)PPIX did not cause such perturbations until additional equivalents were added. Moreover, the deep negative peak centered around 200 nm red-shifted approximately 1 nm upon the addition of one equivalent of Fe(III)PPIX, while the spectrum of the zinc porphyrin associated with BNT II remained the same. After binding six equivalents of hemin this same peak shifted approximately 2 nm from its original value, while the addition of the same number of equivalents of Zn(II)PPIX altered the spectrum by only 0.5 nm. Complete CD titration experiments are listed in **Appendix III, pages A-28 and A-29.**

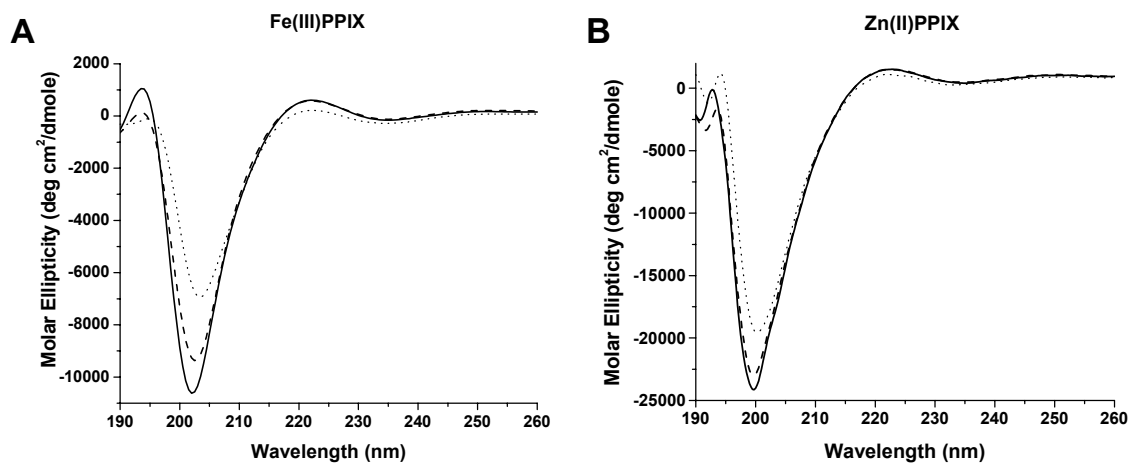


Figure 3.7. Circular dichroism spectra of BNT II and the corresponding spectral changes upon addition of **(A)** Fe(III)PPIX at (—) 0 eq., (----) 1.36 eq., and (.....) 6.12 eq. and **(B)** Zn(II)PPIX at (—) 0 eq., (----) 1.73 eq., and (.....)6.05 eq.

Tables 3.1 and **3.2** compare the spectral features for the binding of the iron (III) and zinc (II) porphyrins respectively. Typically a negative ellipticity centered around 222 nm is indicative of α -helicity in polypeptides. As demonstrated below, the binding of both metal porphyrins modifies this region of the spectra to the exact same extent upon the addition of six equivalents of each porphyrin (383 deg cm^2/dmole). This suggests that for at least BNT II helicity is not only increased upon binding both Fe(III)PPIX and Zn(II)PPIX, but also the mechanism of this binding seems to be similar. The fact that BNT II bound more equivalents of the zinc porphyrin when compared to Fe(III)PPIX in the binding titration assays performed earlier suggests a secondary zinc binding site may be present that may not be located at a CD active position. Further insight into this hypothesis was not explored due to the fact the zinc porphyrin is not the natural substrate involved in the aggregation of hemozoin. In addition, the limited buffering capacity of the 10 mM sodium acetate solution greatly reduced the amount of porphyrin that could be examined.

While interpretation of the CD spectra for BNT II is obviously made difficult by the high content of histidine which dominates the absorbance properties of the spectra, similarities between recombinant HRP II⁴² and BNT II can be made. In addition to sharing the same spectral markers, both rHRP II and BNT II are stable over a broad range of pHs. Both display a red-shift in the peak centered around 200 nm and a negative divergence of the CD spectra at 222 nm upon hemin binding. While the secondary structure of BNT II has yet to be conclusively established, the

BNT II	π - π^* (nm) (x,y)	n - π^* (nm) (x,y)	π - π^* (nm) (x,y)
No hemin	202.0 (-10675.57)	222.0 (591.28)	234.0 (-165.86)
1.36 eq. Hemin	202.5 (-9301.80)	222.0 (574.60)	235.0 (-128.47)
6.12 eq. Hemin	203.5 (-6940.78)	222.0 (208.37)	235.0 (-279.36)

Table 3.1. CD spectral markers for Fe(III)PPIX titration with BNT II averaged over five individual scans. Each value in parentheses is the molar ellipticity data obtained at the corresponding wavelength, which was included to illustrate the change in secondary structure upon porphyrin binding.

BNT II	π - π^* (nm) (x,y)	n - π^* (nm) (x,y)	π - π^* (nm) (x,y)
No Zn(II)PPIX	199.75 (-24138.37)	222.0 (1480.49)	235.0 (423.96)
1.73 eq. Zn(II)PPIX	199.75 (-23031.47)	222.0 (1445.47)	235.0 (510.88)
6.05 eq. Zn(II)PPIX	200.0 (-19585.62)	222.0 (1097.26)	233.0 (271.80)

Table 3.2. CD spectral markers for Zn(II)PPIX titration with BNT II averaged over five individual scans. Each value in parentheses is the molar ellipticity data obtained at the corresponding wavelength, which was included to illustrate the change in secondary structure upon porphyrin binding.

fact that hemin chloride interaction elicits a structural change in the peptide supports a prerequisite of a higher ordered structural requirement in the biomineralization of hemozoin.

3.4.2. BNT IIA (The Ala-His-His-Ala-Ala-Asp-Ala-His-His Domain)

3.4.2a. Interaction with Heme

The electronic absorption spectrum for the interaction of hemin chloride with BNT IIA has a single Soret peak centered near 417 nm (**Figure 3.8**). Again, like

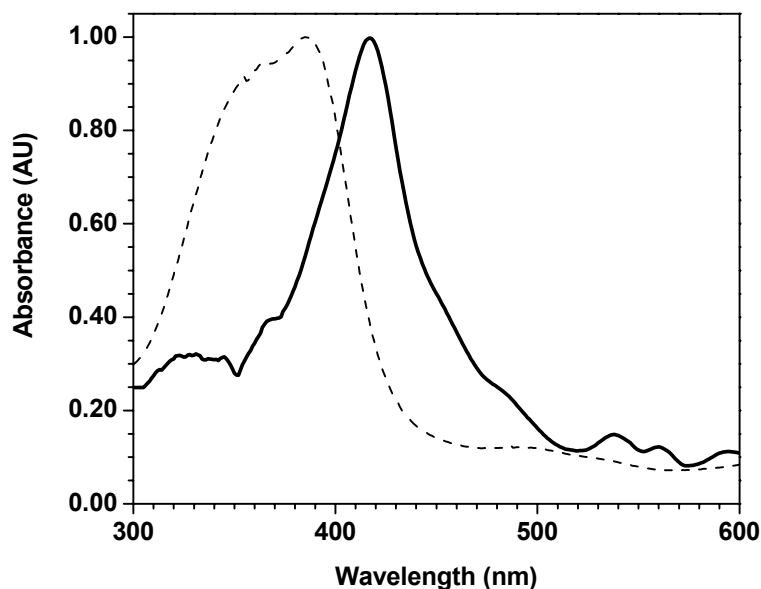


Figure 3.8. UV-Vis spectrum of the interaction of hemin chloride with BNT IIA, represented by the (—) solid line. Samples of approximately 1 equivalent of hemin chloride were added to 1-5 nmoles of template in 100 mM acetate buffer, pH 4.8. Hemin chloride in buffer alone is represented by the (---) dashed line. Spectra were normalized to enhance the red-shift of the Soret band upon substrate binding.

BNT II, the peptide BNT IIA in the absence of hemin has no appreciable absorbance in the 300-600 nm region (data not shown). Therefore, upon binding, the Soret region of the spectrum red-shifted approximately 32 nm from the original Soret region at 385 nm for hemin chloride alone. Visible changes to the absorption spectra again were observed after the addition of only 1 equivalent of heme and normalized to enhance the red-shift in the Soret region upon substrate binding. Saturable binding was noted when the increase in absorbance reached a plateau and afterwards began to decrease.

The alternative putative binding domain, BNT IIA, bound 8.70 ± 0.81 equivalents of hemin chloride (**Figure 3.9**), which is approximately 1 equivalent less than BNT II. When considering the arrangement of the amino acids in either the 3-10 helix or left-handed polyproline II conformations as suggested earlier, BNT II has an arranged face of $[(\text{HHDHHDHHDHHD})_2]_4$ while BNT IIA shares a similar face of $[(\text{HDHHDHHDHHDH})_2]_4$. With sterics likely playing a factor in the design of the templates, and a lack of a crystal structure, it becomes nearly impossible to explain the binding values with any certainty at this point, since the arranged faces of the two peptides are similar in amino acid composition.

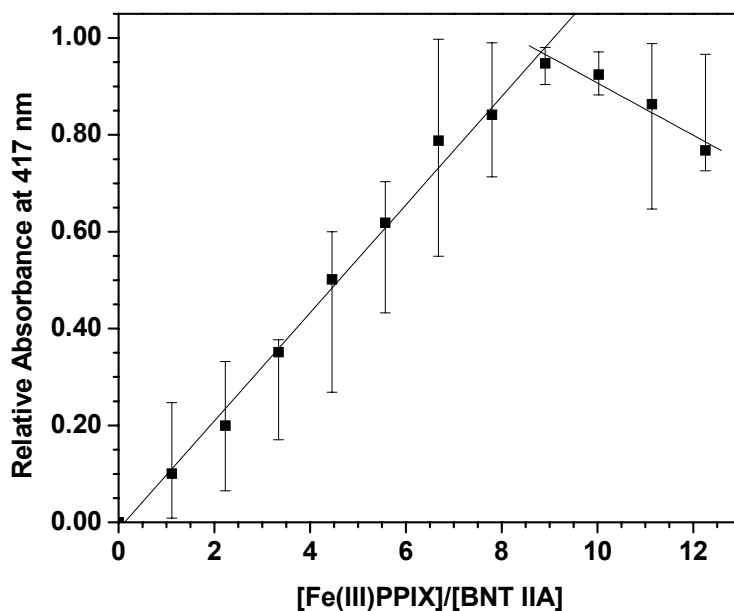


Figure 3.9. Hemin chloride titration binding curve for BNT IIA. The plot was generated from the UV-Vis difference absorption spectra based on methods established by Morgan.^{37,38} The data presented is the averaged result of five independent binding titration experiments. Individual binding experiments are shown in **Appendix II, page A-6**.

Like BNT II, the BNT IIA binding curve did not exhibit a plateau region seen with typical saturable substrate binding assays. Such results are indicative of porphyrin aggregation.

3.4.2b. Interaction with Zn(II) Protoporphyrin IX

When porphyrin binding was assayed with Zn(II)PPIX, BNT IIA bound 3.96 ± 0.45 equivalents of Zn(II)PPIX (**Figure 3.10**), which is about half as many equivalents as noted with Fe(III)PPIX binding.

The fluorescence quenching experiments involving BNT IIA supported the reduced binding capability of Zn(II)PPIX (**Figure 3.11**), when compared to BNT II.

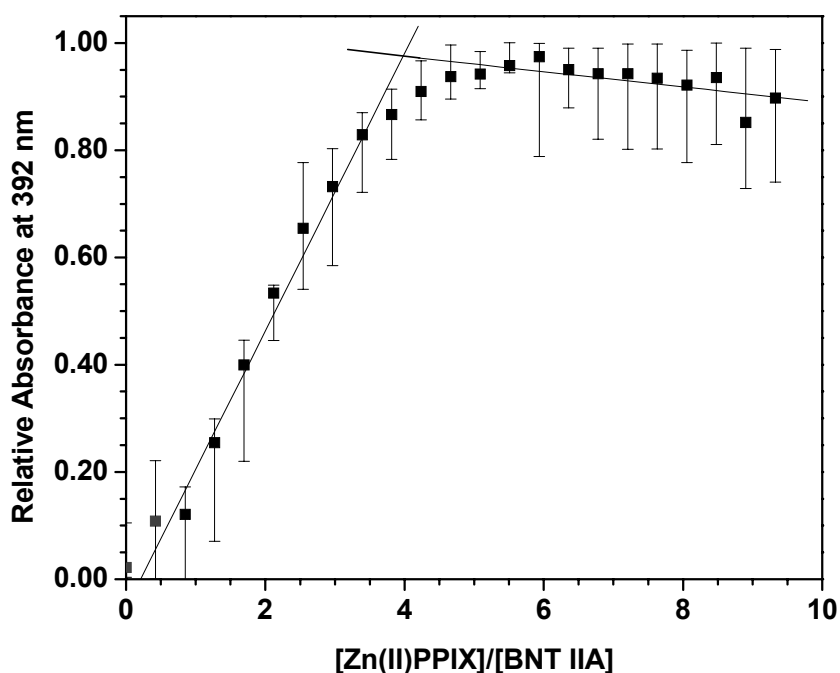


Figure 3.10. Zn(II)PPIX titration binding curve for BNT IIA. The plot was generated from the UV-Vis difference absorption spectra based on methods established by Morgan.^{37,38} The data presented is the averaged result of eight independent binding titration experiments. Individual binding experiments are shown in **Appendix II, pages A-7 and A-8.**

At a 0.1:1 ratio of BNT IIA to Zn(II)PPIX the fluorescence of the chromophore was already quenched. In contrast with BNT II at this same ratio of template to porphyrin, BNT IIA was no longer interacting with the excess porphyrin in solution. A fifty percent quench in the fluorescence was noted at a BNT IIA to porphyrin ratio of 0.02:1.

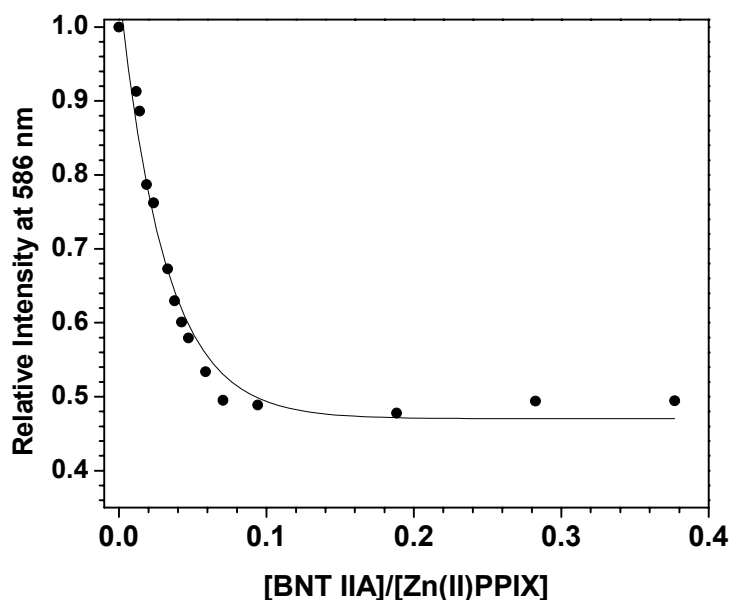


Figure 3.11. Fluorescence quenching studies of Zn(II)PPIX with BNT IIA. Samples were excited at 410 nm and monitored at the emission maxima of the fluorophore.

3.4.2c. Heme Aggregation Activity

The BNT IIA dendrimer promoted 2.60 ± 0.60 nmoles of insoluble aggregated heme product based on an average of twelve individual experiments after background hemozoin formation was subtracted, which for this set of experiments was 1.60 ± 0.10 nmoles of aggregated heme.

3.4.2d. Circular Studies

After initial CD studies with BNT II, circular dichroism spectroscopy was only used to monitor heme binding, since Fe(III)PPIX is the natural substrate involved in hemozoin formation. Additionally, since the full binding capacity could not be achieved due to the limited buffering capacity of the 10 mM sodium acetate solution, changes in the circular dichroism spectra upon hemin binding were evaluated after approximately 1 equivalent of hemin was added and then again at half of the experimentally determined full binding capacity. For example, BNT IIA bound 8.70 equivalents of hemin chloride under the experimental conditions employed in the porphyrin binding assay, so in the circular dichroism experiments, binding at half-capacity was assessed at approximately 4 equivalents of hemin.

As seen in **Figure 3.12**, BNT IIA has a deep negative peak centered around 198 nm. Like BNT II, BNT IIA displays a positive peak at 222 nm and also a negative trough near 234 nm. The deep negative peak however, is much broader than that of BNT II. The addition of approximately 1 equivalent of hemin chloride did not alter the spectrum significantly either, as occurred with BNT II. The spectrum did red-shift upon the addition of higher equivalents of hemin chloride. Spectral shifts associated with binding approximately one equivalent of hemin and at half maximal binding are listed in **Table 3.3** (See **Appendix III, page A-30** for complete CD titration experiments for BNT IIA). It is interesting to note the spectral marker near 234 nm diminishes at higher equivalents of hemin, as demonstrated in **Figure 3.12** by

the dotted line representing 4.88 eq. of hemin, and a new minimum centers around 227 nm.

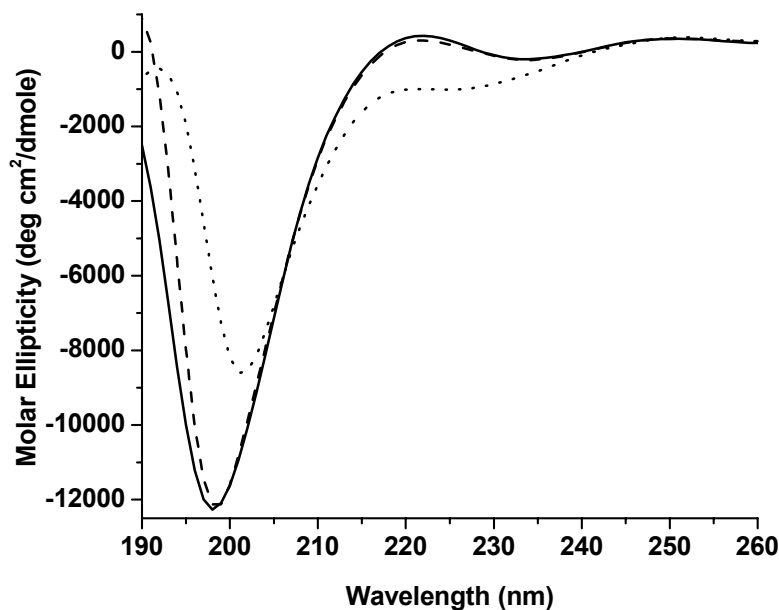


Figure 3.12. Circular dichroism spectra of BNT IIA (—) and the corresponding spectral changes upon the addition of hemin chloride. Spectra are shown upon the addition of 0.81 (----) equivalents of substrate and 4.88 equivalents (.....) of substrate ($\frac{1}{2}$ of the full binding capacity experimentally determined for BNT IIA). Actual spectral shifts and signal intensities are listed in **Table 3.3**

BNT IIA	π - π^* (nm) (x,y)	n - π^* (nm) (x,y)	π - π^* (nm) (x,y)
No hemin	198.0 (-12263.11)	222.0 (425.38)	234.0 (-203.47)
0.81 eq. Hemin	198.3 (-12135.38)	222.0 (279.22)	233.0 (-218.94)
4.88 eq. Hemin	201.0 (-8611.48)	222.0 (-977.79)	227.0 (-1008.51)

Table 3.3. CD spectral markers for Fe(III)PIX titration with BNT IIA averaged over five individual scans. Each value in parentheses is the molar ellipticity data obtained at the corresponding wavelength, which was included to illustrate the change in secondary structure upon porphyrin binding.

3.5. Discussion

Within the HRP II sequence, which is comprised of 76% of histidine and alanine residues, the prevalence of an Ala-His-His repeat becomes apparent. Upon further examination of this trimeric repeat, a higher organizational scheme is revealed. An Ala-His-His-Ala-His-His-Ala-Ala-Asp domain is repeated 16 times while an alternative domain, Ala-His-His-Ala-Ala-Asp-Ala-His-His, is repeated 23 times. With the establishment of BNT II as a functional peptide mimic of HRP II by Zielger *et al.*,³⁶ we elucidated the role of this putative nucleation domain, Ala-His-His-Ala-His-His-Ala-Ala-Asp, against the alternative hypothetical nucleation domain, Ala-His-His-Ala-Ala-Asp-Ala-His-His, sequenced within another peptide dendrimer deemed BNT IIA (the first Alternate of BNT II). Our bionucleating templates each possessed four dendrimeric branches with the respective sequences repeated twice per branch, resulting in each peptide dendrimer possessing 8 copies of the particular putative nucleation domain. Distinctions between the two domains allowed for the evaluation of the significance of the Ala-His-His repeat in the two postulated hemozoin templating sequences. Placement of the Ala-His-His repeat to the end of the nucleation domain, as in BNT IIA, will reveal information as to both the binding and nucleating capabilities of the template when the Ala-His-His repeat is interrupted, as well as revealing which domain is the most probable hemozoin nucleation domain within the HRP II sequence.

When investigating antimalarial strategies targeting hemoglobin catabolism and the processes therein, the reaction medium cannot be disregarded since hemozoin

formation is confined to the parasite's digestive vacuole, which sustains an acidic environment (pH 4.5-5.5). Such acidity can have a twofold effect on both reactivity and stability. First, since the pK_a of histidine is 5.8, positively charged His⁺ is unavailable to bind to metals. Secondly, heme insolubility and other aggregation/precipitation issues occur when the pH is acidic, requiring meticulous and tedious workups of such studies in order to obtain results free of non-hemozoin Fe(III) aggregates.

Free, unbound heme has a low, broad Soret peak centered at 385 nm as detected by UV-Vis spectroscopy. In heme binding assays, observing an increase in the Soret absorbance and/or red-shift in the Soret peak is indicative of substrate binding while decreases in absorbance and/or a blue-shift in the Soret peak characterizes substrate binding interference or inhibition. The natural histidine-rich protein II in acidic medium (pH 4.5-5.5) bound heme with a Soret peak red-shifted to 414 nm. Linear multimers of HRP II sequences [(Ala-His-His-Ala-His-His-Ala-Ala-Asp)₂ and (Ala-His-His-Ala-His-His-Ala-Ala-Asp)₃, but at pH 7.4] were also capable of heme binding, with a detectable Soret peak centered at 413 nm.⁴³ Our peptide dendrimers, BNT II and BNT IIA, had Soret peaks indicative of substrate binding as well, with peaks centered around 419 nm and 417 nm respectively. Although the absorbance wavelengths varied according to the template (**Table 3.4**), both were slightly red-shifted from that of HRP II.

The absorbance maximas involving the Zn(II)PPIX substrate also varied according to the template, with detectable Soret peaks at 380 nm and 392 nm for

BNT II and BNT IIA respectively (**Table 3.4**). The absorption spectra of the zinc porphyrin binding assays did experience an increase in intensity in the Soret absorbance, but both were blue-shifted from the Soret peak of Zn(II)PPIX, which is centered around 400 nm.

Template	Fe(III)PPIX Absorbance Maxima (nm)	Zn(II)PPIX Absorbance Maxima (nm)
BNT II	419	380
BNT IIA	417	392

Table 3.4. Absorbance maximas for templates BNT II and BNT IIA with Fe(III)PPIX and Zn(II)PPIX.

Initial porphyrin binding studies indicated that BNT II and BNT IIA had relatively similar Fe(III)PPIX binding affinities (9.83 ± 0.21 and 8.70 ± 0.81 eq. respectively) (**Figure 3.13**). Assuming the histidine residues are involved in binding, both BNT II and BNT IIA have the same number of Ala-His-His repeats and consequently bound similar equivalents of the natural iron substrate. BNT IIA however, had a drastically reduced ability to bind the zinc porphyrin, binding only 3.96 ± 0.45 equivalents of substrate, while BNT II was capable of binding 13.40 ± 0.31 equivalents. In fact, when reviewing earlier work presented by Ziegler *et al.*,³⁶ a first generation peptide dendrimer, BNT I, which had the Ala-His-His-Ala-His-His-Ala-Ala-Asp sequence repeated once per branch (half as many as BNT II), bound more of the zinc porphyrin (6.80 ± 0.50 eq.) than the second generation template BNT IIA (**Figure 3.13**), which disrupted the Ala-His-His repeat. From the data presented, the perturbed spatial distributions of the amino acids within the nucleating domain,

specifically the interruption of the Ala-His-His repeat, affected binding between the zinc substrate and template. The discrepancies in the binding data may be suggestive of nonspecific interactions between the substrate and template or possibly indicative of specific interactions between the polymer chains of the dendrimeric peptide.

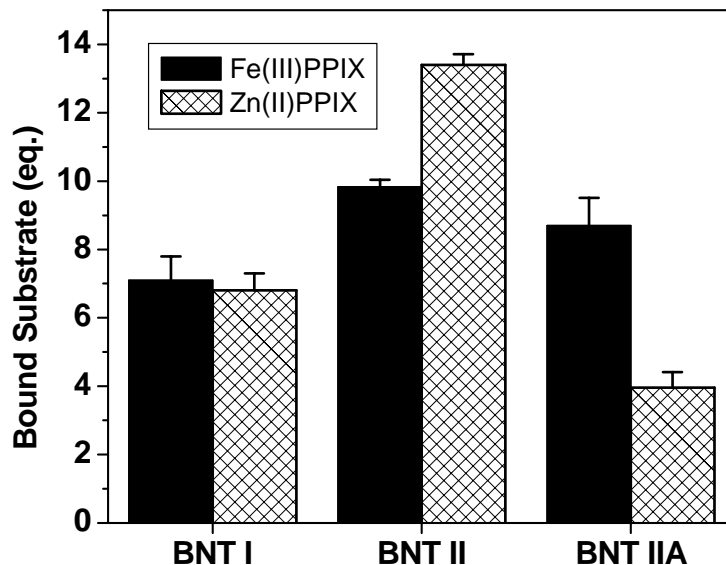


Figure 3.13. Substrate binding of the hypothesized putative nucleation domains. BNT II and BNT IIA with Fe(III)PPIX and Zn(II)PPIX. The first generation dendrimer, BNT I was added to expand the discussion of the templates with the permission of Zielger *et al.*³⁶

The fluorescence quenching studies provided an alternative means by which to examine the zinc porphyrin interactions since both templates shared similar iron porphyrin efficacies, but had vastly different values for Zn(II)PPIX. As a precaution, it was crucial that the concentration of the zinc porphyrin remained constant (1×10^{-5} moles/L), while varying the concentration of the peptide templates to ensure a monomeric state of porphyrin. If porphyrin concentrations become too high, the

monomers aggregate to dimers, which fail to fluoresce. Additionally, since the experiment is performed in aqueous solutions, fluorescence intensity readings do not increase linearly as the concentration of the porphyrin increases, as it would be if carried out in organic medium and therefore more reproducible results are obtained if the concentration of the porphyrin is unvaried. This method also negated the salt effect since the concentration of buffer is kept constant throughout the experimentation, seeing how salts can promote porphyrin aggregation.

The fluorescence quenching studies did support the reported disproportion in the zinc protoporphyrin binding data between BNT II and BNT IIA. Typically the fluorescence of Zn(II)PPIX continues to decrease as there are less monomers in solution, resulting from the template binding to the zinc porphyrin. The rate of decrease in fluorescence intensity for both templates follows a first order exponential decay pattern (**Figure 3.14**), suggesting the mode of binding with the zinc porphyrin may be similar between the two templates. The fluorescence quenching of Zn(II)PPIX displayed a three fold increase with BNT II compared to BNT IIA (0.03:1 vs. 0.01:1 ratios of template to porphyrin), which was the same excess noted in the UV-Vis binding titration experiments (13.40 and 3.96 equivalents for respectively). Actual stoichiometries for the fluorescence quenching studies were not determined since a number of porphyrin self-aggregation processes could occur at the working concentration of Zn(II)PPIX.

As noted before, heme binding alone does not elicit hemozoin formation. Results obtained from the *in vitro* heme aggregation assays, indicated BNT II

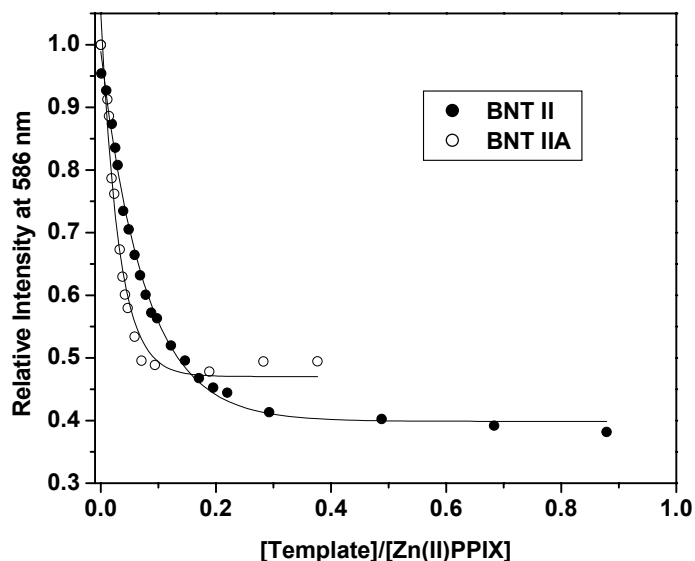


Figure 3.14. Fluorescence quenching of Zn(II)PPIX with putative domain peptides BNT II and BNT IIA.

aggregated twice as much hemozoin as both BNT I (again from Zielger³⁶) and BNT IIA (**Figure 3.15**). Even though BNT II and BNT IIA bound nearly equal amounts of the iron porphyrin, hemozoin production was drastically reduced in the latter mutant. Seemingly, again the interruption of the Ala-His-His repeat in BNT IIA impeded the production of hemozoin by as much as half. Upon further sequence examination of BNT IIA, the full sequence of the Ala-His-His-Ala-His-His-Ala-Ala-Asp domain can be located once along the chain length. Consequently, the production of hemozoin mediated by BNT IIA is equivalent to that mediated by BNT I, which also has this 9-mer sequence repeated only once per dendrimeric branch.

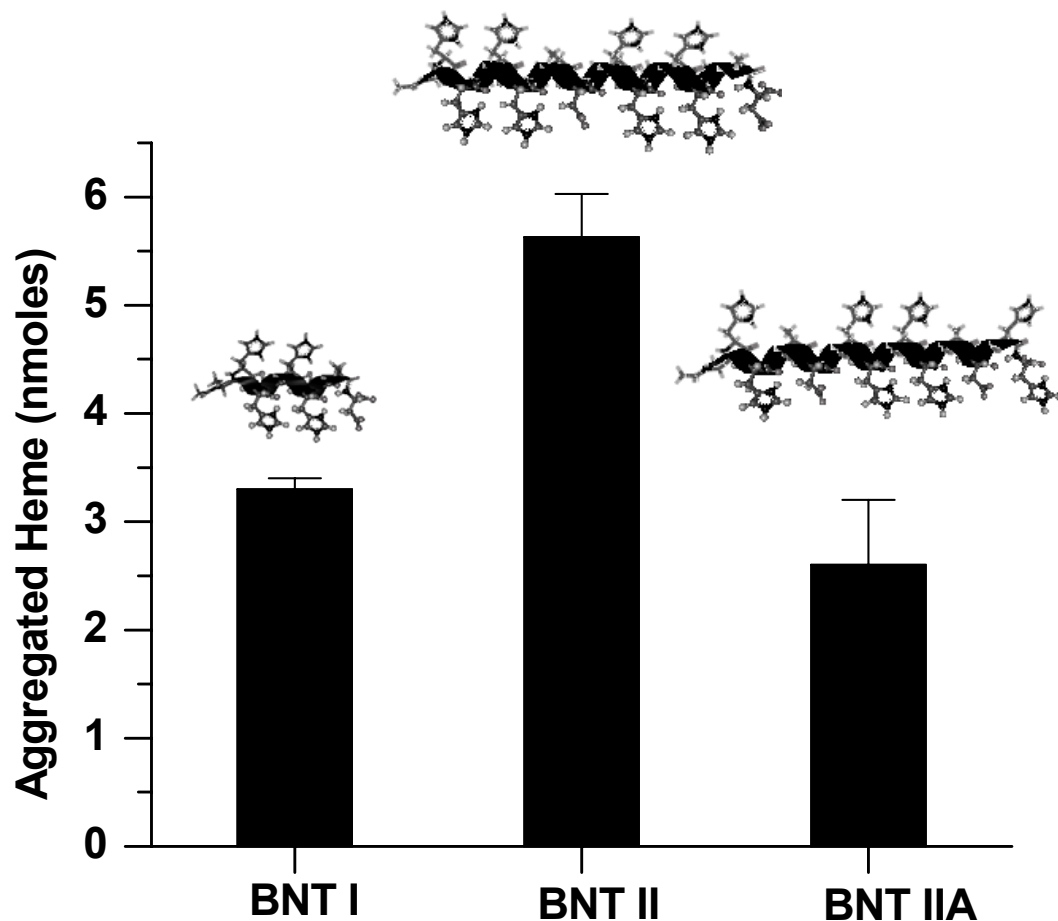


Figure 3.15. Hemozoin production mediated by the putative nucleation domains. Molecular models of the templates as 3-10 helices are added for dimensional clarity. BNT I was added to expand the discussion of the templates with the permission of Zielger *et al.*³⁶

The unusually high content of histidine in HRP II and our bionucleating templates warrants additional considerations when analyzing the data collected. Histidine exists in a partially protonated, partially deprotonated form at physiological pH, thus changes in pH are likely to influence the biological effects exerted by these residues. The effect of pH on proteins rich in histidine has been well documented, demonstrating that such proteins are extremely pH sensitive, being modified not only

by the solution phase, but also by subsequent binding interactions.⁴⁴ Since metal and heme binding are pH dependent, substrate binding diminishes when histidine residues become protonated. Such tightly controlled binding capabilities are likely to influence other cellular interactions in addition to the parasitic homeostasis involved in the biomineralization of hemozoin. Thus, it becomes imperative to characterize such binding sites and uncover the role of the abundant histidine residues in HRP II.

With the peptides modeled as potential right-handed 3-10 helices and left-handed polyproline type II conformations, every second and third residue in both 9-mer putative nucleation domains (amino acids in positions 2,3,5,6,8 and 9) are packed towards the outside, being exposed to solvent, while the conserved alanine residues (at positions 1,4 and 7) are on the opposite face, collapsing inward as a result of the hydrophobic interchain interactions. This suggests that the high histidine content alone may not be sufficient for procuring the heme binding sites involved in the formation of the biomineral, and is supported by the fact that polyhistidine, itself existing in a random coil configuration, failed to promote the formation of insoluble heme aggregates.³⁶

Circular dichroism spectroscopy is widely used for studying peptide and protein conformations. The role of specific residues can be explored through site-directed mutagenesis studies capitalizing on the sensitivity of this spectroscopic method to detect and characterize any structural alterations resulting from the corresponding amino acid substitution. A recent study included such analyses on HRP I peptides in attempt to induce immunogenicity through amino acid mutations

that increased helicity.⁴⁵ Our efforts incorporated the use of circular dichroism spectroscopy to not only detect the spectral differences associated with the specific template mutations, but to also identify any secondary structural changes that may be induced upon hemin binding.

Conformational analysis by circular dichroism spectroscopy gives rise to two fundamental questions that remain unresolved despite recent advances in x-ray crystallography and both high resolution and multidimensional NMR. The first debate regards how exactly protein or peptide native structure is encoded in the amino acid sequence.⁴⁶ The second dispute examines the individual properties of the amino acid residues and the corresponding contribution to both the local environment and overall secondary structure of the protein or peptide, attempting to correlate conformation and activity.⁴⁷

The folding of a protein or peptide into a higher ordered structure is a fundamental requirement necessary to induce or invoke a proper biological response or activity. Templates, when used in the design of protein mimics, have been successful at reinforcing and directing such intramolecular folding. Template assembled protein mimics have been constructed to self-assemble into three α -helical bundles^{48,49} and collagen-like triple helices.⁵⁰ Moreover, the use of such templates can stabilize the overall structure by reducing the entropy involved in protein/peptide folding.⁵⁰ Our templates however, are more involved than traditional protein mimics, being that the BNTs can be characterized as both peptides and polymeric dendrimers. With this in mind, while protein folding principles rely mainly on a linear encoding of

torsion angles along the peptide backbone (ϕ, ψ) and side-chain interactions, polymer and dendrimer modeling suggests solvation and interchain interactions are also pertinent in determining secondary structure.⁴⁶

The tetrabranched 18-mer peptide, BNT II, possessed a more ordered conformation than both BNT I and the linear constructs (**Chapter 2, Figure 2.14**), a feature shared by other MAPS peptides,^{51,52} as well as template-assembled collagen mimetics.^{50,53} The enhanced secondary structure of BNT II over (AHHAHHAAD)₂ is not surprising given the nucleating domain is presented four times. This multiplicity is further demonstrated by the fact the linear 18-mer peptide had to be approximately 3.8 times more concentrated than the similar MAPS construct in order to obtain any appreciable CD signal (unpublished results).

The interpretation of the increase in intensity in the CD signal between BNT I and BNT II however, may not be conclusively explained via circular dichroism experiments. Recognizing the templates are dendrimers, the increase in CD signal noted for BNT II may not reflect an increase in secondary structure per se, but may instead reflect an increase in more CD active groups since the generation of the dendrimer has increased also, a trait seen with other peptide dendrimers.⁵⁴ Though this property is not uncommon for circular dichroism studies involving dendrimers, the secondary structure enhancement is not rooted in the multiplicity factor alone. Inter and intramolecular interactions, including both hydrogen bonding and electrostatic forces, could also augment secondary structure. Ellipticity itself may be rooted in the binding strength of intermolecular hydrogen bonding between the

dendritic peptide segments.^{55,56} As seen with BNT II during thermal denaturation experiments (**Figure 3.16**), both inter and intramolecular aggregations effect the conformation of the peptide dendrimer. Such aggregative forces may play a prominent role in the nucleation and assemblage of hemozoin, as seen in the *in vitro* hemozoin aggregation assays, in which BNT II nucleated twice as much aggregated heme as BNT I.

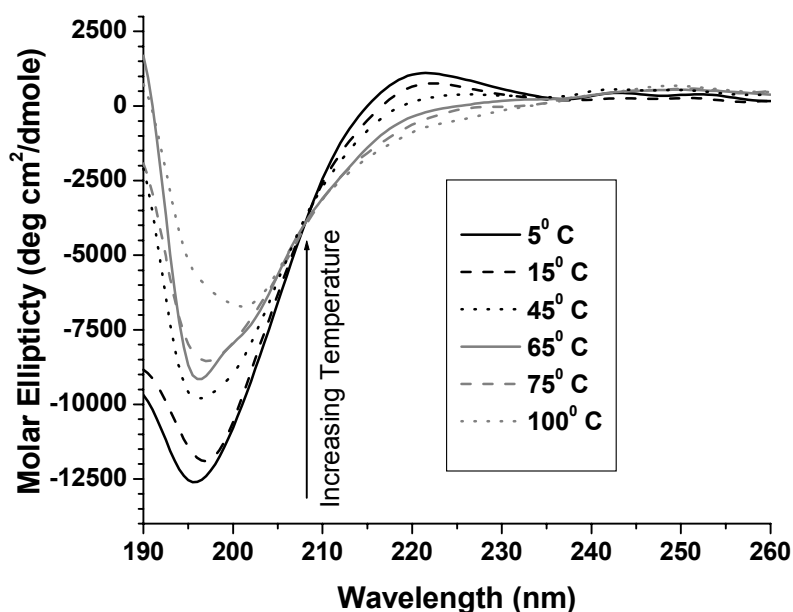


Figure 3.16. Thermal denaturation of BNT II. As the temperature of the sample increased, the negative ellipticity at ~197 nm increased, while the ellipticity at ~220 nm decreased.

Considering the more rigid structural constraints imparted by the MAPS core, the circular dichroism features typically classified by particular secondary structures in globular proteins may inadequately characterize the BNTs. An improved CD model for the BNTs may include the natural and templated collagen triple helix,^{57,58}

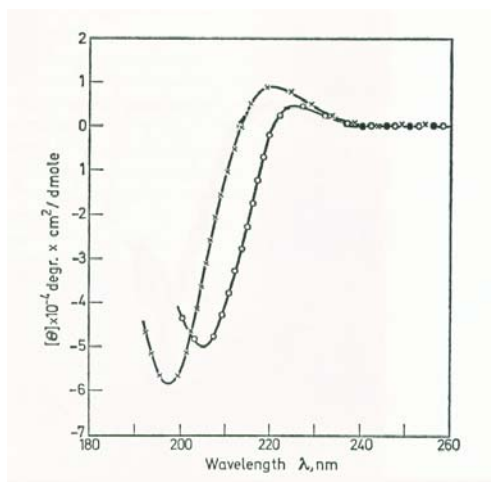


Figure 3.17. Circular dichroism spectra for (-x-x-x-) collagen and (-o-o-o-) poly-L-proline II. Reproduced from reference 59.

which has three individual helices intertwined with each other. The circular dichroism spectrum of collagen exhibits a CD spectrum similar to polyproline II, having a large negative trough around 197 nm and a small positive shoulder at 220 nm (**Figure 3.17**).⁵⁹ These spectral features are shared by both BNT II and BNT IIA (**Figure 3.18**), which blue-shift slightly from the typical polyproline II

conformation, which has a strong negative band at 200 nm and a weak positive band at 226 nm. In fact, the CD spectrum of BNT IIA closely resembles the spectrum of a dendrimeric lysine branched “minicollagen” peptide reported by Fields *et al.*⁵³ More interesting is the fact the thermal denaturation experiments also behave like those performed on collagen, where the ellipticity at 225 nm decreases with increasing temperature, a signature of the denaturation of the collagen

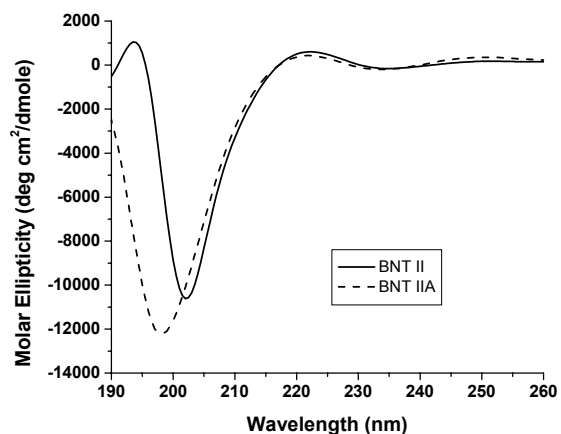


Figure 3.18. Circular dichroism spectra of putative domain peptides BNT II (—) and BNT IIA (---).

triple helix.⁵⁷ This ellipticity associated for BNT II is slightly blue-shifted at 220 nm (Figure 3.16), but fails to explain why a similar thermal denaturation study with the linear peptide (Ala-His-His-Ala-His-His-Ala-Ala-Asp)₂ harbored the same results (Figure 3.19).

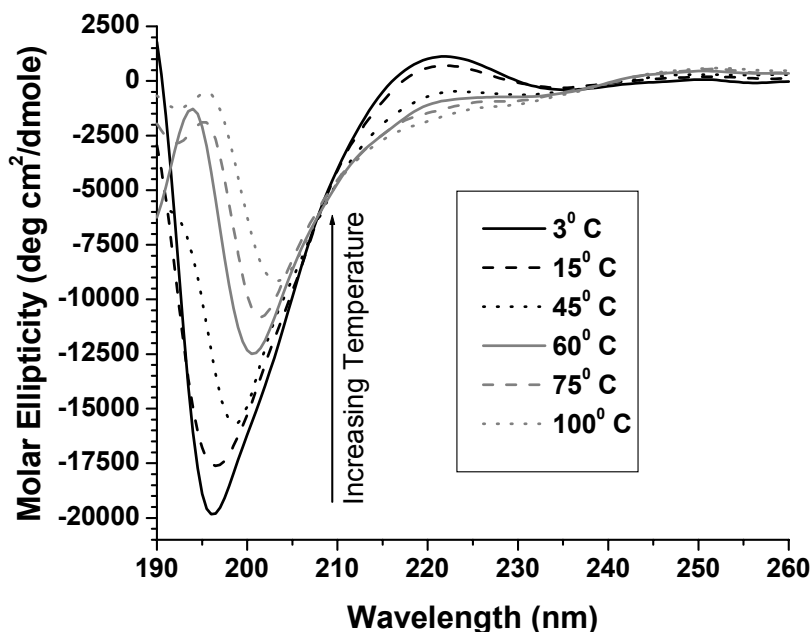


Figure 3.19. Thermal denaturation of the linear multimer of BNT II, (Ala-His-His-Ala-His-His-Ala-Ala-Asp)₂. As the temperature of the sample increased, the negative ellipticity at ~197 nm increased, while the ellipticity at ~220 nm decreased.

As stated before, circular dichroism studies were also utilized as a spectroscopic tool with which to enhance our understanding of iron (III) protoporphyrin IX binding to our modeled templates, where we could monitor the change in secondary structure as a function of increasing heme concentration. The influences of metal binding on the secondary structure of histidine-rich peptides are

abundant. Though both linear and dendrimeric Ala-His-His-Ala-His-His-Ala-Ala-Asp nucleating domains bound a significant amount of heme, only the peptide chains with 18 amino acids exhibited any secondary structure (again see **Chapter 2, Figure 2.14**). Increasing the chain length to an appropriate size may give rise to a favorable conformational feature along the peptide backbone, which could result in more favorable interactions between the peptide and substrate.

An additional point of consideration in the CD experiments involves the amino acid sequence and the placement of the histidine residues. Broo *et al.* reported the environment around a histidine residue in a folded peptide could alter the pKa of that histidine residue.^{60,61} With this in mind, not only does heme binding change with each mutation, but also conformational changes could be attributed to both changes in the sequence and each subsequent heme molecule that is bound. The heme group is however a symmetrical chromophore, exhibiting no inherent optical activity. Any subtle changes in the CD spectrum must arise from the peptide existing in a more fixed orientation as a consequence of the binding, or from the heme molecule possessing an asymmetrical axial ligation or molecular plane distortion once bound to the BNT. If the latter were of any real consequence, the templates that bound the iron porphyrin would only display changes in intensity in the CD spectrum upon binding additional equivalents of heme, rather than the wavelength shifts that are noted.

In retrospect concerning the evaluation of the histidine residues, it must be noted that BNT II and BNT IIA (and every mutant included in Chapter 4) maintained a hydrophobic core of alanine residues at positions 1,4, and 7 along the domain

sequence. Though initially these core residues were not given consideration to mutations since the bionucleating templates design criteria was based solely on binding capabilities and hemozoin production, it may have been of interest to incorporate amino acid residues which were aimed at disrupting this core to examine any effects on the secondary structure,⁶² and if any such spectral changes could be correlated to the results obtained from the substrate binding curves. However, in light of the designed peptides, such alterations would indeed effect hemozoin formation since the three dimensional scaffold necessary for templating heme onto the substrates would be disrupted.

Finally, though the tetravalent lysine MAPS core shows no appreciable secondary structure in our own (data not shown) and independent circular dichroism studies,⁶³ the contributions from the core on the peptide segments can not be ignored. The rigidity imparted by the MAPS core makes it difficult to unambiguously correlate the conformation and activity of the BNT peptides. The CD results however, show some evidence that helical conformation may be important for hemozoin formation. Both BNT II and BNT IIA displayed some alteration in the template secondary structure upon heme binding (**Figure 3.7A, Table 3.1 and Figure 3.12, Table 3.3**). BNT II, which bound more heme and aggregated more hemozoin than BNT IIA, displayed pronounced spectral changes in comparison to BNT IIA. This increased negative ellipticity upon substrate binding is not uncommon in metal binding motifs⁶⁴ and other peptide dendrimers.⁶⁵

3.6. Conclusions

Contradictory to the problems associated with the expression of HRP II in *Escherichia coli*,⁶⁶ using dendrimeric MAPS templates in the *de novo* design of a HRP II mimic permits the facile assembly and functionalization of peptides at the single amino acid level. Unlike linear peptide chains, the BNTs adopt a higher ordered structure.

The interaction of the hemin chloride and zinc protoporphyrin IX substrates with the bionucleating templates, BNT II and BNT IIA, provided insight into the interaction of the porphyrins with HRP II. The absorption spectra of the substrates with both templates were altered in the saturation binding experiments, indicative of substrate association with each template. Additionally, the fluorescence of the Zn(II)PPIX chromophore was quenched upon substrate:template interactions. Finally, such interactions were also noted in the circular dichroism spectra, as detected by changes not only in signal intensity, but also in the recorded wavelength maxima and minima.

Two histidine rich amino acid sequences were proposed to be the critical residues involved in hemozoin formation, the Ala-His-His-Ala-His-His-Ala-Ala-Asp sequence in the dendrimeric template BNT II and the Ala-His-His-Ala-Ala-Asp-Ala-His-His sequence in the alternate template, BNT IIA. Despite both sequences having the same number and type of amino acid residues, the results indicate the arrangement of such amino acids is critical in hemozoin formation. BNT II bound 9.83 ± 0.21 equivalents of heme, while BNT IIA bound a nearly similar amount of 8.70 ± 0.81

equivalents of the same substrate. This suggests that the substrate binding recognition site within the two sequences has not been interrupted, since both have similar efficacies. The zinc porphyrin binding site along the chains of BNT II and BNT IIA however has been disrupted. BNT II bound more Zn(II)PPIX (13.40 ± 0.31 eq.) than heme (9.83 ± 0.21 eq.), while BNT IIA showed a reduced binding capability (3.96 ± 0.45 eq. of Zn(II)PPIX vs. 8.70 ± 0.81 eq. of Fe(III)PPIX). Such results suggest different binding sites for each metal porphyrin.

Though BNT II and BNT IIA have similar iron porphyrin efficacies, the sterics of the dendrimer core could alter the alignment of the peptide chains, and therefore contribute to the small discrepancies in the heme binding data. Such perturbations may be small however, but in light of the results obtained from the *in vitro* heme aggregation assay, where BNT II nucleated twice as much insoluble heme aggregates as BNT IIA, are of real consequence. Subtle changes in the arrangement of amino acids along the peptide chain and between dendrimeric branches could prevent the requisite bond formation in the nucleation of hemozoin, in which the propionate of one heme group serves as the axial ligand to another. Recalling the first generation dendrimer from Ziegler³⁶ nucleated half the amount of β -hematin as the second generation BNT II, it is interesting to note that BNT IIA formed comparable amounts of the insoluble heme aggregates in comparison to BNT I. Upon examination, BNT I had the Ala-His-His-Ala-His-His-Ala-Ala-Asp sequence domain repeated once per dendrimeric branch. The 18 residue sequence of BNT IIA also repeated this same 8-mer sequence once per dendrimeric branch (**Figure 3.20**).

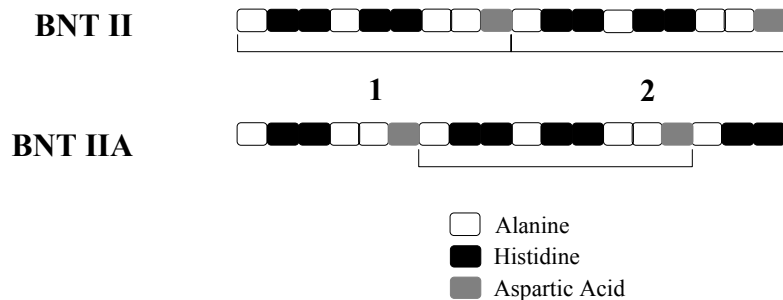


Figure 3.20. Representation of the amino acid sequences of BNT II and BNT IIA. The Ala-His-His-Ala-His-His-Ala-Ala-Asp repeat is isolated along the peptide chains, indicating the frequency of this particular sequence.

Results indicate the 9-mer amino acid sequence for BNT II (Ala-His-His-Ala-His-His-Ala-Ala-Asp) is the most probable nucleating domain, based on the ability to not only bind heme, but also nucleate β -hematin. Subsequent experiments were designed to **elucidate the role of the nucleating domain active site amino acids in the formation of hemozoin based on synthetic site-directed mutagenesis studies using BNT II** and are presented in Chapter 4.

References

- [1] Gardner, M. J.; Hall, N.; Fung, E.; White, O.; Berriman, M.; Hyman, R. W.; Carlton, J. M.; Pain, A.; Nelson, K. E.; Bowman, S.; Paulsen, I. T.; James, K.; Eisen, J. A.; Rutherford, K.; Salzberg, S. L.; Craig, A.; Kyes, S.; Chan, M. S.; Nene, V.; Shallom, S. J.; Suh, B.; Peterson, J.; Angiuoli, S.; Pertea, M.; Allen, J.; Selengut, J.; Haft, D.; Mather, M. W.; Vaidya, A. B.; Martin, D. M. A.; Fairlamb, A. H.; Fraunholz, M. J.; Roos, D. S.; Ralph, S. A.; McFadden, G. I.; Cummings, L. M.; Subramanian, G. M.; Mungall, C.; Venter, J. C.; Carucci, D. J.; Hoffman, S. L.; Newbold, C.; Davis, R. W.; Fraser, C. M.; Barrell, B. "Genome sequence of the human malaria parasite *Plasmodium falciparum*." *Nature* **2002**, *419*, 498-511.
- [2] Loria, P.; Miller, S.; Foley, M.; Tilley, L. "Inhibition of the peroxidative degradation of haem as the basis of action of chloroquine and other quinoline antimalarials." *Biochem. J.* **1999**, *339*, 363-370.
- [3] Egan, T. J. "Haemozoin formation as a target for the rational design of new antimalarials." *Drug Des. Rev.* **2004**, *1*, 93-110.
- [4] Pagola, S.; Stephens, P. W.; Bohle, D. S.; Kosar, A. D.; Madsen, S. K. "The structure of the malaria pigment β -hematin." *Nature* **2000**, *404*, 307-310.
- [5] Slater, A. F. G.; Cerami, A. "Inhibition by chloroquine of a novel heme polymerase enzyme activity in malarial trophozoites." *Nature* **1992**, *355*, 167-169.
- [6] Slater, A. F. G. "Chloroquine: Mechanism of drug action and resistance in *Plasmodium falciparum*." *Pharmacol. Ther.* **1993**, *57*, 203-235.
- [7] Egan, T. J.; Ross, D. C.; Adams, P. A. "Quinoline antimalarial drugs inhibit spontaneous formation of β -hematin (malaria pigment)." *FEBS Lett.* **1994**, *352*, 54-57.
- [8] Dorn, A.; Stoffel, R.; Matile, H.; Bubendorf, A.; Ridley, R. G. "Malarial hemozoin/ β -hematin supports heme polymerization in the absence of protein." *Nature* **1995**, *374*, 269-271.
- [9] Ridley, R. G.; Dorn, A.; Matile, H.; Kansy, M. "Haem polymerization in malaria (*reply*)." *Nature* **1995**, *378*, 138-139.

- [10] Dorn, A.; Vippagunta, S. R.; Matile, H.; Bubendorf, A.; Vennerstrom, J. L.; Ridley, R. G. "A comparison and analysis of several ways to promote hemozoin (heme) polymerization and an assessment of its initiation *in vitro*." *Biochem. Pharmacol.* **1998**, *55*, 737-747.
- [11] Fitch, C. D.; Cai, G. Z.; Chen, Y. F.; Shoemaker, J. D. "Involvement of lipids in ferriprotoporphyrin IX polymerization in malaria." *Biochim. Biophys. Acta* **1999**, *1454*, 31-37.
- [12] Tripathi, A. K.; Tekwani, B. L. "Mechanism of formation of β -hemozoin in malaria parasite: Lipids edge over proteins as possible mediators." *J. Parasit. Dis.* **1999**, *23*, 61-70.
- [13] Tripathi, A. K.; Garg, S. K.; Tekwani, B. L. "A physicochemical mechanism of hemozoin (β -hemozoin) synthesis by malaria parasite." *Biochem. Biophys. Res. Commun.* **2002**, *290*, 595-601.
- [14] Sullivan, D. J. J.; Gluzman, I. Y.; Russell, D. G.; Goldberg, D. E. "On the molecular mechanism of chloroquine's antimalarial activity." *Proc. Natl. Acad. Sci., USA* **1996**, *93*, 11865-11870.
- [15] Sullivan, D. J. J.; Gluzman, I. Y.; Goldberg, D. E. "Plasmodium hemozoin formation mediated by histidine-rich proteins." *Science* **1996**, *271*, 219-222.
- [16] Choi, C.; Cerda, J. F.; Chu, H. A.; Babcock, G. T.; Marletta, M. A. "Spectroscopic characterization of the heme binding sites in plasmodium falciparum histidine-rich protein-2." *Biochemistry* **1999**, *38*, 16916-16924.
- [17] Slater, A. F.; Swiggard, W. J.; Orton, B. R.; Flitter, W. D.; Goldberg, D. E.; Cerami, A.; Henderson, G. B. "An iron-carboxylate bond links the heme units of malaria pigment." *Proc. Natl. Acad. Sci., USA* **1991**, *88*, 325-329.
- [18] Basilico, N.; Monti, D.; Olliaro, P. L.; Taramelli, D. "Non-iron porphyrins inhibit β -hemozoin (malaria pigment) polymerisation." *FEBS Lett.* **1997**, *409*, 297-299.
- [19] Blauer, G.; Akkawi, M. "B-hemozoin." *Biochem. Mol. Biol. Int.* **1995**, *35*, 231-235.
- [20] Blauer, G.; Akkawi, M. "Investigations of B- and β -hemozoin." *J. Inorg. Biochem.* **1997**, *66*, 145-152.

- [21] Basilico, N.; Pagani, E.; Monti, D.; Olliario, P. L.; Taramelli, D. "A microtitre-based method for measuring the haem polymerization inhibitory activity (HPIA) of antimalarial drugs." *J. Antimicrob. Chemother.* **1998**, *42*, 55-60.
- [22] Bohle, D. S.; Helms, J. B. "Synthesis of β -hematin by dehydrohalogenation of hemin." *Biochem. Biophys. Res. Commun.* **1993**, *193*, 504-508.
- [23] Egan, T. J.; Marques, H. M. "The role of heme in the activity of chloroquine and related antimalarial drugs." *Coord. Chem. Rev.* **1999**, *192*, 493-517.
- [24] Ridley, R. G. "Medical need, scientific opportunity and the drive for antimalarial drugs." *Nature* **2002**, *415*, 686-693.
- [25] Ridley, R. G.; Dorn, A.; Vippagunta, S. R.; Vennerstrom, J. L. "Haematin (haem) polymerization and its inhibition by quinoline antimalarials." *Ann. Trop. Med. Parasitol.* **1997**, *91*, 559-566.
- [26] Vippagunta, S. R.; Dorn, A.; Matile, H.; Bhattacharjee, A. K.; Karle, J. M.; Ellis, W. Y.; Ridley, R. G.; Vennerstrom, J. L. "Structural specificity of chloroquine-hematin binding related to inhibition of hematin polymerization and parasite growth." *J. Med. Chem.* **1999**, *42*, 4630-4639.
- [27] Buller, R.; Peterson, M. L.; Almarsson, Ö.; Leiserowitz, L. "Quinoline binding site on malaria pigment crystal: A rational pathway for antimalarial drug design." *Cryst. Growth Des.* **2002**, *2*, 553-562.
- [28] Kaschula, C. H.; Egan, T. J.; Hunter, R.; Basilico, N.; Parapini, S.; Taramelli, D.; Pasini, E.; Monti, D. "Structure-activity relationships in 4-aminoquinoline antiplasmodials. The role of the group at the 7-position." *J. Med. Chem.* **2002**, *45*, 3531-3539.
- [29] Pandey, A. V.; Bisht, H.; Babbarwal, V. K.; Srivastava, J.; Pandey, K. C.; Chauhan, V. S. "Mechanism of malarial heme detoxification inhibition by chloroquine." *Biochem. J.* **2001**, *355*, 333-338.
- [30] Choi, C. Y. H.; Schneider, E. L.; Kim, J. M.; Gluzman, I. Y.; Goldberg, D. E.; Ellman, J. A.; Marletta, M. A. "Interference with heme binding to histidine-rich protein-2 as an antimalarial strategy." *Chem. Biol.* **2002**, *9*, 881-889.
- [31] Egan, T. J. "Discovering antimalarials: A new strategy." *Chem. Biol.* **2002**, *9*, 852-853.

- [32] Howard, R. J.; Andrutis, A. T.; Leech, J. H.; Ellis, W. I.; Cohen, L. A.; Kirk, K. L. "Inhibitory effect of histidine analogues on growth and protein synthesis by *Plasmodium falciparum* in vitro." *Biochem. Pharmacol.* **1986**, *35*, 1589-1596.
- [33] Pandey, A. V.; Joshi, R. M.; Tekwani, B. L.; Singh, R. L.; Chauhan, V. S. "Assay of β -hematin formation by malaria parasite." *J. Pharm. Biomed. Anal.* **1997**, *20*, 203-207.
- [34] Kim, P.; Pau, C.-P. "Comparing tandem repeats and multiple antigenic peptides as the antigens to detect antibodies by enzyme immunoassay." *J. Immunol. Methods* **2001**, *257*, 51-54.
- [35] Noedl, H.; Wernsdorfer, W. H.; Miller, R. S.; Wongsrichanalai, C. "Histidine-rich protein II: a novel approach to malaria drug sensitivity testing." *Antimicrob. Agents Chemother.* **2002**, *46*, 1658-1664.
- [36] Ziegler, J.; Chang, R. T.; Wright, D. W. "Multiple-antigenic peptides of histidine-rich protein II of *Plasmodium falciparum*: Dendrimeric biomineralization templates." *J. Am. Chem. Soc.* **1999**, *121*, 2395-2400.
- [37] Morgan, W. T. "The histidine-rich glycoprotein of serum has a domain rich in histidine, proline and glycine that binds heme and metals." *Biochemistry* **1985**, *24*, 1496-1501.
- [38] Burch, M. K.; Morgan, W. T. "Preferred heme binding sites of histidine-rich glycoprotein." *Biochemistry* **1985**, *24*, 5919-5924.
- [39] Morgan, W. T. "Human serum histidine-rich glycoprotein. I. Interactions with heme, metal ions, and organic ligands." *Biochim. Biophys. Acta* **1978**, *533*, 319-333.
- [40] Orjih, A. U. "On the mechanism of hemozoin production in malaria parasites: activated erythrocyte membranes promote β -hematin synthesis." *Exp. Biol. Med.* **2001**, *226*, 746-752.
- [41] Papalexis, V.; Siomos, M.-A.; Campanale, N.; Guo, X.-g.; Kocak, G.; Foley, M.; Tilley, L. "Histidine-rich protein 2 of the malaria parasite, *Plasmodium falciparum*, is involved in detoxification of the by-products of haemoglobin degradation." *Mol. Biochem. Parasitol.* **2001**, *115*, 77-86.

- [42] Lynn, A.; Chandra, S.; Malhitra, P.; Chauhan, V. S. "Heme binding and polymerization by *Plasmodium falciparum* histidine rich protein II. Influence of pH on activity and conformation." *FEBS Lett.* **1999**, *459*, 267-271.
- [43] Huy, N. T.; Serada, S.; Trang, D. T. X.; Takano, R.; Kondo, Y.; Kanaori, K.; Tamima, K.; Hara, S.; Kamei, K. "Neutralization of toxic heme by *Plasmodium falciparum* histidine-rich protein 2." *J. Biochem.* **2003**, *133*, 693-698.
- [44] Borza, D.-B.; Morgan, W. T. "Histidine-proline-rich glycoprotein as a plasma pH sensor. Modulation of its interaction with glycosaminoglycans by pH and metals." *J. Biol. Chem.* **1998**, *273*, 5493-5499.
- [45] Bermúdez, A.; Alba, P.; Espejo, F.; Vargas, L. E.; Parra, C.; Rodríguez, R.; Reyes, C.; Patarroyo, M. E. "Fitting modified HRP-I peptide analogue 3D structure into HLA-DR molecules induces protection against *Plasmodium falciparum* malaria." *Int. J. Biochem. Cell Biol.* **2005**, *37*, 336-349.
- [46] Dill, K. A. "Polymer principles and protein folding." *Protein Sci.* **1999**, *8*, 1166-1180.
- [47] Bierzynski, A. "Methods of peptide conformation studies." *Acta Biochim. Pol.* **2001**, *48*, 1091-1099.
- [48] Ghadiri, M. R.; Choi, C. "Secondary structure nucleation in peptides. Transition metal ion stabilized α -helices." *J. Am. Chem. Soc.* **1990**, *112*, 1630-1632.
- [49] Ghadiri, M. R.; Case, M. A. "De novo design of a novel hetero dinuclear metalloprotein with three parallel (bundled) helices." *Angew. Chemie. Int. Ed.* **1993**, *32*, 1594-1597.
- [50] Goodman, M.; Bhumralkar, M.; Jefferson, E. A.; Kwak, J.; Locardi, E. "Collagen mimetics." *Biopolymers* **1998**, *47*, 127-142.
- [51] Majer, Z.; Holly, S.; Tóth, G. K.; Váradi, G.; Nagy, Z.; Horváth, A.; Rajnavölgyi, E.; Laczkó, I.; Hollósi, M. "Mapping the intersubunit region of influenza hemagglutinin: comparative CD and FTIR spectroscopic studies on multiple antigenic peptides." *Arch. Biochem. Biophys.* **1995**, *322*, 112-118.
- [52] Gómara, M. J.; Ercilla, G.; Alsina, M. A.; Haro, I. "Assessment of synthetic peptides for hepatitis A diagnosis using biosensor technology." *J. Immunol. Methods* **2000**, *246*, 13-24.

- [53] Fields, C. G.; Grab, B.; Lauer, J. L.; Fields, G., B "Purification and analysis of synthetic, triple-helical "minicollagens" by reversed-phase high-performance liquid chromatography." *Anal. Biochem.* **1995**, *231*, 57-64.
- [54] Love, C. S.; Hirst, A. R.; Chechik, V.; Smith, D. K.; Ashworth, I.; Brennan, C. "One-component gels based on peptidic dendrimers: dendritic effects on materials properties." *Langmuir* **2004**, *20*, 6580-6585.
- [55] Hirst, A. R. "Self-assembly of two-component peptidic dendrimers: dendritic effects on gel-phase materials." *Org. Biomol. Chem.* **2004**, *2*, 2965-2971.
- [56] Hirst, A. R.; Smith, D. K.; Feiters, M. C.; Geurts, H. P. M. "Two-component dendritic gel: effect of spacer chain length on the supramolecular chiral assembly." *Langmuir* **2004**, *20*, 7070-7077.
- [57] Holmgren, S. K.; Bretscher, L. E.; Taylor, K. M.; Raines, R. T. "A hyperstable collagen mimic." *Chem. Biol.* **1999**, *6*, 63-70.
- [58] Kinberger, G. A.; Cai, W.; Goodman, M. "Collagen mimetic dendrimers." *J. Am. Chem. Soc.* **2002**, *124*, 15162-15163.
- [59] Jirgensons, B. *Optical Activity of Proteins and other Macromolecules*; 2nd ed.; Springer-Verlay: New York, 1973, 129-133.
- [60] Broo, K. S.; Brive, L.; Ahlberg, P.; Baltzer, L. "Catalysis of hydrolysis and transesterification reactions of p-nitrophenyl esters by a designed helix-loop-helix dimer." *J. Am. Chem. Soc.* **1997**, *119*, 11362-11372.
- [61] Broo, K. S.; Brive, L.; Sott, R. S.; Baltzer, L. "Site-selective control of the reactivity of surface-exposed histidine residues in designed four-helix-bundle catalysts." *Fold. Des.* **1998**, *3*, 303-312.
- [62] Sugimoto, N.; Zou, J.; Kazuta, H.; Miyoshi, D. " α - β structural transition of short oligopeptides by water/organic solvent titration." *Chem. Lett.* **1999**, *7*, 637-638.
- [63] Shao, J.; Tam, J. P. "Unprotected peptides as building blocks for the synthesis of peptide dendrimers with oxime, hydrazone, and thiazolidine linkages." *J. Am. Chem. Soc.* **1995**, *117*, 3894-3899.
- [64] Kosa, J. L.; Michelsen, J. W.; Louis, H. A.; Olsen, J. I.; Davis, D. R.; Beckerle, M. C.; Winge, D. R. "Common metal ion coordination in the LIM domain proteins." *Biochemistry* **1994**, *33*, 468-477.

- [65] Sakamoto, M.; Ueno, A.; Hisakazu, M. "Multipeptide-metalloporphyrin assembly on a dendrimer template and photoinduced electron transfer based on the dendrimer structure." *Chem. Eur. J.* **2001**, *7*, 2449-2458.
- [66] Schneider, E. L.; King, D. S.; Marletta, M. A. "Amino acid substitution and modification resulting from *Escherichia coli*. Expression of recombinant *Plasmodium falciparum* histidine-rich protein II." *Biochemistry* **2005**, *44*, 987-995.

Chapter 4

Site-directed Mutagenesis Studies of BNT II

4.1. The Mutants of BNT II - An Introduction

With the 9-mer sequence of BNT II, Ala-His-His-Ala-His-His-Ala-Ala-Asp, being the most probable nucleating domain, based on the ability not only to bind heme, but also to nucleate β -hematin, subsequent experiments were designed to elucidate the role of the nucleating domain active site amino acids in the formation of hemozoin based on synthetic site-directed mutagenesis studies. Thirty-two histidine and alanine residues and eight aspartic acid residues comprise the parent BNT II template, excluding amino acid contributions from the MAPS core. The high binding activity of this HRP II mimic suggests the histidine residues at positions 2,3,5, and 6 (and therefore also positions 11,12,14, and 15) may be functionally and structurally important for activity based on results obtained against the alternative hypothesized nucleation domain of BNT IIA, Ala-His-His-Ala-Ala-Asp-Ala-His-His (See **Chapter 3** for the putative domain studies). Furthermore, the diminished hemozoin formation activity of BNT IIA suggests the trimeric Ala-His-His repeat must be necessarily conserved, providing either the appropriate binding site or spatial requirement for β -hematin aggregation. These sequence requirements spawned the development of BNT II mutants (**Table 4.1**).

The first mutant synthesized was BNT IIC, which attempted to probe the Ala-His-His repeat by replacing the histidine residues with alanine in an attempt to ascertain if heme binding was solely dominated by histidine residues. This mutant was however insoluble under the experimental conditions employed (pH 4.8).

Before attempting to investigate the trimeric repeat again, a single point mutation was made, not only for the eased peptide assembly from a synthetic standpoint, but also to explore the necessity of the conserved aspartic acid residue along the 9-mer sequence. Here the aspartic acid residues were replaced with nonpolar alanine residues in mutant BNT IID.

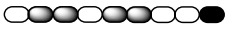

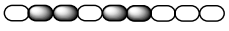



BNT II		Ala	His	His	Ala	His	His	Ala	Ala	Asp
BNT IIC		Ala	Ala	Ala	Ala	Ala	Ala	Ala	Ala	Asp
BNT IID		Ala	His	His	Ala	His	His	Ala	Ala	Ala
BNT IIX		Ala	His	Ala	Ala	His	Ala	Ala	Ala	Asp
BNT ILY		Ala	Ala	His	Ala	Ala	His	Ala	Ala	Asp
BNT IIZ		Ala	His	His	Ala	His	His	Ala	Ala	Lys

Table 4.1. Site-directed mutagenesis of the 9-mer sequence of BNT II. Mutated amino acids residues are outlined with ----.

With the inability to assess if the histidine residues in the original BNT II sequence were the single-handed determinant in heme binding and hemozoin biomineralization, the trimeric repeat was then evaluated in terms of the relative position of this amino acid on the putative nucleating face. With the templates modeled as potential right-handed 3-10 helices and left-handed polyproline II conformations, every third or approximately 3.4 residues is involved in a helical turn.

Mutant BNT IIX disturbed these turns by mutating the histidine residues with alanine at the third and sixth positions along the 9-mer sequence. Mutant BNT IYY explored the reverse arrangement of the histidine residues, conserving the deemed helical spatial requirements of the histidine residues at these positions, while making alanine mutations at positions two and five.

Finally, since BNT IID surveyed the conservation of the aspartic acid residue in terms of polarity, BNT IIZ reconsidered this amino acid in terms of charge. By replacing the aspartic acid with lysine, which will be deprotonated under the experimental conditions, we can clarify whether electrostatic interactions are requisite in heme binding.

4.2. General Information

All experiments performed on the BNT II mutants were the same as those described for the parent template BNT II, including Fe(III)PPIX and Zn(II)PPIX binding assays, fluorescence quenching studies with Zn(II)PPIX, the *in vitro* heme aggregation assay, and circular dichroism analysis. For complete details on experimental procedures see **Chapter 3, Section 3.2, Functional Screening of the BNTs.**

Regarding mutant solubility in 100 mM acetate buffer, pH 4.8, BNT IIZ, which had lysine replacing aspartic acid in the ninth and eighteen positions along the putative binding domain, displayed an enhanced solubility compared to the parent peptide dendrimer BNT II, which was soluble up to concentrations of approximately 10 mg mL⁻¹. BNT IID, which had the aspartic acid residue mutated to alanine, was

considerably less soluble ($\sim 1\text{-}2\text{ mg mL}^{-1}$) than the other mutants. BNT IIX and BNT IYY exhibited a somewhat reduced solubility compared to BNT II. BNT IYY was slightly more soluble than BNT IIX ($\sim 6\text{ mg mL}^{-1}$ of BNT IYY vs. $3\text{-}4\text{ mg mL}^{-1}$ of BNT IIX). When considering the mutations for the respective templates in light of peptide solubility, it appears that the Ala-Ala-His trimeric repeat of BNT IYY enhances the solubility of the peptide versus the Ala-His-Ala trimeric repeat of BNT IIX. This however, is not surprising given the arrangement of amino acids along the nucleating face if modeled in the right-handed 3-10 helix or the left-handed polyproline II conformation. With three or nearly so amino acid residues per turn, the residue of BNT IIX exposed to the solvent would be alanine, which is hydrophobic, as compared to the hydrophilic histidine residue present at that position in BNT IYY.

4.2.1. Mutant BNT IID – Results and Discussion

(The Ala-His-His-Ala-His-His-Ala-Ala-Ala Mutant Domain)

The electronic absorption spectra for the interaction of hemin with BNT IID had a single Soret peak centered at 413 nm (**Figure 4.1**). Like BNT II, this peptide had no appreciable absorbance in the 300-600 nm region of the spectra (data not shown). Though the spectra again red-shifted from that of hemin chloride alone (385 nm), BNT IID had a much broader spectrum than its parent BNT II (**Chapter 3, Figure 3.2**). Visible changes to the absorption spectra were observed after 1 equivalent of heme was added, but heme aggregation was also apparent in the cuvette. The electronic absorption spectrum was then reevaluated after 0.1 equivalents of heme were added, as shown in **Figure 4.1**.

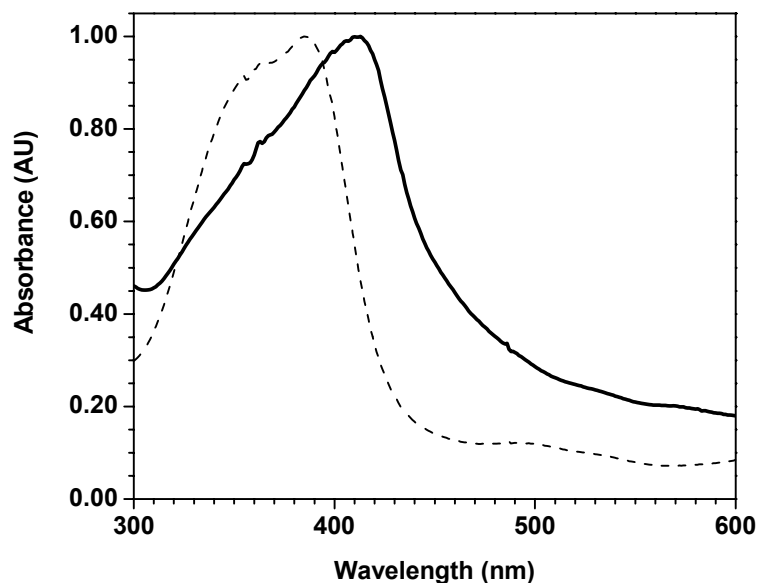


Figure 4.1. UV-Vis spectrum of the interaction of hemin chloride with BNT IID, represented by the (—) solid line. Samples of approximately 0.1 equivalents of hemin chloride were added to 7-10 nmoles of template in 100 mM acetate buffer, pH 4.8. Hemin chloride in buffer alone is represented by the (---) dashed line. Spectra were normalized to enhance the red-shift of the Soret band upon substrate binding.

Initially BNT IID was deemed a non-binding peptide with hemin chloride since a substrate binding curve could not be constructed due to the presence of aggregated heme. However, upon re-examination with an increased amount of template (7-10 nmoles) and reduced number of equivalents of hemin chloride, saturable binding was achieved. The absorbance maxima continued to increase from 413 nm to 417 nm upon the addition of more hemin chloride.

BNT IID bound 1.45 ± 0.17 equivalents of hemin chloride (**Figure 4.2**). Note however, the increased error in the normalized binding data due to the more rapid occurrence of heme aggregation. Upon sequence examination, when compared to its

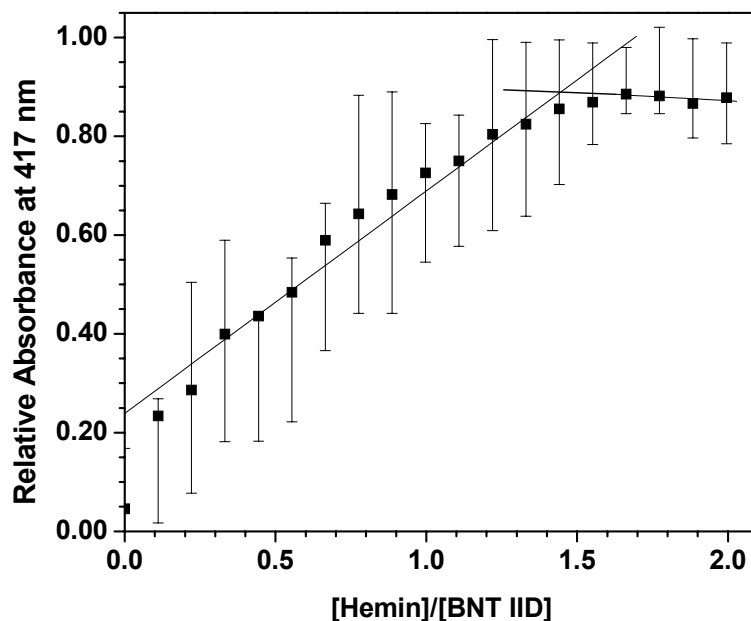


Figure 4.2. Hemin chloride titration binding curve for BNT IID. The data presented is the averaged result of ten independent binding titration experiments. Individual binding titration curves are shown in **Appendix II, pages A-9 and A-10**.

parent BNT II, it appears the aspartic acid is a critical residue in the binding of Fe(III)PPIX. While BNT II was capable of binding nearly 10 equivalents of the iron porphyrin, mutating the aspartic acid with alanine as in BNT IID, drastically reduced the binding capabilities with this porphyrin. At this point it becomes indeterminate whether the reduced binding capabilities are due to the change in polarity at this position, or whether the reactivity of the side chain affected binding.

BNT IID also bound the zinc porphyrin (**Figure 4.3**), binding 3.14 ± 0.71 equivalents of this porphyrin. The binding capability with Zn(II)PPIX was twice as much as that with Fe(III)PPIX, a trend also seen with mutant BNT IIA (**Chapter 3, Section 3.4.2b**).

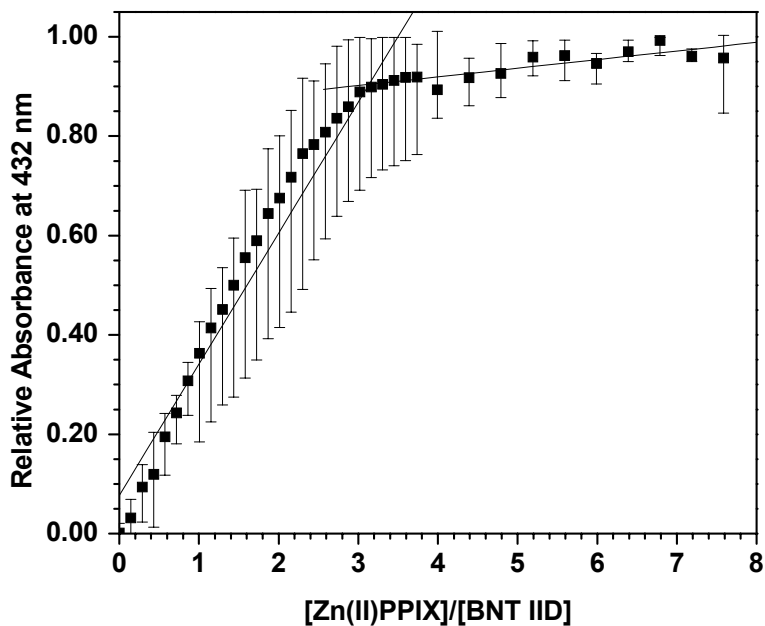


Figure 4.3. Zn(II)PPIX binding titration curve for BNT IID. The data presented is the averaged result of sixteen independent binding experiments. Individual binding titration curves are shown in **Appendix II, pages A-12 and A-13.**

Though the zinc protoporphyrin IX binding assays may appear immaterial because this porphyrin fails to be incorporated into an aggregated material such as β -hematin, both alone and as an extension of preformed hemozoin crystals,¹ this porphyrin is a known malarial antagonist. The fact that Zn(II)PPIX can bind to HRP II in the absence of Fe(III)PPIX, yet still bind to the same sites of the crystal surface of β -hematin as quinoline antimalarials implies a tightly controlled mechanism of hemozoin formation and inhibition. Such interactions cannot be solely dependent on π - π interactions or the zinc porphyrin would behave similarly to that of the iron substrate. Our template dendrimers, which make single amino acid mutations

along a putative binding domain, delve further into which sites are pertinent for binding and the biomineralization of hemozoin.

Results from the binding data of BNT IID suggest that while the aspartic acid residue is critical for the binding of hemin chloride, it plays little role in the binding of zinc(II)protoporphyrin IX. Accompanying discussion will be offered in the conclusions, **Section 4.3**, after the remaining mutants are presented.

The fluorescence quenching experiments involving Zn(II)PPIX with BNT IID demonstrated a reduced binding capability (**Figure 4.4**). At a BNT IID to Zn(II)PPIX ratio of 0.1:1, the fluorescence intensity was reduced by 33% and did not diminish to 50% until the ratio of template to porphyrin was approximately 0.35:1. The fluorescence of the fluorophore was completely quenched at a 0.8:1 ratio of BNT IID to zinc porphyrin.

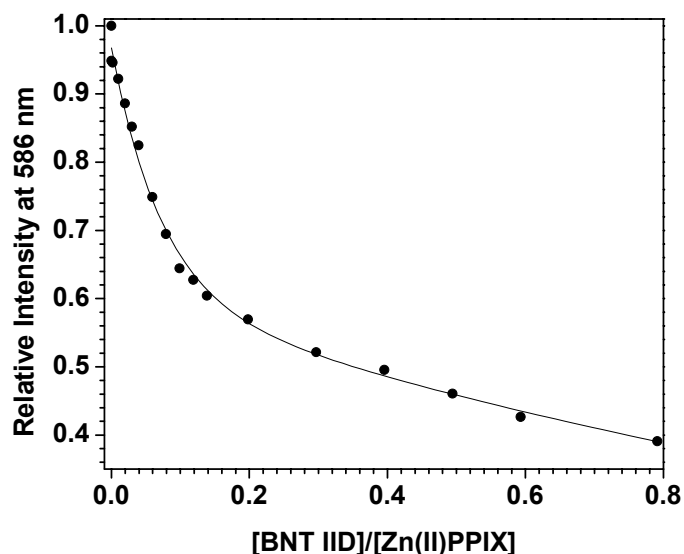


Figure 4.4. Fluorescence quenching studies of Zn(II)PPIX with BNT IID. Samples were excited at 410 nm and monitored at the emission maxima of the fluorophore.

BNT IID aggregated only 0.50 ± 0.20 nmoles of heme according to the *in vitro* heme polymerization assay. This miniscule production of insoluble aggregated heme again supports the role of the aspartic acid residue in the formation of β -hematin.

As seen in the circular dichroism spectra below (**Figure 4.5**), BNT IID has a deep, broad negative peak centered around 195 nm, a positive shoulder at 222 nm and a positive trough at 234 nm. Unlike the spectra of BNT II, the spectra of BNT IID remained positive throughout the remainder of the spectra after 215 nm. The addition of hemin chloride did not alter the spectra significantly. Although the molar ellipticity increased upon hemin binding, the spectra did not red-shift throughout the wavelengths examined. Spectral shifts associated with hemin binding are listed in **Table 4.2**. Complete CD titration experiments are listed in **Appendix III, page A-31**.

The lack of associated spectral changes upon hemin binding could provide a possible explanation as to why BNT IID failed to promote any significant amount of insoluble heme aggregate. In addition to the aspartic acid being a critical residue in the binding of the heme substrate, the lack of secondary structure, not only depicted by the template, but also displayed upon hemin binding, suggests that the conformation offered by the template is not favorable for hemozoin formation.

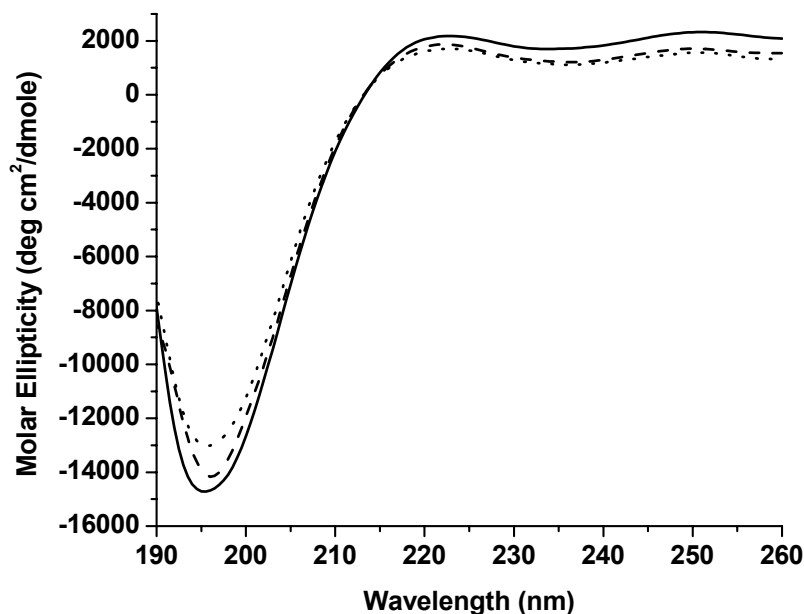


Figure 4.5. Circular dichroism spectra of BNT IID (—) and the corresponding spectral changes upon the addition of hemin chloride. Spectra are shown upon the addition of 0.33 (----) equivalents of substrate and 1.00 (.....) equivalent of substrate. Actual spectral shifts and signal intensities are listed in **Table 4.2**.

BNT IID	π - π^* (nm) (x,y)	n - π^* (nm) (x,y)	π - π^* (nm) (x,y)
No hemin	195.4 (-14752.82)	223.0 (2158.69)	234.0 (1681.49)
0.33 eq. Hemin	196.0 (-14189.81)	222.0 (1841.79)	236.7 (1203.11)
1.00 eq. Hemin	195.7 (-13043.04)	222.0 (1684.50)	236.7 (1099.31)

Table 4.2. CD spectral markers for Fe(III)PIX titration with BNT IID averaged over five individual scans. Each value in parentheses is the molar ellipticity data obtained at the corresponding wavelength, which was included to illustrate the change in secondary structure upon porphyrin binding.

4.2.2. Mutant BNT IIX – Results and Discussion

(The Ala-His-Ala-Ala-His-Ala-Ala-Ala-Asp Mutant Domain)

The interaction of hemin chloride with BNT IIX produced the electronic absorption spectrum in **Figure 4.6**. The peptide dendrimer again had no appreciable absorbance in the 300-600 nm range. Upon the addition of 0.3 equivalents of hemin chloride, the spectrum displayed a single Soret peak centered near 400 nm, which is red-shifted 5 nm from the value recorded with Fe(III)PPIX in acetate buffer, pH 4.8, alone. This interaction of the template, BNT IIX, with hemin chloride is however blue-shifted from iron protoporphyrin IX association with both BNT II and native

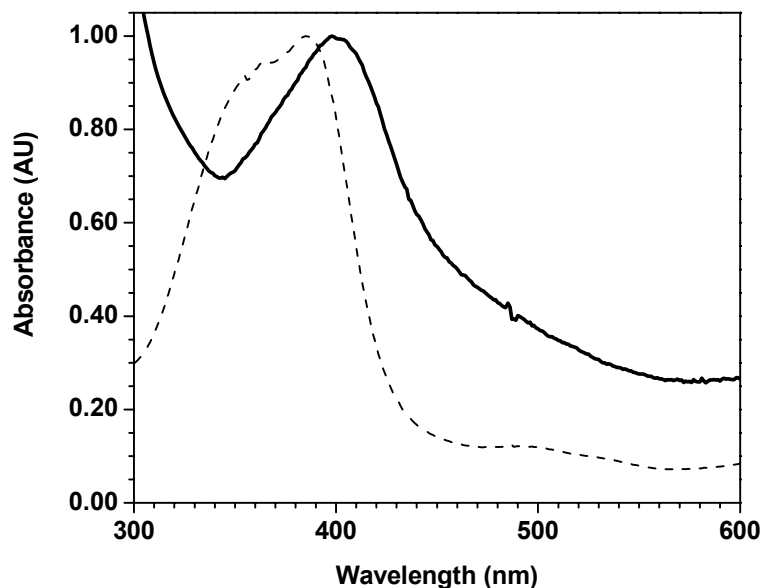


Figure 4.6. UV-Vis spectrum of the interaction of hemin chloride with BNT IIX, represented by the (—) solid line. Samples of approximately 0.3-0.5 equivalents of hemin chloride were added to 9-10 nmoles of template in 100 mM acetate buffer, pH 4.8. Hemin chloride in buffer alone is represented by the (---) dashed line. Spectra were normalized to enhance the red-shift of the Soret band upon substrate binding.

HRP II. The absorbance maxima shifted to 417 nm over the course of the porphyrin binding assay, and thus was analyzed at this wavelength.

As seen in **Figure 4.7**, the binding of hemin chloride with BNT IIX is saturable, although the graph still deviates from a plateau region typically associated with saturable binding (as discussed in **Chapter 3, Section 3.4.1a**). The titration curve shows that 3.37 ± 0.39 equivalents of Fe(III)PPIX bound to BNT IIX at saturation. In comparison to BNT II, which bound 9.83 ± 0.21 equivalents of heme, mutating the third and sixth histidine residues to alanine greatly reduced the binding capabilities of this template.

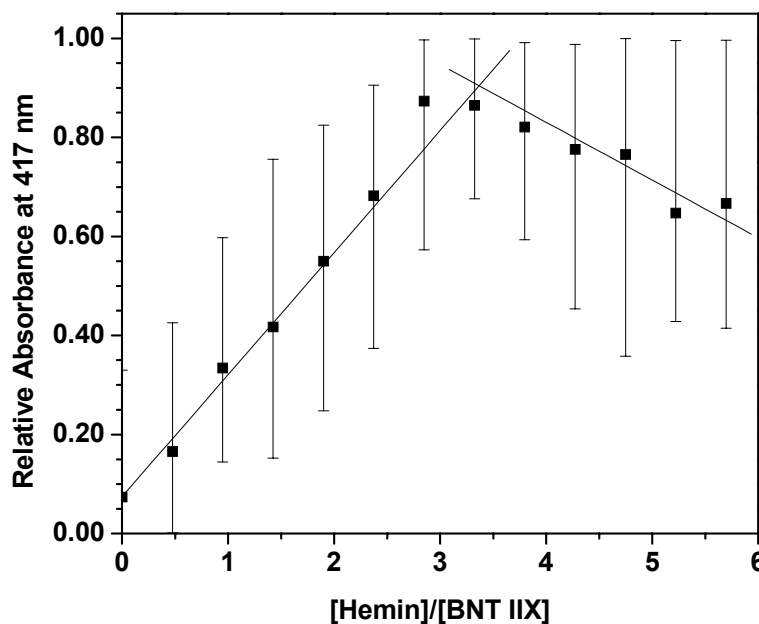


Figure 4.7. Hemin chloride titration binding curve for BNT IIX. The data presented is the averaged result of fifteen independent binding titration experiments. Individual binding titration curves are shown in **Appendix II, pages A-14 thru A-16**.

BNT IIX also interacted with Zn(II)PPIX, coincidentally binding the same number of equivalents of this porphyrin (3.33 ± 1.36) as it did the iron substrate (Figure 4.8).

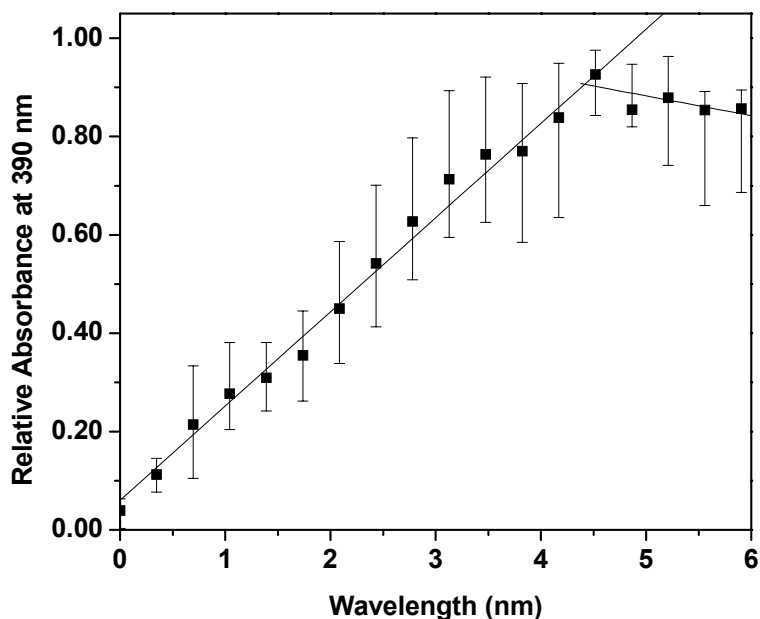


Figure 4.8. Zn(II)PPIX binding titration curve for BNT IIX. The data presented is the averaged result of sixteen independent binding experiments. Individual binding titration curves are shown in **Appendix II, pages A-17 and A-18**.

The fluorescence quenching experiments involving BNT IIX failed to exhibit similar saturation values as the binding titration curves. As seen in **Figure 4.9**, according to the protocol established in the fluorescence quenching experiments, the fluorescence of 40 nmoles of Zn(II)PPIX (1×10^{-5} M) was not quenched until a BNT IIX to porphyrin ratio of 5.5:1. This high number of required template is atypical in comparison to the other BNTs examined thus far. First, fluorescence intensity was reduced by 50% at template to porphyrin ratios whereby other templates

had already completely quenched the fluorescence of the fluorophore. This possibly suggests single point associations for the template BNT IIX and Zn(II)PPIX, since an excess of over five molecules of BNT IIX were needed to quench the fluorescence of a single molecule of fluorophore. Furthermore, the fluorescence of Zn(II)PPIX was quenched by the other templates once the fluorescent intensity was reduced by 60% to a relative intensity near 0.4. The intensity of the fluorescence of Zn(II)PPIX in the presence of BNT IIX was diminished 100% to near baseline fluorescence values.

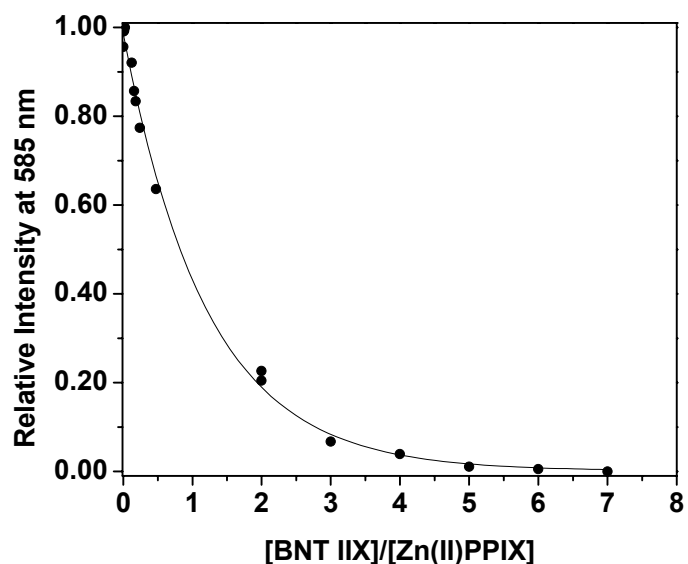


Figure 4.9. Fluorescence quenching studies of Zn(II)PPIX with BNT IIX. Samples were excited at 410 nm and monitored at the emission maxima of the fluorophore.

BNT IIX was also dismal at aggregating insoluble heme product, promoting the formation of 0.40 ± 0.30 nmoles of product.

As displayed in the circular dichroism experiments (**Figure 4.10**), BNT IIX has a deep negative peak centered around 200.5 nm, a positive shoulder at 220.6 nm, and a positive trough at 233.6 nm. The spectrum of BNT IIX in the absence of hemin chloride remained positive throughout the remainder of the spectrum after 215 nm. The addition of hemin chloride did not red-shift the region centered around 200 nm to any significant degree (0.5 nm max), much like BNT IID, which also bound very few equivalents of hemin chloride. The spectra only changed in the region centered around 230 nm, where the ellipticity in this area became negative upon the addition of substrate. Again, the lack of secondary structural change upon hemin binding may be

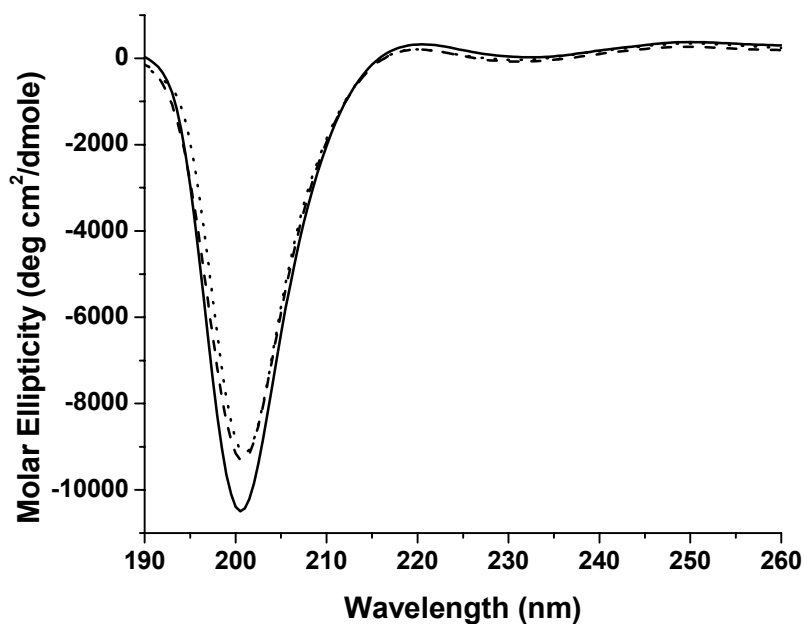


Figure 4.10. Circular dichroism spectra of BNT IIX (—) and the corresponding spectral changes upon the addition of hemin chloride. Spectra are shown upon the addition of 1.34 (----) equivalents of substrate and 2.33 (.....) equivalents of substrate (near $\frac{1}{2}$ of the full binding capacity experimentally determined for BNT IIX). Actual spectral shifts and signal intensities are listed in **Table 4.3**.

implicated in the bleak formation of aggregated heme. Spectral shifts associated with hemin binding are listed in **Table 4.3**. Complete CD titration experiments are listed in **Appendix III, page A-32**.

BNT IIX	$\pi\text{-}\pi^*$ (nm) (x,y)	$n\text{-}\pi^*$ (nm) (x,y)	$\pi\text{-}\pi^*$ (nm) (x,y)
No hemin	200.5 (-10497.39)	220.6 (300.12)	232.6 (18.21)
1.34 eq. Hemin	200.7 (-9321.21)	220.0 (196.29)	231.5 (-48.33)
2.33 eq. Hemin	201.0 (-9158.02)	220.0 (201.68)	231.3 (-95.55)

Table 4.3. CD spectral markers for Fe(III)PPIX titration with BNT IIX averaged over five individual scans. Each value in parentheses is the molar ellipticity data obtained at the corresponding wavelength, which was included to illustrate the change in secondary structure upon porphyrin binding.

4.2.3. Mutant BNT IY – Results and Discussion

(The Ala-Ala-His-Ala-His-Ala-Ala-Asp Mutant Domain)

BNT IY in association with hemin chloride in 100mm sodium acetate buffer, pH 4.8, displayed the electronic absorption spectrum in **Figure 4.11**, having a single Soret peak centered at 412 nm. BNT IY alone had no appreciable absorbance in the 300-600 nm range. Thus, the association of the iron porphyrin with the template red-shifted the Soret region of hemin chloride by 27 nm upon the addition of 0.5 equivalents of heme. Additional equivalents of heme red-shifted the absorbance maxima to 420 nm.

Mutant BNT IY bound 7.82 ± 0.45 equivalents of iron substrate (**Figure 4.12**). Replacing the second and fifth histidine residues with alanine reduced the binding

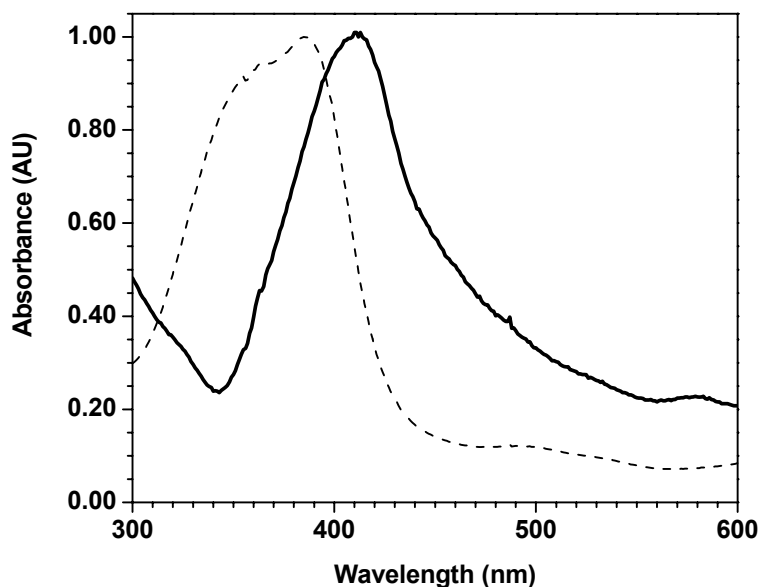


Figure 4.11. UV-Vis spectrum of the interaction of hemin chloride with BNT IY, represented by the (—) solid line. Samples of approximately 0.5-1 equivalents of hemin chloride were added to approximately 3 nmoles of template in 100 mM acetate buffer, pH 4.8. Hemin chloride in buffer alone is represented by the (---) dashed line. Spectra were normalized to enhance the red-shift of the Soret band upon substrate binding.

capabilities of the template in comparison to the parent, BNT II. The binding data however, suggests the conserved histidine residues at positions three and six along the putative domain of BNT II are significant in establishing heme:template interactions, seeing how BNT IY binding is dramatically increased from its sister BNT IIX, which mutated these same residues.

The increased substrate recognition was also experienced with Zn(II)PPIX. BNT IY bound 8.56 ± 0.80 equivalents of zinc protoporphyrin IX, over twice as much as its sister BNT IIX, though a significant amount less than its parent BNT II (~ 13 equivalents).

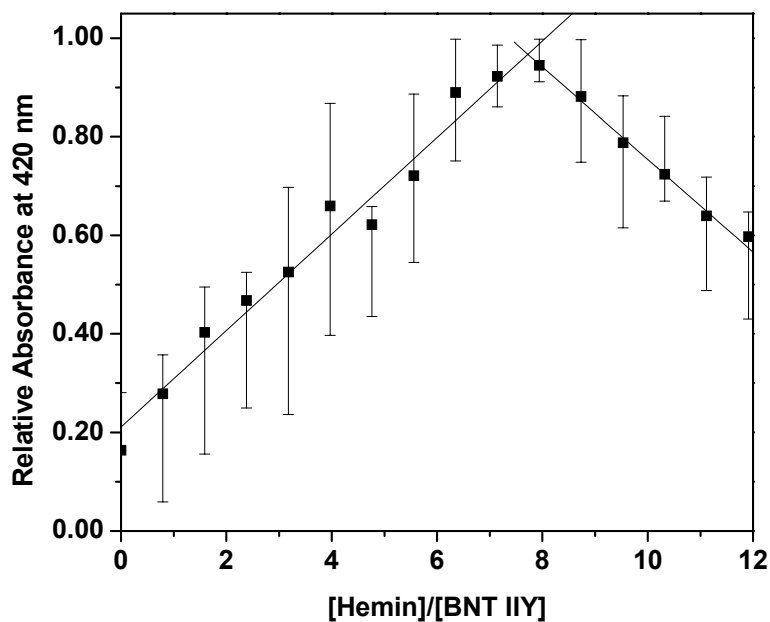


Figure 4.12. Hemin chloride titration binding curve for BNT I1Y. The data presented is the averaged result of nine independent binding titration experiments. Individual binding titration curves are shown in **Appendix II, pages A-19 and A-20.**

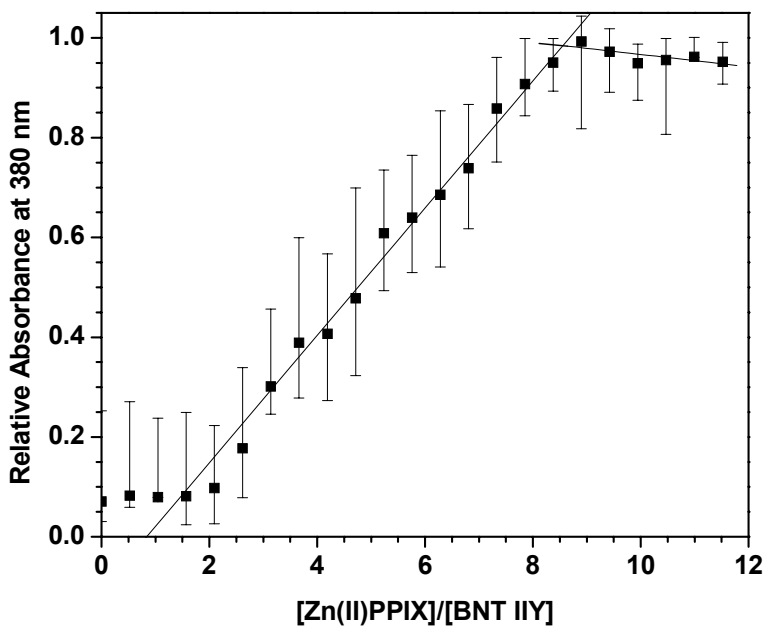


Figure 4.13. Zn(II)PPIX binding titration curve for BNT I1Y. The data presented is the averaged result of seven independent binding experiments. Individual binding titration curves are shown in **Appendix II, pages A-21 and A-22.**

Zn(II)PPIX fluorescence quenching experiments involving BNT IY were different from BNT II and the other mutants examined thus far. Despite binding a fairly high number of Zn(II)PPIX molecules, much like BNT II this mutant was typically a poor fluorophore quencher. Like its sister mutant BNT IIX, the ratio of template to porphyrin at which complete fluorescence quenching was observed was above 1:1. Specifically, the fluorescence was quenched at a 1.61:1 ratio of BNT IY to Zn(II)PPIX, however the fluorescence value only decreased by 20% of the normalized fluorescence. At the 0.1:1 ratio of mutant to fluorophore, commonly examined for BNT II and all mutants, the fluorescence was only diminished by roughly 4%. In light of the amino acid mutations made, alanine replacements at

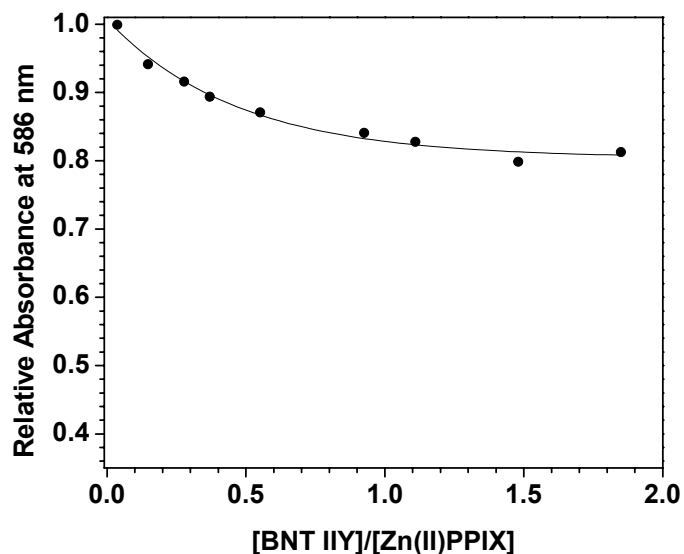


Figure 4.14. Fluorescence quenching studies of Zn(II)PPIX with BNT IY. Samples were excited at 410 nm and monitored at the emission maxima of the fluorophore.

positions 2 and 5 significantly affected mutant ability to quench the fluorophore.

BNT IY promoted 0.27 ± 0.15 nmoles of insoluble aggregated heme based on an average of twelve independent experiments. The background hemozoin formation for the assay was slightly lower than 1-2 nmoles typical with other assays, with the blanks aggregating 0.47 nmoles of heme.

The CD spectrum of BNT IY (**Figure 4.15**) displays a deep negative peak at 210.5 nm and a shoulder and trough at 221 nm and 232 nm respectively, closely sharing the spectral properties of its parent, BNT II. The addition of approximately 1.5 equivalents of hemin failed to alter the shape of the circular dichroism spectrum,

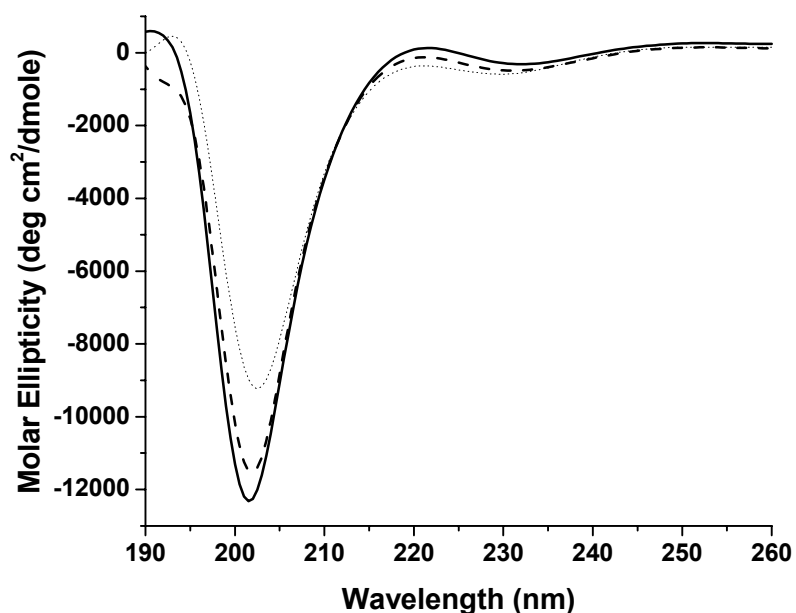


Figure 4.15. Circular dichroism spectra of BNT IY (—) and the corresponding spectral changes upon the addition of hemin chloride. Spectra are shown upon the addition of 1.47 (---) equivalents of substrate and 4.40 (····) equivalents of substrate ($\frac{1}{2}$ of the full binding capacity experimentally determined for BNT IY). Actual spectral shifts and signal intensities are listed in **Table 4.4**.

altering only the molar ellipticity value. The addition of further equivalents of hemin chloride did red-shift the CD spectrum, but only by a maximum of 1 nm. Spectral shifts associated with binding approximately one equivalent of hemin chloride and near half maximal binding are listed in **Table 4.4**. The entire CD titration experiment is listed in **Appendix III, page A-33**.

BNT IY	π - π^* (nm) (x,y)	n - π^* (nm) (x,y)	π - π^* (nm) (x,y)
No hemin	201.5 (-12301.80)	221.6 (128.66)	232.0 (-318.77)
1.47 eq. Hemin	202.0 (-11531.07)	221.3 (-120.58)	231.5 (-488.17)
4.40 eq. Hemin	202.5 (-9242.26)	221.0 (-360.44)	230.0 (-581.39)

Table 4.4. CD spectral markers for Fe(III)PPIX titration with BNT IY averaged over five individual scans. Each value in parentheses is the molar ellipticity data obtained at the corresponding wavelength, which was included to illustrate the change in secondary structure upon porphyrin binding.

When compared to BNT IIX, which mutated the histidine residues opposite of BNT IY (positions 2 and 5 versus 3 and 6), the changes in the CD spectrum are more pronounced than with the sister mutant. Seemingly, the histidine residues conserved in this mutant are more active participants in heme binding. Preserving the amino acids in the third and sixth positions along the chain, support increased binding values and amplify the changes that occur along the peptide backbone upon porphyrin interaction. This provides supporting evidence the putative binding domain has conformationally vital residues every three amino acids.

4.2.4. Mutant BNT IIZ – Results and Discussion

(The Ala-His-His-Ala-His-His-Ala-Ala-Lys Mutant Domain)

The electronic absorption spectrum for the interaction of hemin chloride with BNT IIZ is shown in **Figure 4.16**. Though the peptide had no appreciable absorbance in the 300-600 nm range, its interaction with the iron porphyrin shifted the Soret band 31.5 nm from 385 nm to 416.5 nm upon the addition of only 1 equivalent of heme. The Soret region continued to red-shift approximately 1 nm, after the addition of subsequent equivalents of heme.

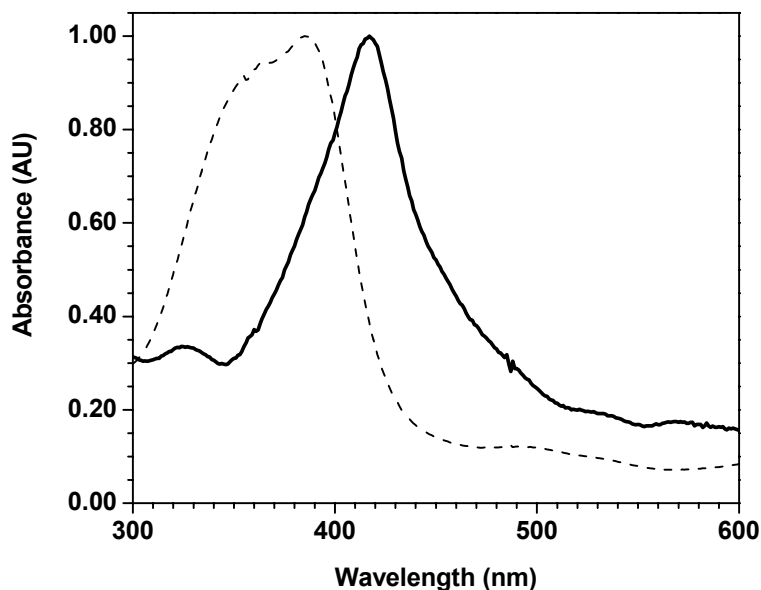


Figure 4.16. UV-Vis spectrum of the interaction of hemin chloride with BNT IIZ, represented by the (—) solid line. Samples of approximately 0.7 equivalents of hemin chloride were added to 3 nmoles of template in 100 mM acetate buffer, pH 4.8. Hemin chloride in buffer alone is represented by the (---) dashed line. Spectra were normalized to enhance the red-shift of the Soret band upon substrate binding.

As shown in **Figure 4.17**, the binding of heme with BNT IIZ is saturable. The titration curve shows that 9.81 ± 0.88 equivalents of heme were bound to BNT IIZ at saturation. BNT II also bound over nine equivalents of substrate, suggesting that the aspartic acid mutation with lysine in the ninth position along the domain sequence of BNT IIZ, had little effect on hemin binding. Electrostatics therefore, is not a prominent force in the binding of the iron substrate.

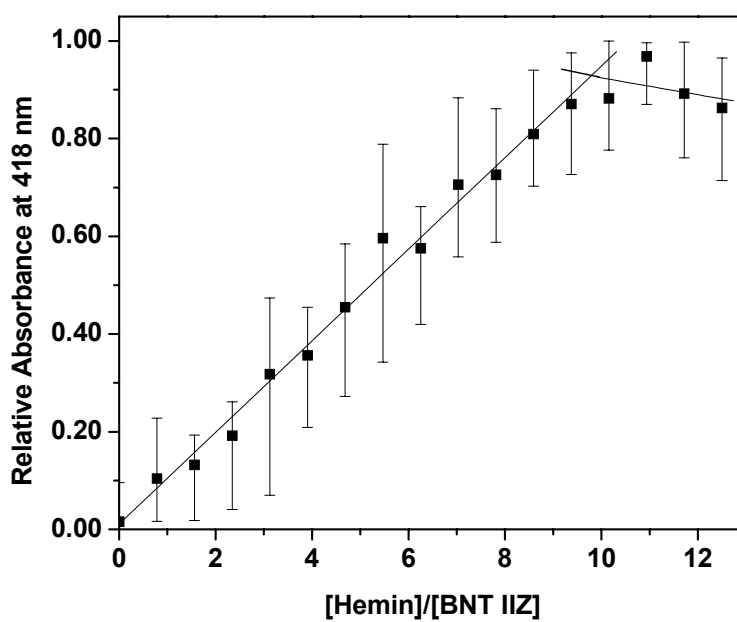


Figure 4.17. Hemin chloride titration binding curve for BNT IIZ. The data presented is the averaged result of eight independent binding titration experiments. Individual binding experiments are shown in **Appendix II, pages A-23 and A-24**.

BNT IIZ also interacted with Zn(II)PPIX, as shown in **Figure 4.18**. The 6.44 ± 0.81 equivalents of zinc bound is less than half of that bound by BNT II. Though hemin binding between these mutants did not seem to be affected by the

lysine mutation, zinc binding was significantly changed suggesting that electrostatic interactions may be a key factor in template association with zinc protoporphyrin IX.

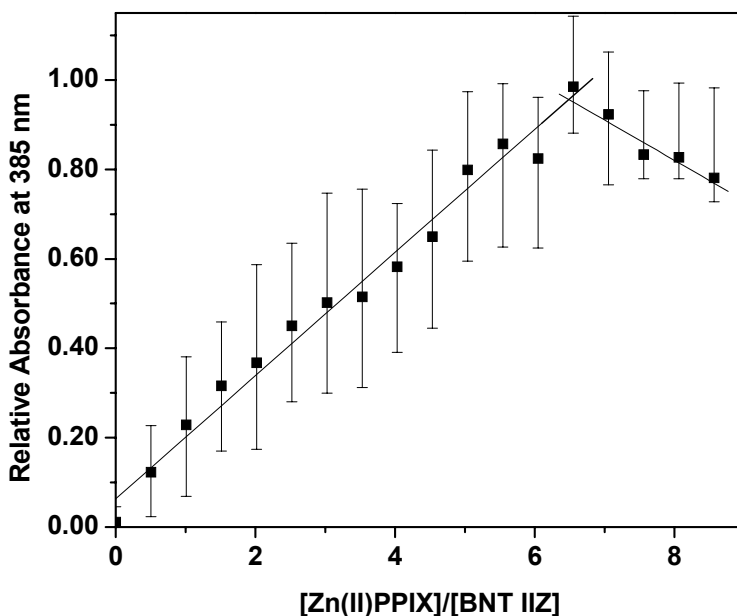


Figure 4.18. Zn(II)PPIX titration binding curve for BNT IIZ. The data presented is the averaged result of thirteen independent binding titration experiments. Individual binding experiments are shown in **Appendix II, pages A-25 thru A-27**.

As expected, since BNT IIZ bound less equivalents of the zinc porphyrin in comparison to BNT II, the fluorescence of Zn(II)PPIX was also quenched more rapidly when associated with this template (**Figure 4.19**). Recalling the fluorescence of BNT II was quenched by nearly fifty percent at a template to porphyrin ratio of 0.1:1, the fluorescence of the chromophore at this same ratio is completely quenched by BNT IIZ. A fifty percent reduction in the fluorescence intensity was displayed at a 0.015:1 ratio of BNT IIZ to Zn(II)PPIX.

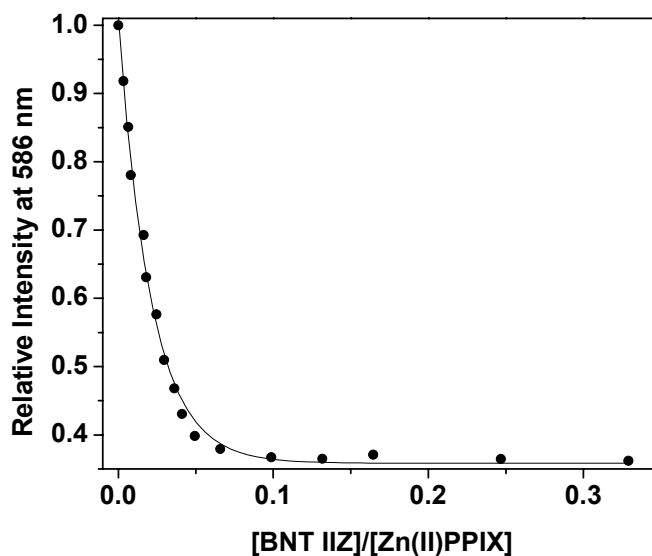


Figure 4.19. Fluorescence quenching studies of Zn(II)PPIX with BNT IIZ. Samples were excited at 410 nm and monitored at the emission maxima of the fluorophore.

BNT IIZ aggregated 2.37 ± 0.43 nmoles of heme. Background hemozoin formation was again lower at 0.5 nmoles. Seemingly BNT IIZ was the only mutant capable of aggregating any appreciable amount of heme.

The secondary structure of BNT IIZ in 10 mM acetate buffer, pH 4.8, is displayed in the CD spectra appearing in **Figure 4.20**. BNT IIZ had a deep negative peak around 198 nm and a small shoulder near 220 nm, but the entire spectrum remained negative in molar ellipticity. Heme binding increased the molar ellipticity value and red-shifted the deep negative peak approximately 1 nm (**Table 4.5**). These features are much like those displayed by BNT II and BNT IIZ, which also bound significant amounts of heme. Regardless of the increased heme binding, BNT IIZ and the aforementioned templates more importantly shifted 1 nm upon

interacting with 1 equivalent of substrate. This suggests that once bound, hemin chloride tightens the conformation of the templates. If this does indeed occur, the binding of subsequent equivalents of the iron porphyrin may align these molecules in the proper orientation for upcoming hemozoin formation. The shoulder near 235 nm appears much weaker in BNT IIZ than in the other mutants. The complete CD titration experiment for BNT IIZ is listed in **Appendix II, page A-34**.

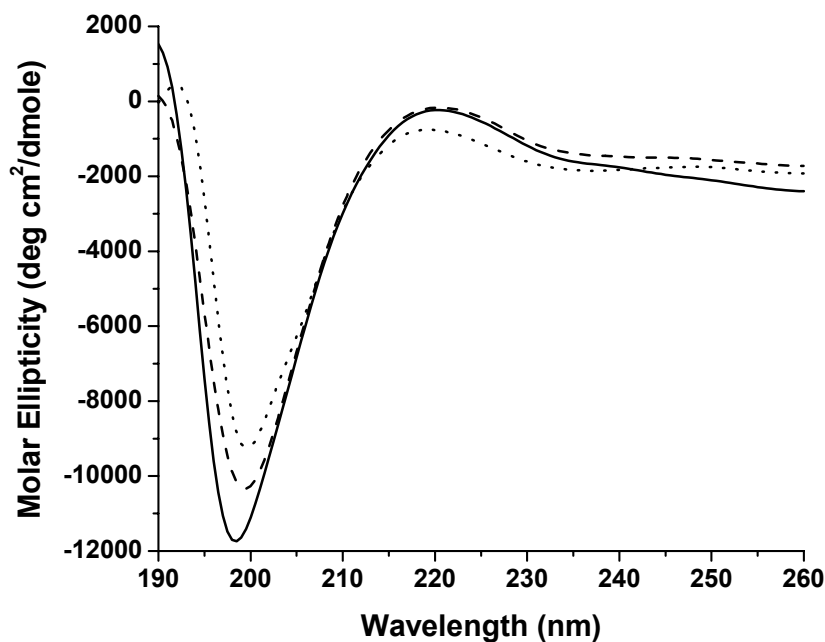


Figure 4.20. Circular dichroism spectra for BNT IIZ (—) and the corresponding spectral changes upon the addition of hemin chloride. Spectra are shown upon the addition of 1.15 (---) equivalents of substrate and 4.60 (····) equivalents of substrate ($\frac{1}{2}$ of the full binding capacity experimentally determined for BNT IIZ). Actual spectral shifts and signal intensities are listed in **Table 4.5**.

BNT IIZ	π - π^* (nm) (x,y)	n - π^* (nm) (x,y)	π - π^* (nm) (x,y)
No hemin	198.4 (-11733.92)	220.3 (-230.73)	235.7 (-1636.68)
1.15 eq. Hemin	199.4 (-10350.31)	220.3 (-167.35)	235.6 (-1419.54)
4.60 eq. Hemin	199.6 (-9271.85)	219.2 (-761.17)	235.7 (-1853.82)

Table 4.5. CD spectral markers for Fe(III)PPIX titration with BNT IIZ averaged over five individual scans. Each value in parentheses is the molar ellipticity data obtained at the corresponding wavelength, which was included to illustrate the change in secondary structure upon porphyrin binding.

4.3. Conclusions

As seen in **Figure 4.21**, the Soret region of the UV-Vis spectra of the mutants in association with hemin chloride differed from that of BNT II upon the addition of 0.3-1 equivalent of substrate. The addition of more hemin chloride caused the Soret region to move even further to 417-420 nm, depending on the mutant. The mutants that bound the least amount of heme (BNT IID and BNT IIX) had the Soret region centered near 417 nm at saturation, blue-shifted from the parent BNT II by 1 nm. BNT ILY and BNT IIZ, which bound a significant amount of heme, possessed Soret bands near 420 nm and 418 nm respectively. BNT IIX was the mutant that displayed the greatest alteration in the Soret region (17 nm) upon saturable binding.

The binding titration experiments demonstrated which amino acid mutations significantly affected the binding of Fe(III)PPIX and Zn(II)PPIX (**Figure 4.22**). BNT II, the Ala-His-His-Ala-His-His-Ala-Ala-Asp domain template, bound approximately 10 equivalents of the iron porphyrin and 13.5 equivalents of the zinc

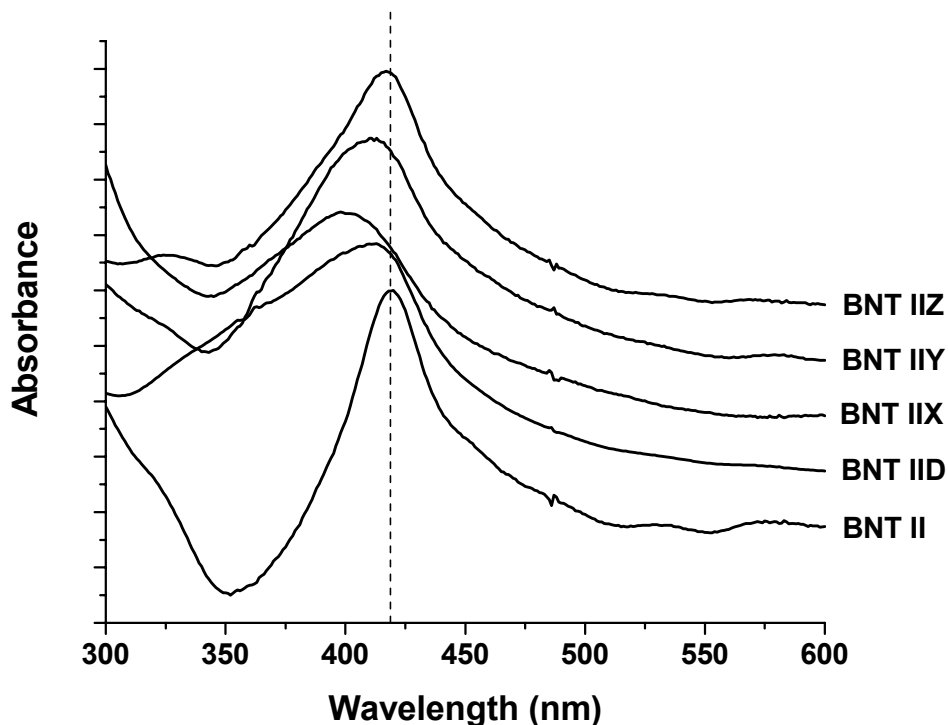


Figure 4.21. UV-Vis spectra of the interaction of hemin chloride with BNT II and its mutants. Samples of approximately 0.3-1 equivalents of hemin chloride were added to 1-10 nmoles of template in 100 mM acetate buffer, pH 4.8.

porphyrin. Removing the aspartic acid residue and replacing it with alanine, affected the binding of both porphyrins to the greatest degree, as seen with mutant BNT IID. Mutant BNT IIX with alanine mutations made to the third and sixth residue also reduced the binding capabilities of the template. Thus far, the histidine and aspartic acid residues appear to be critical in the binding of both Fe(III)PPIX and Zn(II)PPIX. Mutant BNY IY showed that modifying the second and fifth residues did not have the dramatic effect on binding that replacing the third and sixth residues did with mutant BNT IIX. In fact BNT IY binding levels approached those of BNT II. These results support the notion the conformation of the BNTs mirrors that of HRP II in

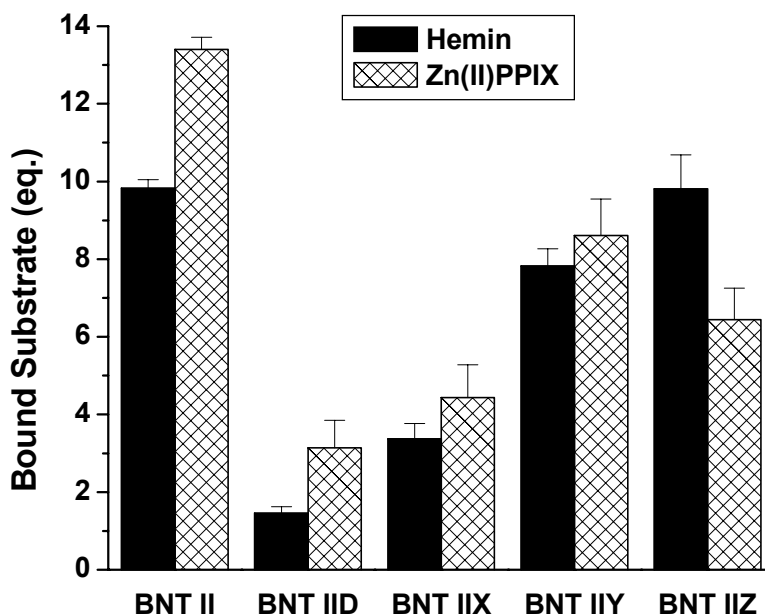


Figure 4.22. Substrate binding of BNT II and its mutants with Fe(III)PPIX and Zn(II)PPIX.

either a 3-10 or polyproline type II secondary structure, since every third amino acid residue plays a prominent role in sequestering substrates.

Mutant BNT IIZ, which replaced aspartic acid with lysine, restored the heme binding capability of the template to levels near its parent BNT II, suggesting that electrostatics do not play a role in heme binding. However, the same is not true for zinc protoporphyrin IX binding. In the mutants discussed thus far, 1-4 equivalents more of zinc protoporphyrin IX bound to the templates in comparison to Fe(III)PPIX binding. The same is not true for BNT IIZ which bound approximately 10 equivalents of hemin and only slightly above six equivalents of Zn(II)PPIX. This implies that although hemin binding may not be contingent on electrostatic

interactions, zinc binding is decreased when this affiliated residue is deprotonated. The positive lysine mutation did reduce the binding capabilities when Zn(II)PPIX was in association with the template. This suggests a different binding site along the peptide dendrimer between the two porphyrins, since polarity greatly reduced the binding of both porphyrins (as with BNT IID), while electrostatic associations were only prominent in zinc binding (as with BNT IIZ).

The fluorescence quenching studies help to pictorially represent some of the differences in Zn(II)PPIX binding amongst the mutant templates. As seen in **Figure 4.23**, the rates of fluorescence quenching varied with each mutant. BNT IIX and BNT IY are of particular interest. The fluorescence intensity of BNT IIX was diminished by 100% upon complete quenching of the fluorophore, while BNT IY reduced its intensity by 20% upon quenching. Moreover, when mutations to the histidine residues occurred, as with BNT IIX and BNT IY, the ratio of template to porphyrin at complete fluorescence quenching was above 1:1, while BNT IID and BNT IIZ, which conserved these amino acid residues, behaved more like its parent BNT II. This suggests that both histidine residues are involved in securing the points of interaction between Zn(II)PPIX and the templates. Beyond this, it appears that while BNT IID and BNT IIZ quench the fluorophore at ratios less than 1:1, the interaction of BNT IIZ with the zinc porphyrin must be slightly more fixed or interlocked, since the rate of quenching is increased with this template in comparison to its parent, BNT II.

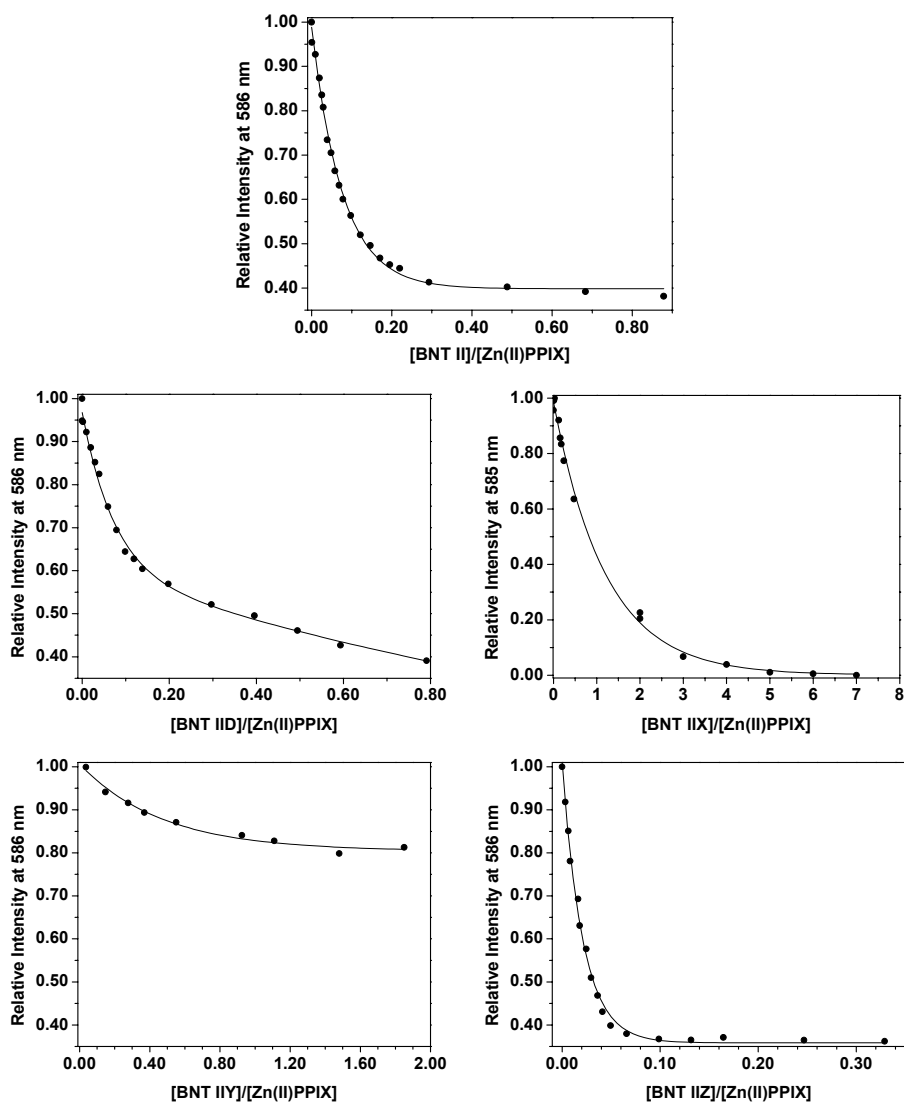


Figure 4.23. Fluorescence quenching studies of Zn(II)PPIX by BNT II and its mutants. Note the scaling differences in the x-axes and also the y-axis change for BNT IIX.

Hemozoin production mediated by BNT II and its mutants is tallied in **Figure 4.24**. Again, the removal of the aspartic acid is not only critical in porphyrin binding, but also in the aggregation of hemozoin, as seen with BNT IID. The most noticeable dissimilarity between binding and hemozoin formation becomes apparent upon examination of BNT IIX and BNT IY. While BNT IY, possessing alanine mutations to the second and fifth positions along the putative domain of BNT II, was capable of binding more porphyrin than BNT IIX, which had the same mutations but instead to the third and sixth amino acids, this trend did not follow suit where hemozoin aggregation was concerned. In fact, replacing either of the histidine residues reduced the amount of hemozoin formed even more so than the aspartic acid

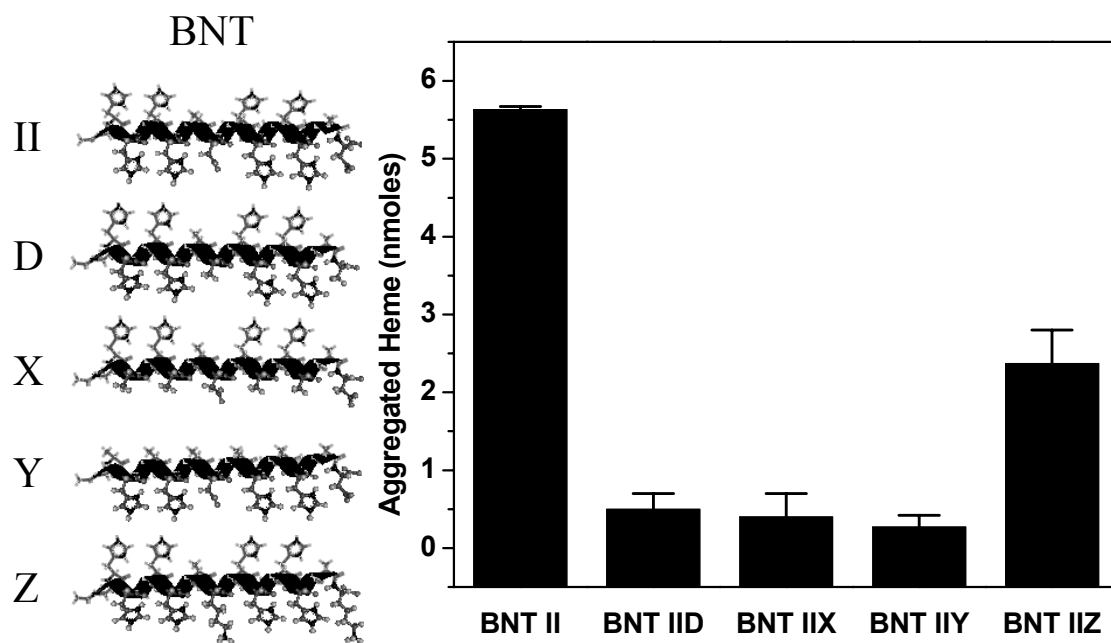


Figure 4.24. Hemozoin production mediated by BNT II and its mutants. Molecular models of the templates as 3-10 helices are added for dimensional clarity.

mutation in BNT IID. Mutating the ninth residue with lysine in BNT IIZ lessened hemozoin production in comparison to its parent BNT II, but this was the only mutant with β -hematin production above 1 nmole after background subtraction.

Though the CD experiments were performed in order to examine the effect of heme binding on secondary structure of the BNTs, other considerations should be given to such examinations since the BNTs are also dendrimers. Secondary structural propensities of dendrimers are modified as a function of the hydrodynamic volume, which is greatly affected by solvent conditions.²⁻⁴ Decreasing the hydrodynamic volume typically increases the secondary structural content. Additionally, any collapse of the dendrimer structure may perturb local secondary structure by possibly increasing the packing of amino acid side chains or by backfolding of the dendrimeric branches.⁵ Both occurrences could decrease or at least change the degree of helicity incurred by the BNT. Such interactions were intentionally minimized by conserving the hydrophobic face of alanine residues in the 1,4, and 7 positions along the binding domain.

The CD spectra of the mutants are shown in **Figure 4.25**. In comparison to BNT II (See **Figure 4.25 inset**), BNT IID which had alanine replacing the aspartic acid along the putative domain sequence, unfolded or loosened the conformation of the original peptide dendrimer, as depicted by the blue-shifted and broadened deep negative peak. After 210 nm the signal intensity of the remainder of the CD spectrum rose above negative molar ellipticity values. BNT IY preserved the original conformation of BNT II to the greatest extent, blue-shifting the deep negative peak

centered near 202 nm for BNT II by 0.5 nm, when the third and sixth histidine residues are left unchanged. BNT IIX, which mutated these positions, altered the same region of the spectra by blue-shifting that region by an additional 1.5 nm. The conformation of BNT IIZ shifted this deep negative peak below 200 nm.

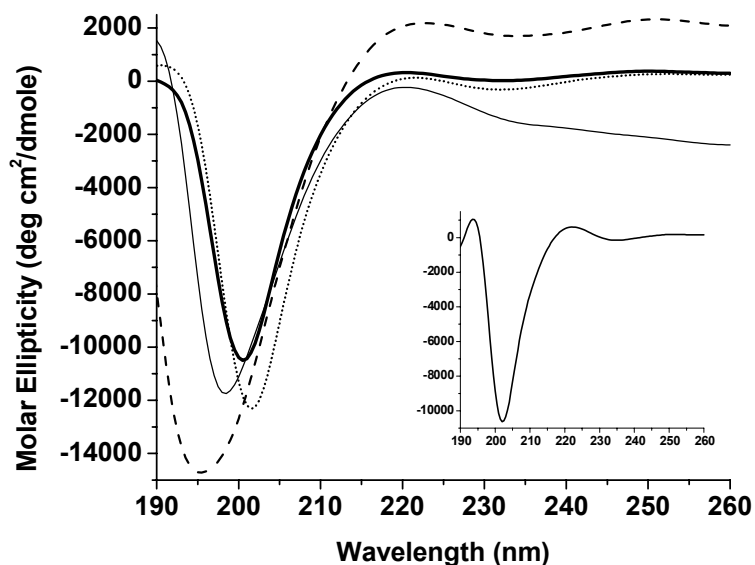


Figure 4.25. CD spectra of 2 nmoles of the mutants of BNT II in 10 mM acetate buffer, pH 4.8. (---) BNT IID, (—) BNT IIX, (···) BNT IIY, and (— ·) BNT IIZ. The inset displays the CD spectrum of BNT II.

The rigidity imparted by the MAPS core makes it difficult to unambiguously correlate the conformation and activity of the BNT peptides. The CD results however, show some evidence that helical conformation may be important for hemozoin formation. BNT IID had the least tendency to adopt any secondary helical conformation alone and upon the titration of hemin chloride, and was found to be least active in both porphyrin binding assays and relatively inactive in the template

mediated formation of hemozoin. BNT IIX had minimal changes in secondary structure upon hemin binding and was also not proficient at either porphyrin binding or hemozoin formation. BNT IIY bound a higher number of equivalents of both porphyrins and possessed a secondary structure in the largest part identical to BNT II, but the template mediated production of hemozoin by this mutant was diminished with the His-His repeat interrupted. Mutant BNT IIZ performed well with its abilities to mimic BNT II in binding capabilities, but the modification seen in the secondary structure most likely can be correlated to the reduction in the number of nmoles of aggregated heme in comparison to BNT II. The CD spectrum of BNT IIZ did cause the most pronounced changes in secondary structure upon hemin binding as depicted by the increase in negative ellipticity upon porphyrin association. Such behavior is not uncommon in metal binding motifs⁶ and other peptide dendrimers⁷.

In summary, the results presented indicate the 9-mer sequence of BNT II, Ala-His-His-Ala-His-His-Ala-Ala-Asp, is the major nucleating domain sequence responsible for eliciting appreciable hemozoin formation. Of the thirty-two histidine and alanine residues and eight aspartic acid residues in the parent template, the high binding activity of the His-His repeat is functionally and structurally important for activity. Any mutation to this repeat diminishes binding activity and greatly reduces the formation of hemozoin. The polarity of the aspartic acid residue is critical in both activities, since an alanine residue mutation fails to bind elevated levels of the porphyrins and participate in the aggregation of hemozoin. While BNT IIZ has similar binding capabilities to BNT II, the replacement of the aspartic acid residue by

lysine at positions eight (and also sixteen) along the putative domain sequence, does not provide the necessary chemical environment to elicit maximal hemozoin formation activity. The electrostatics surrounding this residue is not necessarily relevant for the binding of Fe(III)PPIX, but topological constraints likely play a role in hemozoin formation.

Ultimately, the functional analyses of BNT II and its mutants are to be debated from the perspective of amino acid sequence, since single amino acid mutations permitted the inherent chemical reactivity to be assessed as point mutations. With the experimental design of the porphyrin binding assays and hemozoin aggregation assay, the examination of such mutations should be easily addressed. However, the results of the circular dichroism experiments prompted a refinement of our thinking since the molecular models demonstrated behavioral characteristics more like dendrimers and collagen rather than straightforward peptides. Substrate interactions may not be solely along the peptide chain, but may exist between the dendrimeric peptide branches. Intermolecular interactions may also affect inherent binding and hemozoin nucleation properties.

Initially the two putative hemozoin nucleation domain sequences of BNT II and BNT IIA were examined in order to determine which was the most probable sequence within HRP II to actually participate in hemozoin formation. Initial results indicated that binding of heme alone did not elicit hemozoin formation since both BNT II and BNT IIA bound nearly similar equivalents of heme substrate (**Table 4.6**). Moreover, the examination of the two hypothesized hemozoin nucleation domains of

BNT II and BNT IIA and earlier studies by Ziegler *et. al*⁸ suggested that hemozoin formation was sequence dependent. Aggregated heme formed in the presence of BNT IIA was nearly half of that mediated by BNT II. In fact, the production of hemozoin in association with BNT IIA was similar to the first generation dendrimer, BNT I,⁸ which possessed only one copy of the Ala-His-His-Ala-His-His-Ala-Ala-Asp repeat of BNT II per branch. Upon further examination, this sequence can be located once per branch within the eighteen amino acid residues of BNT IIA. Seemingly BNT II, with twice the number of Ala-His-His-Ala-His-His-Ala-Ala-Asp repeats mediated the formation of hemozoin to levels two times greater than BNT IIA.

Template	9-mer Sequence	Fe(III)PPIX Binding (eq.)	Zn(II)PPIX Binding (eq.)	Aggregated Hemozoin (nmoles)	Secondary Structure of BNT II
BNT II	AHHAHHAAD	9.83±0.21	13.40±0.31	5.63±0.04	-----
BNT IIA	AHHAADAHH	8.70±0.81	3.96±0.45	2.60±0.60	loose
BNT IID	AHHAHHAAA	1.45±0.17	3.14±0.71	0.50±0.20	loose
BNT IIX	AHAAHAAAD	3.37±0.39	3.33±1.36	0.40±0.30	loose
BNT IY	AAHAAHAAAD	7.82±0.45	8.56±0.80	0.27±0.15	Like BNT II
BNT IZ	AHHAHHAAK	9.81±0.88	6.44±0.81	2.37±0.43	Like BNT II

Table 4.6. Summary of the functional analyses of BNT II and its mutants.

The suggested sequence dependency of hemozoin formation led to the examination of specific point mutations with the Ala-His-His-Ala-His-His-Ala-Ala-Asp sequence in attempt to ascertain the amino acid residues along the domain sequence of BNT II that were critical in hemozoin formation. As stated earlier, the third and sixth histidine residues are critical in the binding and aggregation of hemozoin, as is the aspartic acid residue as determined by the functional screening of

the BNT mutants (**Table 4.6**). Mutant BNT IIZ however demonstrated that while the ninth residue is affected by polarity (BNT IID), the consequences of electrostatics are less effectual.

The identification of particular binding sites for both Fe(III)PPIX and Zn(II)PPIX through the above mutations were unsuccessful, as well as correlating heme binding and hemozoin formation. High heme binding activities did not necessarily impart high levels of hemozoin aggregation (particularly BNT IY and BNT IZ). Additionally, patterns in Zn(II)PPIX binding values were of little consequence, with the BNTs appearing to have associative binding activities with a minimum of three molecules of zinc substrate.

The CD binding experiments however, expound some connections between heme binding, hemozoin formation activity and secondary structure. Mutants BNT IID and BNT IIX, which had CD spectra blue-shifted from the spectrum of BNT II, exhibited both poor porphyrin binding capabilities and hemozoin aggregation activities. BNT IY and BNT IZ, which displayed CD spectra similar to BNT II were more efficient at porphyrin binding. Since BNT II and BNT IY conserved the third, sixth, and ninth residues one would expect the binding values to be necessarily the same, however BNT IY bound slightly fewer equivalents of the substrates. The disruption of the His-His repeat with alanine partially unfolds and/or distorts the peptide chain, decreasing porphyrin binding. The lysine residue in BNT IZ does little to perturb the secondary structure of the peptide dendrimer and therefore binding capabilities are restored to levels near the parent BNT II. However, the length of the

amino acid lysine, may occlude the ability of the template to aggregate hemozoin, especially when considering the steric constraints imparted by this residue near the MAPS core.

Mark Kac, noted mathematician once stated that the purpose of models was “to polarize our thinking,” helping to pose questions and make testable predictions. In this way, the BNT peptide mimics served as true models, generating hypotheses that cannot be constructed without such experimentation, while also leaving new unanswered questions as to the extent of amino acid sequence dependency or secondary structural requirement in hemozoin formation.

References

- [1] Iyer, J. K.; Shi, L.; Shankar, A. H.; Sullivan, D. J. J. "Zinc protoporphyrin IX binds heme crystals to inhibit the process of crystallization in *Plasmodium falciparum*." *Mole. Med.* **2003**, *9*, 175-182.
- [2] Gualfetti, P. J.; Bilsel, O.; Matthews, C. R. "The progressive development of structure and stability during the equilibrium folding of the α subunit of tryptophan synthase from *Escherichia coli*." *Prot. Sci.* **1999**, *8*, 1623-1635.
- [3] Gualfetti, P. J.; Iwakura, M.; Lee, C. J.; Kihara, H.; Bilsel, O.; Zitzewitz, J. A.; Matthews, C. R. "Apparent radii of the native, stable intermediates and unfolded conformers of the α -subunit of tryptophan synthase from *e. coli*, a TIM barrel protein." *Biochemistry* **1999**, *38*, 13367-13378.
- [4] Uversky, V. N.; Fink, A. L. "The chicken-egg scenario of protein folding revisited." *FEBS Lett.* **2002**, *515*, 79-83.
- [5] Huang, B.; Pranti, M. A.; Gustafson, T. L.; Parquette, J. R. "The effect of global compactions on the local secondary structure of folded dendrimers." *J. Am. Chem. Soc.* **2003**, *125*, 14518-14530.
- [6] Kosa, J. L.; Michelson, J. W.; Louis, H. A.; Olsen, J. I.; Davis, D. R.; Beckerle, M. C.; Winge, D. R. "Common metal ion coordination in the LIM domain proteins." *Biochemistry* **1994**, *33*, 468-477.
- [7] Sakamoto, M.; Ueno, A.; Hisakazu, M. "Multi-peptide-metalloporphyrin assembly as a dendrimer template and photoinduced electron transfer based on the dendrimer structure." *Chem. Eur. J.* **2001**, *7*, 2449-2458.
- [8] Ziegler, J.; Chang, R. T.; Wright, D. W. "Multiple-antigenic peptides of histidine-rich protein II of *Plasmodium falciparum*: Dendrimeric biomineralization templates." *J. Am. Chem. Soc.* **1999**, *121*, 2395-2400.

Chapter 5

Application of the BNT II Model System:

Inhibition of Hemozoin Aggregation by N_4O_2 Schiff Base Complexes

5.1. Introduction

The proteolysis of hemoglobin and the detoxification of released heme via the biomineralization of hemozoin are vital metabolic processes of the *Plasmodium falciparum* parasite. Since nearly all host hemoglobin is consumed during the trophozoite stage of *P. falciparum*'s life cycle, antimalarials that function to antagonize the essential life processes at this developmental stage are often regarded as having the greatest antiparasitic potentials. However, it is nearly impossible to assess whether antimalarial action is due to diminished hemoglobin catabolism, the inhibition of hemozoin formation, or whether parasite growth is simply arrested via other pathways.

Though most antimalarials are hypothesized to function by disrupting some aspect of the biomineralization of hemozoin¹⁻³ either by interfering with heme,⁴⁻⁷ a heme binding template,⁸⁻¹⁰ or a heme/template complex,^{11,12} differing experimental conditions have plagued the literature with a wealth of conflicting half-maximal inhibitory effects (IC₅₀ values), especially in *in vitro* assays. Inhibitory effects of antimalarial drugs are often attributed to salt concentrations, anions, metal ions and the experimental conditions, which require an acidic reaction medium (pH 4.8-5.5) to mimic the environment of the digestive vacuole of *P. falciparum*, the place where active hemoglobin proteolysis occurs. Despite this, an enormous amount of experimental research still occurs at neutrality.

Additionally, few considered the very nature of the malarial pigment, failing to acknowledge that experimental protocol washing procedures could become a such

tedious, yet innate part of correctly assembling true inhibition activities. Only as recently as the year 2000 did a few research groups begin focusing on the mode of antimalarial inhibition and surmounted the importance of washing protocols.¹³ Extraneous peaks were often present in the Fourier transformed infrared spectra of hemozoin that was used to characterize the final product, but these could often be considerably reduced through additional washing of the pigment. Never before had the differential solubility of the product been so pertinent in its characterization. Aggregates of heme were soluble in sodium bicarbonate buffer (pH 9.1) and sodium dodecyl sulfate (SDS), while hemozoin retained its insolubility in such solutions. The washing protocol therefore, must be able to dissolve all of the ferriprotoporphyrin aggregates that are not genuine hemozoin. Consequently, inadequate washing could lead to an artifactual lack of inhibition since the ferriprotoporphyrin aggregates would be quantitated as the malaria pigment.

Information is also obscured in the fact that certain antimalarials are more effective against particular strains of the parasite. Often a peculiar strain in one geographic location is more virulent than another found only a few hundred miles away. Part of this is due to the fact that chromosomal polymorphisms appear to heal by the addition of telomeric repeat sequences rather than a typical recombination of DNA breakages.¹⁴

By far, the quinoline class of antimalarials, which includes chloroquine, has been one of the most successful classes of drugs ever developed at combating malaria. Research has shown these antimalarials have the ability to disrupt hemozoin

formation.¹⁻³ Despite such early success as an antimalarial, chloroquine prophylaxis has receded due to the ever emerging resistant strains of *Plasmodia*. The development of new drugs for the treatment of malaria is thus of utmost importance.

Since the parasite's proteolysis of hemoglobin releases free heme, a number of metal chelating agents have been examined as potential antimalarials. Sharma and Piwnicka-Worms used a hexadentate ethylenediamine-*N,N'*-bis[propyl(2-hydroxy-*R*-benzylimino)] ligand (R-ENBPI) and a reduced (*R*-benzylamino) analogue (R-ENBPA) to form metal (III) complexes with aluminum, iron, gallium, and indium, developing a novel class of antimalarials that was shown to blockade hemozoin formation. Such multi-dentate metal (III) coordination complexes exhibited a wide range of activity among both chloroquine-sensitive and chloroquine-resistant strains of *P. falciparum*.¹⁵⁻¹⁷ Detailed structural studies emphasized the importance of the spatial arrangement of the ligand periphery in localization and biotransport of these molecules.¹⁶ Goldberg *et al.* meanwhile demonstrated that *in vivo* hemozoin formation was greatly diminished in parasites cultured with both the iron and gallium complexes.¹⁵ None however, examined the specific role of the coordination complex in the inhibition of β -hematin aggregation. With this in mind and the fact such topological constraints warrant further investigations into three dimensional growth processes such as the biomineralization of hemozoin, we examined the basis for the observed inhibitory effects of these N_4O_2 Schiff bases using our histidine-rich protein II (HRP II) biomimetic model peptide, BNT II .

5.2. Synthesis and Characterization of N₄O₂ Complexes

All reagents were purchased from commercial sources and used as received. Hemin chloride (Fe(III)PPIX), protoporphyrin IX (PPIX), and deuterated methylene chloride-*d*₂ (CD₂Cl₂), chloroform-*d* (CDCl₃), methanol-*d*₃ (CD₃OH), dimethylsulfoxide-*d*₆ (DMSO), sodium acetate-*d*₃ (CD₃CO₂Na), glacial acetic acid-*d*₄ (CD₃COOD), and water (D₂O) were purchased from Sigma-Aldrich (St. Louis, MO).

The ligand and metal (III) complexes were prepared according to a method previously described by Sharma *et al.*¹⁸ Briefly, the prepared N₄O₂ ligand was reacted with the appropriate amount of metal salt in ethanol. The metal (II) complex was synthesized according to methods previously described by Polyakov.¹⁹ Isolated complexes were characterized by proton nuclear magnetic resonance spectroscopy (¹H NMR), infrared spectroscopy (IR), and electrospray ionization mass spectrometry (ESI). The corresponding spectra were omitted from this publication since the physical characterizations of these compounds were previously reported by the aforementioned authors.^{18,15,16,19} Instead, proof of each characterization is briefly summarized.

IR analyses of dried reaction mixtures in KBr matrixes were performed on a Perkin-Elmer 1760 X FT-IR spectrophotometer (Boston, MA). Typically, 256 scans were collected at a resolution of 4 cm⁻¹ from 4000-400 cm⁻¹. UV-Vis measurements were carried out on a Cary 3-E UV-Vis spectrophotometer (Walnut Creek, CA). Fluorescence measurements were performed on a Photon Technology International QM-1 spectrofluorometer (Lawrenceville, NJ). NMR studies were recorded on a

Bruker ACP-300 MHz spectrometer (Newark, DE) at room temperature. Chemical shifts were reported in δ (ppm).

5.2.1. Ligand Synthesis. 2-(2'-Hydroxy-3'-methoxyphenyl)-1,3-bis[4-aza-5-(2''-hydroxy-3''-methoxyphenyl)but-4'-en-1'-yl]-1,3'-imidazolidine (H₃Mabi)

N,N'-Bis(aminopropyl)ethylenediamine (858 mg, 4.92 mmole) and o-vanillin (2,244 mg, 14.76 mmole) were dissolved in a minimum amount of ethanol. The reaction was heated to reflux for 3 hours. After cooling to room temperature, the mixture was subjected to rotary evaporation to remove all volatiles. The remaining residue was then dried under reduced pressure typically overnight, until a bright yellow solid formed.

¹H NMR (in CD₂Cl₂) δ 8.15 (s, 2H), 6.60-7.15 (m, 7H), 6.50 (dd, 1H), 4.05 (s, 6H), 3.65 (m, 3H), 2.15-2.85 (m, 6H), 1.85 (m, 4H); **IR (KBr pellet, cm⁻¹)** 1630 ν (C=N).

5.2.2. Synthesis of Metal (III) Complexes [(3-OMe-ENBPI)M⁺]I⁻

5.2.2a Fe(III) Complex - Fe^{III}ENBPI

Equimolar amounts of H₃Mabi ligand (459 mg, 0.78 mmole) and iron (III) acetylacetonate (Fe(acac)₃, 282 mg, 0.79 mmole) were dissolved in a minimum amount of ethanol. The reaction was heated to reflux for 1 hour before potassium iodide (KI, 132 mg, 0.78 mmole) was added to the mixture and permitted to reflux for another 10 minutes. The solution was then removed from heat and allowed to precipitate overnight. The microcrystalline precipitate was then filtered from

solution, washed with cold ethanol and then ether. The remaining residue was then dried under reduced pressure.

¹H NMR (in CD₃OH) δ 25 b, 20 b, 9 s, 5.5 s, 3.5 s, 1 s, -1 s, -8 b; **IR (KBR pellet, cm⁻¹)** 3000–2800 ν (C-H), 1620 ν (C=N), 1540 σ (N-H); **ESI Mass Spec** 496.3 m/z; **UV-Vis λ_{max}** 375 nm (ε = 8765).

5.2.2b Ga(III) Complex - Ga^{III}ENBPI

Equimolar amounts of H₃Mabi ligand (420 mg, 0.72 mmole) and gallium (III) acetylacetonate (Ga(acac)₃, 267 mg, 0.72 mmole) were dissolved in a minimum amount of ethanol. The reaction was heated to reflux for 1 hour before KI (120.9 mg, 0.72 mmole) was added to the mixture and permitted to reflux for another 10 minutes. The solution was then removed from heat and allowed to precipitate overnight. The microcrystalline precipitate was then filtered from solution, washed with cold ethanol and then ether. The remaining residue was then dried under reduced pressure.

¹H NMR (in CD₂Cl₂) δ 8.14 (s, 2H), 7.05 (d, 2H), 6.8 (d, 2H), 6.65 (t, 2H), 3.85 (s, 6H), 3.2-3.6 (m, 6H), 1.9 (m, 2H), 1.6 (m, 2H); **IR (KBr pellet, cm⁻¹)** 1630 ν (C=N) **ESI Mass Spec** 509.2 m/z; **UV-Vis λ_{max}** 390 nm (ε = 4470).

5.2.3. Synthesis of Metal (II) Complex [(3-OMe-ENBPI)M]

4.2.3a Mg(II) Complex - Mg^{II}ENBPI

The magnesium complex was prepared as a batch reaction. Magnesium sulfate (MgSO₄, 6.0 g, 0.05 mole) and N,N'-bis(3-aminopropyl)ethylenediamine (3.49 g, 0.02 mole) were dissolved in 300 ml of methylene chloride (CH₂Cl₂). O-vanillin (2.28g, 0.015 mole) dissolved in 60 ml of CH₂Cl₂ was then added

dropwise to the above solution. The reaction mixture was then allowed to stir for 24 hours at room temperature. The resulting solid was then filtered from solution and permitted to dry under low vacuum. The dried solid residue was then crystallized from nitromethane.

¹H NMR (in CDCl₃) δ 7.81 (s, 2H), 6.72 (d, 2H), 6.61 (d, 2H), 6.31 (t, 2H), 4.15 (m, 2H), 3.89 (m, 2H), 3.79 (s, 6H), 2.92 (m, 8H), 2.00 (d, 2H), 1.56 (m, 2H), 1.37 (m, 2H); **IR (KBr pellet, cm⁻¹)** 3329 ν (N-H), 3049 ν (C-H_{arom}), 2911 and 2861 ν (C-H_{alip}), 1629 ν (C=N); **ESI Mass Spec** 465.1 m/z; **UV-Vis** λ_{\max} 353 nm ($\epsilon = 2990$).

5.3. Experimental Methods

5.3.1. BNT Binding Assay

Following the UV-Vis difference titration methods of Morgan,^{20,21} 1-10 nmoles of BNT II dissolved in 100 mM sodium acetate buffer, pH 4.8, were added to a 1.0 mL semi-micro quartz cell (10 mm, Starna Cells, Atascadero, CA). Blanks contained 1.0 mL of the aforementioned buffer. Aliquots of stock solutions of the N₄O₂ complex substrate (~ 1 mM) dissolved in DMSO were then titrated into both the blank and reference cuvettes. Samples were equilibrated for fifteen minutes prior to measurements on a Cary 3-E UV-Vis spectrophotometer (Walnut Creek, CA).

5.3.2. In Vitro Heme Aggregation Assay

BNT II was assayed for hemozoin formation by incubating 2-2.5 nmol of template and 50-100 μ M hemin chloride (dissolved in 0.1 M NaOH) in a total volume of 2.0 mL of 25-500 mM sodium acetate buffer, pH 4.8, for 48 hours at 37 °C in the

presence of varying concentrations of drug dissolved in DMSO. Control blanks of DMSO showed that the solvent had no effect on the assay. The volume of hemin added was less than 10% of the total volume of the solution in order to maintain buffering capacity. After 48 hours the samples were vortexed, transferred to 50 mL polycarbonate Oak Ridge centrifuge tubes, and centrifuged at 19,000 g for 1 hour at 4 °C on a Sorvall RC-5B refrigerated superspeed centrifuge equipped with a SS-34 fixed angle rotor. The supernatant was discarded and the pellet resuspended in 5 mL of 0.1 M sodium bicarbonate, pH 9.1, to solubilize any free heme. The centrifuge tubes were then vortexed every ½ hour for two hours before centrifuging again and decanting the supernatant. The pellet was treated with an additional sodium bicarbonate wash and centrifuged. The remaining pellet was washed with water, vortexed, and centrifuged until the pH of the decanted supernatant was neutral. The final pellet of aggregated heme was quantitated on the basis of its absorbance at 400 nm ($\epsilon = 100,000$). Briefly, the pellet was dissolved in 1.0 mL of 0.1 M NaOH and vortexed every 15 minutes for 1 hour before recording the absorbance measurement on a Cary 3-E UV-Vis spectrophotometer (Walnut Creek, CA).

5.3.3. Porphyrin Aggregation Fluorescence Studies

Stock solutions of the fluorophore (the N_4O_2 complexes) dissolved in DMSO and heme quencher, which was 1.0 mM hemin chloride dissolved in 100 mM NaOH, were used. According to the assay, an appropriate amount of 100 mM sodium acetate buffer, pH 4.8, was added to a 4.0 mL quartz fluorometer cell (10 mm, Starna Cells, Atascadero, CA), along with varying amounts of the fluorophore (20-40 μ M).

Aliquots of a stock solution of Fe(III)PPIX dissolved in 0.1 M NaOH were then added to the cuvette (final hemin concentration: 4-320 μ M). The sample was scanned rapidly from 450-700 nm upon addition of the fluorophore on a Photon Technologies QM-1 T format spectrofluorometer (Lawrenceville, NJ). All samples were excited at the respective excitation maxima and monitored at the emission maxima of the corresponding fluorophore. This included excitation values of 310 nm for Fe^{III}ENBPI, 380 nm for Ga^{III}ENBPI, and 350 nm for Mg^{II}ENBPI.

5.3.4. NMR Stability Studies

Briefly, 4.0 mL of 50 mM deuterated acetate buffer was prepared by adding 4.3 mg deuterated sodium acetate (CD₃CO₂Na-d₃) dissolved in 2.0 mL deuterated water (D₂O) and 2.87 mL deuterated glacial acetic acid diluted in 1.997 mL D₂O. The pH was adjusted to 4.8 by the dropwise addition of deuterated sodium hydroxide (NaOD). Next 7-10 mg of the ENBPI complex dissolved in 1.0 mL deuterated dimethylsulfoxide (DMSO-d₆) were added to 1.0 mL of the above prepared acetate buffer. The sample was then filtered into an NMR tube and the initial time zero measurement recorded. The sample was then incubated at 37⁰C for the duration of the experimental time intervals. Samples were permitted to return to room temperature before recording additional spectra.

5.4. Results and Discussion

Previous studies by Zielger *et al.* demonstrated that a dendrimeric peptide, BNT II, based on the putative heme binding domain of the histidine-rich protein II of *Plasmodium falciparum*, served as a functioning analogue for this protein in an *in*

vitro hemozoin aggregation assay.²² In conjunction with his ongoing studies, undergraduate summer research projects, and as an introduction for myself into BNT II chemistry, this template was utilized as a means to probe the inhibitory effects of the synthesized Schiff base compounds.

5.4.1. Inhibitory Effects

Once the compounds (**Figure 5.1**) were fully characterized, the dose responses of hemozoin formation to the Fe^{III}ENBPI, Ga^{III}ENBPI, and Mg^{II}ENBPI complexes were evaluated. In 25 mM acetate buffer, pH 4.8, the half-maximal inhibitory effects (IC₅₀) for both Fe^{III}ENBPI and Ga^{III}ENBPI (9.5 and 58 μM respectively) were similar those reported by reported by Goldberg (4 and 40 μM, respectively). The neutral Mg^{II}ENBPI did not inhibit hemozoin aggregation.

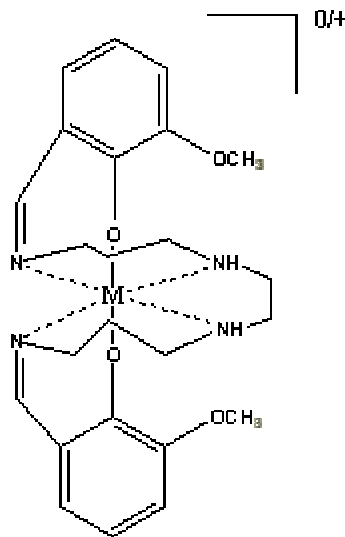


Figure 5.1. Representation of the N₄O₂ Schiff base complex. M = Fe(III), Ga(III), or Mg(II).

When considering the proposed mechanisms of inhibiting hemozoin aggregation, three possible scenarios arise. First, (1) the drug can intercalate the growing face of the hemozoin crystal preventing further crystal development.^{11,12} Second, (2) hematin could also be displaced from substrates such as lipids or HRP II, in such that drug binding to the substrate would enable free heme concentrations to become lethal to *P. falciparum*.⁸⁻¹⁰ Finally, (3) the drug could physically interact with

hematin via π - π stacking of its aromatic structure with that of heme,²³⁻²⁶ preventing further crystalline hemozoin growth.

First and foremost, the drugs did not appreciably bind to BNT II (data not shown), eliminating drug inhibition by scenario (2). Furthermore, when considering the topology of the complexes investigated, planar stacking of the drug onto the growing face of a hemozoin crystal in scenario (1) is not likely since the N_4O_2 Schiff base complexes do not offer this orientation. The fact however, that the neutral Schiff base compound, $Mg^{II}ENBPI$, is not inhibitory while the cationic complexes are, suggests the charge of the complex may be critical for the inhibition of heme aggregation. Upon consideration of the structure of hemozoin, whereby the critical linkage involves the oxygen from a propionate of one heme monomer serving as the axial ligand to the ferric ion of another¹¹ with hydrogen bonding between the propionic acid side chains of the porphyrin rings,²⁷ one could envision the N_4O_2 cationic Schiff base compounds preventing the critical axial linkage for the dimerization of heme units by electrostatic interaction with the anionic propionate moiety of heme. If the drug formed a drug:heme salt complex, the requisite propionate linkage in hemozoin aggregation would not be available.

If the mode of action of the antimalarial coordination complexes were charge dependent based on specific interactions originating from the propionate of heme, then such interactions should also be susceptible to competitive receptors, such as the acetate buffer used in the assays. Experiments performed in 500 mM acetate buffer were not inhibitory for both $Fe^{III}ENBPI$ and $Ga^{III}ENBPI$. In 100 mM acetate buffer,

Ga^{III}ENBPI was an ineffective inhibitor while Fe^{III}ENBPI had an IC₅₀ of 15 μM (See **Table 5.1** below). In contrast, assays performed in 25 mM acetate buffer with increasing amounts of sodium chloride had no effect on the IC₅₀ values (**Figure 5.2**) Drug concentrations were selected near maximal inhibitory concentrations - 50 μM

Table 5.1. Acetate buffer dependence of the IC₅₀ of N₄O₂ Schiff base complexes for the BNT II mediated aggregation of hemozoin.

Schiff Base Complex	IC ₅₀ μM		
	25 mM acetate buffer	100 mM acetate buffer	500 mM acetate buffer
Fe ^{III} ENBPI	9.5	15	NI
Ga ^{III} ENBPI	58	NI	NI
Mg ^{II} ENBPI	NI	NI	NI

NI = No Inhibition

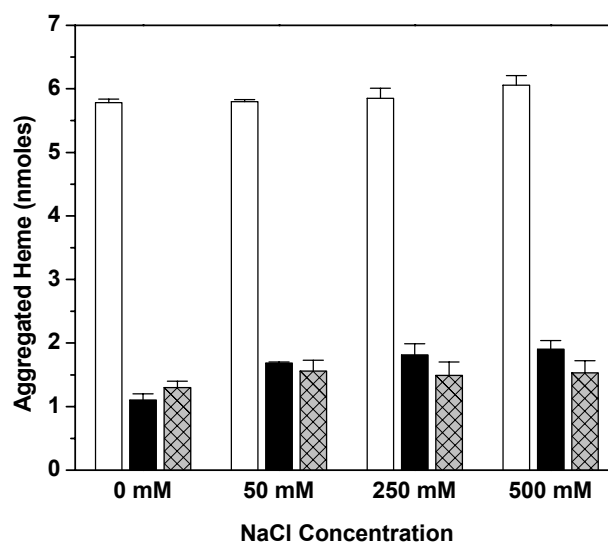


Figure 5.2. Effect of increasing salt concentration on hemozoin aggregation and drug inhibition. Assays were performed in 25 mM acetate buffer with increasing concentrations of NaCl. Vertical bar identification: white (left), no drug, black (middle), 50 μM Fe^{III}ENBPI, and right (gray) 200 μM Ga^{III}ENBPI.

Fe^{III}ENBPI and 200 μ M Ga^{III}ENBPI. This suggests the interactions between the drugs and heme may not be simply charge dependent, but also contingent on the specific carboxylate moiety.

The sensitivity of the cationic ENBPI complexes to acetate buffer concentration is distinct from other classes of heme aggregation inhibitors, such as the quinolines, hydroxyxanthenes, and porphyrins, which are seemingly unaffected by such conditions. In fact, two laboratories independently reported that heme inhibition by porphyrins is unaffected by acetate buffer concentration, one being our template mediated heme aggregation assay,²² the other being a heme polymerization inhibition activity assay²⁸ which does not utilize a template in the reaction medium.²⁹

The ability of the ENBPI complexes to directly associate with heme is further substantiated by means of fluorescence quenching experiments performed in various concentrations of acetate buffer, pH 4.8 (**Figure 5.3**). The titration of dilute solutions of the individual ENBPI complexes with Fe(III)PPIX resulted in the partial quenching of the fluorophore. At ratios of 1:1 Fe(III)PPIX to ENBPI complex, the fluorescence values were 70% of the original intensity for Fe^{III}ENBPI, 50% for Ga^{III}ENBPI, and 60% for Mg^{II}ENBPI. Complete quenching of Fe^{III}ENBPI was achieved with approximately 4 fold excess of Fe(III)PPIX, while Ga^{III}ENBPI required nearly 6 fold excess of the iron porphyrin. Mg^{II}ENBPI, the noninhibitory complex, was quenched when roughly 7.5-8 fold excess of heme was used. All curves followed a second order exponential decay quenching pattern.

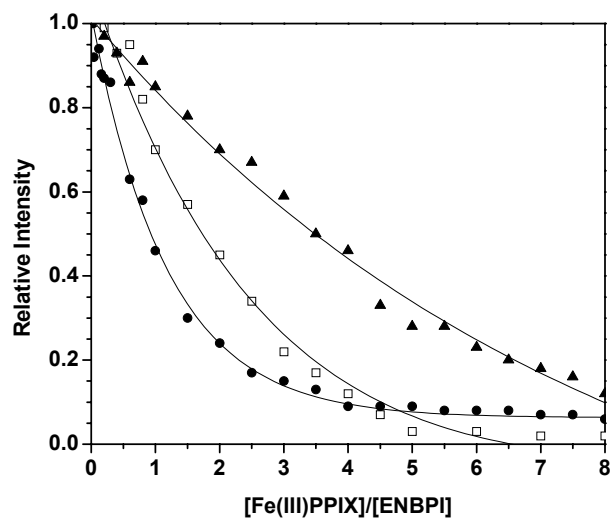


Figure 5.3. Fluorescence quenching study of ENBPI complexes by Fe(III)PPIX in 50 mM acetate buffer, pH 4.8. Each data point represents the average of three individual experiments with a standard deviation of < 5% for each point. ● Ga^{III}ENBPI, □ Fe^{III}ENBPI, and ▲ Mg^{II}ENBPI.

Quenching studies at increasing concentrations of acetate buffer (**Figure 5.4**) demonstrated a systematic decrease in the quenching of fluorescence as the concentration of the acetate buffer increased for the cationic ENBPI complexes. Fluorescence quenching of the Fe^{III}ENBPI complex was slowed to the same degree at higher concentrations of acetate buffer (200 and 500 mM), while the Ga^{III}ENBPI complex did not experience this trend at the concentrations investigated. Mg^{II}ENBPI showed little sensitivity to the acetate buffer concentration, especially at acetate buffer concentrations greater than 25 mM. Moreover, the intensity of the fluorescence emissions of the complexes remained relatively stable over time, up to 48 hours in both 25 mM and 500 mM acetate buffer, pH 4.8, at 37⁰C.

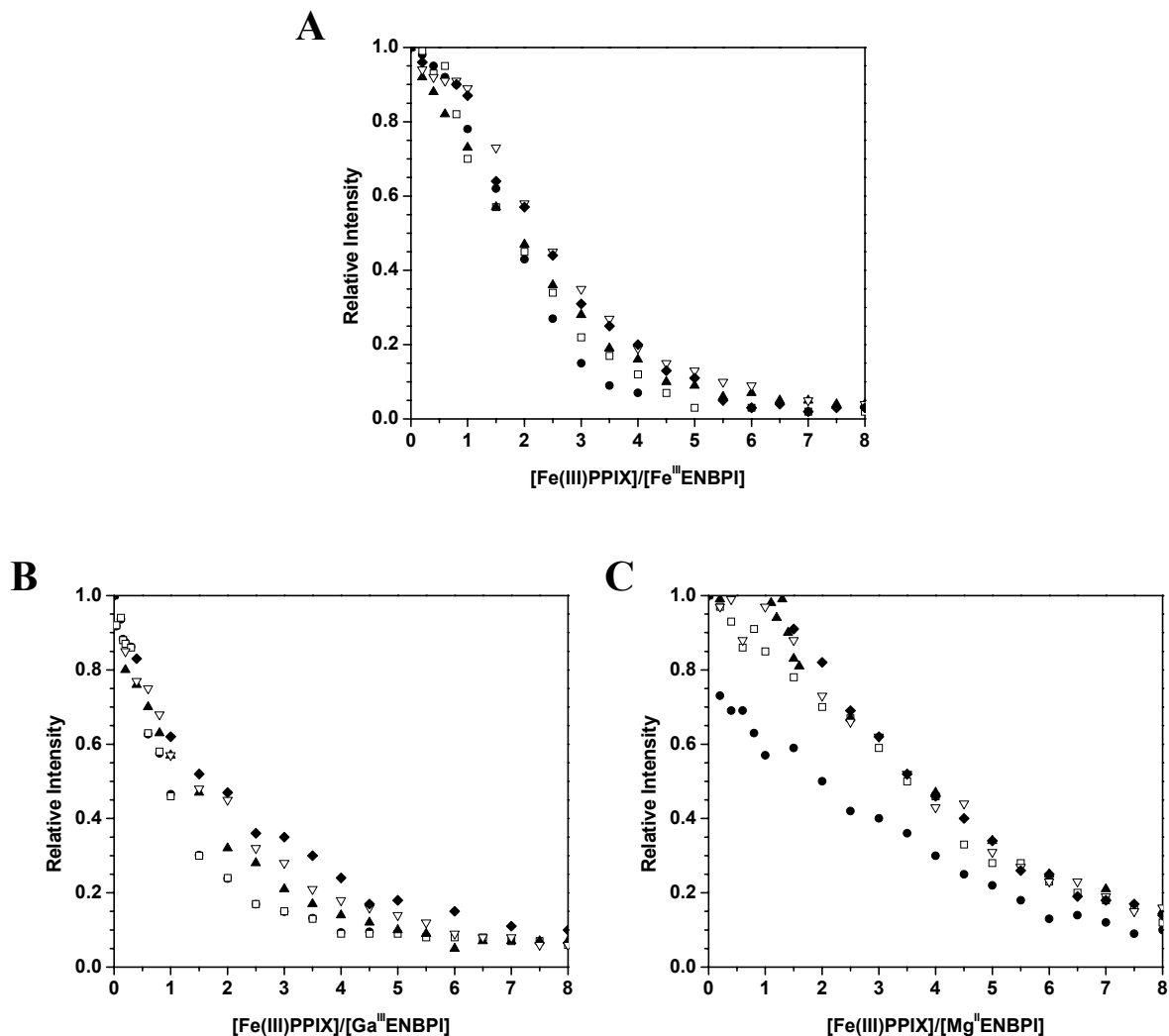


Figure 5.4. Fluorescence aggregation studies of fluorophores: (A) $\text{Fe}^{\text{III}}\text{ENBPI}$, (B) $\text{Ga}^{\text{III}}\text{ENBPI}$, and (C) $\text{Mg}^{\text{II}}\text{ENBPI}$ with heme in various concentrations of acetate buffer. Briefly, $20\ \mu\text{M}$ of each complex dissolved in DMSO was added to $4\text{--}320\ \mu\text{M}$ of heme dissolved in $0.1\ \text{M}$ NaOH. All samples were excited at respective excitation maxima ($\text{Fe}^{\text{III}}\text{ENBPI}$ – $310\ \text{nm}$, $\text{Ga}^{\text{III}}\text{ENBPI}$ – $380\ \text{nm}$, and $\text{Mg}^{\text{II}}\text{ENBPI}$ – $350\ \text{nm}$) and monitored at the emission maxima of each fluorophore.

● $25\ \text{mM}$ acetate, □ $50\ \text{mM}$ acetate, ▲ $100\ \text{mM}$ acetate, ▽ $200\ \text{mM}$ acetate, and ◆ $500\ \text{mM}$ acetate.

Representative studies for the cationic and neutral Schiff base compounds are listed in **Figure 5.5**.

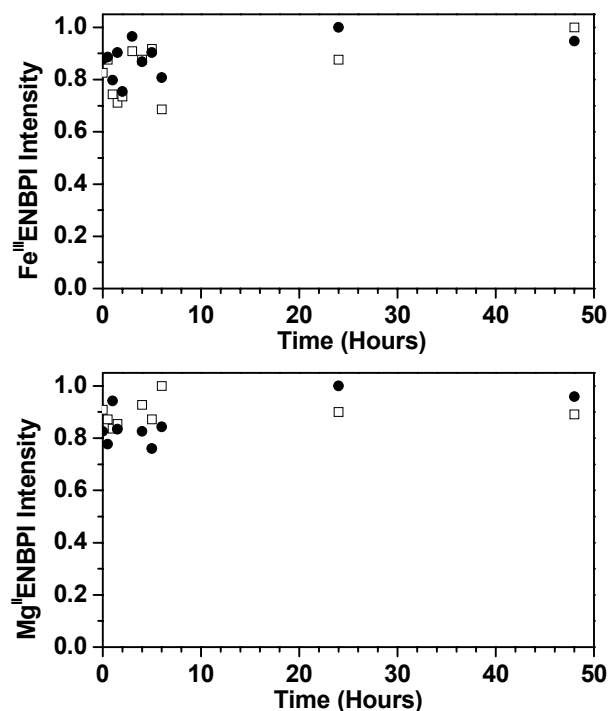


Figure 5.5. Fluorescence emission time study for representative ENBPI complexes. Samples were excited at the respective excitation maxima. Experiments were performed in pH 4.8 buffer at 37 °C. □ 25 mM acetate buffer, ● 500 mM acetate

Controls for the effect of possible demetalation reactions were negative.¹⁵ NMR stability studies of these same complexes in 25 mM or 500 mM acetate buffer, displayed no signs of hydrolysis. The Fe^{III}ENBPI complex was stable in 25 mM acetate buffer for 48 hours (data not shown), much like the stability reported at neutrality (pH 7.4, 72 hours) by Sharma *et al.*¹⁸ The Mg^{II}ENBPI complex (**Figure 5.6**) was also stable under the acidic assay conditions. The NMR spectra were

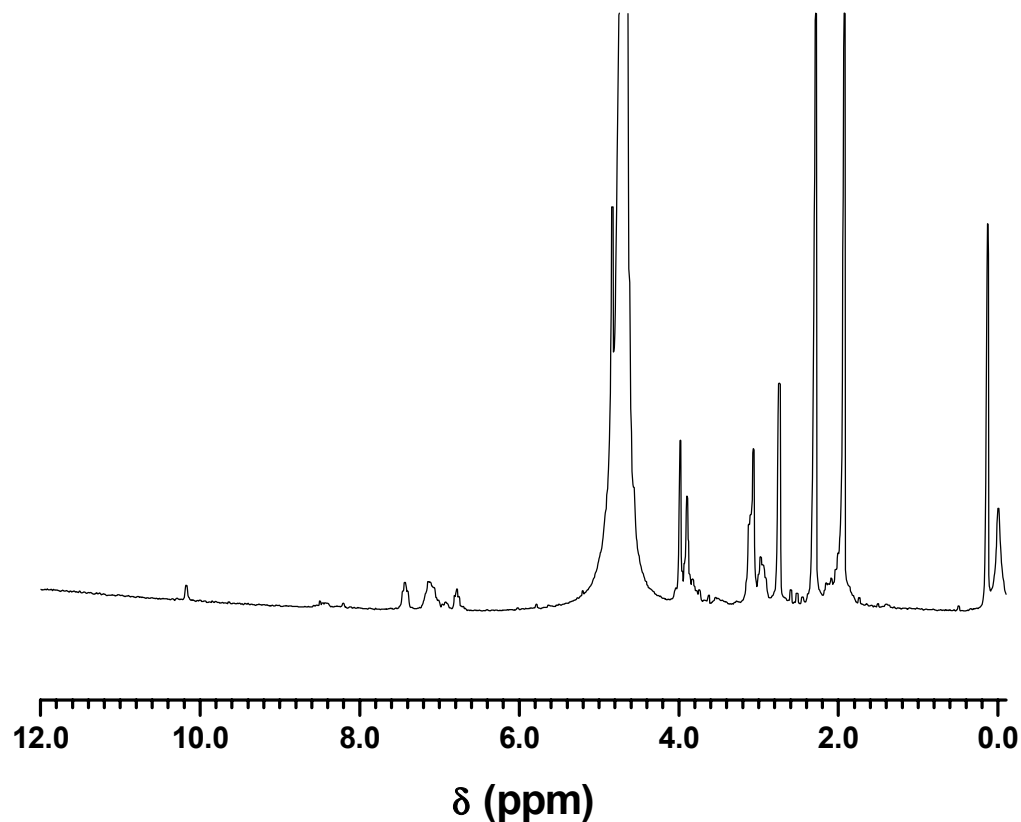


Figure 5.6. Typical NMR spectrum of $\text{Mg}^{\text{II}}\text{ENBPI}$ in 25mM acetate buffer.

superimposable before and after incubation in water at 37°C throughout the duration of the 48 hour experimental time period (**Figure 5.7**). Additionally, the stability was assessed via the integration ratios in **Figure 5.8**. The aldimino resonance signal (N-metal) at δ 7.36 did not decrease in intensity throughout the study. Furthermore, little compound decomposition occurred, as signified by the lack of aldimino proton at δ 8.15, which represents protons resulting from demetalation. This result differs from that recorded by Polyakov *et al.*, whom not only described the aldimino proton

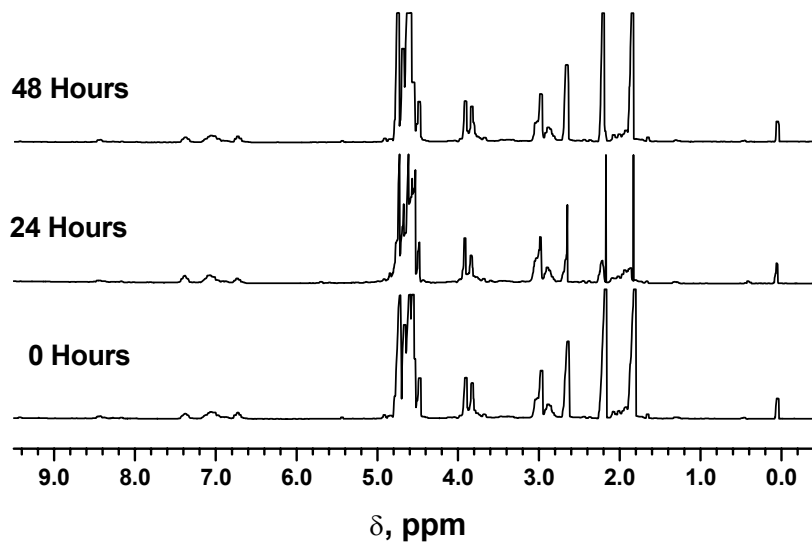


Figure 5.7. Representative NMR stability study of $\text{Mg}^{\text{II}}\text{ENBPI}$. The spectra did not change over the course of the experiment.

resonance at δ 8.1, but also demonstrated an additional reduced stability under acidic conditions.¹⁹

5.5. Conclusions

Given the relative importance of iron in the metabolic processing of *Plasmodium falciparum*, metal chelating agents are often examined as potential antimalarials. If the administered drug is lethal to the parasite, the question often then becomes which plausible mechanism of interaction halted or disrupted the very sustenance of the malaria parasite. With known antimalarials such as chloroquine, being more effective at specific stages of parasite growth,³⁰ understanding antimalarial drug action may seem like a daunting task. With the ENBPI complexes possessing an excellent correlation between the inhibition of hemozoin, both *in vitro*

and *in vivo*, and the ability of these compounds to arrest parasite development in both chloroquine sensitive and chloroquine resistant strains,¹⁵⁻¹⁷ a more detailed account was deemed necessary. Here we report the basis for the inhibition is most likely the formation of a salt complex between the anionic propionate of heme and the cationic drug complex.

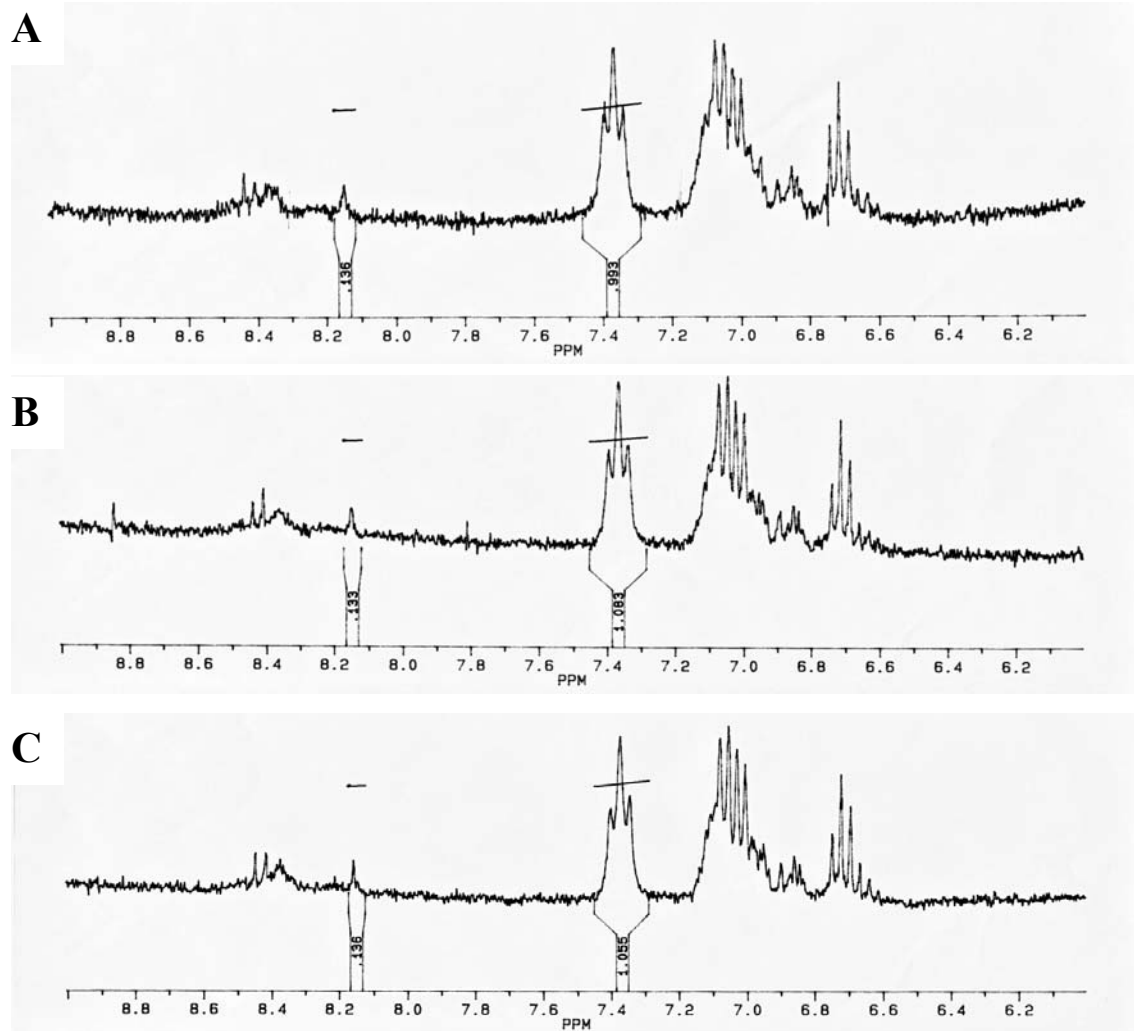


Figure 5.8. Representative NMR stability study of $Mg^{II}ENBPI$. The ratio of the small peak at 8.15 ppm relative to the triplet at 7.36 ppm did not change over the course of the experiment. Sample times include: (A) initial NMR, (B) 24 hour incubation, (C) 48 hour incubation.

References

- [1] Chou, A.; Chevli, R.; Fitch, C. "Ferriprotoporphyrin IX fulfills the criteria for identification as the chloroquine receptor on malaria parasites." *Biochemistry* **1980**, *15*, 1543-1549.
- [2] Slater, A. F. G.; Cerami, A. "Inhibition by chloroquine of a novel heme polymerase enzyme activity in malarial trophozoites." *Nature* **1992**, *355*, 167-169.
- [3] Sullivan, D. J., Jr.; Gluzman, I. Y.; Russell, D. G.; Goldberg, D. E. "On the molecular mechanism of chloroquine's antimalarial action." *Proc. Natl. Acad. Sci., USA* **1996**, *93*, 11865-11870.
- [4] Ridley, R. G.; Dorn, A.; Vippagunta, S. R.; Vennerstron, J. L. "Haematin (heme) polymerization and its inhibition by quinoline antimalarials." *Ann. Trop. Med. Parasitol.* **1997**, *91*, 559-566.
- [5] Egan, T. J.; Marques, H. M. "The role of heme in the activity of chloroquine and related antimalarial drugs." *Coord. Chem. Rev.* **1999**, *192*, 493-517.
- [6] Vippagunta, S. R.; Dorn, A.; Matile, H.; Bhattacharjee, A. K.; Karle, J. M.; Ellis, W. Y.; Ridley, R. G. "Structural specificity of chloroquine-hematin binding related to inhibition of hematin polymerization and parasite growth." *J. Med. Chem.* **1999**, *42*, 4630-4635.
- [7] Ridley, R. G. "Medical need, scientific opportunity and the drive for antimalarial drugs." *Nature* **2002**, *415*, 686-693.
- [8] Pandey, A. V.; Bisht, H.; Babbarwal, V. K.; Srivastava, J.; Pandey, K. C.; Chauhan, V. S. "Mechanism of malarial heme detoxification inhibition by chloroquine." *Biochem. J.* **2001**, *355*, 333-338.
- [9] Choi, C. Y. H.; Schneider, E. L.; Kim, J. M.; Gluzman, I. Y.; Goldberg, D. E.; Ellman, J. A.; Marletta, M. A. "Interference with heme binding to histidine-rich protein-2 as an antimalarial strategy." *Chem. Biol.* **2002**, *9*, 881-889.
- [10] Kaschula, C. H.; Egan, T. J.; Hunter, R.; Basilico, N.; Parapini, S.; Taramelli, D.; Pasini, E.; Monti, D. "Structure-activity relationships in 4-aminoquinoline antiplasmodials. The role of the group at the 7-position." *J. Med. Chem.* **2002**, *45*, 3531-3539.

- [11] Pagola, S.; Stephens, P. W.; Bohle, D. S.; Kosar, A. D.; Madsen, S. K. "The structure of the malaria pigment β -hematin." *Nature* **2000**, *404*, 307-310.
- [12] Buller, R.; Peterson, M. L.; Almarsson, Ö.; Leiserowitz, L. "Quinoline binding site on malaria pigment crystal: A rational pathway for antimalarial drug design." *Cryst. Growth Des.* **2002**, *2*, 553-562.
- [13] Baelmans, R.; Deharo, E.; Munoz, V.; Sauvain, M.; Ginsburg, H. "Experimental conditions for testing the inhibitory activity of chloroquine on the formation of β -hematin." *Exp. Parasitol.* **2000**, *96*, 243-248.
- [14] Pologe, L. G.; Ravetch, J. V. "Large deletions result from breakage and healing of *P. falciparum* chromosomes." *Cell* **1988**, *55*, 869-874.
- [15] Goldberg, D. E.; Sharma, Y.; Oksman, A.; Gluzman, I. Y.; Wellems, T. E.; Piwnica-Worms, D. "Probing the chloroquine resistance locus of *Plasmodium falciparum* with a novel class of multidentate metal (III) coordination complexes." *J. Biol. Chem.* **1997**, *272*, 6567-6572.
- [16] Sharma, Y.; Beatty, A.; Goldberg, D. E.; Piwnica-Worms, D. "Structure of a novel antimalarial gallium (III) complex with selective activity against chloroquine-resistant *Plasmodium falciparum*." *Chem. Commun.* **1997**, *22*, 2223-2224.
- [17] Sharma, V.; Piwnica-Worms, D. "Metal complexes for therapy and diagnosis of drug resistance." *Chem. Rev.* **1999**, *99*, 2545-2560.
- [18] Sharma, V.; Crankshaw, C. L.; Piwnica-Worms, D. "Effects of multidrug resistance (*MDR1*) P-glycoprotein expression levels and coordination metal on the cytotoxic potency of multidentate (N_4O_2) (ethylenediamine)bis[propyl(R-benzylimino)]metal (III) cations." *J. Med. Chem.* **1996**, *39*, 3483-3490.
- [19] Polyakov, V. R.; Sharma, V.; Crankshaw, C. L.; Piwnica-Worms, D. "Synthesis, molecular structure, and properties of a neutral Schiff base phenolic complex of magnesium." *Inorg. Chem.* **1998**, *37*, 4740-4742.
- [20] Burch, M. K.; Morgan, W. T. "Preferred heme binding sites of histidine-rich glycoprotein." *Biochemistry* **1985**, *24*, 5919-5924.

- [21] Morgan, W. T. "The histidine-rich glycoprotein of serum has a domain rich in histidine, proline, and glycine that binds heme and metals." *Biochemistry* **1985**, *24*, 1496-1501.
- [22] Ziegler, J.; Chang, R. T.; Wright, D. W. "Multiple-antigenic peptides of histidine-rich protein II of *Plasmodium falciparum*: dendrimeric biomineralization templates." *J. Am. Chem. Soc.* **1999**, *121*, 2395-2400.
- [23] Pandey, A. V.; Joshi, R. M.; Tekwani, B. L.; Singh, R. L.; Chauhan, V. S. "Assay of β -hematin formation by malaria parasite." *J. Pharm. Biomed. Anal.* **1997**, *20*, 203-207.
- [24] Kim, P.; Pau, C.-P. "Comparing tandem repeats and multiple antigenic peptides as the antigens to detect antibodies by enzyme immunoassay." *J. Immunol. Methods* **2001**, *257*, 51-54.
- [25] Egan, T. J. "Discovering antimalarials: A new strategy." *Chem. Biol.* **2002**, *9*, 852-853.
- [26] Noedl, H.; Wernsdorfer, W. H.; Miller, R. S.; Wongsrichanalai, C. "Histidine-rich protein II: a novel approach to malaria drug sensitivity testing." *Antimicrob. Agents Chemother.* **2002**, *46*, 1658-1664.
- [27] Bohle, D. S.; Kosar, A. D.; Madsen, S. K. "Propionic acid side chain hydrogen bonding in the malarial pigment β -hematin." *Biochem. Biophys. Res. Commun.* **2002**, *294*, 132-135.
- [28] Egan, T. J.; Ross, D. C.; Adams, P. A. "Quinoline antimalarial drugs inhibits spontaneous formation of β -hematin (malaria pigment)." *FEBS Lett.* **1994**, *352*, 54-57.
- [29] Egan, T. J.; Hempelmann, E.; Mavuso, W. W. "Characterization of synthetic β -hematin and the effects of the antimalarial drugs quinidine, halofantrine, desbutylhalofantrine and mefloquine on its formation." *J. Inorg. Biochem.* **1999**, *74*, 101-107.
- [30] Orjih, A. U. "Heme polymerase activity and the stage specificity of antimalarial action of chloroquine." *J. Pharmacol. Exp. Ther.* **1997**, *282*, 108-112.

Chapter 6

Concluding Remarks

6.1. Hemoglobin Proteolysis as an Antimalarial Strategy

Hemoglobin proteolysis is essential for parasite survival, and therefore provides a wealth of catabolic targets for the development of novel antimalarials. While earlier investigations targeted the disruption of proteolytic events, recent research focuses on arresting parasite development after the catabolism of hemoglobin; either during the ensuing formation of hemozoin from free released iron (III) protoporphyrin IX or during events outside the digestive vacuole once the biomineral has formed.

While hemoglobin ingestion and digestion are energetically expensive to the parasite, quantitative estimates of the actual proteolysis remain highly controversial. Some research demonstrates that only ~ 16% of the amino acids from hemoglobin proteolysis is utilized by the *Plasmodium falciparum* parasites,¹ despite hemoglobin digestion estimates as high as 80%. In addition to obtaining requisite amino acids, Lew *et al.* have suggested that parasites proteolyze hemoglobin as a mechanism to prevent the host red blood cell from premature lysis.² Sound evidence of this evolutionary strategy however, fails to exist until advances in the validation of host cell volume measurements and hemoglobin concentration experiments *in vivo* improve. Nevertheless, parasite growth remains directly correlated to hemoglobin proteolysis and thus halting any stage of hemoglobin consumption will definitively arrest parasite development.

Quests to understand antimalarial drug action through the inhibitory activity of hemozoin aggregation is also contentious, due to the fact that an overwhelming

number of possible mechanisms exist, with each hypothesis being a reasonable and partially substantiated event. Heme, hemozoin, and templates such as HRP II and lipids have all been shown to act as drug receptor sites, preventing the aggregation of heme. With malarial antagonists being operational amid different receptors, uncovering novel antimalarial drug strategies has become a daunting task. Stereoelectronic models are now being used to search for new potential antimalarial compounds.³

6.2. Biochemical Involvement of HRP II

Consequently, the *in vivo* measurement of cellular HRP II levels has also long been correlated to parasitemia, as well as to parasite development, increasing in concentration during the late ring and trophozoite stages of development, while remaining at a relatively constant level during schizont development and the later rupture and red blood cell reinvasion stages. Thus, it appears that HRP II production is mediated by *Plasmodium falciparum*'s metabolic activity, remaining associated with the parasites and/or erythrocytes.

Significant increases in the concentration of this protein are not noted in the culture medium in *in vitro* experiments. However, the inhibition of parasite development with common antimalarials, such as mefloquine and artesunate, is reflected in the inhibition of HRP II production,⁴ following a sigmoidal inhibition curve similar to traditional *in vitro* drug sensitivity assays. In hindsight, impeding HRP II production could disrupt the metabolic activity of *Plasmodium falciparum* to an extent that parasitemia may be controlled or decreased. Knowing how HRP II

secretion and production are growth-related and affected by antimalarials is only one avenue of investigation. Why not know which particular amino acids or repeats within the protein sequence are associated with the viability of the parasite?

In addition to its proposed role in the detoxification of heme, HRP II has also been evidenced to bind actin, suggesting it plays a role in the stabilization of actin filaments in an acidic environment (pH 6.0-6.5).⁵ This acidic pH dependence of HRP II in both actin binding and heme binding and hemozoin formation is also noted with the knob-associated HRP (KAHRP) and its binding to the cytoplasmic domain of the *Plasmodium falciparum* erythrocyte membrane protein 1 (PfEMP1),⁶ which has regions rich in histidine and lysine.

HRP II from *Plasmodium falciparum* was found to also decrease the lipopolysaccharide (LPS) induced production of interleukin-8,⁷ demonstrating yet another reason to examine the sequence specificity of HRP II activity, not only in hemozoin formation, but also since it may play additional role(s) in monocyte activation.

Despite its numerous avenues of biochemical involvement, even if HRP II is not definitively implicated in the nucleation and formation of hemozoin or other such events, such site-directed mutagenesis studies are warranted for the advancement of the current scientific understanding of this protein in immunochromatographic assays. Currently, the detection of the HRP II antigen⁸⁻¹⁰ is the only alternative to the microscopic diagnosis of malaria. HRP II however, has a long half-life *in vivo* which has limited its application in developing tests to monitor therapeutic efficacy.

6.3. Role of BNT II Model Systems

In retrospect, since hemozoin formation is a biomineralization process, understanding the stages of assemblage becomes essential for understanding antimalarial drug interactions. With a model system such as the BNTs, hemozoin formation could be evaluated at the single amino acid residue level. By the determination of single anchor points along the template that elicit hemozoin production, drug:template interactions can be better assessed. With multiple sites of interactions and the specific affinities therein for different antimalarials, many drugs have diverse modes of interaction. The parasites additionally have many modes of resistance including the overexpression of target proteins, mutations of target proteins, enzyme modifications, and alterations in efflux pumps. With such overwhelming dynamics in the life cycle of *Plasmodium falciparum* interplayed with possible scenarios for antimalarial drug interactions and insecticide resistance in the vector, a fundamental understanding at the single amino acid residue level will lead to novel control strategies in both the immunology of the tropical disease of malaria and biochemistry of *P. falciparum*.

While conflicting reports on mode of hemozoin formation continue to be presented in the literature, the exact mechanism of malarial pigment growth will be disputed until science overcomes some of the technological problems associated with studying life processes within a living organism. Crystals of synthetic β -hematin vary in microscopic morphologies (**Figure 6.1 and 6.2**),^{11,12} but are still biochemically similar to hemozoin formed by *Plasmodium falciparum* and other hemozoin

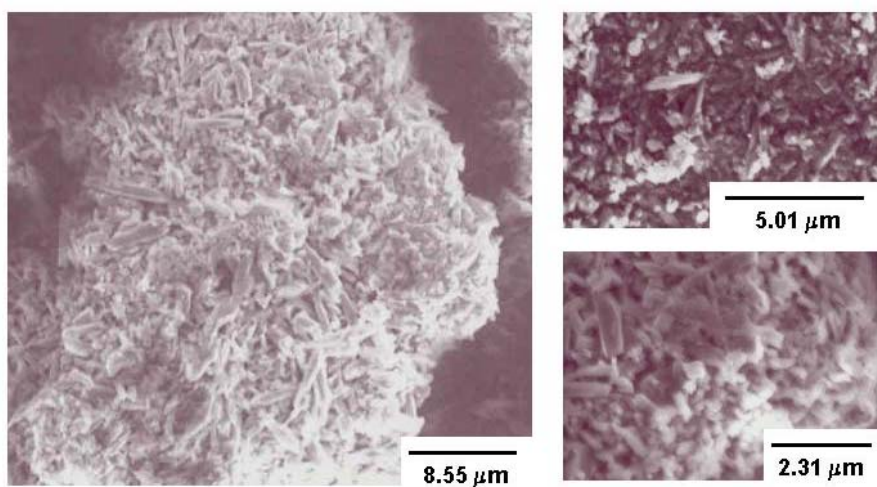


Figure 6.1. Scanning electron microscopy of β -hematin synthesized by the dehydrohalogenation of 2,6-lutidine according to methods published by Bohle.

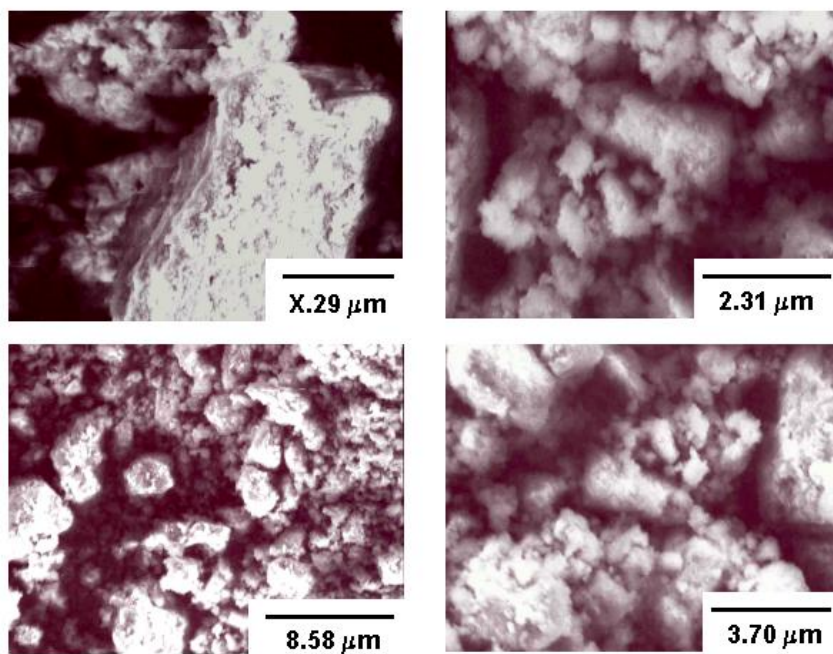


Figure 6.2. Scanning electron microscopy of β -hematin synthesized in aqueous solution according to methods published by Blauer.

producing species. The spectra of hemozoin and synthetic β -hematin are similar, including the Raman imaging¹³ and Fourier transform infrared (FT-IR) spectroscopy.¹⁴⁻¹⁶ Though *in vitro* growth conditions may mimic hemozoin formation and yield approximations for inhibition, such biochemical events are directly controlled by the parasite. With this in mind, the BNT dendrimers are no less an effective mimic than the other templates, whether lipid or protein based.

6.4. Summary

While advances have been made, questions still arise and are resultant from the different methodologies employed in studying hemozoin formation. Though a recent paper by Tripathi *et al.*¹⁷ highlights the importance of the removal residual heme aggregates from hemozoin formation assays before pigment quantification, which our laboratory definitively agrees with the authors on, their research still poses another question upon further examination. The authors examine the *in vitro* process of β -hematin formation with heme alone, parasite lysate extracts and lipid extracts. Curiously, the lipid mediated formation of hemozoin was found to be concentration dependent to 10 $\mu\text{g/mL}$ for most fatty acids except for oleoyl glycerol, which was notably more soluble under the experimental conditions. If a lipid mediated route to hemozoin formation was employed by *Plasmodium falciparum*, then the parasite would not only have to regulate hemoglobin degradation, but also fatty acid synthesis, which the parasite may very well do, but preliminary results suggest that fatty acid synthesis is decreased during parasite proteolysis.¹⁸ This would cause the parasite to expend an enormous amount of energy to simply sustain its life. In addition to this,

would fatty acid concentration be another unexplored antimalarial strategy? Increasing fatty acid concentration would decrease hemozoin formation and the excess free heme could still effectively kill the parasite.

The exploitation of a functional model system like BNT II is seemingly boundless. Studies beyond site-directed mutagenesis work are readily envisioned in order to better understand the critical interactions between the substrate and template. The relevance of histidine, which is critical for heme binding and hemozoin formation, can be evaluated further by modifying the residue with diethylpyrocarbonate¹⁹⁻²¹ and studying the effects thereto.

References

- [1] Krugliak, M.; Zhang, J.; Ginsburg, H. "Intraerythrocytic *Plasmodium falciparum* utilizes only a fraction of the amino acids derived from the digestion of host cell cytosol for the biosynthesis of its proteins." *Mol. Biochem. Parasitol.* **2002**, *119*, 249-256.
- [2] Lew, V. L.; Macdonald, L.; Ginsburg, H.; Krugliak, M.; Tiffert, T. "Excess hemoglobin digestion by malaria parasites: a strategy to prevent premature host cell lysis." *Blood Cells Mol. Dis.* **2004**, *32*, 353-359.
- [3] Portela, C.; Afonso, C. M. M.; Pinto, M. M. M.; Ramos, M. J. "Computational studies of new potential antimalarial compounds - Stereoelectronic complementarity with the receptor." *J. Comput. Aided Mater. Des.* **2003**, *17*, 583-595.
- [4] Noedl, H.; Wongsrichanalai, C.; Miller, R. S.; Myint, K. S. A.; Looareesuwan, S.; Sukthana, Y.; Wongchotigul, V.; Kollaritsch, H.; Wiedermann, G.; Wernsdorfer, W. H. "*Plasmodium falciparum*: effect of anti-malarial drugs on the production and secretion characteristics of histidine-rich protein II." *Exp. Parasitol.* **2002**, *102*, 157-163.
- [5] Benedetti, C. E.; Kobarg, J.; Pertinhez, T. A.; Gatti, R. M.; De Souza, O. N.; Spisni, A.; Meneghini, R. "*Plasmodium falciparum* histidine-rich protein II binds to actin, phosphatidylinositol 4,5-biphosphate and erythrocyte ghosts in a pH-dependent manner and undergoes coil-to-helix transitions in anionic micelles." *Mol. Biochem. Parasitol.* **2003**, *128*, 157-166.
- [6] Voigt, S.; Hanspal, M.; LeRoy, P. J.; Zhao, P.; Oh, S. S.; Chishi, A. H. "The cytoadherence ligand *Plasmodium falciparum* erythrocyte membrane protein 1 (PfEMP1) binds to the *P. falciparum* knob-associated histidine-rich protein (KAHRP) by electrostatic interactions." *Mol. Biochem. Parasitol.* **2000**, *110*, 423-428.
- [7] Bosshart, H.; Heinzelmann, M. "Endotoxin-neutralizing effects of histidine-rich peptides." *FEBS Lett.* **2003**, *553*, 135-140.
- [8] Shiff, C. J.; Premji, Z.; Minjas, J. N. "The rapid manual ParaSight-F- test. A new diagnostic tool for *Plasmodium falciparum* infection." *Trans. R. Soc. Trop. Med. Hyg.* **1993**, *87*, 646-648.

- [9] Beadle, C.; Long, G. W.; Weiss, W. R.; McElroy, P. D.; Maret, S. M.; Oloo, A. J.; Hoffman, S. L. "Diagnosis of malaria by detection of *Plasmodium falciparum* HRP-2 antigen with a rapid dipstick antigen-capture assay." *Lancet* **1994**, *343*, 564-568.
- [10] Wongsrichanalai, C. "Rapid diagnostic techniques for malaria control." *Trends Parasitol.* **2001**, *17*, 307-309.
- [11] Bohle, D. S.; Kosar, A. D.; Stephens, P. W. "Phase homogeneity and crystal morphology of the malaria pigment β -hematin." *Acta Crystallogr. D. Biol. Crystallogr.* **2002**, *58*, 1752-1756.
- [12] Norland, G. S.; Briones, N.; Sullivan, D. J. "The shape and size of hemozoin crystal morphology distinguishes diverse plasmodium species." *Mol. Biochem. Parasitol.* **2003**, *130*, 91-99.
- [13] Wood, B. R.; Langford, S. J.; Cooke, B. M.; Glenister, F. K.; Lim, J.; McNaughton, D. "Raman imaging of hemozoin within the food vacuole of *Plasmodium falciparum* trophozoites." *FEBS Lett.* **2003**, *554*, 247-252.
- [14] Slater, A. F. G.; Swiggard, W. J.; Orton, B. R.; Flitter, W. D.; Goldberg, D.; Cerami, A.; Henderson, G. B. "An iron-carboxylate bond links the heme units of malaria pigment." *Proc. Natl. Acad. Sci., USA* **1991**, *88*, 325-329.
- [15] Blauer, G.; Akkawi, M. "Investigations of B- and β -hematin." *J. Inorg. Biochem.* **1997**, *66*, 145-157.
- [16] Wood, B. R.; Langford, S. J.; Cooke, B. M.; Lim, J.; Glenister, F. K.; Duriska, M.; Unthank, J. K.; McNaughton, D. "Resonance raman spectroscopy reveals new insight into the electronic structure of β -hematin and malaria pigment." *J. Am. Chem. Soc.* **2004**, *126*, 9233-9239.
- [17] Tripathi, A. K.; Shabana, I.; Walker, L. A.; Tekwani, B. L. "Spectroscopic determination of de novo hemozoin/ β -hematin formation in an *in vitro* assay." *Anal. Biochem.* **2004**, *325*, 85-91.
- [18] Waller, R. F.; Ralph, S. A.; Reed, M. B.; Su, V.; Douglas, J. D.; Minnikijn, D. E.; Cowman, A. F.; Besra, S. G.; McFadden, G. I. "A type II pathway for fatty acid biosynthesis presents drug targets in *Plasmodium falciparum*." *Antimicrob. Agents Chemother.* **2003**, *47*, 297-301.
- [19] Morgan, W. T. "Interactions of the histidine-rich glycoprotein of serum on metals." *Biochemistry* **1981**, *20*, 1054-1061.

- [20] Morgan, W. T. "The histidine-rich glycoprotein of serum has a domain rich in histidine, proline, and glycine that binds heme and metals." *Biochemistry* **1985**, *24*, 1496-1501.
- [21] Evrard, C.; Fastrez, J.; Soumillion, P. "Histidine modification and mutagenesis point to the involvement of a large conformational change in the mechanism of action of phage lamda lysozyme." *FEBS Lett.* **1999**, *460*, 442-446.

Appendix I

Sample program for Model 90 Peptide Synthesizer for 1 mmole synthesis, generously supplied by AnaSpec, Inc.. Modifications were tailored according to the experimentally developed peptide synthesis protocol outlined in *Section 2.5.2b. - Automated Synthesis of Templates.*

RV-1 = reaction vessel 1
Mech = mechanical shaker
AA = amino acid

DMF = dimethylformamide
PIP = piperidine
COUP = coupling mixture

1. Fill RV-1 from DMF, 40.00 mL.
2. Mix RV-1 with Mech for 1.0 min.
3. Empty RV-1.

Swelling

- 4.
5. Fill RV-1 from PIP, 50.00 mL.
6. Mix RV-1 with Mech for 10.0 min.
7. Empty RV-1.
8. Fill RV-1 from PIP, 50.00 mL.
9. Mix RV-1 with Mech for 40.0 min.
10. Empty RV-1.

Deprotection

11. Fill RV-1 with DMF, 50.00 mL.
12. Mix RV-1 with Mech for 1.5 min.
13. Empty RV-1.
14. Repeat from step 11, 4 times.
15. Stop.

Wash

- 16.
17. Fill RV-1 from AA-1, 25.0 mL.
18. Fill RV-1 from COUP, 15.0 mL.
19. Mix RV-1 with Mech for 60.0 min.
20. Empty RV-1.

Coupling

21. Fill RV-1 from DMF, 50.0 mL.
22. Mix RV-1 with Mech for 1.5 min.
23. Empty RV-1.
24. Repeat from step 21, 4 times.
25. Stop.

Wash

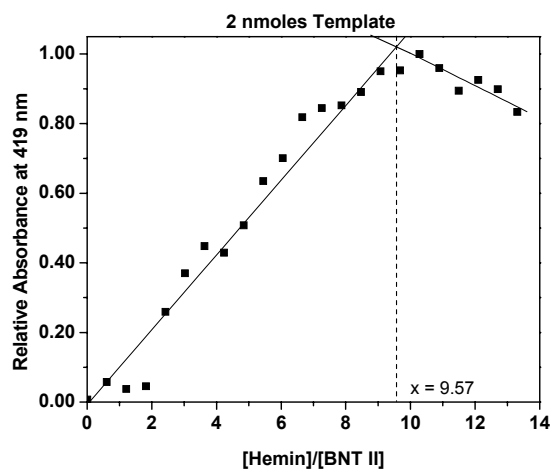
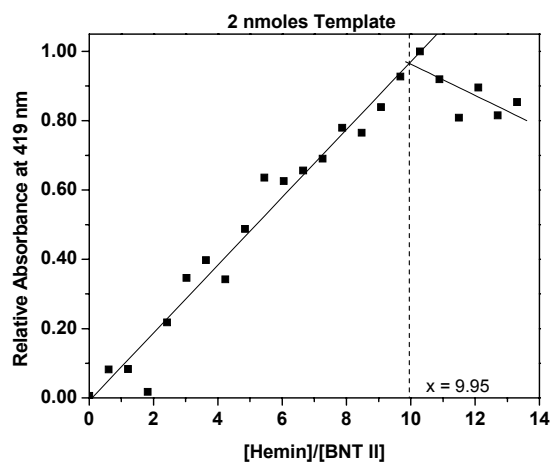
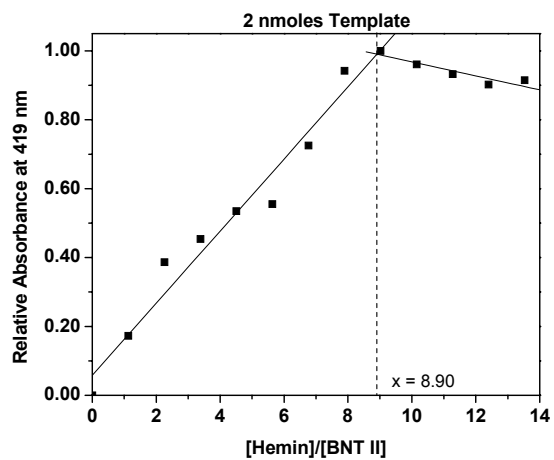
- 26.
27. Fill RV-1 from PIP, 50.0 mL.
28. Mix RV-1 with Mech for 10.0 min.
29. Empty RV-1.
30. Fill RV-1 from PIP, 50.0 mL.

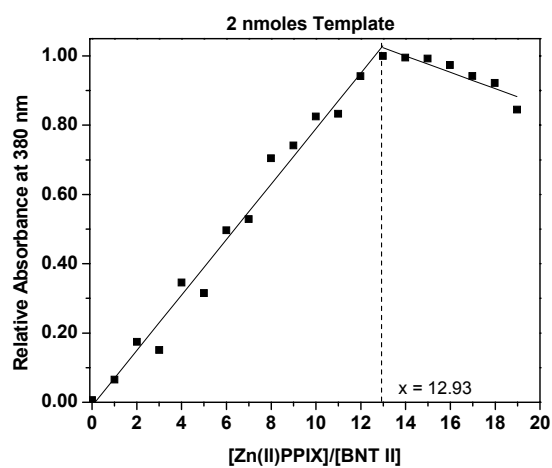
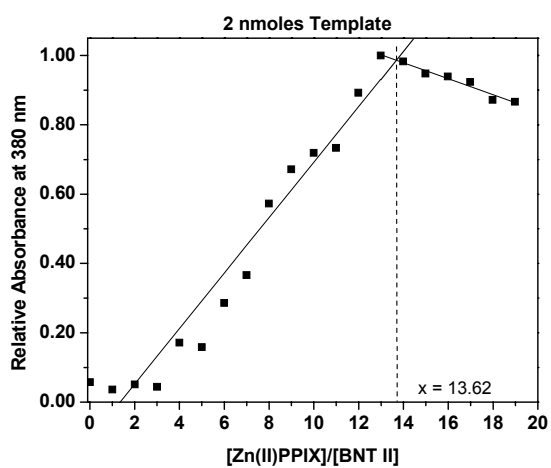
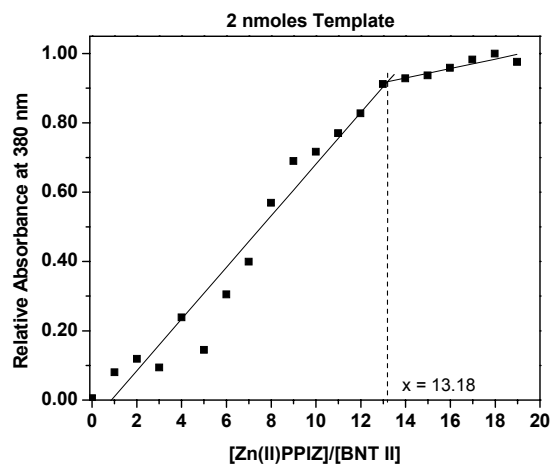
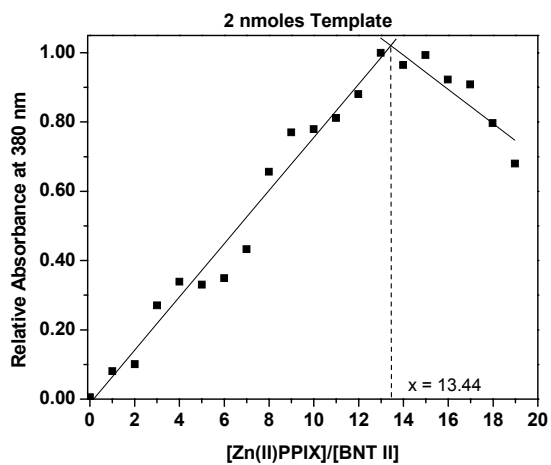
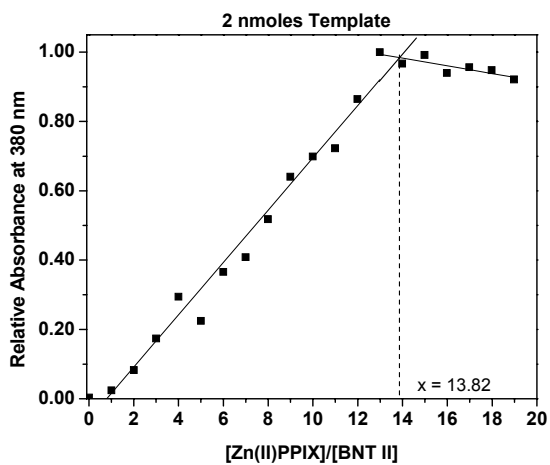
31. Mix RV-1 from Mech for 40.0 min.
32. Empty RV-1.
33. Fill RV-1 from DMF, 50.0 mL.
34. Mix RV-1 with Mech for 1.5 min.
35. Empty RV-1.
36. Repeat from step 33, 4 times.
37. Stop.
- 38.
39. Fill RV-1 from AA-2, 25.0 mL.
40. Fill RV-1 from COUP, 15.0 mL.
41. Mix RV-1 with Mech for 60.0 min.
42. Empty RV-1.
43. Fill RV-1 from DMF, 50.0 mL.
44. Mix RV-1 with Mech for 1.5 min.
45. Empty RV-1.
46. Repeat from step 43, 4 times.
47. Stop.
- 48.
49. Fill RV-1 from PIP, 50.0 mL.
50. Mix RV-1 with Mech for 10.0 min.
51. Empty RV-1.
52. Fill RV-1 from PIP, 50.0 mL.
53. Mix RV-1 from Mech for 40.0 min.
54. Empty RV-1.
55. Fill RV-1 from DMF, 50.0 mL.
56. Mix RV-1 with Mech for 1.5 min.
57. Empty RV-1.
58. Repeat from step 55, 4 times.
59. Stop.
- 60.
61. Fill RV-1 from AA-3, 25.0 mL.
62. Fill RV-1 from COUP, 15.0 mL.
63. Mix RV-1 with Mech for 60.0 min.
64. Empty RV-1.
65. Fill RV-1 from DMF, 50.0 mL.
66. Mix RV-1 with Mech for 1.5 min.
67. Empty RV-1.
68. Repeat from step 65, 4 times.
69. Stop.
- 70.
71. Fill RV-1 from PIP, 50.0 mL.
72. Mix RV-1 with Mech for 10.0 min.
73. Empty RV-1.

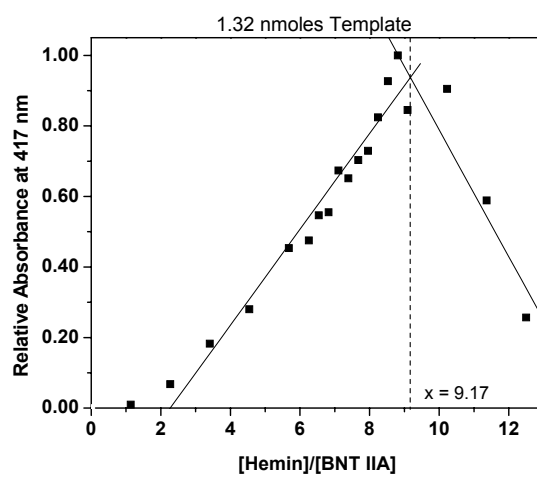
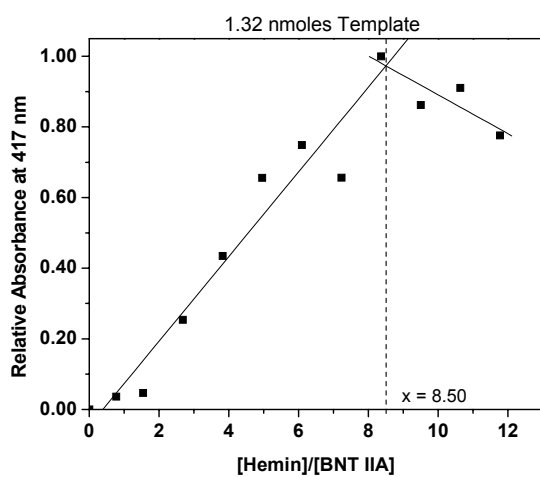
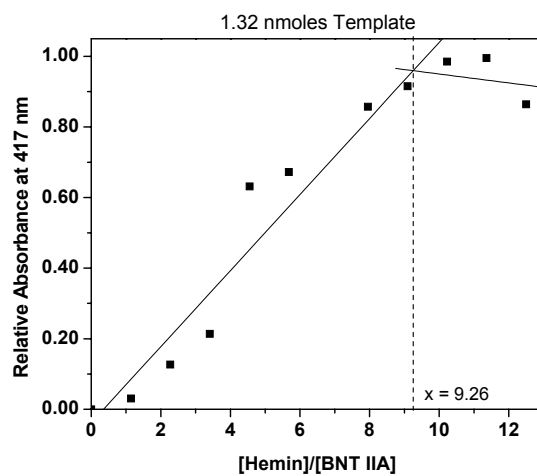
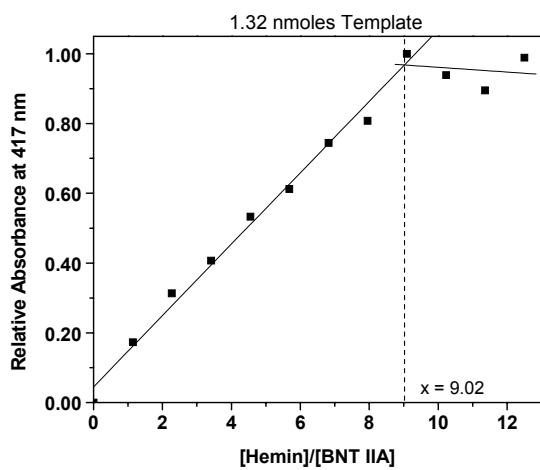
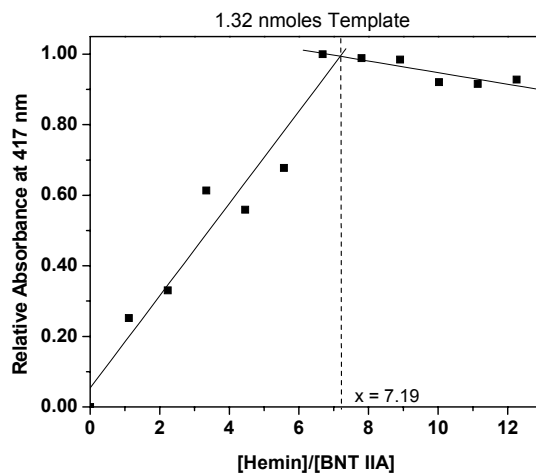
74. Fill RV-1 from PIP, 50.0 mL.
75. Mix RV-1 from Mech for 40.0 min.
76. Empty RV-1.
77. Fill RV-1 from DMF, 50.0 mL.
78. Mix RV-1 with Mech for 1.5 min.
79. Empty RV-1.
80. Repeat from step 77, 4 times.
81. Stop.
- 82.
83. Fill RV-1 from AA-4, 25.0 mL.
84. Fill RV-1 from COUP, 15.0 mL.
85. Mix RV-1 with Mech for 60.0 min.
86. Empty RV-1.
87. Fill RV-1 from DMF, 50.0 mL.
88. Mix RV-1 with Mech for 1.5 min.
89. Empty RV-1.
90. Repeat from step 87, 4 times.
91. Stop.
- 92.

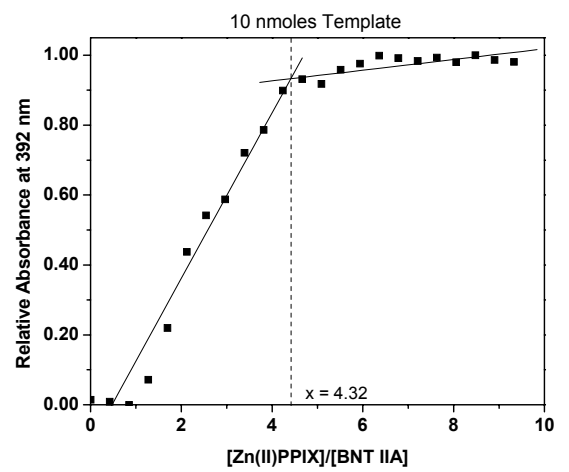
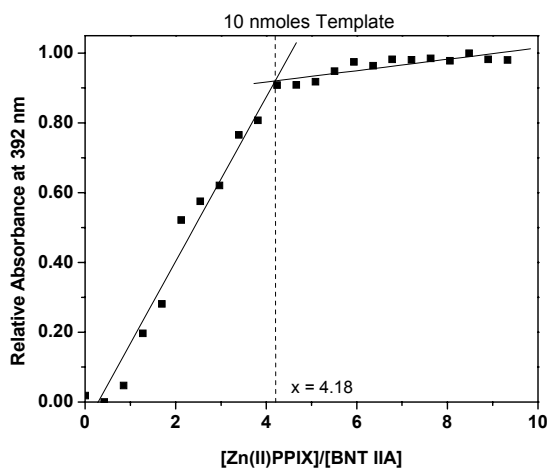
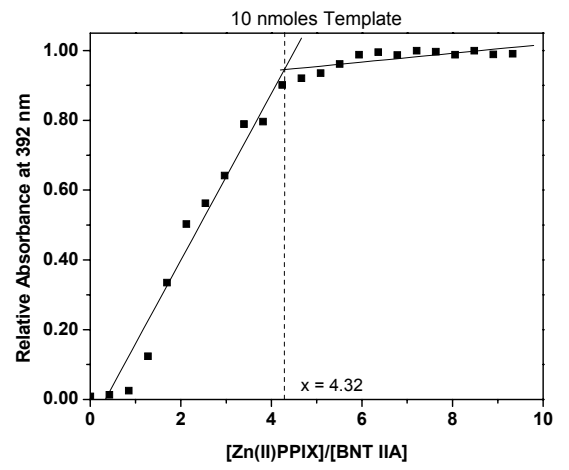
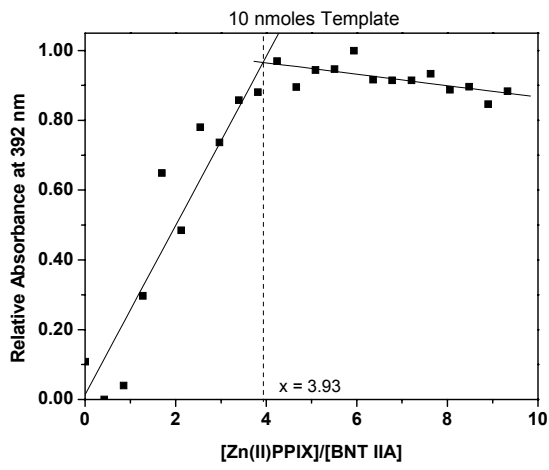
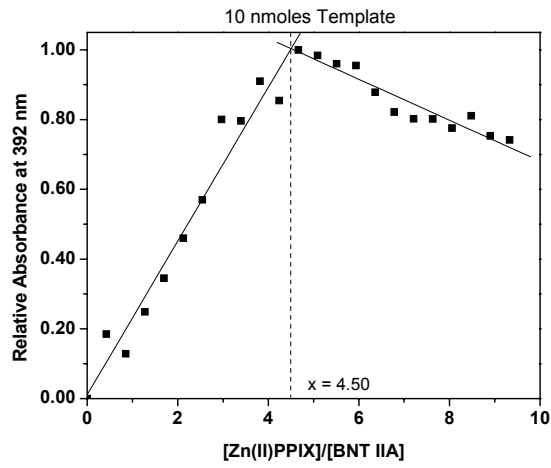
Appendix II

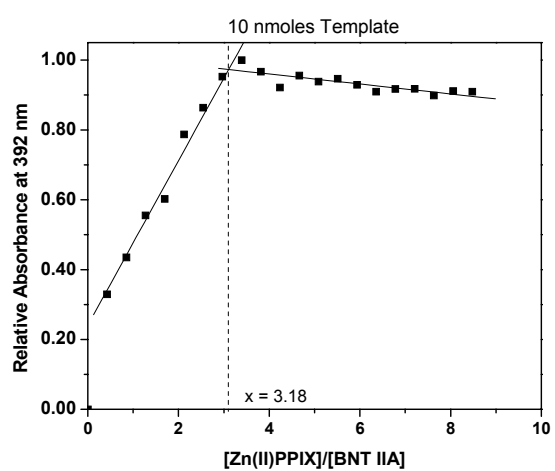
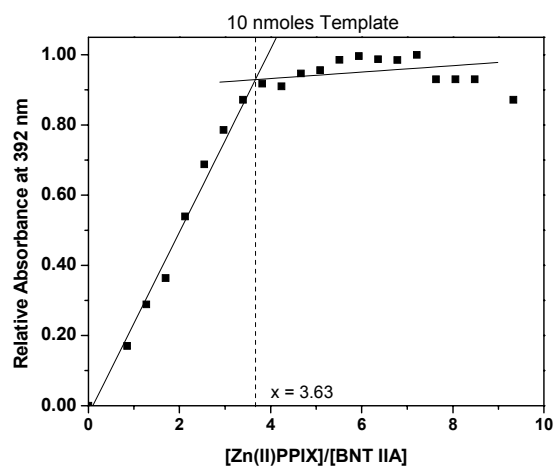
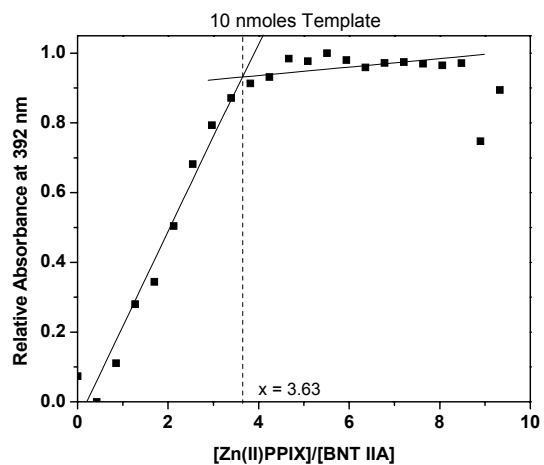
Titration Binding Curves

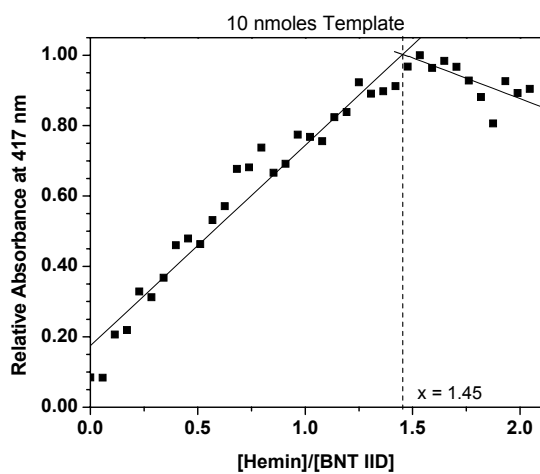
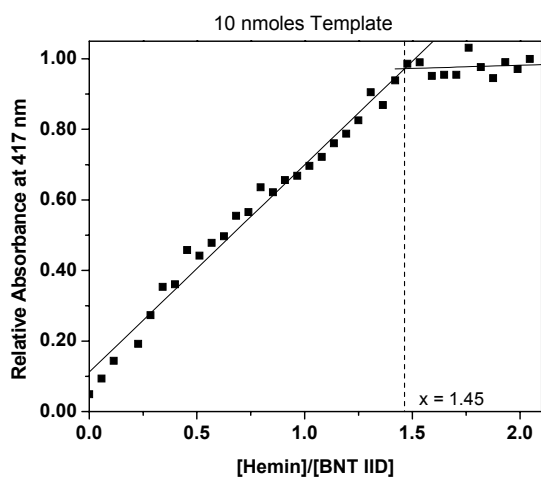
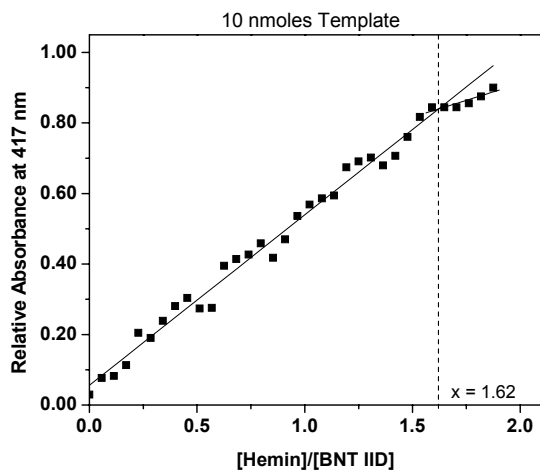
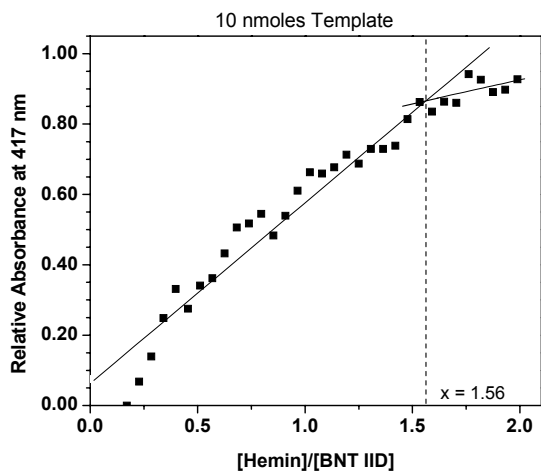
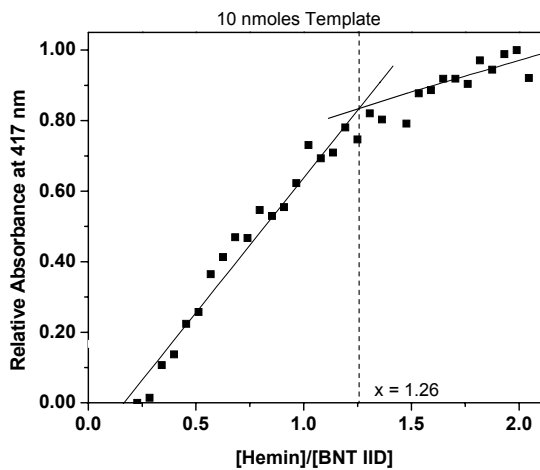


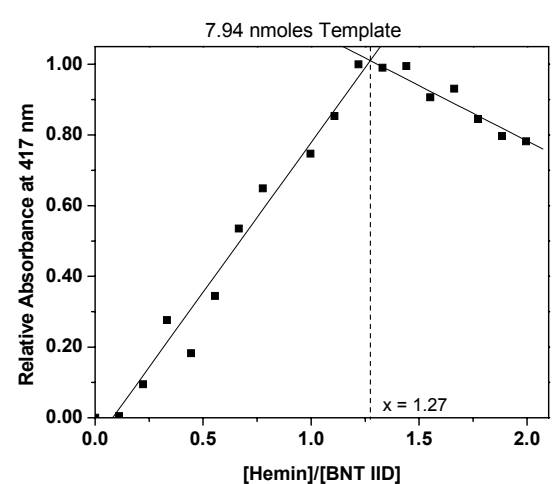
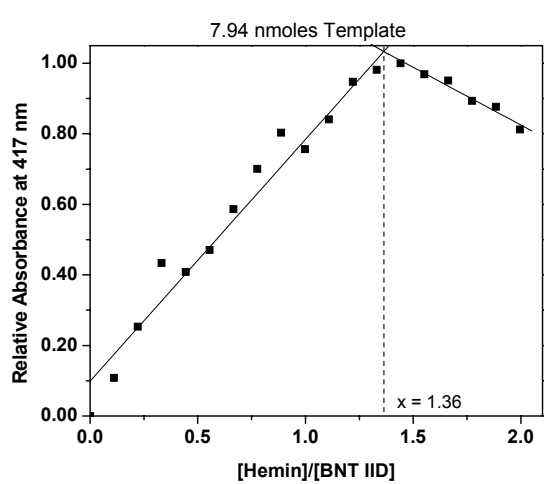
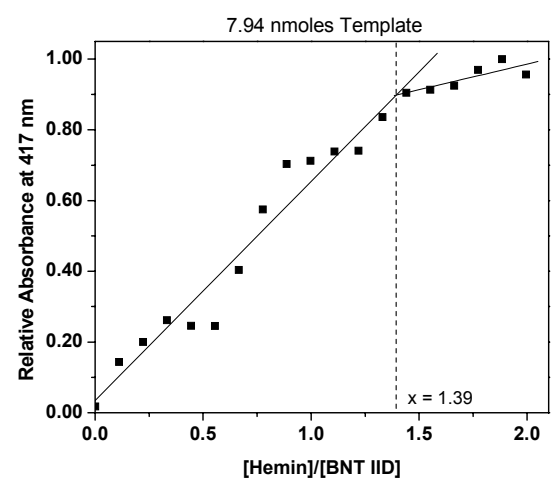
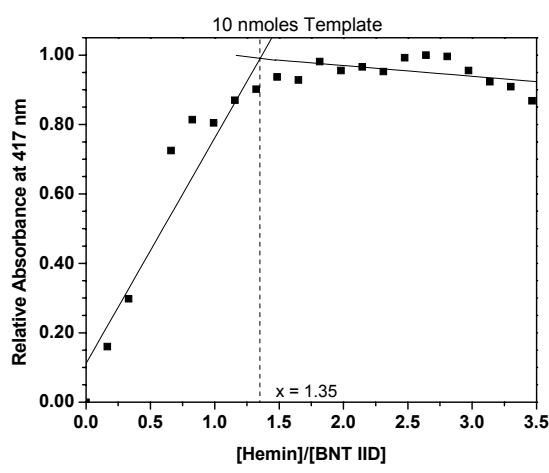
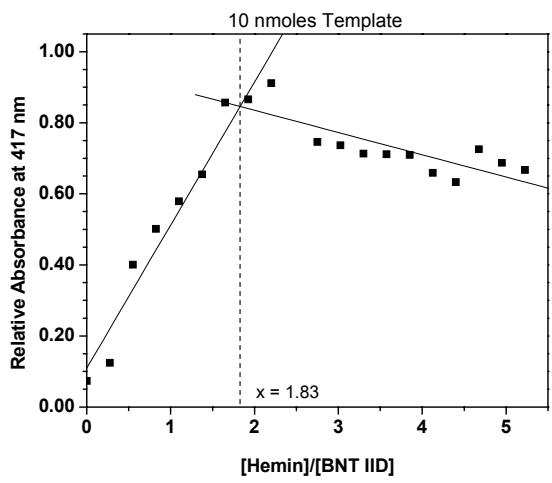


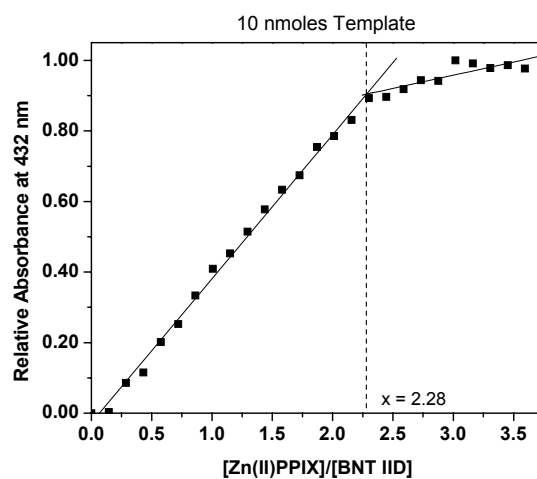
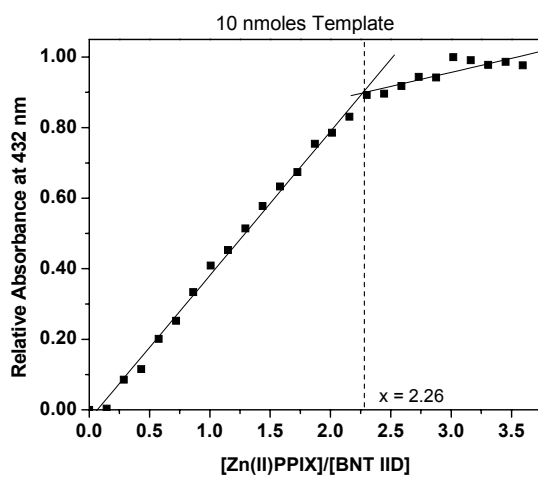
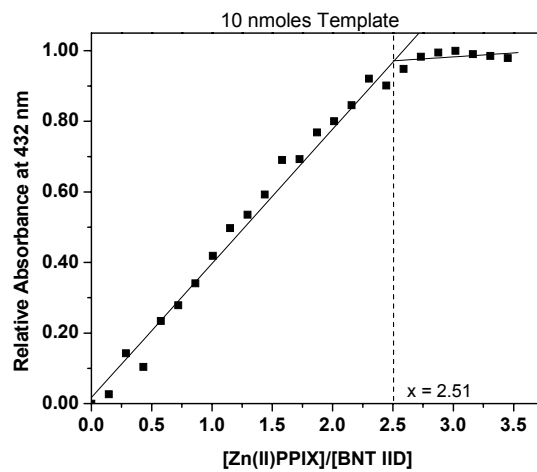
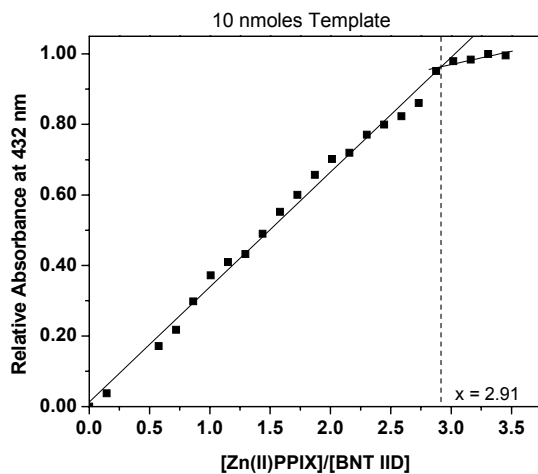
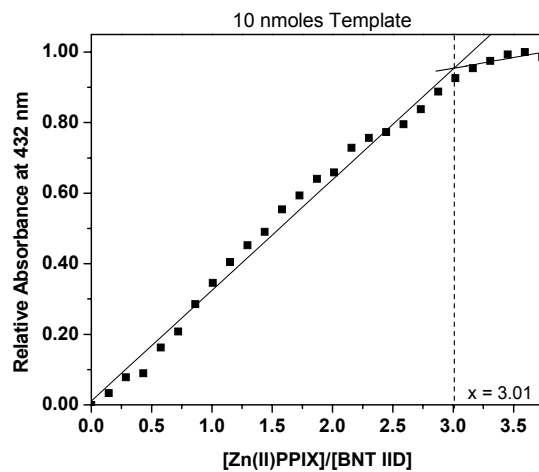


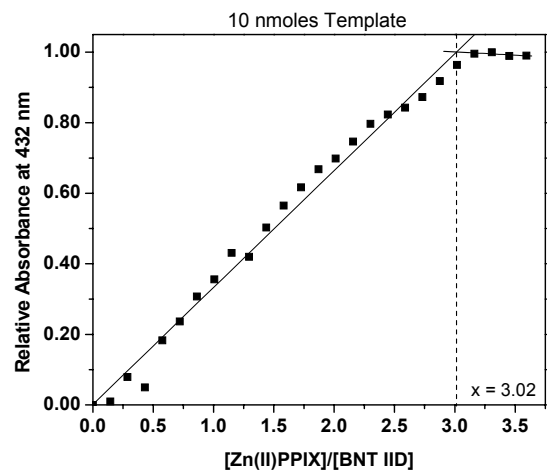
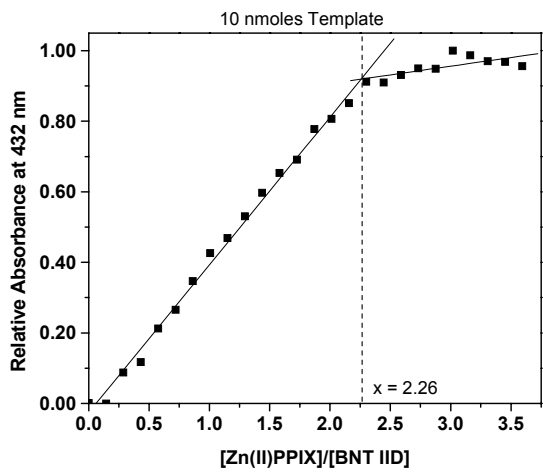
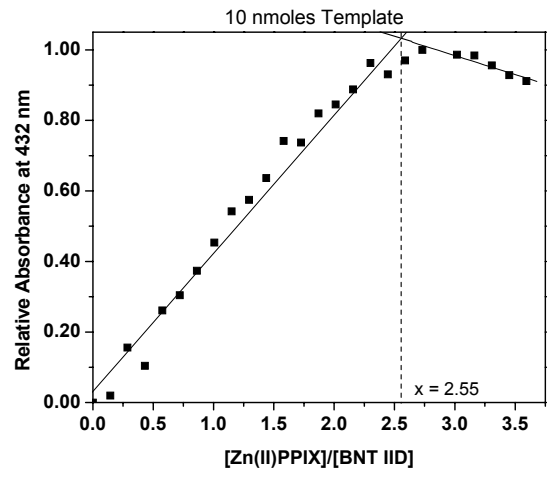
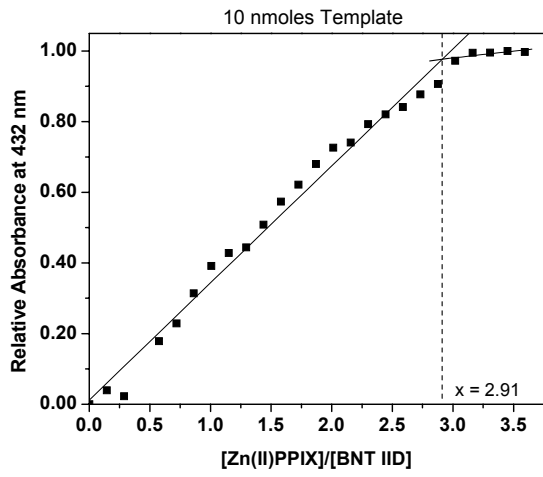
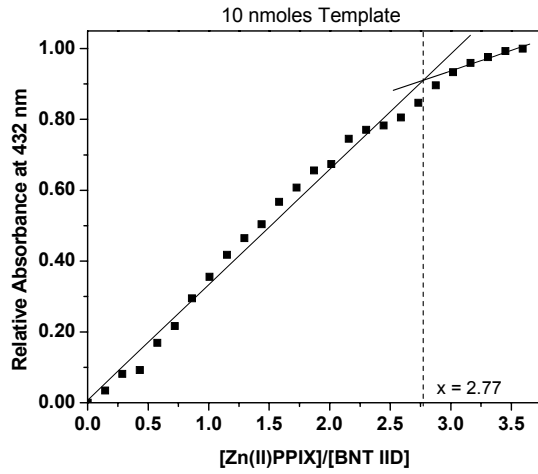


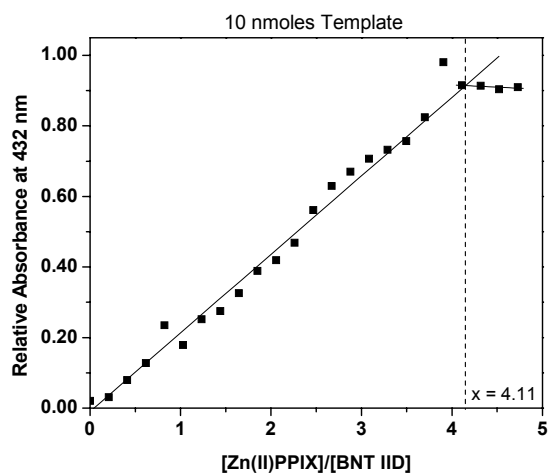
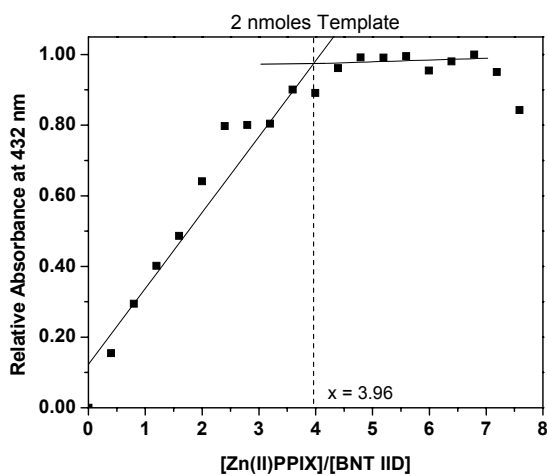
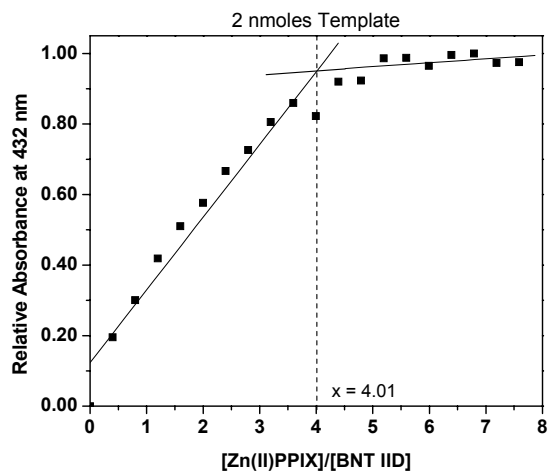
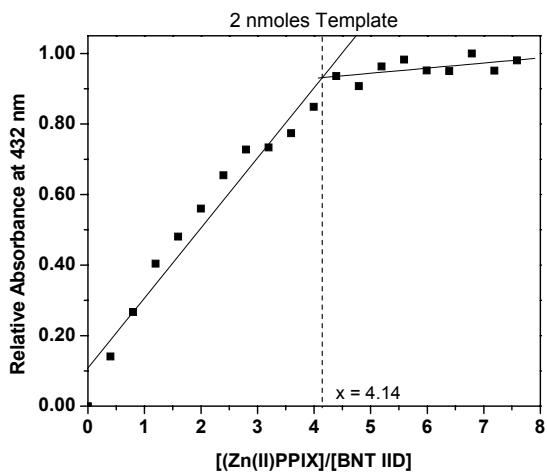
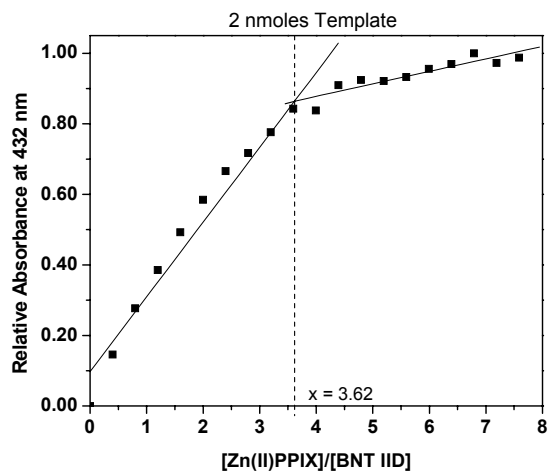
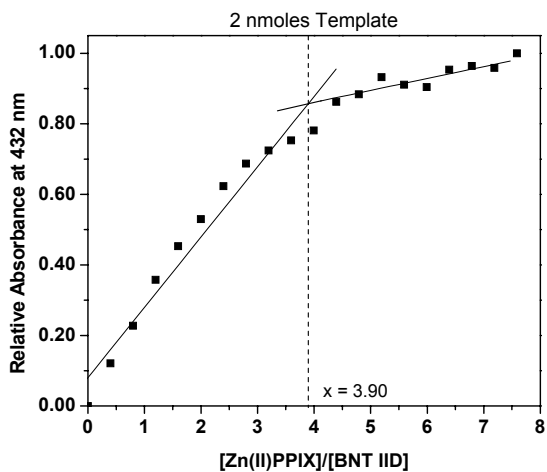


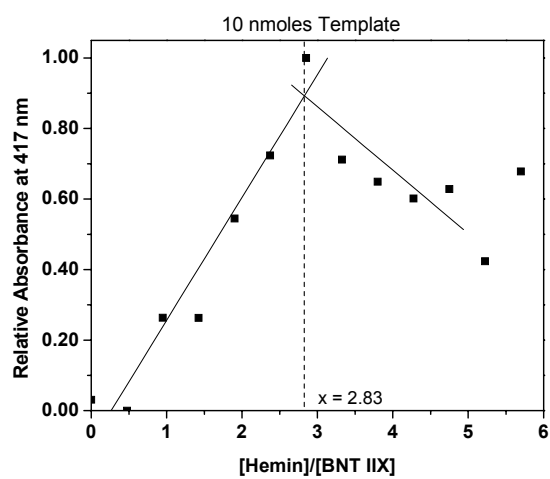
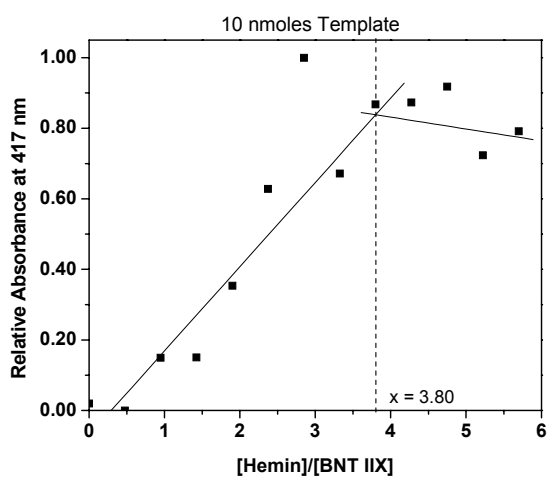
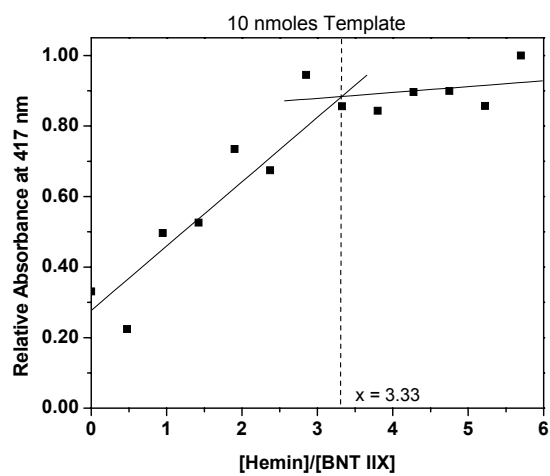
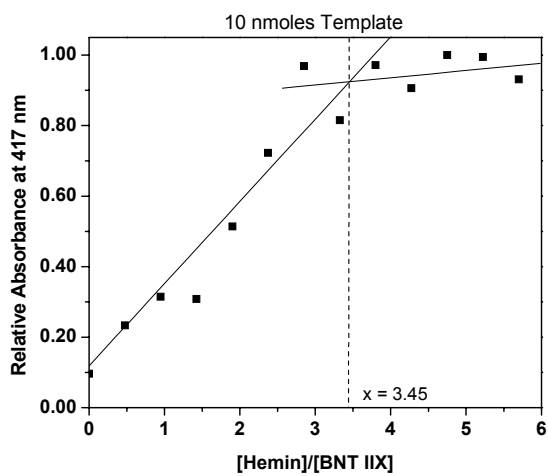
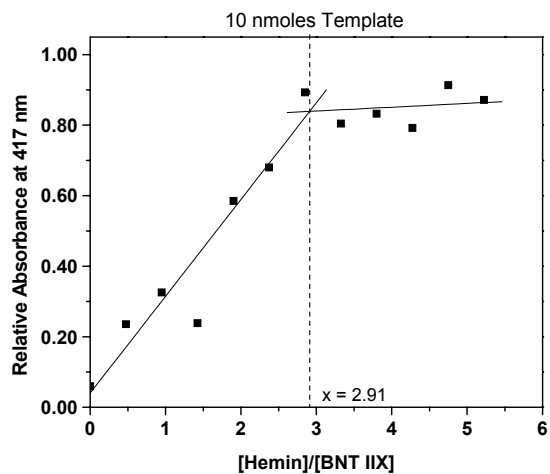


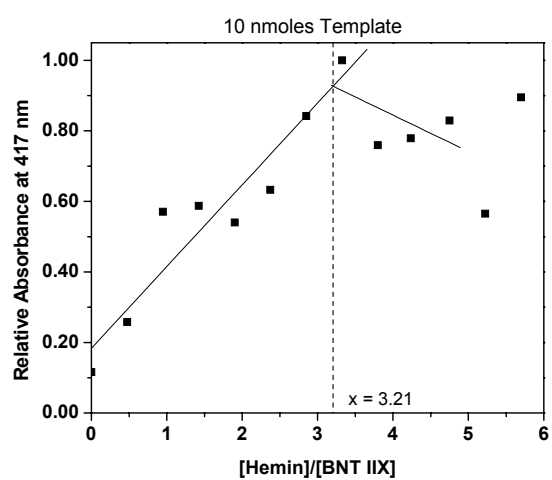
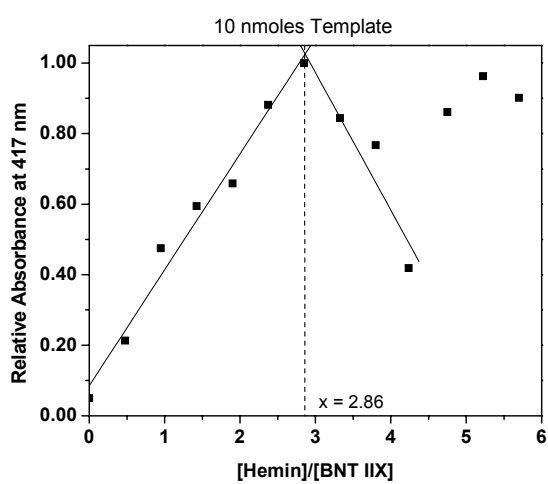
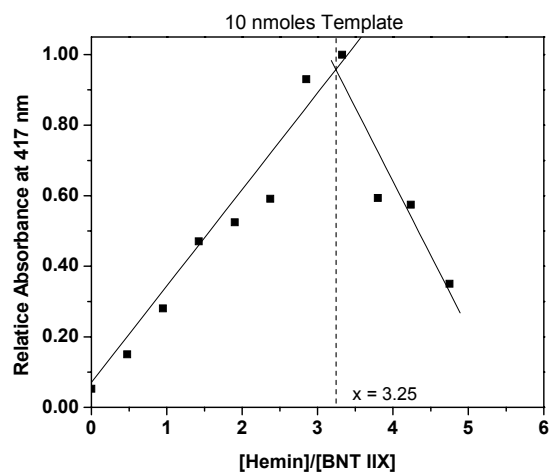
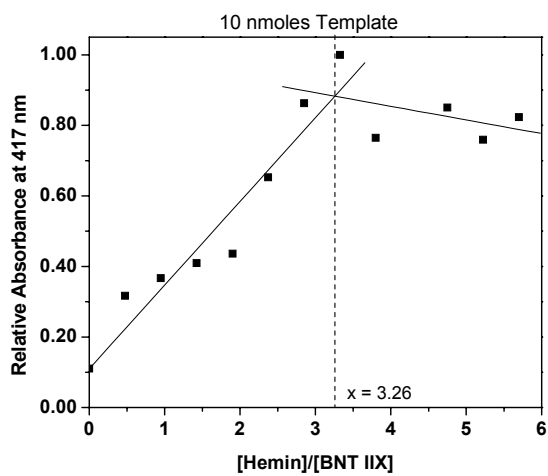
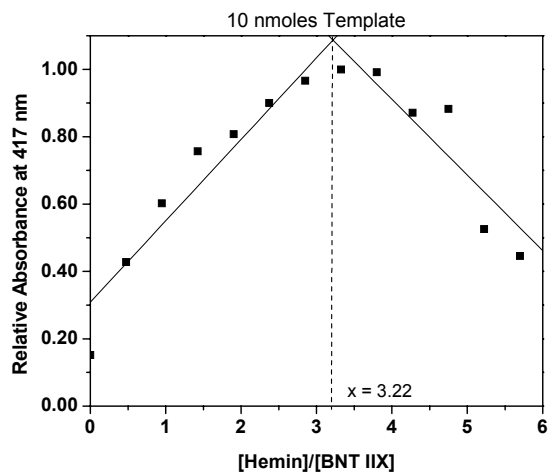


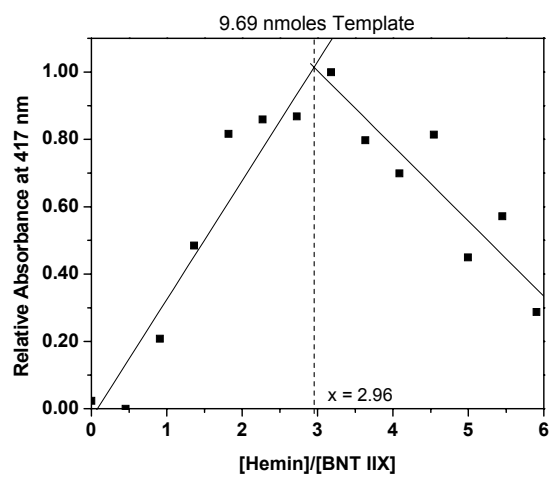
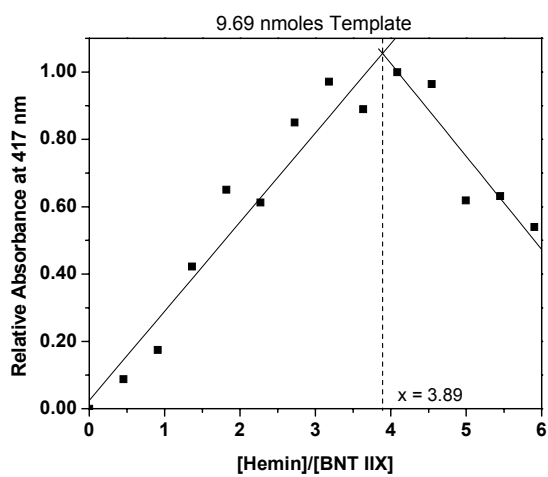
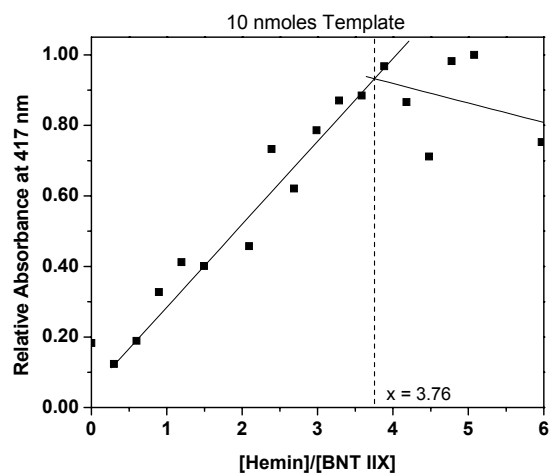
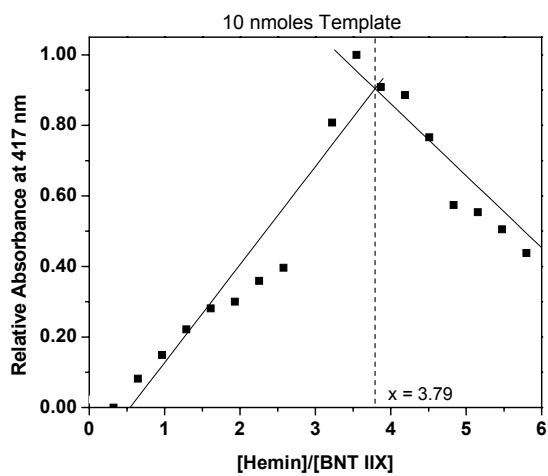
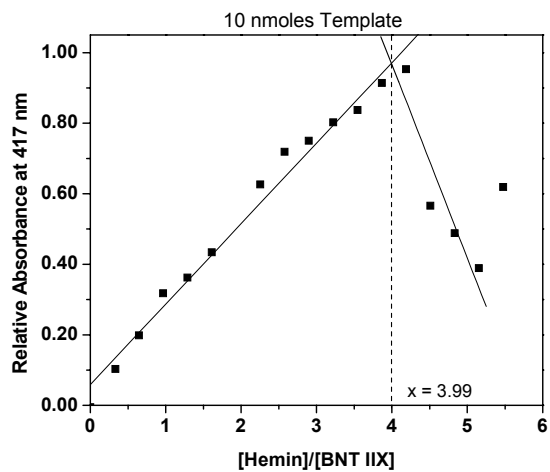


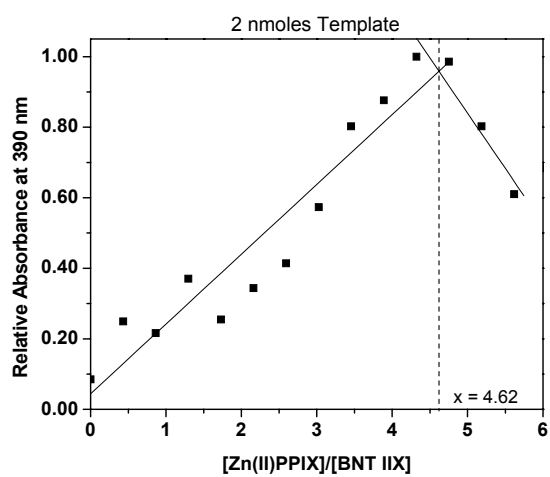
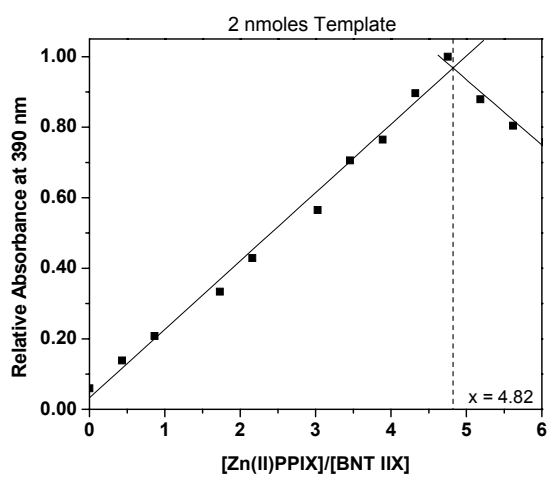
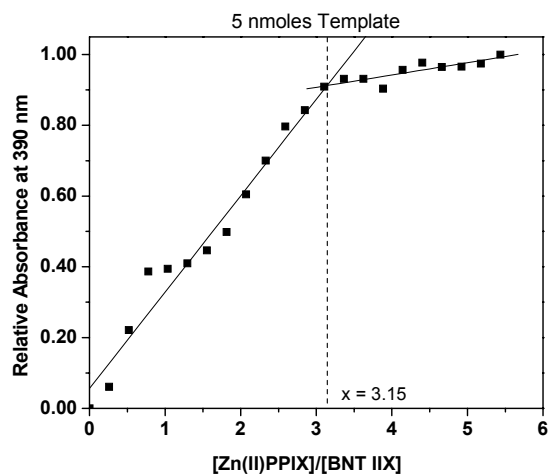
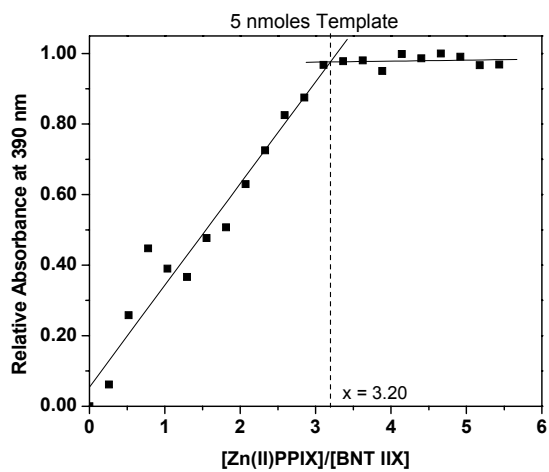
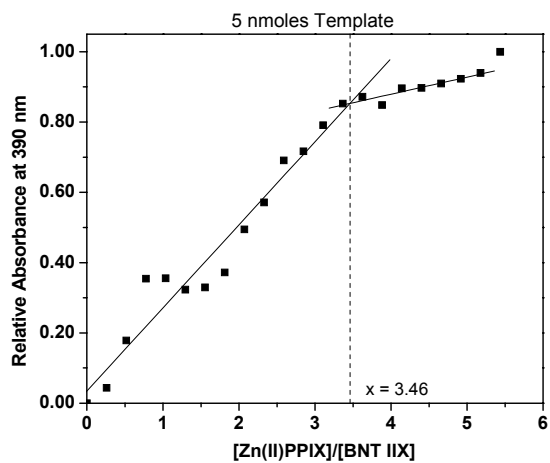


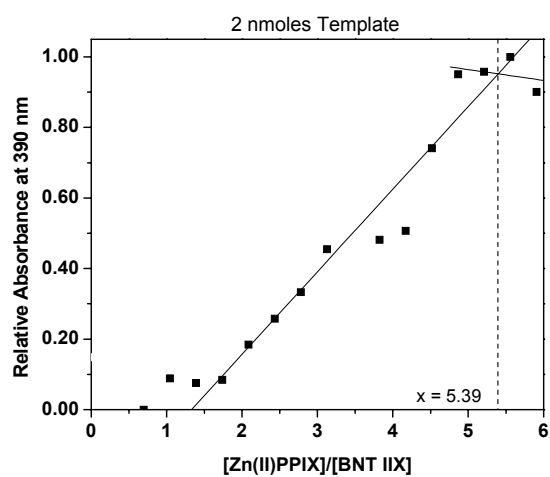
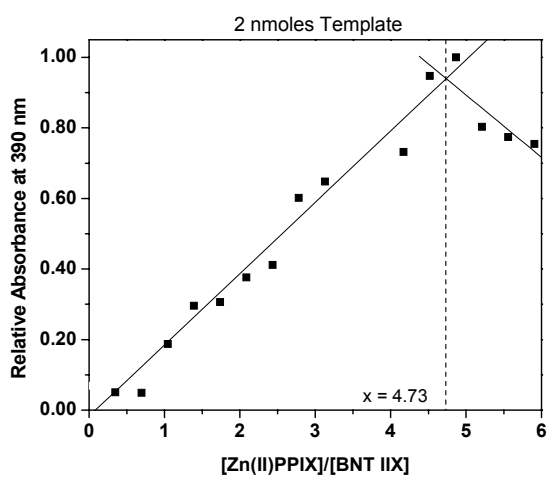
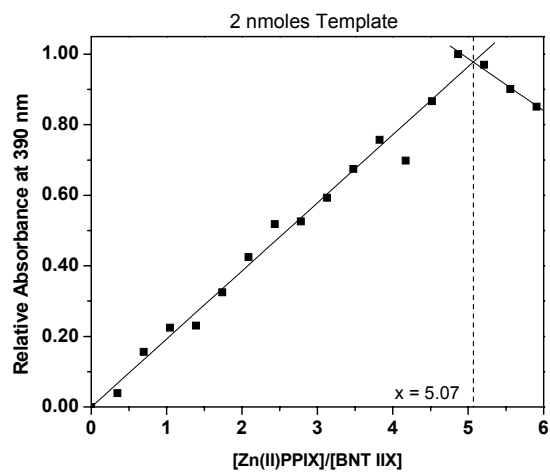
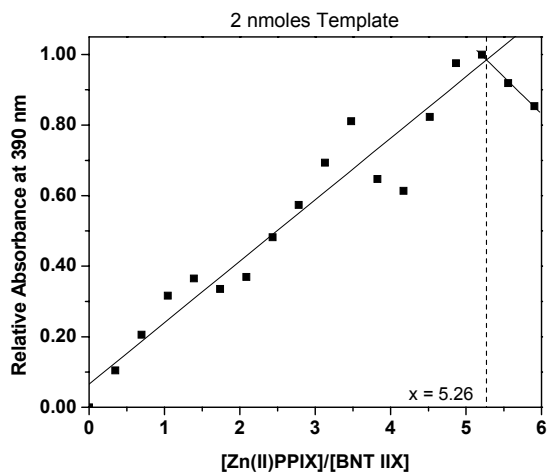
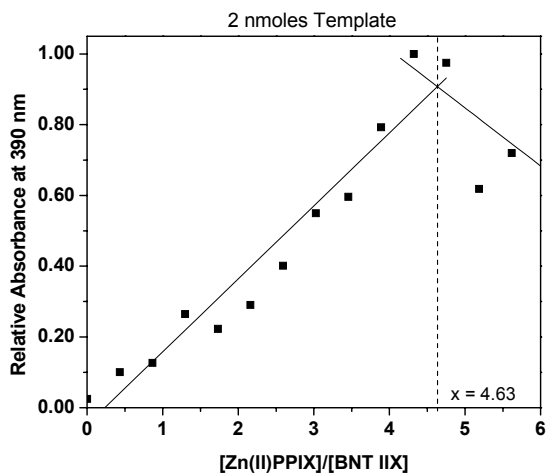


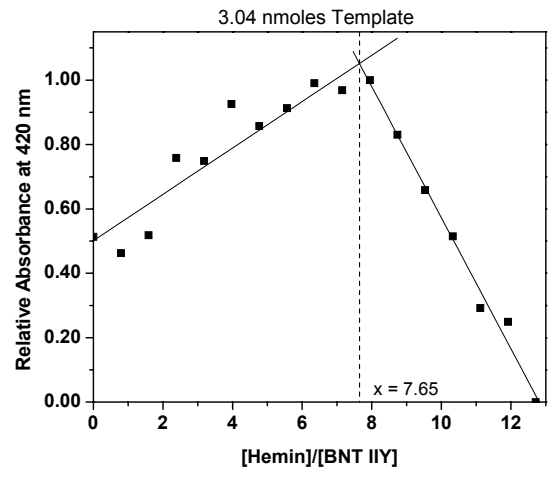
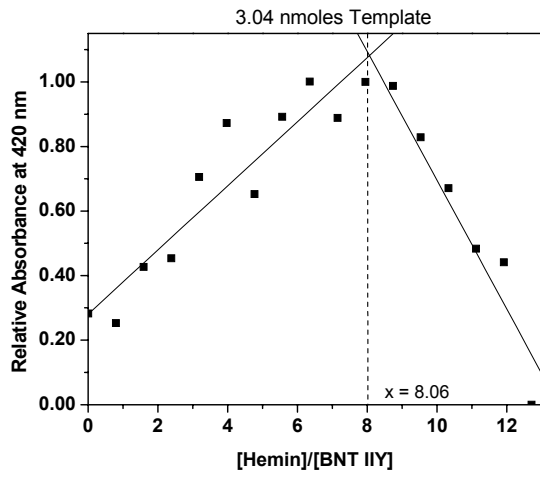
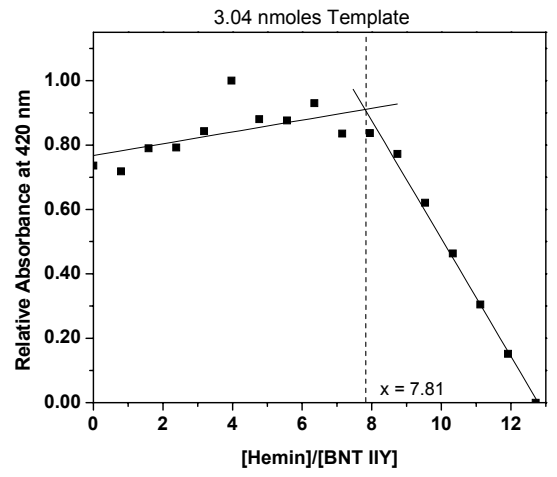
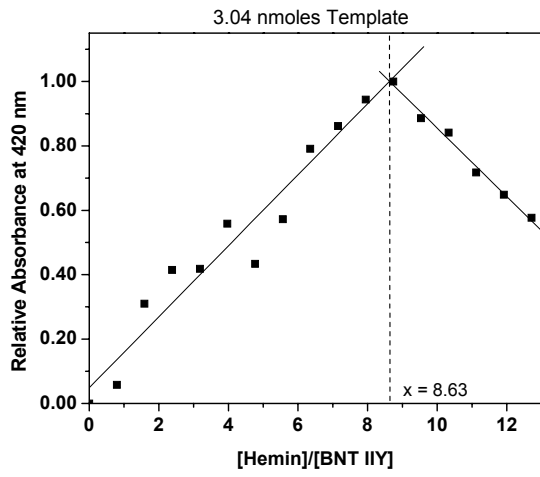


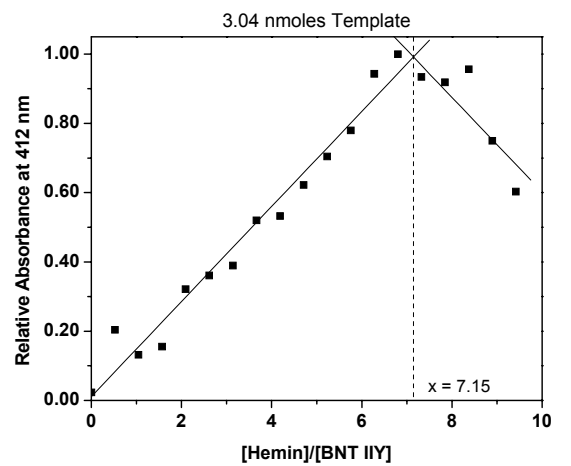
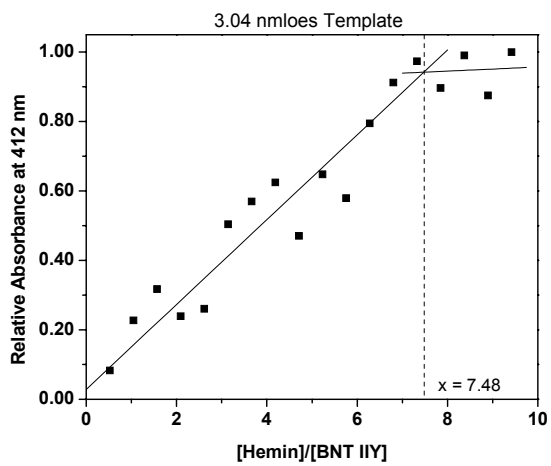
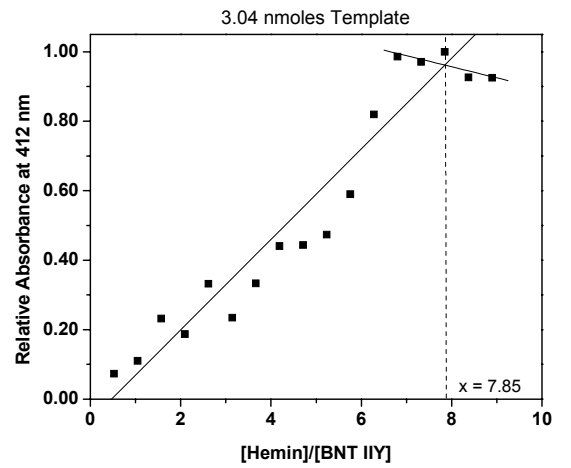
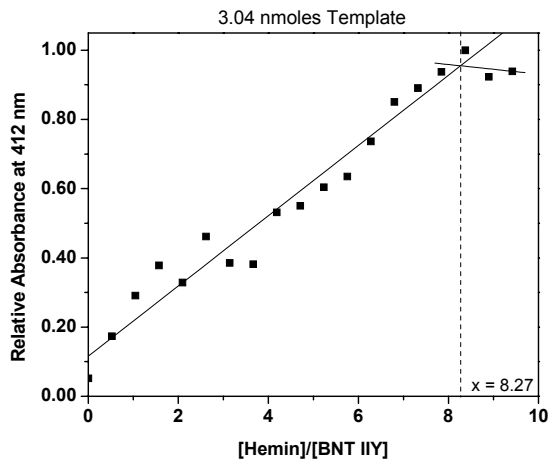
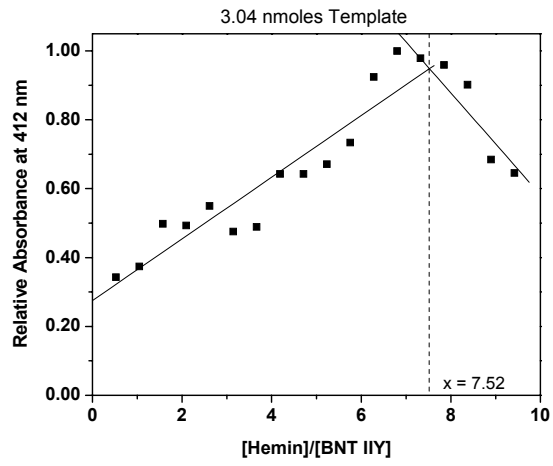


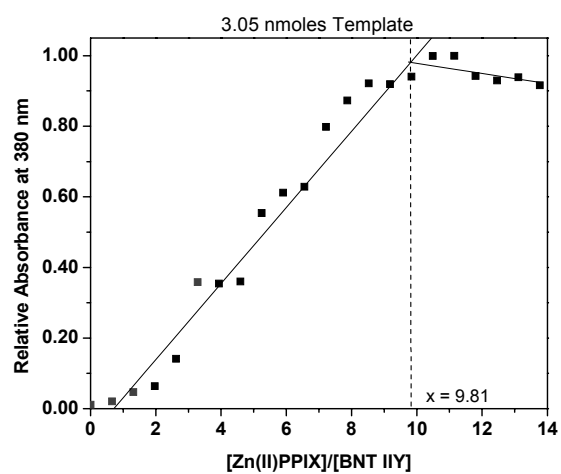
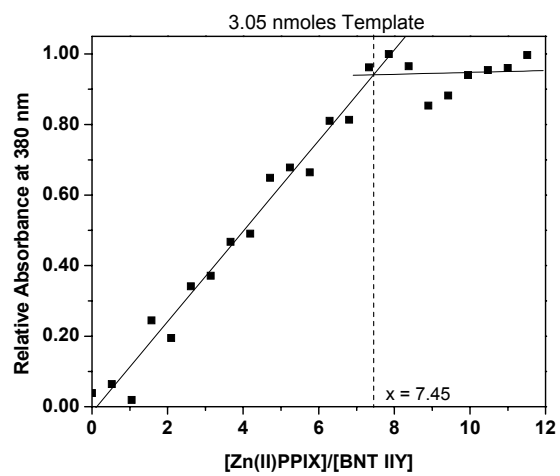
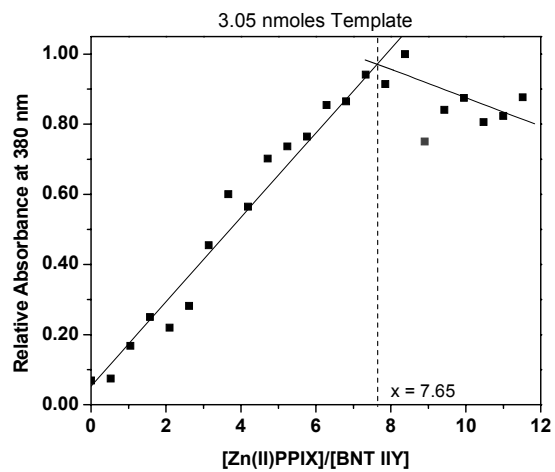


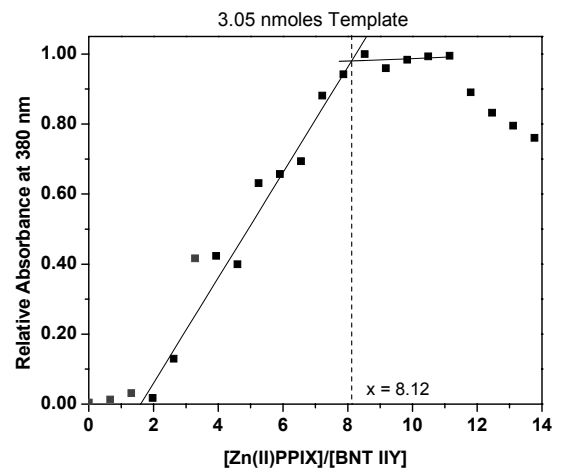
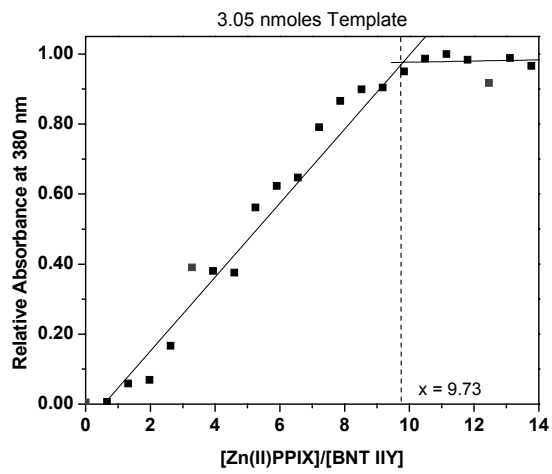
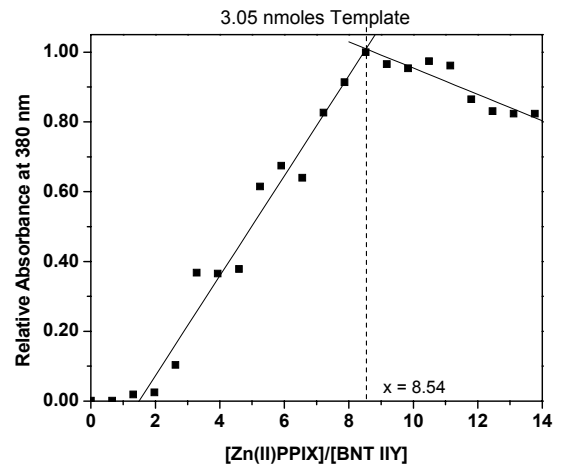
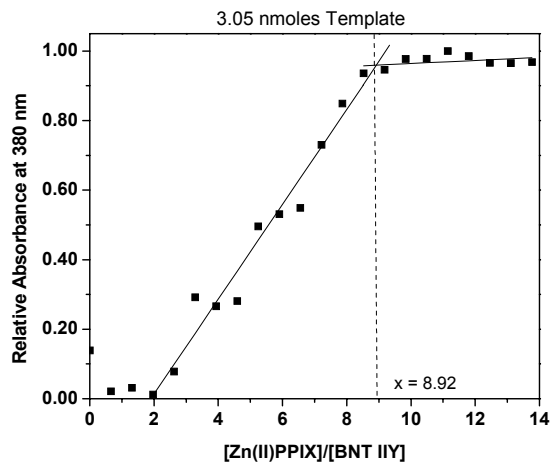


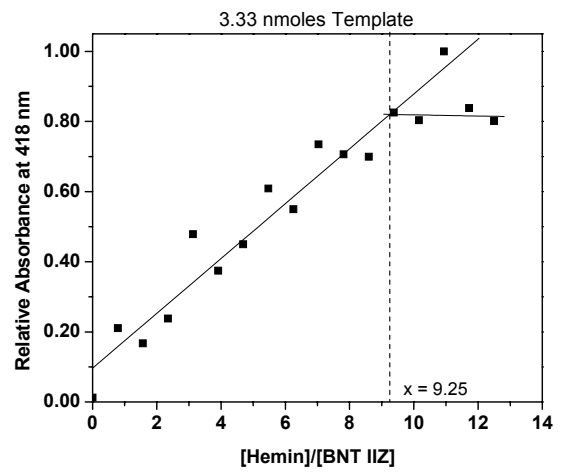
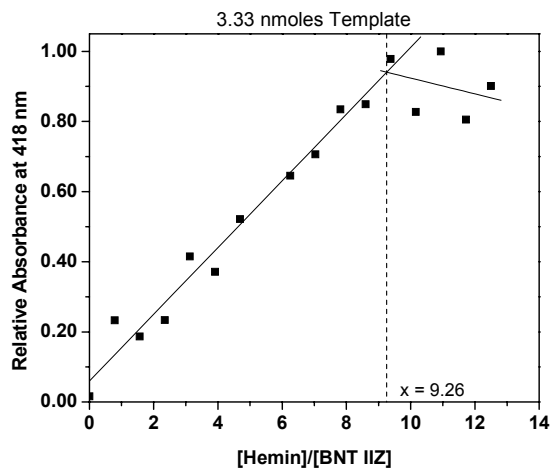
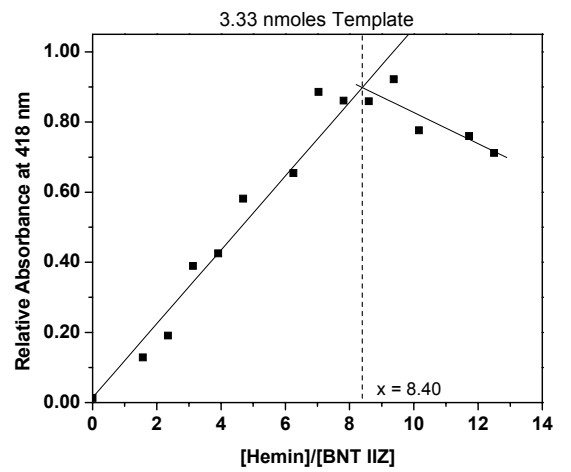
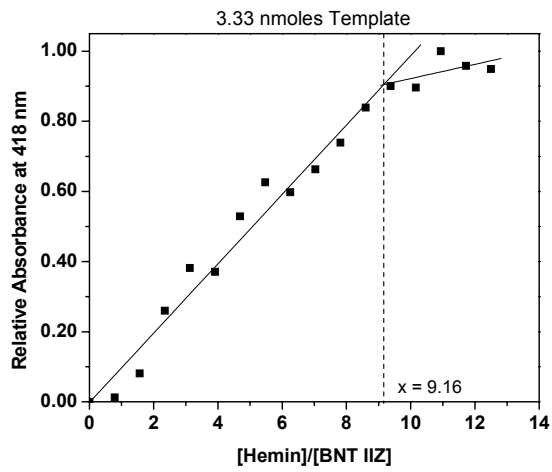


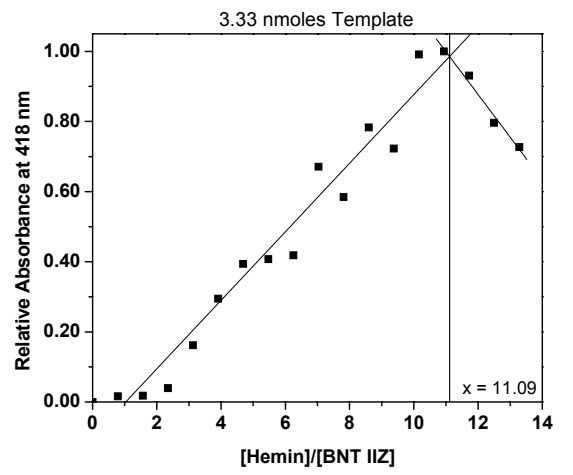
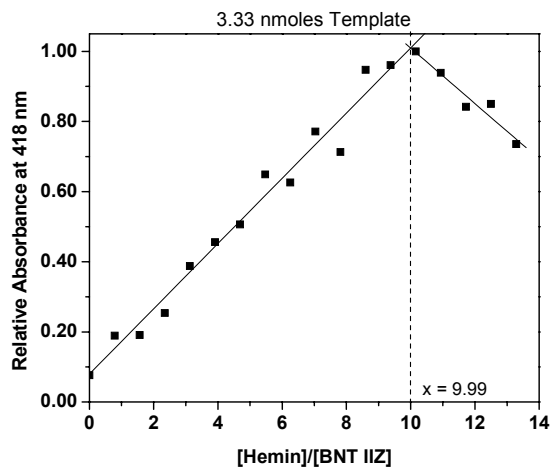
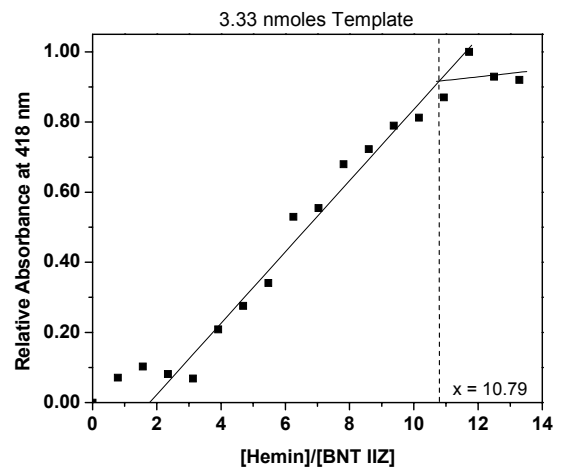
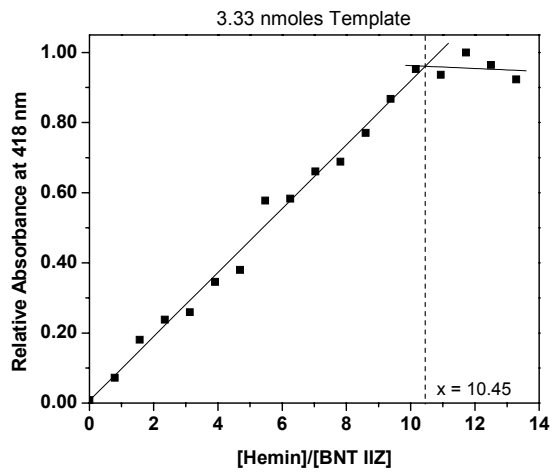


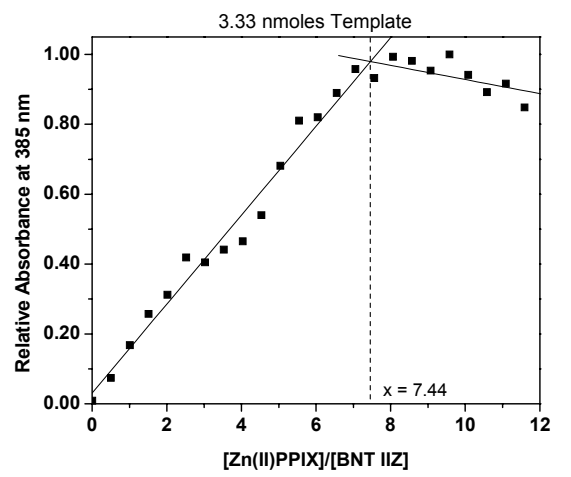
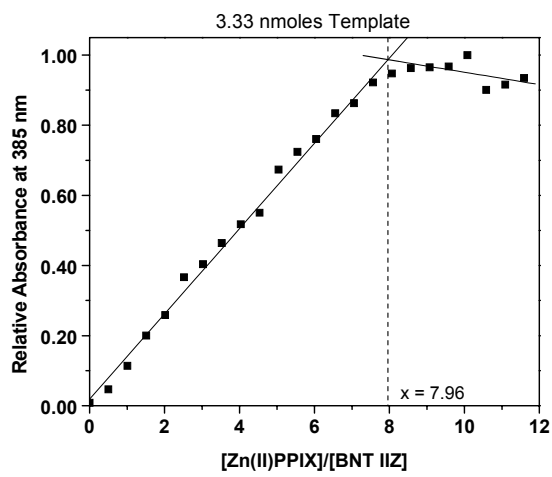
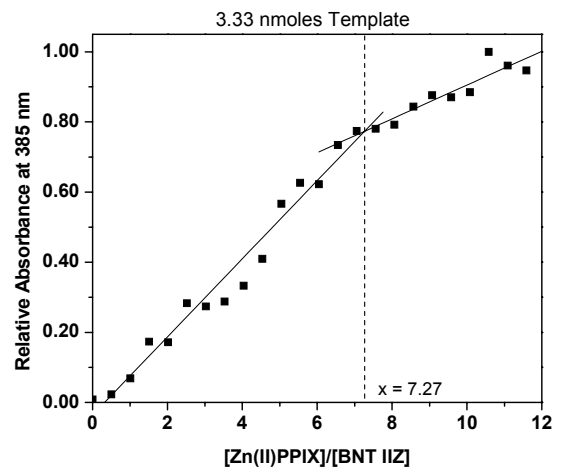
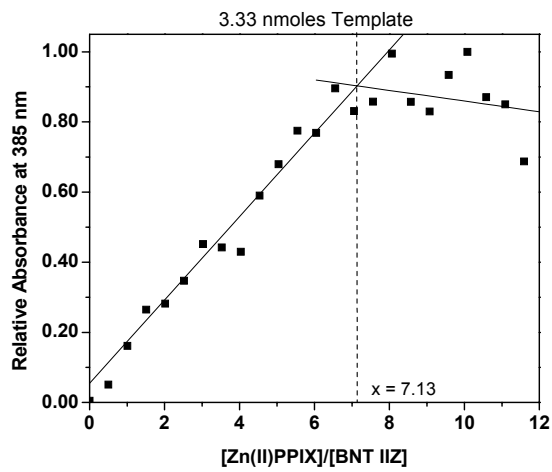


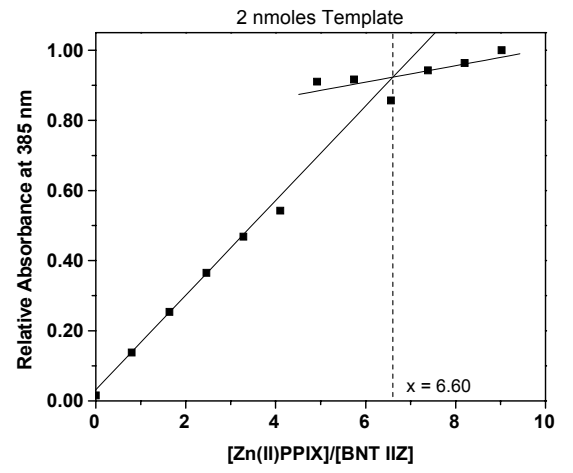
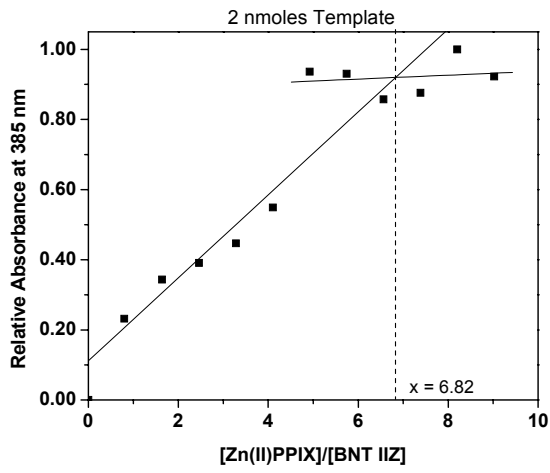
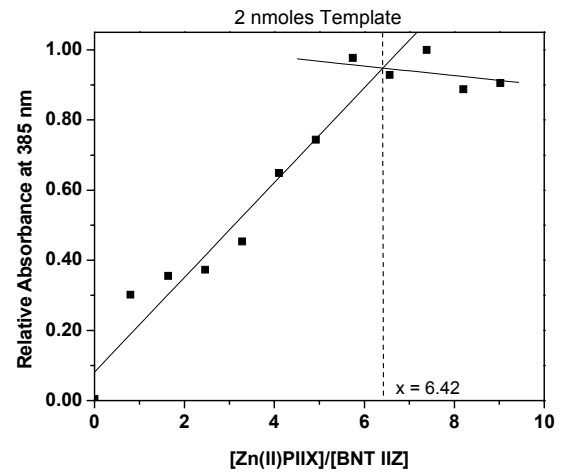
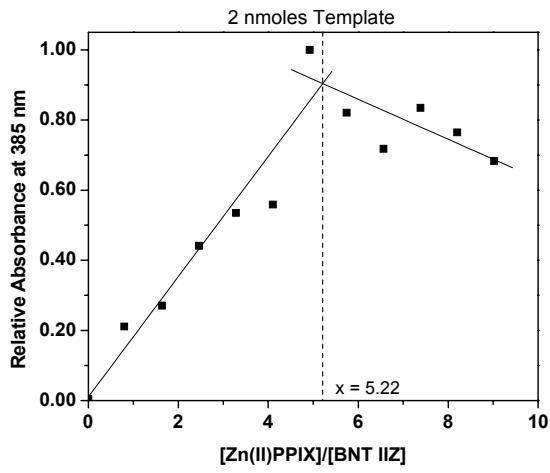


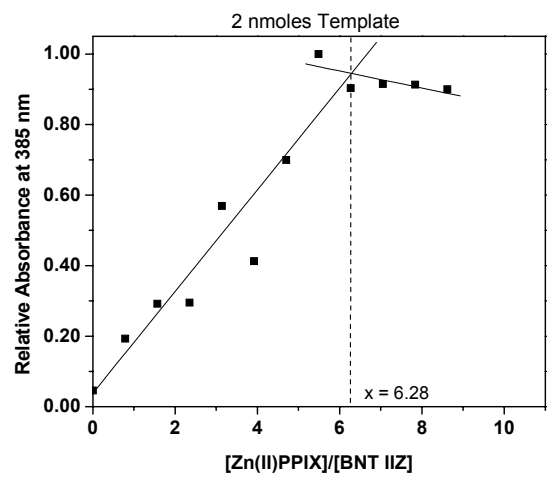
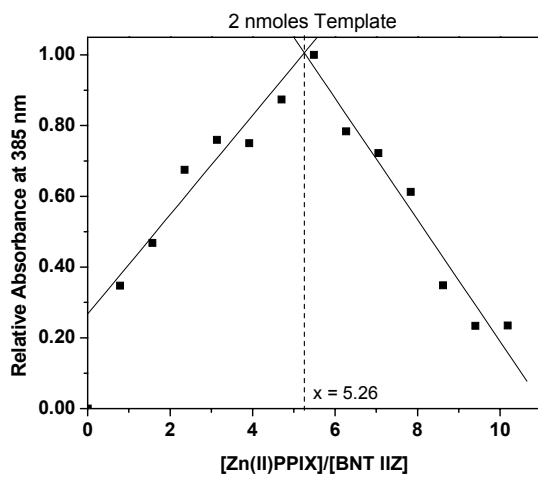
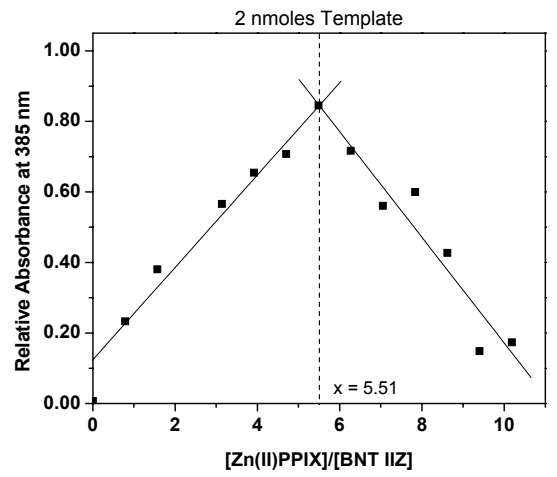
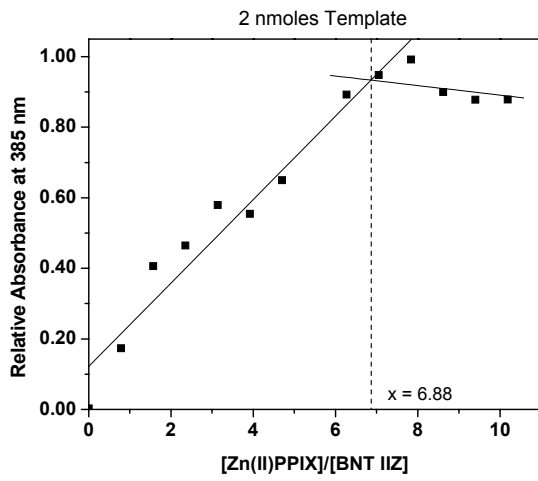
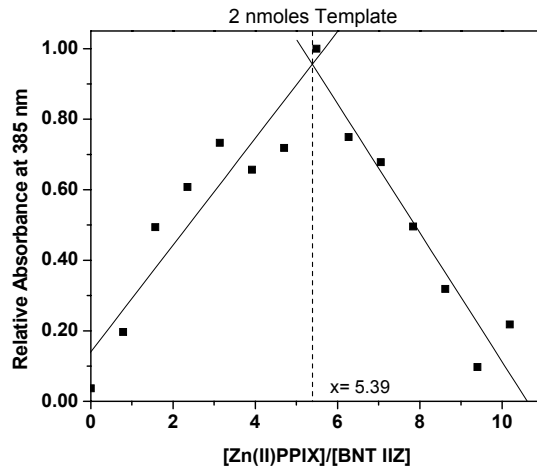






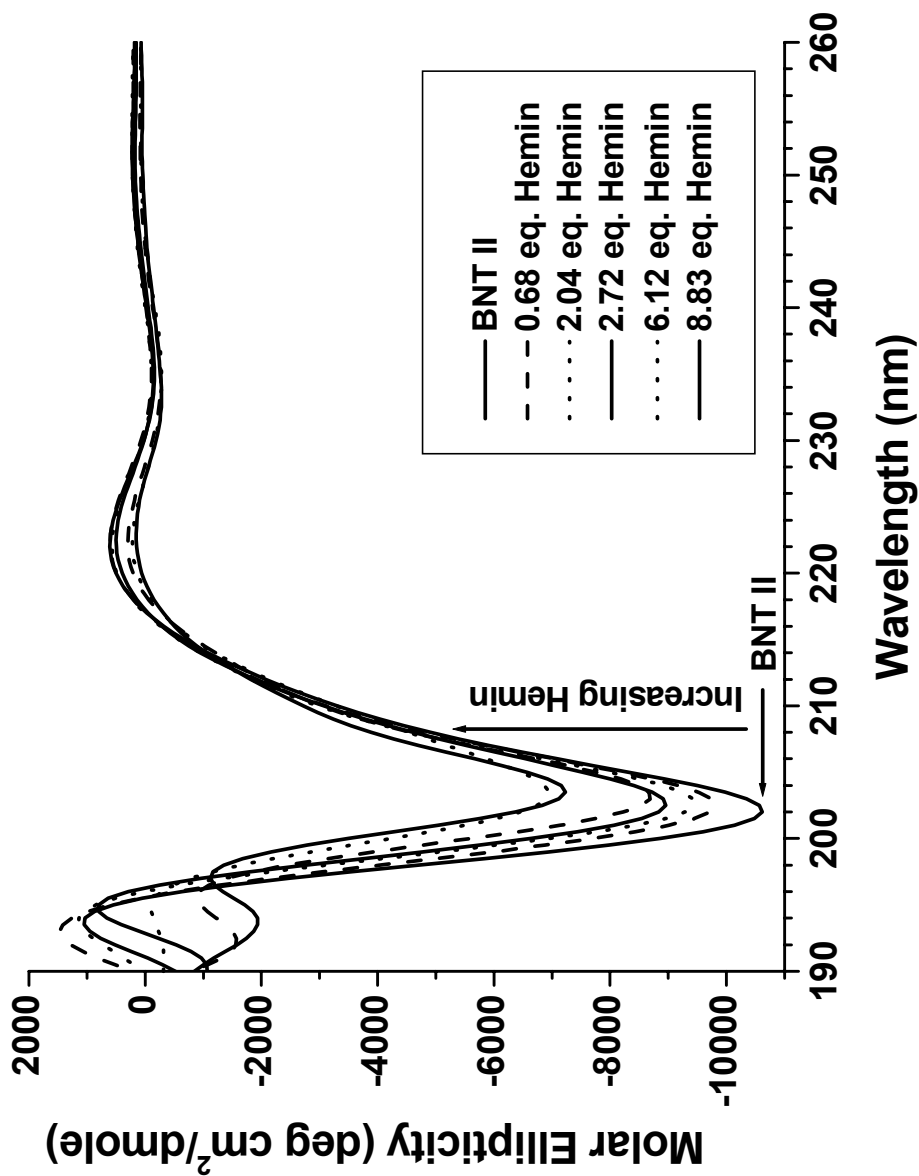




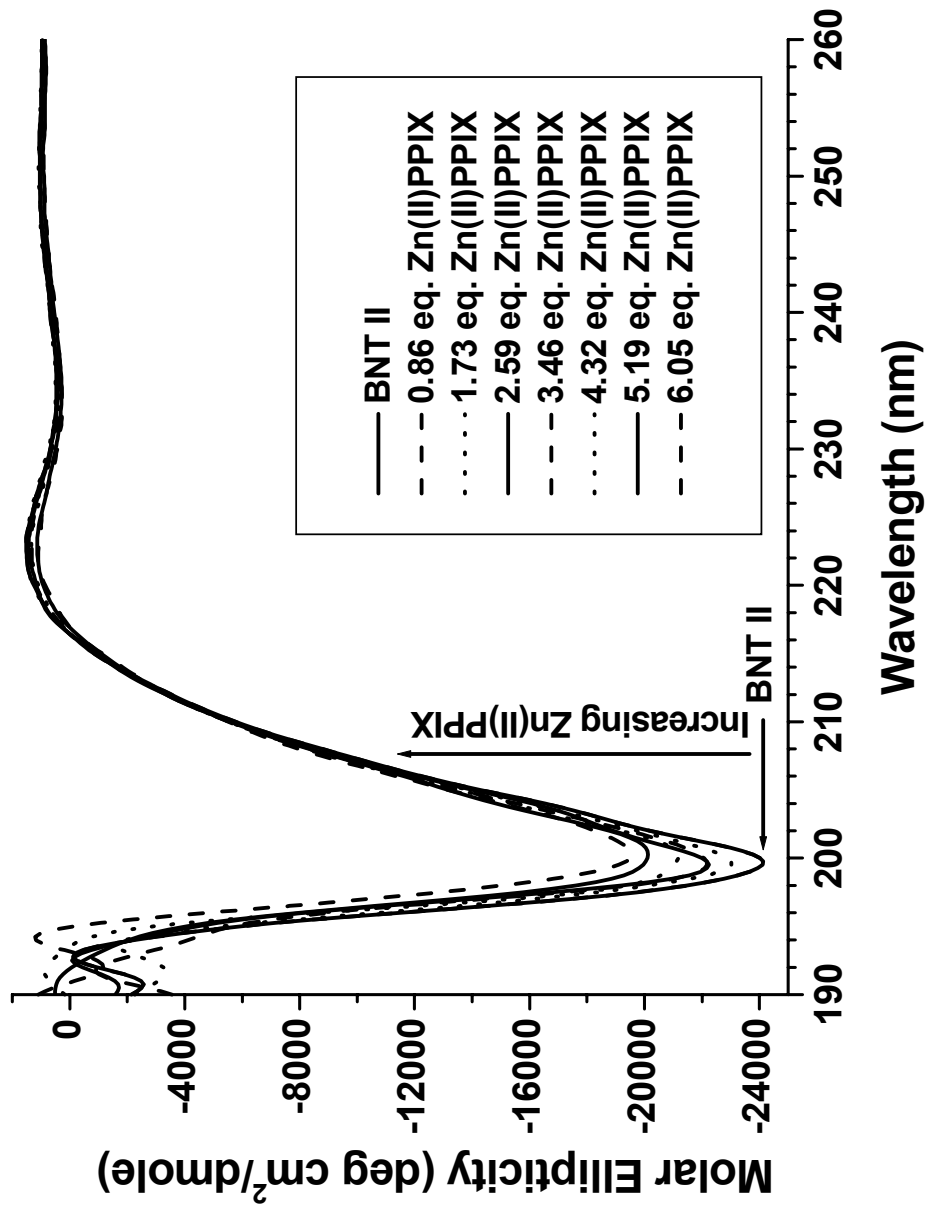


Appendix III

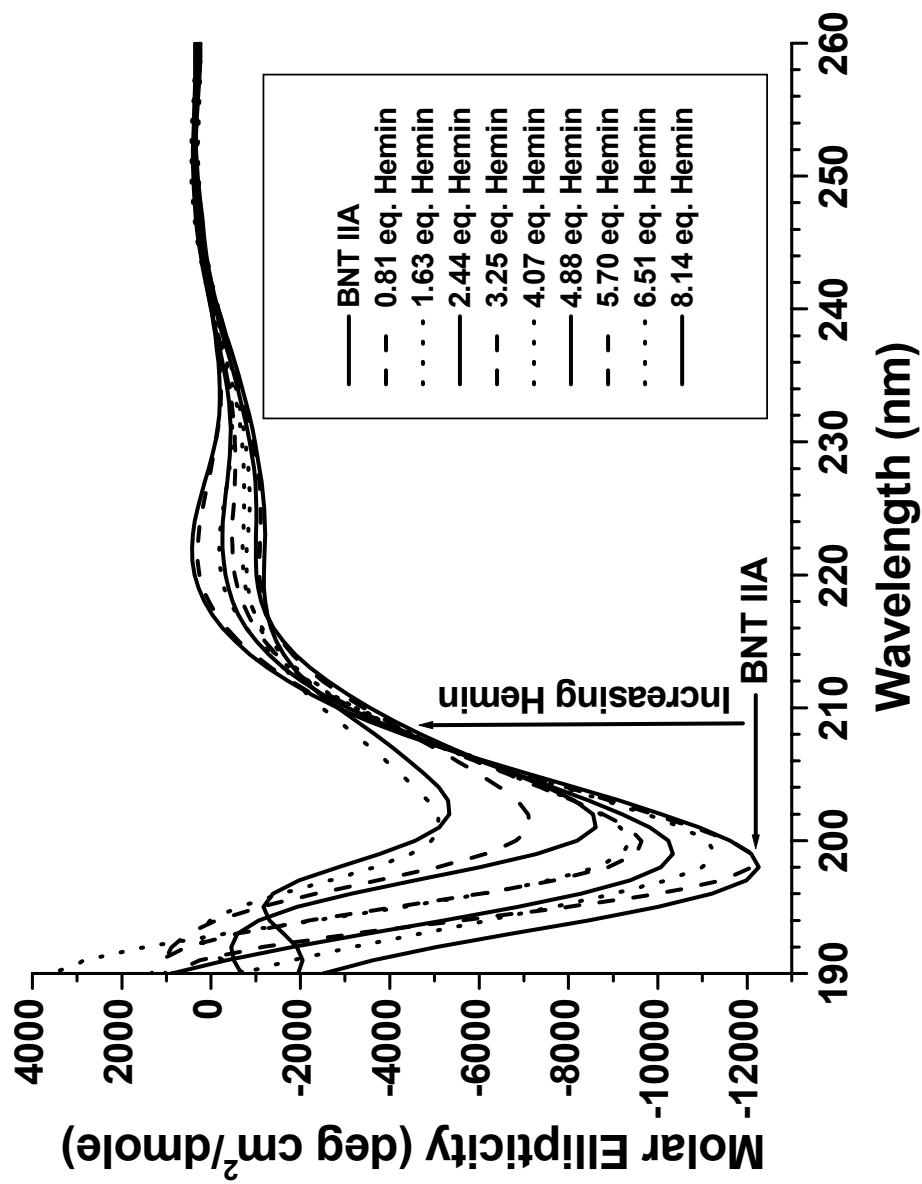
Circular Dichroism Titration Experiments



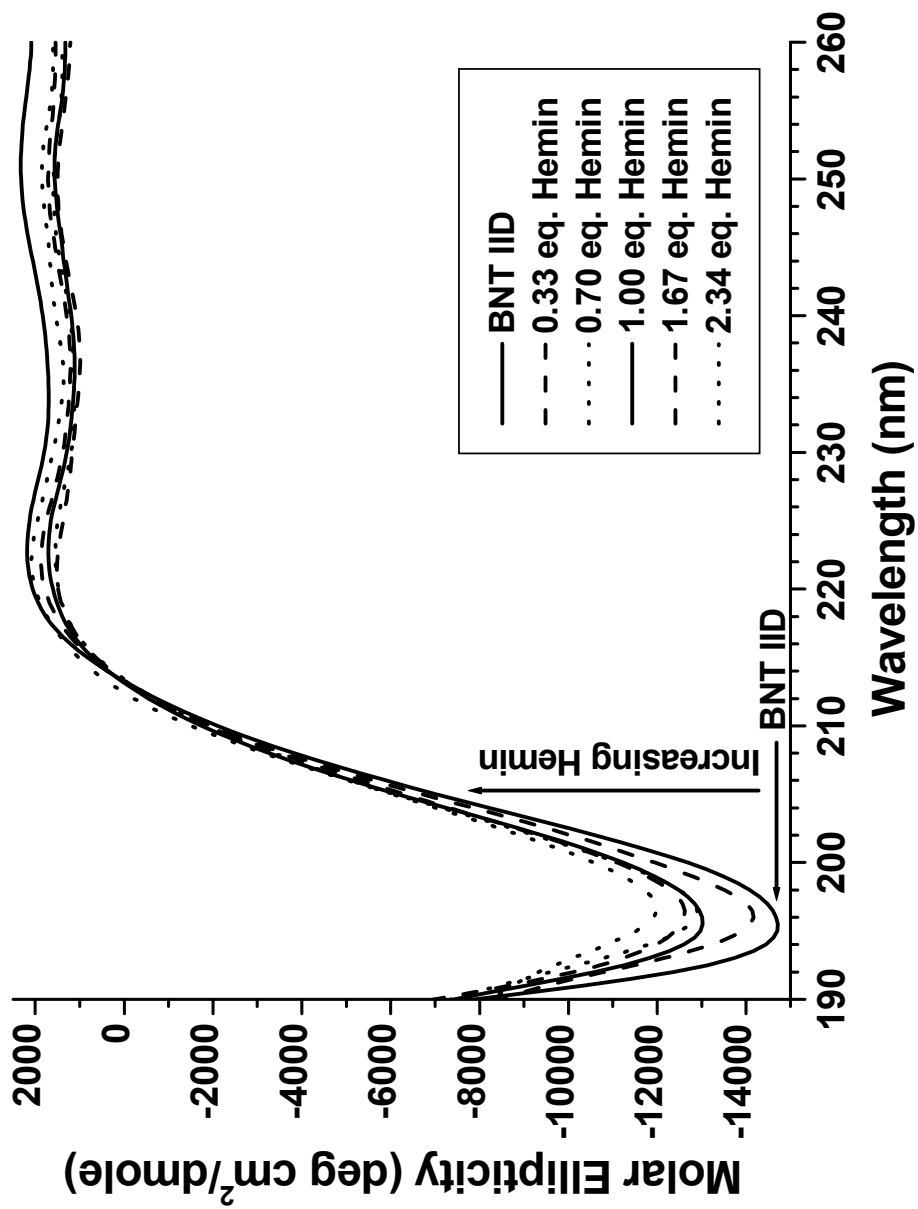
CD spectra of the titration of Fe(III)PPIX with BNT II. The negative ellipticity centered around 202 nm decreased and red-shifted upon increasing concentration of porphyrin.



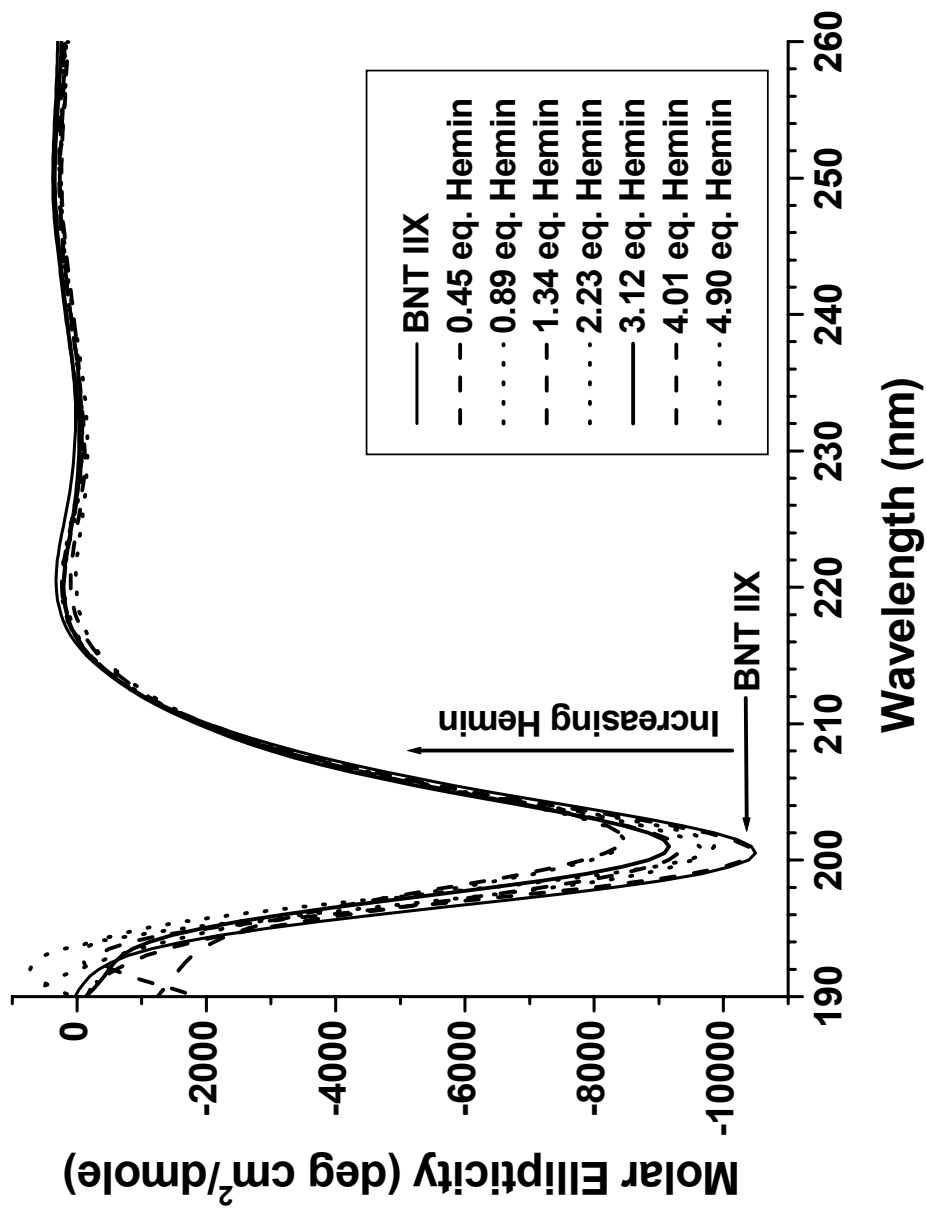
CD spectra of the titration of Zn(II)PPiX with BNT II. The negative ellipticity centered around 200 nm decreased and red-shifted upon increasing concentration of porphyrin.

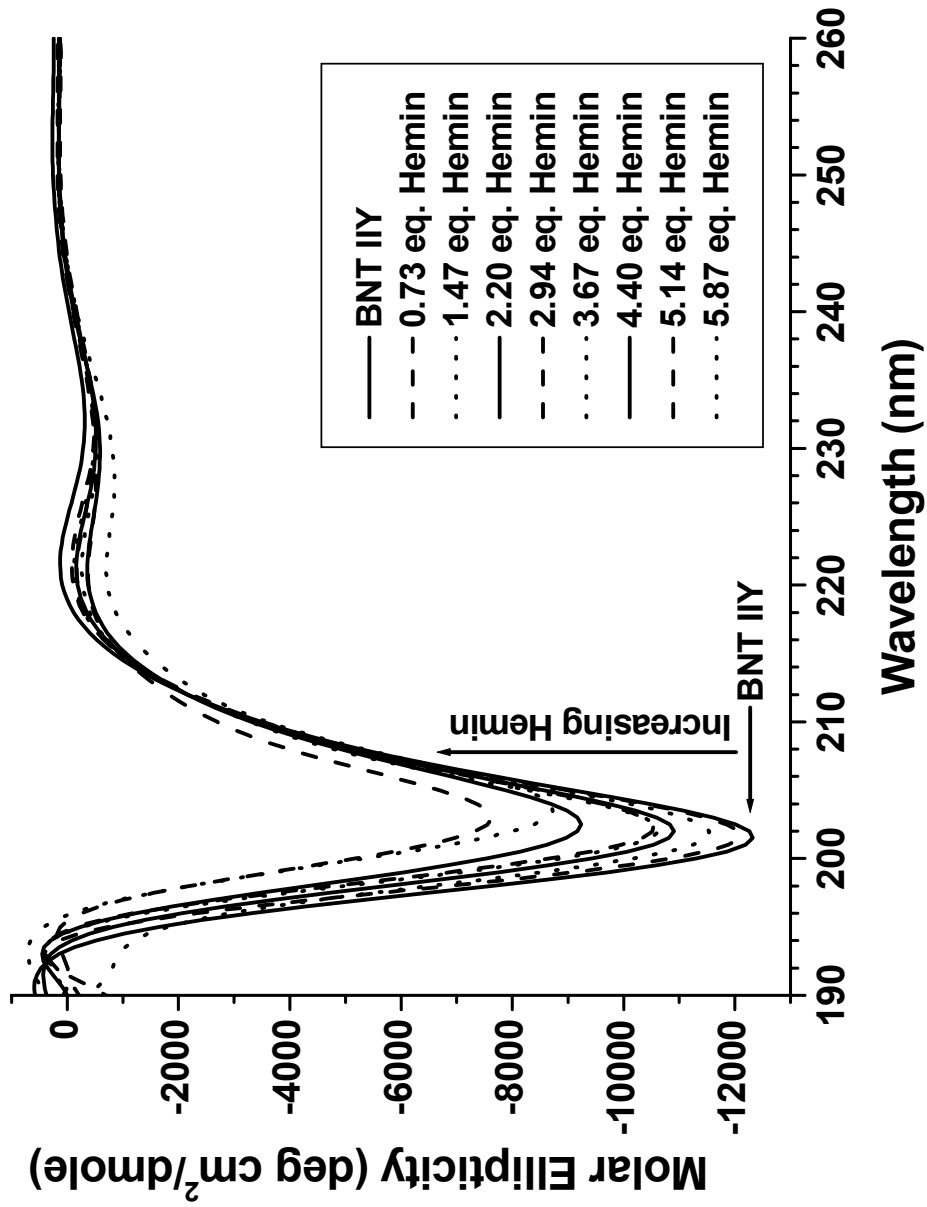


CD spectra of the titration of Fe(III)PPIX with BNT IIA. The negative ellipticity centered around 198 nm decreased and red-shifted upon increasing concentration of porphyrin.

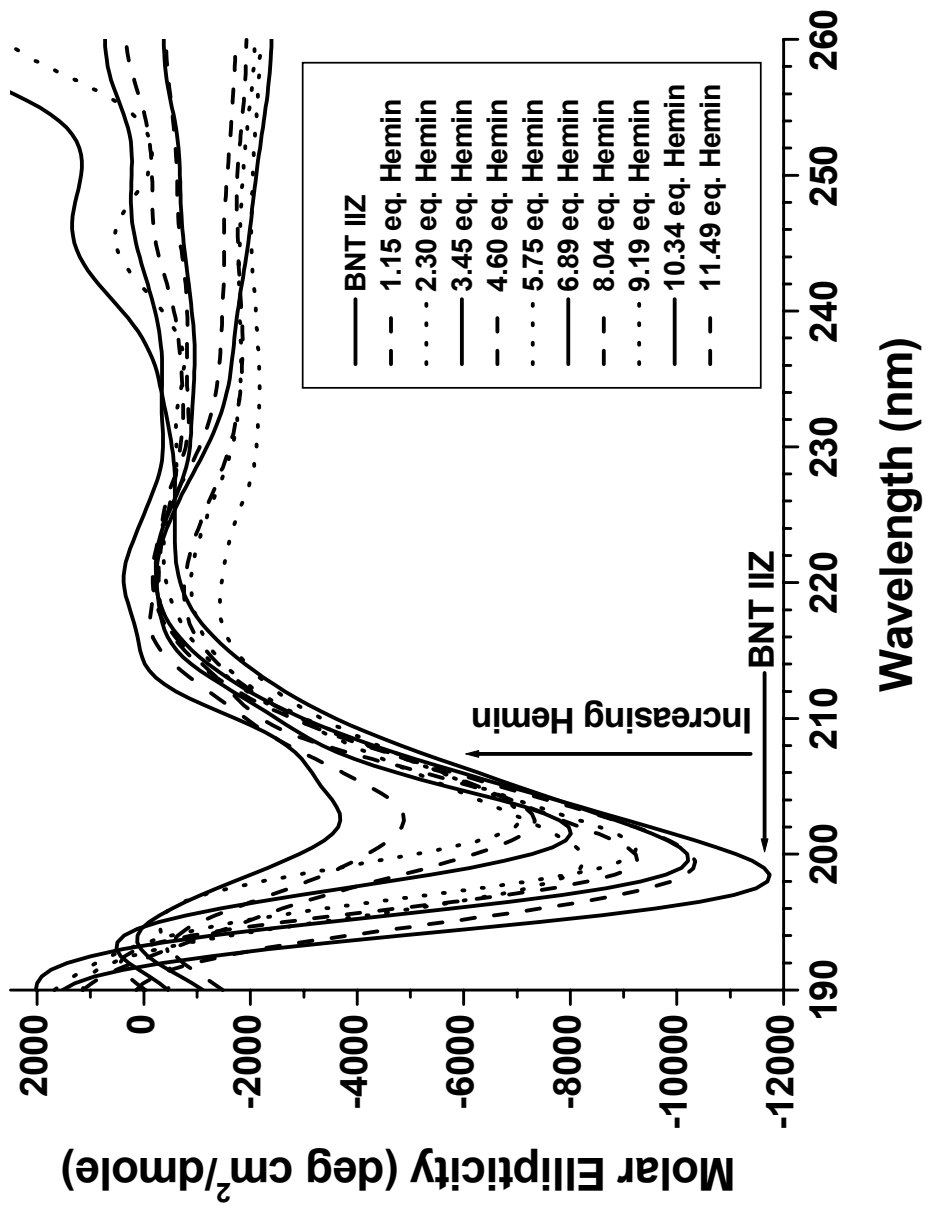


CD spectra of the titration of Fe(III)PPIX with BNT IID.
 The negative ellipticity centered around 195 nm decreased slightly upon increasing concentration of porphyrin.





CD spectra of the titration of Fe(III)PPIX with BNT IIY. The negative ellipticity centered around 201 nm decreased and red-shifted upon increasing concentration of porphyrin.



CD spectra of the titration of Fe(III)PPIX with BNT IIZ. The negative ellipticity centered around 198 nm decreased and red-shifted upon increasing concentration of porphyrin.